



UNIVERSITÀ DEGLI STUDI DI PADOVA

DIPARTIMENTO DI INGEGNERIA CIVILE, EDILE E AMBIENTALE

SCUOLA DI DOTTORATO DI RICERCA IN SCIENZE DELL'INGEGNERIA
CIVILE ED AMBIENTALE – CICLO XXV

Sede amministrativa: Università degli Studi di Padova

DUCTILITY AND BEHAVIOUR FACTOR OF WOOD STRUCTURAL SYSTEMS

Theoretical and experimental development of a high
ductility wood-concrete shearwall system

Director of PhD School : Prof. Stefano Lanzoni

Supervisor: Prof. Roberto Scotta

External Evaluator: Prof. Ario Ceccotti

PhD candidate:

Luca Pozza

January, 2013

To my parents Renato e Carla and
to Miriam, my smart Sweetheart.

Summary

This dissertation focuses on the seismic behavior, ductility and dissipative capacity of modern timber buildings. A number of innovations in the field of timber structures are reported with special regard to the modeling techniques suitable for timber joints and to the characterization of the seismic behavior of modern timber systems.

A preliminary overview on the seismic-resistant timber building technology and on their evolution from the past to nowadays is reported in the introduction of this thesis work. A review of the state of art about the available seismic codes is also reported and the main lack and incongruence with the current constructive practice are pointed out.

The basic terms and concepts used in structural modeling and nonlinear analysis of timber structure are provided in the first part of this dissertation. The specific behavior of wood joints under cyclic actions and therefore under earthquakes is described with emphasis to the pinching effect and strength and stiffness degrading. A literature review on the main numerical models proposed to reproduce the hysteretic load-slip curve of single fasteners, joints and whole wooden elements is presented and discussed. A proposal for a new wood joint numerical model that can be easily implemented into a standard commercial Finite Element code is reported. The reliability of such new developed model to reproduce the fasteners hysteresis behavior is presented and critically discussed in comparison with experimental results.

The second part of this thesis work is based on the evidence that the growing spread of the use of timber structures has led to the development of numerous innovative construction systems but at the same time a lack of code provisions for seismic timber structure still remains, in particular concerning the ductility (or behavior) factor q to be used for the design of different timber systems. This part of dissertation analyzes the definitions of the q -factor given in the scientific literature and its relevance in the design of seismic resistant structures. The traditional methods for estimating the q -factor are investigated and an innovative procedure for expeditious q -factor estimation is presented. The theoretical aspects of this new analytical-experimental procedure are reported and the main advantages and limitations are critically discussed.

The seismic behavior of the Cross Laminated Timber structure is in deep studied in the third part of this dissertation. Such building system is largely spreading in the constructive practice but no design guidelines are provided in the seismic codes yet, especially for what concerning the definition of their sound behavior factor. Aim of this part of dissertation is to define the influence of some significant building characteristics, such as building technology, storeys number, slenderness, design criteria etc., on the q -factor value. Such influences were studied referring to a numbers of building configuration and by means of nonlinear analyses carried out using specific

hysteretic spring lamp-mass models. Based on such numerical assessment a proposal for an analytical formulation suitable to calculate the q-factor of CrossLam buildings has been developed and is presented. The validation and the applicability limits of the proposed formulation are presented and critically discussed.

The final part of the dissertation investigates from the structural efficacy of newly developed construction technology which uses an external concrete shelter made of precast R.C. slabs to improve the performance of standard platform-frame shear walls. The idea consists of external plating made of thin reinforced concrete slabs screwed to the wooden frame of the walls. The concrete slab acts as a diaphragm against the horizontal forces. The structural response of this shearwalls under monotonic and cyclic loading conditions has been assessed by means of experimental tests. The tests outcomes are presented and compared with those from code provisions. Fulfillment of the requirements given by current codes as regards the attribution to the Higher Ductility Class is also verified. The influence of concrete skin on the seismic response of the shearwalls is also evaluated by means of numerical analysis and the assured “q” ductility factor is estimated.

Keywords: timber engineering, timber systems, timber buildings, seismic design, pinching, hysteretic model, ductility, by-linearization criteria, yielding limit, failure limit, wood connection, Cross Laminated Timber system, shearwall, behavior factor, ductility factor, q-factor.

Sommario

In questo lavoro di tesi si analizza il comportamento sismico, la duttilità e la capacità dissipativa dei moderni edifici con struttura in legno. Le principali innovazioni sviluppate in questa tesi di dottorato riguardano le tecniche di modellazione dei sistemi di connessione usati nelle strutture lignee e la caratterizzazione sismica dei moderni edifici in legno.

L'introduzione della tesi evidenzia le caratteristiche che rendono le strutture in legno idonee per l'impiego in zona sismica e riporta una analisi storica delle principali tipologie di edifici sismo-resistenti a struttura in legno e la loro evoluzione dal passato ai giorni nostri. Si riporta inoltre un'analisi critica dello stato normativo Europeo ed Extraeuropeo sulle progettazione sismica degli edifici a struttura in legno evidenziando le principali lacune e incongruenze con la pratica costruttiva corrente.

Il lavoro di tesi sviluppato affronta sostanzialmente quattro argomenti dettagliati in parti indipendenti. Le prime due sono di carattere generale e riguardano tutte le strutture in legno mentre le rimanenti sono specifiche di sistemi costruttivi innovativi e non ancora completamente caratterizzati sismicamente e normati.

La prima parte della tesi è dedicata alla descrizione del comportamento isteretico che caratterizza le connessioni utilizzate nelle strutture in legno e dei modelli numerici disponibili in letteratura per una riproduzione fedele di tale comportamento evidenziandone le potenzialità, i limiti di applicazione e l'efficienza numerica. Viene inoltre proposto un modello isteretico innovativo per riprodurre il comportamento delle connessioni tipicamente utilizzate nelle strutture in legno riproducibile anche mediante codici agli elementi finiti di tipo commerciale e non specificatamente orientati alla ricerca. Questa prima parte della tesi si conclude con la validazione e la descrizione dei principali vantaggi e limiti di applicazione della modello numerico proposto.

La seconda parte della tesi riguarda la definizione del fattore di struttura q dei sistemi costruttivi in legno innovati e di recente diffusione che non sono annoverati nelle normative sismiche. In questa parte della tesi vengono descritti i metodi tradizionali utilizzati per la stima del fattore di struttura evidenziandone i vantaggi e i principali limiti. Viene proposta una procedura innovativa di tipo misto analitico-sperimentale che consente una valutazione speditiva del valore del fattore di comportamento q . Questa parte del lavoro di tesi si conclude riportando la validazione della procedura proposta nonché gli aspetti teorici i limiti di applicabilità.

La terza parte della tesi approfondisce lo studio sul sistema costruttivo a parete massiccia del tipo CrossLam. Preliminarmente viene riportato lo stato dell'arte sull'attività di ricerca sinora svolta su tale sistema costruttivo. L'obiettivo di questa parte del lavoro di tesi consiste nella definizione dell'effetto di determinate caratteristiche dell'edificio come il numero di piani, la snellezza, la

composizione delle pareti, i criteri di progetto ecc. sul valore del fattore di struttura da utilizzare nella progettazione sismica dell'edificio stesso. Tale correlazione viene studiata mediante una serie di simulazioni numeriche su diverse configurazioni di edifici. I risultati ottenuti sono stati sintetizzati in una nuova formulazione analitica per la definizione del fattore di struttura q a partire dalle specifiche caratteristiche dell'edificio. Infine si riporta la validazione di tale formulazione analitica e si descrivono i principali vantaggi e limiti.

L'ultima parte di questo lavoro di tesi consiste nello sviluppo teorico e sperimentale di un nuovo sistema costruttivo misto legno-calcestruzzo ad alta duttilità e performance anti-sismiche. Il sistema sviluppato consiste nell'applicazione di un rivestimento esterno in lastre di calcestruzzo alle tradizionali pareti di taglio a telaio d legno. La risposta strutturale, la duttilità e il comportamento isteretico sono stati verificati mediante dei test sperimentali condotti su differenti configurazioni di pareti. Infine sono state condotte delle simulazioni numeriche, con modelli numerici appositamente sviluppati e tarati sulla base dei test sperimentali, mediante le quali è stato possibile stimare il valore del fattore di struttura q da utilizzare per il progetto sismico di questo nuovo sistema costruttivo.

Parole chiave: ingegneria del legno, sistemi in legno, edifici in legno, progettazione sismica, pinching, modello isteretico, duttilità, criteri di bi-linearizzazione, limite di snervamento, sistemi di connessione, sistema CrossLam, sistema pareti di taglio, fattore di struttura, fattore di riduzione, fattore q , rivestimenti strutturali

Acknowledgments

I wish to express my deepest gratitude to Dr Roberto Scotta for giving me the opportunity to widen my knowledge and to improve my passion for wooden structures and seismic engineering by means of this work. His suggestions and his tuition helped me to mature both on a scientific and a personal level.

I gratefully thank Prof Renato Vitaliani, Prof Anna Saetta, Dr Luisa Berto, Dr Massimiliano Lazzari, Dr Leopoldo Tesser, my workmates and PhD graduate students in the Department of Engineering at the University of Padua Giuseppe, Diego, Tommaso, Paolo and Davide, who welcomed me in their research unit and encouraged me to be always at my best. My special gratefulness goes to my dear fellow student Lorenzo, whose heartening support helped me to get through every difficult moment.

I also extend my appreciation to my external evaluator Prof Ario Ceccotti for his generous readiness, for our challenging scientific discussions, for his precious suggestions which improved my scientific work.

I am especially indebted with my sweetheart Miriam, who has always been a constant source of love, help and inspiration.

I am extremely blessed to have a wonderful family: my sisters Mila and Alice, my brother Filippo and my loving parents Carla e Renato who have unceasingly encouraged my studies and supported me both with moral and financial backing.

This research project was funded by “MAURO BERTANI GROUP” to whom I address my appreciation together with my graduate advisor Dr Roberto Scotta and the Graduate School at the University of Padua for investing in the scientific research as a tool for innovation and technological advance.

I further acknowledge Mr Gianfrancesco Biancon, holder of “POLIFAR Srl”, for giving his logistical and financial support which allowed the development of a part of this PhD thesis.

Table of Contents

Table of Contents	11
Introduction.....	1
I.1 Seismic behaviour of timber structures	1
I.1.1 Factors influencing seismic design of wooden structures	2
I.1.1.1 Wood properties.....	2
I.1.1.2 Joints and connections.....	3
I.1.1.3 Building lateral stability.....	4
I.1.1.4 Building anchorage	5
I.1.1.5 Typical timber buildings vulnerabilities	6
I.1.2 Historical timber structures.....	7
I.1.2.1 Wood-masonry house of Lefkas island - Greek	7
I.1.2.2 “Pompalino” building in Lisbon - Portugal	8
I.1.2.3 “Himis” building - Turkey	9
I.1.2.4 Pagodas – Japan	10
I.1.2.5 Wood-block system.....	11
I.1.3 Modern timber structures	12
I.1.3.1 Heavy Timber Frame constructions	14
I.1.3.2 Platform Frame wood construction	16
I.1.3.3 Cross Laminated Timber construction	17
I.1.3.4 Hybrid wood-concrete constructions	20
I.2 Seismic regulations for wooden structures	22
I.2.1 European seismic regulations	22
I.2.1.1 Specific rules for timber structures.....	23
I.2.1.2 Comments and notes	24
I.2.2 Extra - European seismic regulations.....	25
I.2.2.1 Canadian regulations	25
I.2.2.2 U.S. regulations.....	26
I.2.2.3 Japanese regulations	26
I.2.2.4 Chinese regulations	26
I.3 Objectives and Scope	27
I.4 Dissertation overview	27
References - Introduction	29
Chapter 1 - Hysteresis models for wood joints	31
1.1 Wood fasteners hysteretic characteristic	33

1.2	Hysteresis models	35
1.2.1	General hysteresis models	35
1.2.2	Current models for wood system	36
1.2.2.1	Foschi hysteresis model	37
1.2.2.2	Dolan hysteresis model	38
1.2.2.3	Richard & Yasumura hysteresis model.....	40
1.2.2.4	CUREE hysteresis model	41
1.2.2.5	Ceccotti & Vignoli hysteresis model.....	43
1.2.2.6	Rinaldin hysteresis model.....	44
1.2.2.7	K. Elwood hysteresis model.....	46
1.3	Comments.....	47
	References - Chapter 1.....	48
Chapter 2	– Proposal and validation of a new hysteresis model for wooden joints	51
2.1	Introduction	53
2.2	Proposal for a simplified hysteresis model for wood connections	53
2.3	Model calibration procedure	55
2.4	Test Simulation on a Single Connection Element	56
2.5	Test Simulation on a Single Wall Panel	58
2.6	Simulation of shaking table tests of whole buildings	60
2.7	Conclusions.....	62
	References - Chapter 2.....	63
Chapter 3	- Procedures for determining the behaviour q-factor of timber building systems	65
3.1	Background on q-factor definition	67
3.2	Overview on timber constructive system q-factor.....	69
3.2.1	Q-factor for timber buildings.....	69
3.3	Basic procedure for q-factor evaluation	71
3.3.1	Conventional methods based on experimental tests	72
3.3.1.1	Q-factor definition by means of quasi-static cyclic tests	72
3.3.1.2	Q-factor definition by means of shaking table test.....	73
3.3.2	Conventional methods based on numerical simulations	74
3.3.2.1	Q-factor definition by means of NLDAs.....	75
3.3.2.2	q-factor definition by means of NLSAs.....	76
3.3.2.3	Summary of numerical methods	77
3.3.3	Comments about the “near collapse” condition.....	78
3.4	Conclusions.....	78
	References – Chapter 3.....	80

Chapter 4	– Proposal and validation of a procedure for the q-factor estimation of timber buildings	83
4.1	Introduction	85
4.2	Description of the analytical-experimental proposal	85
4.3	Bi-linearization criteria.....	87
4.3.1	Yielding point definition.....	88
4.3.2	Failure limit definition	90
4.3.3	Bi-linearization methods for timber structures	90
4.4	Validation of the proposed procedure	91
4.5	Assessment of the q-factor of various building systems	94
4.5.1	Case study wall specimens	94
4.5.2	Capacity curves	96
4.5.3	q-factor estimation	99
4.6	Conclusions	104
	References – Chapter 4.....	105
Chapter 5	– Numerical evaluation of the q-factor for various CLT building configurations.....	107
5.1	Introduction	109
5.2	Seismic research on CLT building - State of art	110
5.3	Overview on the CLT construction practice	113
5.4	Parameters influencing the q-factor value	114
5.5	Parametric analyses to assess the influence of slenderness, design criteria, wall composition and joints arrangement on the CLT building q-factor	115
5.5.1	Reference CLT building.....	116
5.5.2	Assessment of building test configurations.....	118
5.5.3	Seismic design criteria of the shear walls.....	121
5.5.4	Numerical model of the building	123
5.5.4.1	Numerical model of the case studies building	123
5.5.4.2	Numerical model calibration	124
5.5.5	NonLinear Static and Dynamic Analyses on the buildings	126
5.5.5.1	Calibration of NonLinear Static Analyses	126
5.5.5.2	Calibration of NonLinear Dynamic Analyses	126
5.5.5.3	Analyses results	127
5.5.6	Q-factor evaluation for the different building configurations	132
5.6	Influence of the fasteners overstrengthening on the q-factor value	133
5.7	Conclusions	135
	References – Chapter 5.....	137

Chapter 6 – Proposal and validation of an analytical formula for the evaluation of the q-factor of CLT buildings.....	139
6.1 Proposal for an analytic procedure for the CLT building q-factor evaluation.....	141
6.1.1 Building synthetic indexes.....	141
6.1.2 Analytical formulations to assess the q-factor.....	144
6.1.2.1 Linear formulation	146
6.1.2.2 Power formulation.....	146
6.1.2.3 Calibration of the proposed formulations	146
6.1.3 Effects of the connectors design criteria	149
6.1.4 Effects of the principal elastic period on the q-factor value.....	150
6.1.4.1 Case study buildings.....	150
6.1.4.2 Analysis of q-factor values.....	151
6.1.5 Full formulation of the ductility factor	156
6.2 Validation of the developed analytical procedure.....	157
6.2.1 Case study n. 1 - NEES Wood building	157
6.2.2 Case study n. 2 - SOFIE building.....	159
6.3 Energetic evaluations.....	161
6.3.1 Energetic balance equation	161
6.3.2 Evaluation of the hysteretic energy dissipation.....	163
6.3.3 Energy balance for increasing PGA.....	165
6.4 Conclusions.....	166
References – Chapter 6.....	167
Chapter 7 – Theoretical and experimental development of a high ductility wood-concrete shearwall system.....	169
7.1 Introduction	171
7.2 Plated wooden shearwall – Concept.....	173
7.3 Cyclic and monotonic tests	175
7.3.1 Test wall configurations	175
7.3.2 Test setup and instrumentation.....	175
7.3.3 Test procedure.....	175
7.3.4 Test outcomes	176
7.4 Analysis of experimental result	178
7.4.1 Estimation of the ductility	178
7.4.2 Wall equivalent viscous damping.....	179
7.4.3 Wall strength degradation	180
7.4.4 Comparison with static and seismic design provisions	181
7.4.4.1 Strength and stiffness evaluation according to Eurocode 5.....	181

7.4.4.2	Ductility class definition	182
7.5	Numerical model of the tested modular panel	182
7.5.1	Modeling of the single fasteners	184
7.5.2	Numerical model of whole shearwalls	184
7.6	Assessment of the q-ductility factor	186
7.6.1	Case study building	186
7.6.2	Seismic design of the case study building	187
7.6.3	Numerical model of the case study building	188
7.6.4	Evaluation of the q-factor.....	189
7.7	Conclusions	190
	References - Chapter 7	191
Appendix A	- Geometrical and resistant characteristics of the newly developed wood-concrete building system.....	193
A.1	Introduction	193
A.2	Geometrical characteristics and structural details	193
A.2.1.	Structural layout.....	195
A.2.2.	Connection system between RC slab and wood frame	196
A.2.3.	Mechanical connections at the foundation.....	197
A.2.4.	Mechanical connections at the inter-storey	198
A.2.5.	Joint system between adjacent modular panels	198
A.3	Lateral load bearing capacity and stiffness.....	200
A.3.1	Analytical evaluation of wall panel lateral shear resistance	200
A.3.1.1.	Stapled OSB panel shear resistance	201
A.3.1.2.	Screwed concrete slab shear resistance	202
A.3.1.3.	Single modular wall panel lateral resistance	203
A.3.2	Analytical evaluation of wall panel lateral shear stiffness	207
A.3.2.1.	Bracing system stiffness	208
A.3.2.2.	Base bolt stiffness	210
A.3.2.3.	Holdown stiffness	211
A.3.2.4.	Single modular wall panel lateral stiffness	212
A.3.3	Strength and stiffness of composed and windowed walls	212
A.3.2.4.	Composed wall lateral shear and stiffness.....	212
A.3.2.5.	Windowed wall lateral shear and stiffness	213
	References - Appendix A.....	215
	List of Figures.....	217
	List of Tables	221

Introduction

I.1 Seismic behaviour of timber structures

There are many general advantages in using timber for building purposes. It is an environmentally friendly, easily recyclable material. The energy consumption during production is very low compared to that of other building materials. Timber has a low weight in relation to strength, which is advantageous for transport, handling and production. Furthermore, wood has aesthetic qualities, which give great possibilities in architectural design. However, key to the success of the wooden structures is their excellent performance in earthquake.

Timber constructions subjected to earthquake actions provide relevant advantages if compared to traditional materials. Related to its strength, timber has a low mass therefore during earthquake actions the mass excited to oscillations (“seismic mass”) is lower than with other materials, and therefore resulting forces are thus smaller. Furthermore the large amount of damping derived from friction of contacting surfaces reduces the destructive structural response to the seismic ground shaking. On the basis of these advantages and unlike the fire resistance and the durability due to the biotic attack the seismic performance has never been considered a problem in the determination of the reliability of wood as construction material.

The usage of timber as a construction material dates back to ancient history, with specific techniques differently developed within several countries. In Europe wood has never been used singly as construction material suitable to build earthquake-resistant structures but has always been combined with traditional materials such as brickwork or stone. The usage of wooden structural elements in order to improve the seismic resistance of masonry buildings has been a practice widespread as consequence of disastrous earthquakes that destroyed buildings made with traditional constructive systems. Examples of these constructive systems are the mixed wood-stone building of the Greek islands [I.1], the building system named “Pompalino” developed in Portugal after the earthquake of Lisbon in 1755 [I.2] and the traditional “himis” in Turkey [I.3], another version of the wood framed walls filled with masonry which survey to the serious earthquake that caused 25 000 victims in Izmit in 1999. Moreover in China and Japan there are excellent samples of seismic-resistant architecture: the century-old monumental temples and pagodas have survived a number of strong ground motions.

However the more common and widespread building systems is the wood-frame constructions which are largely used as residential buildings in USA, Canada, North Europe and Japan. One of

the proven features of wood-frame construction is its excellent life safety performance in earthquakes. The results from a scientific research performed in Canada [14] on the behaviour of wood-frame structure after severe earthquakes highlights a very low number of victims compared to the number of buildings involved by the earthquake. These data support the theory that timber buildings are safer than non-timber ones.

Despite the previous examples represent the excellence in the earthquake-resistant architecture, experience shows that even a wooden structure may suffer significant damage due to an intense seismic event. Such circumstance is clearly emphasized by the Loma Prieta (USA-1989), Northridge (USA-1994) and Kobe (Japan 1995) earthquakes.



Fig. 1.1 - Destruction of a residential house after Northridge earthquake 1994 [1.5] (left) and Kobe earthquake 1995 [1.6] (right)

These negative examples show that the seismic resistance of the wooden buildings is given by a combination of factors and not only by the material lightness. Once defined such seismic resistant factors it is possible to understand the behaviour of the historical timber building and design modern timber structure safety also in seismic zones.

1.1.1 Factors influencing seismic design of wooden structures

The factors that provide good performance of timber structure in seismic events are: low weight of timber structures, ductility of joints, clear layout of timber houses and good lateral stability of the house as a whole. On the contrary for wooden buildings vulnerable parts are: the anchorage of the house, the diaphragm action of floors and the first soft storey which sometimes has been left without sufficient lateral bracing (for example crawl spaces, garages).

1.1.1.1 Wood properties

Intrinsic characteristics of wood make it not only suitable but even recommended for use in seismic areas. Anyway it is also important to consider the weaknesses of this material and design criteria to ensure adequate levels of security as well as an acceptable cost. As a structural material, wood offers some advantages over other materials in earthquake performance. Wood generally used for structure has a density of 500 kg/m^3 , about 1/5 of that of the concrete. However the resistance of wood is similar to the concrete one, with the advantage that wood resist also in tension. The ratio strength/density is quite equal to that of steel; consequently, ground accelerations do not generate as much energy in wood buildings as in other buildings.

Under cyclic actions, wood usually performs linearly and elastically. Failures are brittle and these are caused by natural defects in wood, such as knots. In detail timber is brittle in tension, especially when the tension is perpendicular to grains. Therefore, perpendicular tension stresses should be avoided. Timber behaves in a ductile manner when loaded under compression, especially compression perpendicular to the grain. This is advantageous in seismic design as, for example, in the traditional carpentry joints used in the pagodas or traditional blockbau houses. However wood in itself has a low capability for dissipating energy, thus the behaviour of timber structures during seismic events is fully dependent on the behaviour of the joints under cyclic loading. The detailing of joints is thus very important in seismic design.

1.1.1.2 Joints and connections

Joints represent crucial issue for the seismic resistance of timber structures. There are substantially three different typologies of joints: glued joints, mechanical joints and carpentry ones.

Glued joints perform linearly and elastically. These do not involve plastic deformations and they do not dissipate energy. For this reason timber structures with glued joints should be classified as structures that do not dissipate energy and possess no plastic strains. The plasticity and energy dissipation property can be introduced to the connections, if the connections are "semi-rigid" as most mechanical connections used for timber structures are, instead of perfectly rigid joints as, for example, glued joints. Well-designed mechanical connections perform usually in a semi-rigid manner.

Mechanical joints in timber structures usually perform in a semi-rigid manner and plastic strains may develop, if fastener spacing and end distances match the design rules. The successful performance of mechanical connections is due to high ductility, lack of sensitivity to cyclic loads and their ability to dissipate energy. To ensure the dissipation of energy, it is possible to take advantage of the slenderness of the fastener. The slenderness is defined as the ratio between the wood member thickness and the fastener diameter. Fasteners with high slenderness ratios dissipate more energy since the plastic yield points are, in this case, always formed in the fastener. Fasteners with low slenderness ratios perform more elastically and do not dissipate as much energy. In addition, the wood splitting may be prevented by increasing the member thickness in comparison to the fastener diameter. To avoid an unacceptable strength loss in cyclic loading, three general principles should be followed. Details should be designed so that elements cannot easily pull out, brittle material failures should be avoided and materials should be used which retain their mechanical properties during cyclic loading. Mechanical joints are largely used in modern timber structure and different typologies of joint can be realized depending on the fasteners employed. As an example the following Fig. 1.2 reports the typical fasteners used in mechanical joints.



Fig. 1.2 – Typical fastener used in mechanical joints [1.7]

The carpentry joints (i.e. woodwork joints) are made by means of notches, inlay and grooves on wood elements without using any mechanical connectors. Fig. 1.3 reports as an example some typical woodwork joints such as mortise and tenon joints, lap joints etc..

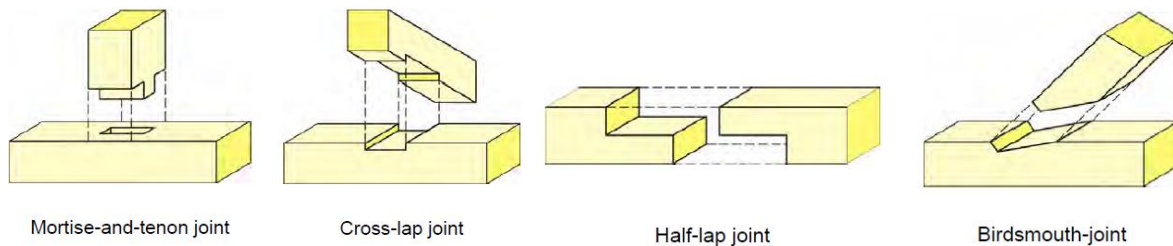


Fig. 1.3 – Typical woodwork joints [1.7]

These woodwork joints transfer the action by means of perpendicular compression stresses. As states above timber behaves in a ductile manner under perpendicular to grain compression. Furthermore the friction between the numerous wood-wood contact surfaces confers to these joints a good energy dissipation capacity.

The most significant use of these woodwork joints in timber engineering regards the realization of monumental building such as the Japanese pagodas. The following Fig. 1.4 reports a detail of a woodwork joints used to realize the roof of a Japanese pagoda [1.8].



Fig. 1.4 – Detail of the woodwork joints of a Japanese pagoda [1.8]

I.1.1.3 Building lateral stability

Lateral loads are transferred to the foundations by structures providing lateral bracing. In a timber building, the most appropriate manner to provide bracing is by using shear walls. A schematic diagram of the functioning of structural shearwalls against lateral loads is shown in Fig. 1.5, where a simple 'box-like' building is loaded laterally. The floor diaphragm is assumed to behave as a high beam and this is loaded by a seismic action depending on the floor mass and on the ground acceleration.

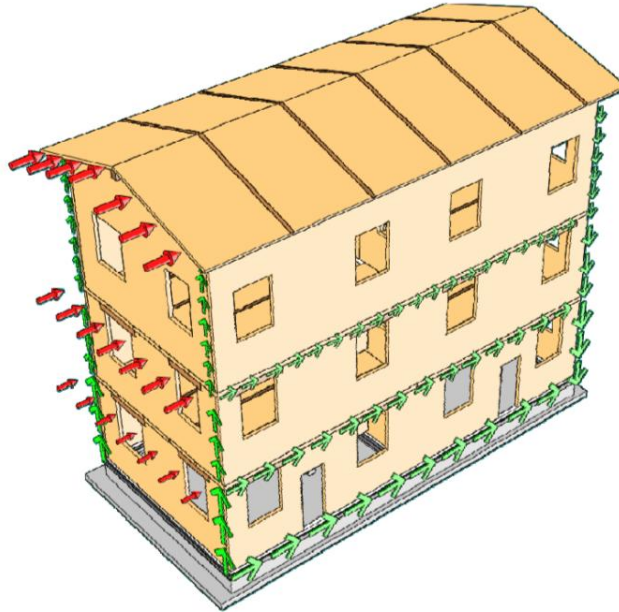


Fig. I.5 – Schematic diagram of the path of lateral forces in a simple building [I.9]

The floor diaphragm is supported at the ends by shear walls, which in turn transfer the load to the foundations. Such structural configurations may be side by side or one on top of the other as in a multi-storey house. In multi-storey houses the lateral loads cumulate to the lower storeys. The structural parts should, of course, be properly attached to each other in order to ensure that an intact path for the lateral forces does exist. This includes the connection between the floors and supporting shear walls and between the shear walls and the foundations.

I.1.1.4 Building anchorage

In order to transfer the lateral loads to the foundations, the building has to be anchored to the storey below and then on to the foundations. Anchoring is normally required at the ends of shear walls to account for uplift forces (due to overturning when the building own weight does not compensate for the effects of the lateral load) and at the bottom plate to account for the sliding (slip from base shear), see Fig. I.6. Uplift and sliding forces are anchored independently with special connectors.

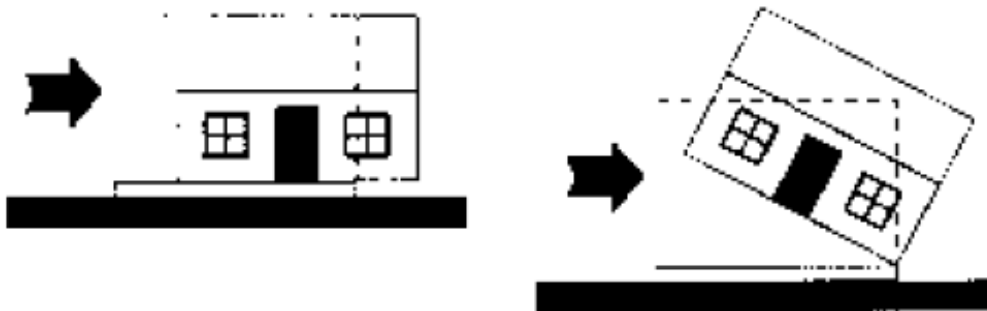


Fig. I.6 – The two anchoring cases: sliding caused by base shear and uplift caused by overturning [I.10]

Such anchorages are realized by means of specific mechanical connectors specifically designed to resist to tensile or shear action. Generally such anchorage consists of steel bracket nailed or screwed to the wooden shearwall as depicted in the following Fig. I.7.



Fig. I.7 – Typical anchorage system of Platform Frame building (left) [I.11] and CLT building (right) [I.9]

An accurate design of such anchor systems is a crucial issue to ensure an adequate level of structural robustness, dissipative capacity and safety against the seismic actions.

I.1.1.5 Typical timber buildings vulnerabilities

Generally timber building presents a very simple and regular structural layout both in plane and in height. However, if earthquake engineering principles are not respected also in timber structure may occur serious problems.

The typical example of poor earthquake design is represented by the soft-storey buildings. Such constructions are largely spread and have a soft first story due to the existence of large garage doors or retail store window openings. Such soft-storey buildings are prone to large lateral movements (displacements and rotations) and even pancake collapses in the first story during earthquakes. As an example San Francisco has about 4400 pre-1973 wood-frame buildings with three or more storeys and five or more residential units, considered likely to have soft-storey conditions. The 1989 Loma Prieta earthquake caused extensive damage of such building highlighting the constructive limitation of building typology. As an example the following Fig. I.8 reports two soft-storey buildings seriously damaged after the Loma Prieta earthquake.



Fig. I.8 – S. Francisco soft-storey building damage – Loma Prieta earthquake 1989 [I.12]

As in any kind of building the inadequate structural design or inadequate supervision during the building process that causes the damages induced by seismic events.

I.1.2 Historical timber structures

Historic buildings with wooden structure have developed in highly seismic regions and generally as a result of devastating earthquakes. The more relevant historical earthquake-resistant timber structure are: the mixed wood-stone building of the Lefkas island - Greek [I.1], the “Pompalino” building system Lisbon - Portugal [I.2], the “himis” building in Turkey [I.3] and the Japanese pagodas [I.13]. Another construction technique largely spread in the past in the European and Middle East areas is the wood-block system [I.14]. Below is reported a brief description of the main characteristics of these building systems.

I.1.2.1 Wood-masonry house of Lefkas island - Greek

The Lefkas Island is characterized by high seismic hazard. In 1825 a severe earthquake destroyed all buildings therefore the English authority issued the regulations for seismically safe. Such standards imposed the realization of multi-storey building using a specific constructive systems characterized by the 1st storey walls made by stone or masonry which represent the load bearing system of the upper storeys realized within a wooden structure. This wooden structure was realized by means of frame braced by diagonal elements. Each frame was stiffened by the angular elements located in the corners as depicted in the following Fig. I.9.

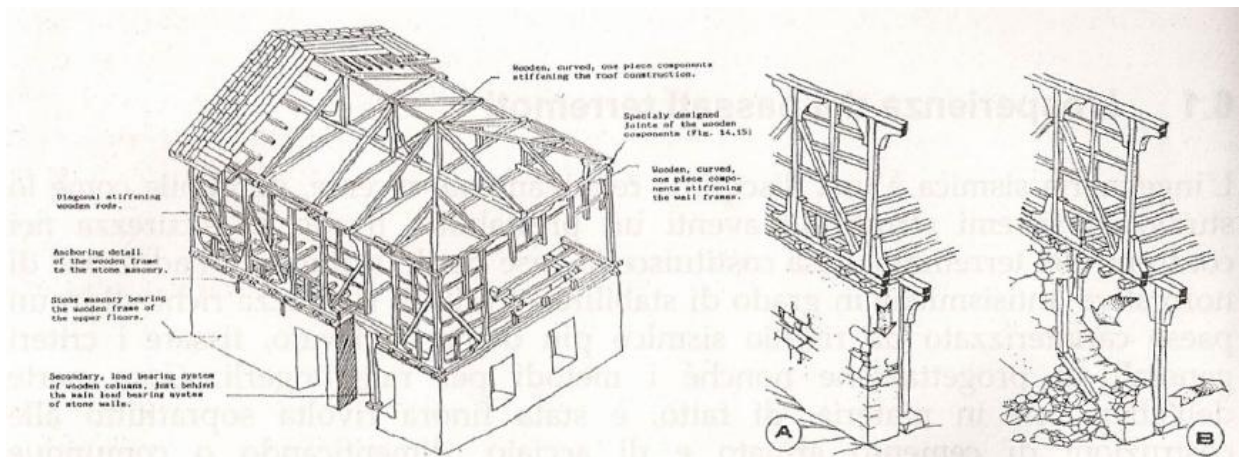


Fig. I.9 – View of the seismic-resistant building of Lefkas Island – Greek (left). Resistant mechanisms under earthquake (right). In static condition masonry bear vertical load (A) but in case of partial collapse of the wall under earthquake the gravity load are bore by the wooden pillars (B) [I.1]

The particularity of this mixed wood-masonry building is represented by the usage of an additional timber system placed in parallel with the walls of the ground floor suitable to bear the vertical loads. Such coupling of wooden pillars and masonry wall allows to withstand earthquakes of high intensity that can also cause the partial collapse of the masonry walls but without causing the building collapse. In fact the wooden system in parallel with the masonry bears the vertical load and prevents the collapse of the building as shown in Fig. I.9.

The seismic resistance of this constructive system is based on the difference in the deformation capacity under seismic loads of wood and masonry. This coupling ensures high seismic performance although Lefkas Island is highly seismic, and nowadays there are numerous examples of buildings made with this constructive system without damages.

I.1.2.2 “Pompalino” building in Lisbon - Portugal

The “Pompalino” system was developed as a result of the earthquake that destroyed the city of Lisbon in 1755. After the earthquake this building system was chosen as the anti-seismic construction system by an experienced team of engineers appointed by the Marquis of Pompal.

This building system consists of a timber frame system made of square fields braced with crosses. The triangles formed of the elements of the frame were filled with masonry. As a result this building system consists in a wooden cage (the “gaiola”) filled with masonry which allows the construction of buildings up to 5 floors. The following Fig. I.10 reports an example of this “Pompalino” building.



Fig. I.10 – Lisbon area rebuild with “Pompalino” system after 1755 (left) and typical “gaiola” wall [I.2]

The basic idea of this building system is the usage of wooden structural elements in order to improve the seismic resistance of masonry buildings. This building typology is also widespread in non-seismic areas of Europe such as in France, named “Colombage” system, in Germany “Fackwerk” system and in England “Half-timbered” system (see Fig. I.11).



Fig. I.11 – Example of a “Colombage” building in France [I.15] (left) and of a “Fackwerk” building in Germany (right) [I.16]

The structural system of reinforced masonry house with wooden frames was also used in Italy for the reconstruction of some buildings in Calabria after the earthquake of 1783 [I.17].

I.1.2.3 “Himis” building - Turkey

In Turkey there are several wooden and mixed wood-masonry building systems. An extensively treatment about the historical Turkish wooden building can be found in [1.14]. The well-known building system used in Turkey is the traditional “himis” [1.3], another version of the wood framed walls filled with masonry which survey to the serious earthquake that caused 25 000 victims in Izmit in 1999.

The structural layout of the “himis” building consists of wood bearing structure composed by frame braced by diagonal elements filled-in by masonry or stone. According to the characteristic of regions some variations are observed between structures in different areas as infill material, types of wood, etc.. In detail there are three main types of “himis”: sun-dried brick fill, stone fill and brick-fill [1.14].

The Sun-Dried brick fill himis system used as filling material sun-dried bricks. It is the most primitive and poor technique used to realize the himis buildings. The following Fig. I.12 reports some buildings achieved with this technique.

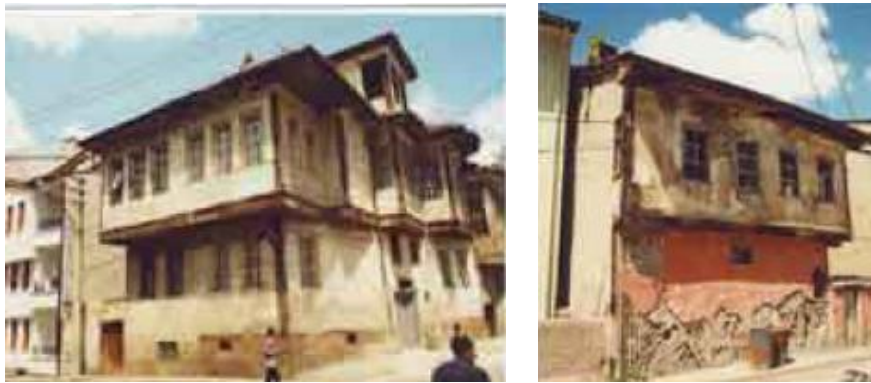


Fig. I.12 – Example of sun-Dried Brick infill himis structures [1.14].

The stone fill himis systems are commonly used in areas characterized by coast and forest. In this system, spaces between members of wooden frame are filled with stones, which dimensions vary between 10-15 cm. Some examples are shown in Fig. 1.13.



Fig. 1.13 – Example of stone infill himis structures [1.14].

The brick fill himis system was first use in 16th century. In this method brick is used for infill material and the thickness of the wall was approximately equal to the size of half brick. Filling the bricks into

wall can be shaped into horizontal, vertical and crosswise. In Fig. I.14 is reported an example of this brick fill himis.



Fig. I.14 – Example of Brick infill himis structures [I.14].

The proper seismic behavior of these building typologies is confirmed by numerous comparative studies carried out by Langenbach R. [I.18].

I.1.2.4 Pagodas – Japan

Traditional timber pagodas in Japan are believed to have high seismic performance. This is because there is no documented record of the destruction of a multi-story timber pagoda during an earthquake, despite their height and low rigidity. The height of timber pagodas ranges from 15 meter to over 50 meter. The structure has a square and symmetrical plan, usually three spans by three spans. The aspect ratio has a tendency to increase and the structure becomes slender for newer pagodas. The structural system of timber pagodas in Japan is composed of the center column and the surrounding multi story frame as shown in Fig. I.15.

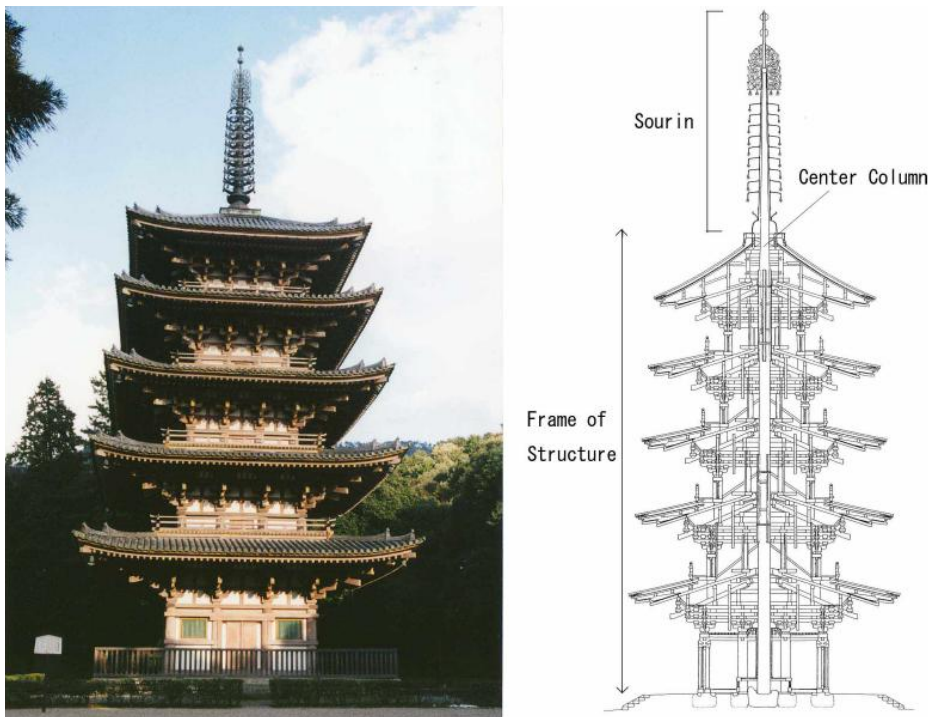


Fig. I.15 – Example of the section and picture of Daigo-ij Pagoda [I.13]

The center column is structurally independent of the surrounding frame structure, and is based on the foundation or on top of the beam of the first floor or suspended from the frame. On top of the center column, metal ornamentation called the “sour in” is installed. The columns of the surrounding frame are all based on top of the beam of the lower story, and have small aspect ratio.

The seismic performance of timber pagodas has been of interest to seismologists as well as structural engineers, and many analytical studies have been performed and hypotheses proposed. The seismic resistance of traditional timber pagodas has not yet been clarified quantitatively because of the lack of experimental data. However it seems that the high seismic performance may be due to particular building methodology. The usage of wood-wood joints to realize the structure ensures great flexibility and energy dissipation due to the friction that develops between the carpentry joint surfaces.

I.1.2.5 Wood-block system

This system is a typical constructive technique of the mountain and rural villages of the European and Middle East area characterized by high timber volume. In this construction system the walls are made overlapping round logs that cross in the corner. Two different solutions of corner joints were typically used. In the first solution a half-lap joint were used while in the second one the wood is removed in both the upper and lower face of the log as depicted in the following Fig. I.16.

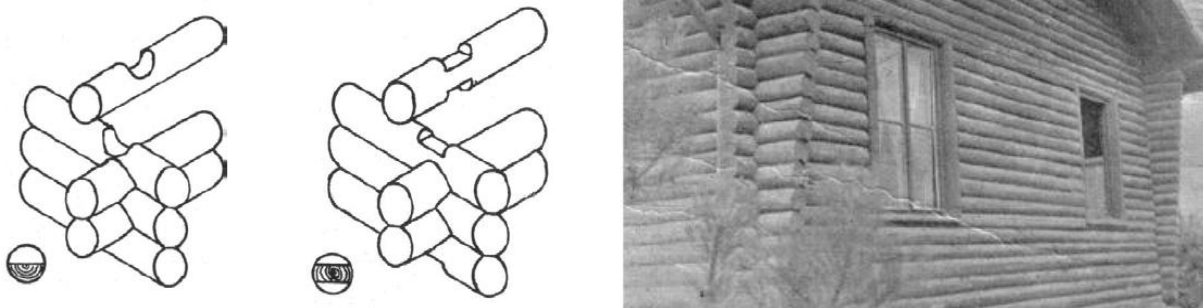


Fig. I.16 – Simple wood-block system [I.14]

The resistance to the horizontal action of this timber system is exclusively due to the friction in the contact surface of the overlapped logs. Such circumstance joined with the vertical load condition perpendicular to the grain imposed the usage of this constructive technique only for small one storey building. Nowadays this building system is steel used in north Europe and alpine area for single storey building named Log-house.

I.1.3 Modern timber structures

The usage of wood in the past was closely linked to the maximum size of the structural elements that could not exceed those of trees. For this reason traditional use of wood as a structural material was relegated to the construction of small-rise buildings, small scale roofs and of structures and stiffening frames to be coupled to masonry structures.

The modern use of wood as a building material is really different from the historical one. Currently new engineered wood materials, mainly glued laminated timber beams (glulam) and innovative timber panels, allow wood to be used for long-span structures (large roofs, pedestrian and road traffic bridges) and multi-storey buildings.

Firstly the invention of laminated timber has allowed to overcome the limitations of the tree and realized large scale structures. Early applications used mechanical fasteners, such as bolts, dowels and rods, to connect the laminations. However, the potential of the lamination technique was not fully exploited until synthetic glues became generally available in the early twentieth century. Glued laminated timber or glulam became one of the first engineered wood products, and is still very competitive in modern construction. By bending the laminations before gluing, it can be produced in curved shapes. Theoretically, cross-section depth is unlimited, but for practical reasons maximum depths are of the order of 2 m. This makes glulam an ideal material to create structures for large spans. A variety of structural systems based on straight and curved glulam members has been developed for roofs with spans of up to 100 m. As an example, the following Fig. I.17 reports Glulam arch roof for Stockholm central railway station, built in 1925 [I.19].



Fig. I.17 – Glulam arch roof for Stockholm central railway station - 1925. [I.19]

Tall buildings and large structures with wood-based panels and systems are not something new in European and North America construction sector. As an example in Canada many 5- to 9-storey timber buildings were built in the early 20th century and they're still in use today. As an example, the following Fig. I.18 shows an 8-storey office buildings built in Vancouver in 1905 and in Toronto in 1920 using the brick-and-beam technique.



Fig. 1.18 – 8-storey brick-and-beam office buildings built in Vancouver in 1905 (left) and in Toronto in 1920 (right) [1.20]

Anyway, a decline in the construction of such building were observed over the second half of the 20th century due to the technological advantages in alternative construction material such as steel and concrete and the desire by both developers and designers to go taller. Restrictions imposed by previous building codes on the maximum height of building made of combustible materials have also contributed to this downfall.

However, recent development of innovative engineered wood-based products and systems in addition to the introduction of objective and performance based building codes have contributed to reviving the interest using wood-base products in mid and potentially high rise construction.

On the material side, new generation of engineered wood-based products have been developed which provide to designers and engineers alternative materials, comparable or better performance systems and better environmental attributes compared to other construction materials.

Substantially there are three key wood-based material developed in the 20th century that have provided such opportunity: (1) glued laminated timber (glulam), (2) wood based board (Oriented Strand Board and Plywood) and (3) Cross Laminated Timber panel (CLT). The usage of such innovative engineered wood-based products allows realizing different medium and high-rise structure as follows:

- Heavy Timber Frame construction
- Platform Frame wood construction
- Cross Laminate Timber construction
- Hybrid wood-concrete construction

A brief description of such structural system is reported below. The main characteristics and usages of each constructive typology are presented and discussed.

I.1.3.1 Heavy Timber Frame constructions

Glulam represents a viable alternative to traditional materials (steel and concrete) both in terms of structural efficiency and costs. In the last years evolution of the manufacturing technology of laminated timber has allowed to realize very complex structures of considerable dimension, the so called heavy frame construction.

The competitiveness of heavy timber frame structure has been demonstrated in thousands of buildings during the past fifty years, many of which are still in use. Heavy timber buildings were structures designed and used primarily for industrial and storage purposes. Nowadays there are many applications of this construction system to realize industrial buildings as depicted in the following Fig. I.19.



Fig. I.19 – Novello factory – Varese Italy [I.21]

Nowadays, its use has been expanded to include much other occupancy. It is commonly used for assembly and mercantile buildings, such as schools, churches, auditoriums, gymnasiums, supermarkets, and for various other structures. The following Fig. I.20 reports some examples of modern applications of heavy frame systems.

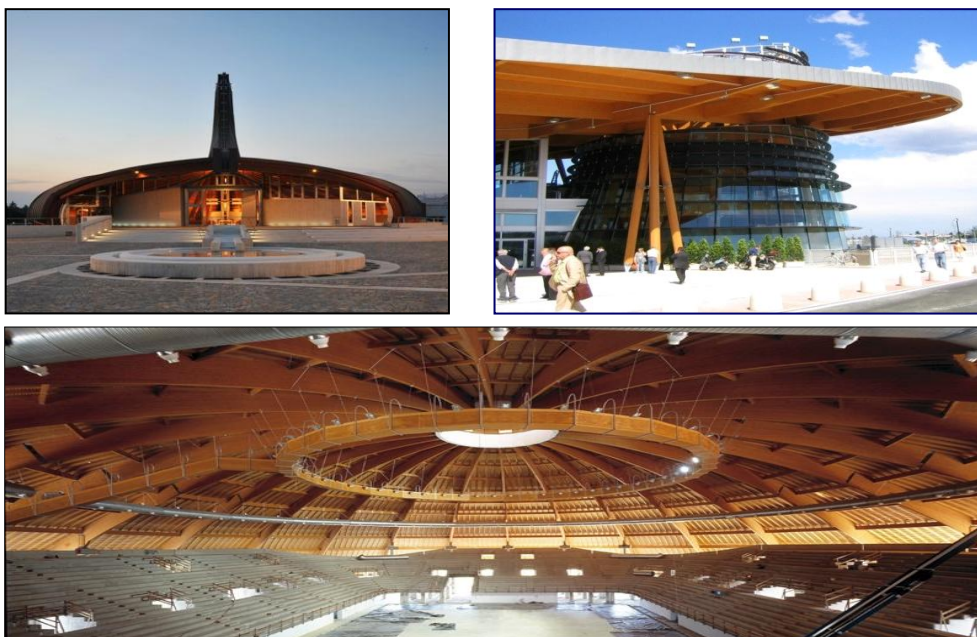


Fig. I.20 – S. Francesco Church – Imola, Italy (top left), Carrefour Shopping Center – Milan, Italy (top right) and Palasport – Livorno, Italy (bottom) [I.21]

Many of modern heavy timber buildings are large in area and consist of a single storey. However, modern multi-storey heavy timber building has proved to be entirely practical and satisfactory. The crucial issue of multi-storey heavy frame building is represented by the moment-resistant joints used to connect pillars to beams. Such joints are traditionally realized using steel plate fixed by means of dowel or bolts. As example the following Fig. I.21 reports an outline of the typical beam-column intersections [x].

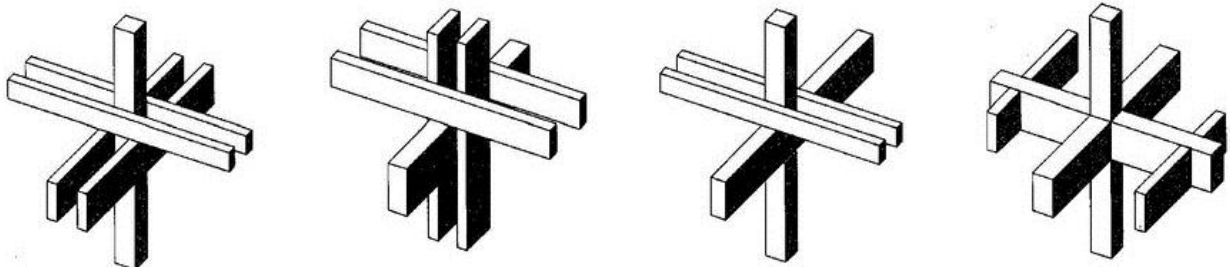


Fig. I.21 – Typical beam-column intersections [I.7]

In the last 20 years some innovative systems have been developed for the realization of column-beam joints. The most relevant is a hybrid systems based on post-tensioning techniques [I.22]. A schematic representation of such joints is depicted in following Fig. I.22.

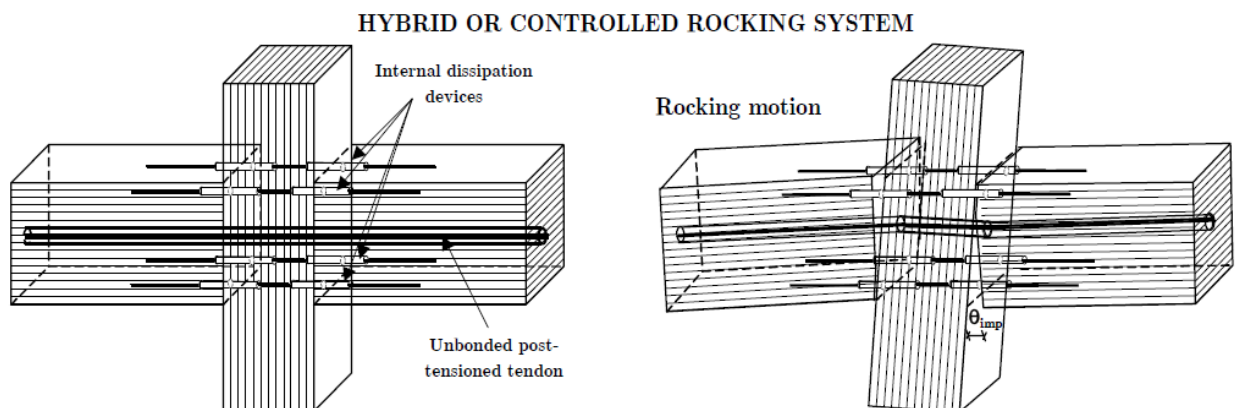


Fig. I.22 – Basic concept of hybrid jointed for heavy frame systems [I.22]

This innovative moment-resistant solution have been developed for the seismic design of multi-storey timber buildings, following current international trends towards performance based seismic design and technological solutions for high seismic performance, based on limited levels of damage. Furthermore re-centering properties, leading to negligible residual deformations and limited cost of structural repairing, are provided by unbonded post-tensioned tendons.

Although in the last years there have been significant technological advances in manufacturing techniques of beam-column joints the realization of multi-storey buildings with heavy timber frame structure has been very limited. Nowadays the most widespread construction technology for multi-storey timber buildings involves the use of shearwalls and heavy frame timber systems is quite exclusively used to realize one-storey large scale structure.

I.1.3.2 Platform Frame wood construction

Light-frame wood construction was invented in North America in the early 1800s. Its track record, both in building performance and assembling expertise, has been well-established over that time. Many wood buildings across North America, built at the turn of the 20th century, are standing proof of the reliability of this system. Wood construction provides high strength with relatively low weight, and the high strength-to-weight ratio makes wood a good choice for earthquake-resistant construction.

In this type of construction, wood members are thin, standard size, and closely spaced. Floors are built one at a time, so that each floor becomes the building platform for the new one above. Three components form most of the framing: studs run vertically and form the skeleton of the walls; joists run horizontally and form the floors; and rafters or trusses underpin the roof. When a wall is braced with diagonal wood members or enclosed with lightweight wooden panels, it now has lateral resistance and becomes a shear wall system — light, strong and structurally efficient. All the pieces work together to hold up the building against gravity, wind and earthquakes. The following Fig. I.23 shows a scheme of the platform frame system.

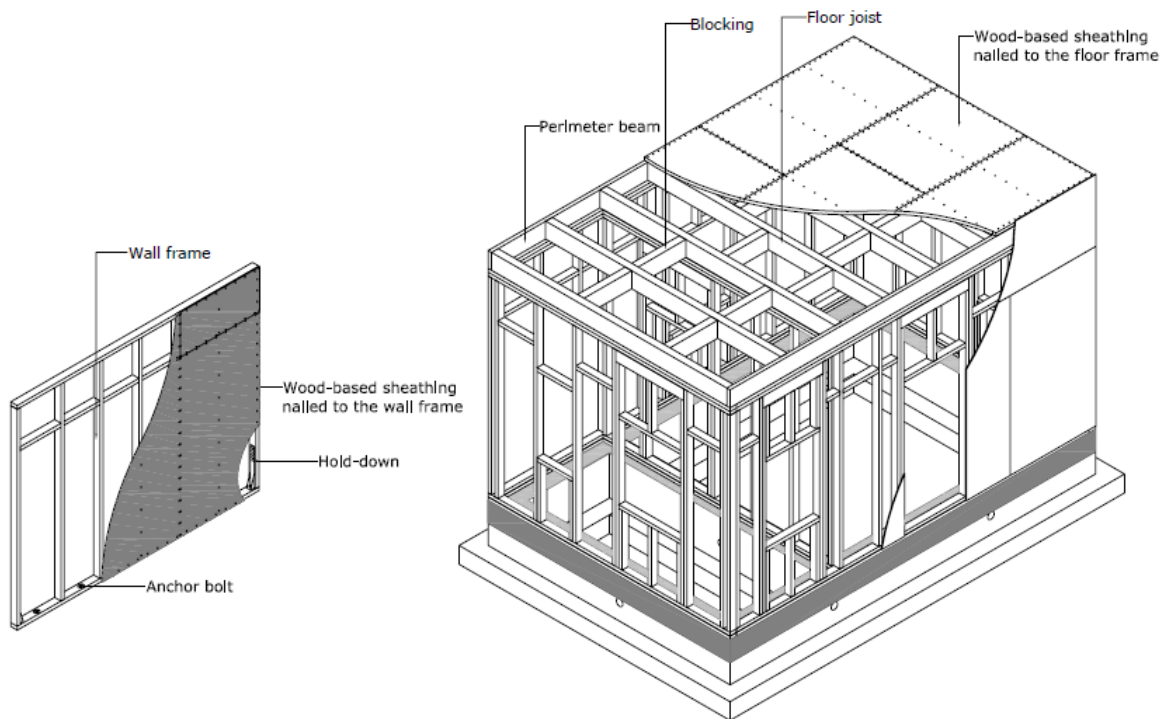


Fig. I.23 – Structural scheme of platform frame system [I.23]

Nowadays wood-framed buildings are by far the most prevalent type of timber construction used for homes and apartment buildings around the world. Moreover wood-framed construction is also used for retail, office, school and government occupancies.

In North America platform frame system was largely used to realize medium rise building (up to 4 storeys) since the 1920s. Since 1980 this constructive technique was used to realize the first samples of high rise building. The seismic performances of such high-rise structure were investigated by full scale shaking table test. The most relevant research project is the NEES Wood project [I.24] which verifies the earthquake-resistant adequateness of a six-storey Platform frame building.

In Europe the first samples of multi-storey building are represented by the 4- and 5- storey building realized in Växjö -Sweden in the early 1990s (see Fig. I.24)



Fig. I.24 – Medium rise Platform Frame building in Växjö - Sweden [I.25]

Once built the first multi-storey buildings in Sweden the use of the Platform Frame system has spread around the Europe for the construction of low and medium rise building. Despite the optimal earthquake-resistant characteristics, Platform Frame system has not spread in seismic areas of Europe. The main reasons that prevented its spread in such areas are structural lightness and low massiveness. Such characteristics represent a weak point in hot climates zones and in countries culturally linked to the heavy masonry structures such as Italy.

Furthermore Platform Frame system results not suitable to realize high-rise building (up to 10 storeys). For all these reasons, in recent years the use of the Platform Frame system is decreasing in favor of massive wall systems (i.e. CLT) or hybrid systems that combine wooden structures with earthquake-resistant concrete or steel elements.

I.1.3.3 Cross Laminated Timber construction

Cross Laminated Timber (CLT) is a relatively new building system in European and North American construction. CLT is an innovative wood product that was first developed in the early 1990s in Austria and Germany and ever since has been gaining popularity in residential and non-residential applications in European area where there are currently several CLT producers. It is a potentially cost competitive wood-based solution that complements the existing light and heavy frame options, and is a suitable candidate for some applications which currently use concrete, masonry and steel [I.20].

CLT panels consist of several layers of dimensional lumber boards stacked crosswise (typically at 90 degrees) and glued together on their wide faces and, sometimes, on the narrow faces as well. A cross-section of a CLT element has at least three glued layers of boards placed in orthogonally alternating orientation to the neighboring layers. CLT products are usually fabricated with three to seven layers and even more in some cases. Panel sizes vary by manufacturers; typical widths are 0.6 m, 1.2 m, and 3 m (could be up to 4–5 m in particular cases) while length can be up to 18 m and the thickness can be up to 400 mm. Similarly to glulam beam transportation regulations may impose limitations to CLT panel size. The CLT panel are connected together and to foundation in situ by means of mechanical connectors such as steel angular bracket and holdown, nails screws etc.. Fig. I.25 illustrates a CLT panel configuration and the typical connection elements.

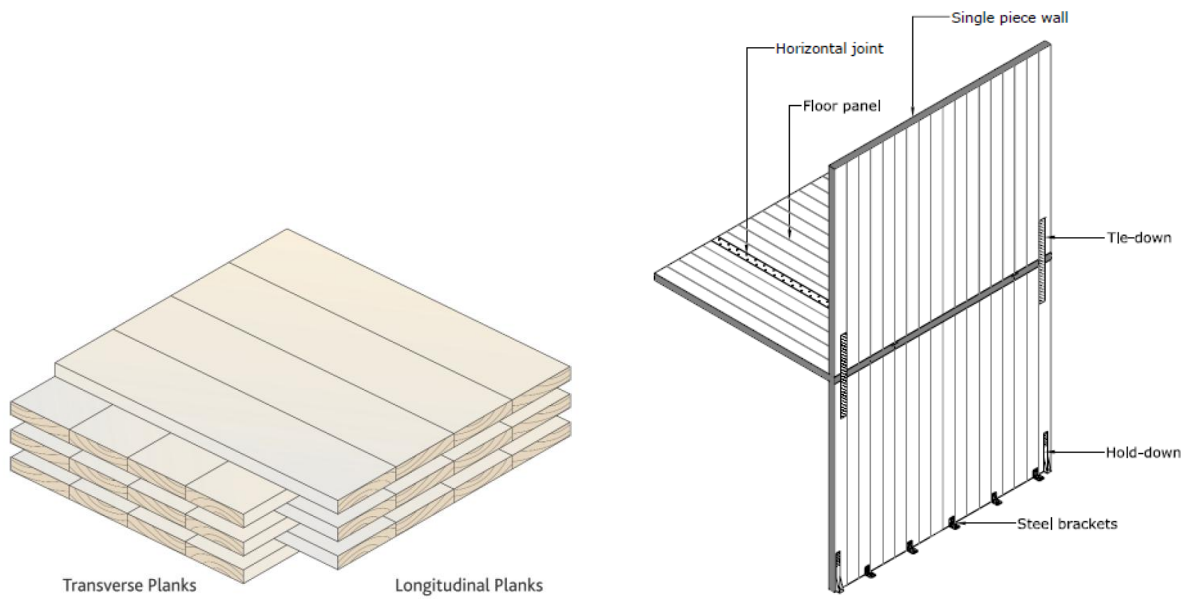


Fig. I.25 – CLT panel configuration [I.20] (left) and typical connection assemblies (right) [I.23]

CLT used for prefabricated wall and floor systems offer many advantages. The cross-laminating process provides improved dimensional stability to the product which allows for prefabrication of wide and long floor slabs and single storey long walls. Additionally, cross-laminating provides relatively high in-plane and out-of-plane strength and stiffness properties in both directions, giving it a two-way action capability similar to a reinforced concrete slab. The ‘reinforcement’ effect provided by the cross-lamination in CLT increases the splitting resistance of CLT for certain types of connection systems.

On the environmental side, CLT possesses a number of positive environmental characteristics common to almost all wood products.

The use of CLT panels in buildings has increased over the last few years in Europe. Numerous impressive buildings (e.g. up to 9 storeys) and other types of structures built around the world using CLT have become a good testimony of the many advantages that this product can offer to the construction sector (see Fig. I.26, Fig. I.27, Fig. I.28, and Fig. I.29.).



Fig. I.26 – Murray Grove 9-storey CLT Building, London [I.20]



Fig. I.27 – Multi-family buildings in Austria [I.20]



Fig. I.28 – 8-storey CLT buildings Melbourne – Australia [I.26]



Fig. I.29 – Social houses. 9-storey CLT buildings in Italy [I.27]

CLT structures behave well under seismic conditions as confirmed by the extensive research activities performed in Italy as part of the SOFIE project undertaken by the Trees and Timber Institute of the National Research Council of Italy (CNR-IVALSA) [1.28]. During such research project full scale shaking table tests were performed in order to characterized the seismic behaviour of multi-storey buildings. Despite the shaking table tests have clearly shown the excellent performance of this seismic construction system, there is a lack on the available seismic codes. No guidelines and design rules are still given for this building typology. An extensive treatment about the seismic behaviour of CLT building is reported in the chapters 5 and 6 of this dissertation.

1.1.3.4 Hybrid wood-concrete constructions

The previously defined constructive systems can be coupled with a other construction material such as steel or concrete. Generally reinforced concrete shearwalls and cores are used to resist the lateral loads and act as seismic force resisting systems while wooden structure bear the gravity loads. As an example the following Fig. 1.30 reports the scheme of a hybrid wood concrete post and beam building.



Fig. 1.30 – Structural concept of the 6-storey hybrid wood-concrete building [1.20]

The seismic force resisting systems are realized by means of concrete core and shearwalls positioned in such a way to maximizing resistance to torsion under lateral loads. The gravity loads are transferred to the foundation by means of glulam pillars. The floor and roof diaphragms are also made of glulam. The following Fig. 1.31 reports an example of a hybrid heavy frame structure with steel bracing.



Fig. I.31 – Heavy frame timber structure with steel bracing [I.29]

Such constructive technique that provides two different resistant systems for vertical and horizontal actions can be applied also to Platform Frame and CLT buildings. The following Fig. I.32 reports as an example a hybrid construction with CLT shearwalls and concrete core.



Fig. I.32 – Hybrid CLT-concrete system [I.20]

The main critical issue of this type of construction is represented by the connection between the wood structure and the earthquake-resistant elements made by concrete or steel. Such connections must be adequately design to transfer the seismic action form the floor to the bracing system.

1.2 Seismic regulations for wooden structures

The progress of technical regulations represents a measure of the importance of a certain material within the building market [1.6]. Studies concentrated on wooden buildings [1.30] highlight that there are no regulatory barriers to the use of wood or wood-based products in the construction of residential buildings. This is mainly due to the fact that governments, through their regulations, cannot be prejudiced towards any particular material.

Regulatory requirements are functional and not prescriptive in almost countries and any material can be employed as long as the functional requirements can be met. However, there are many limitations to the use of wood and wood-based products, which need to be addressed and ultimately eliminated. First of all there is a lack of codes and standards for many wood products. A typical example of such lack is represented by CLT. Another regulatory limitation to the enhanced use of wood-based products in residential construction relate to the fire performance and sound insulation specifications, especially when materials and building elements are used in multi-storey and/or multi-occupancy residential constructions.

Buildings designed by means of modern codes perform well for earthquakes as confirmed by the significant number of undamaged timber building after severe earthquakes. In seismic area use of wood and wood-based products is mainly limited by the height of the building and the distance between adjacent buildings. Furthermore the maximum number of storeys permitted varies between countries.

This section reports a literature overview about the current seismic codes available in several countries where the usage of wood as a building material is widespread. The positives and avant-gardes are presented and lacks and limitations are highlighted.

1.2.1 European seismic regulations

The harmonized European regulation for the design of structure in seismic regions refers to the Eurocode 8 [1.31]. According to [1.23] all the structures should be designed to withstand the foreseen earthquake for that area. More specifically, in accordance with the so-called “no-collapse requirement”, the structure must be designed for the reference seismic action associated with a typical probability of exceedance of 10% in 50 years, corresponding to a reference return period of 475 years, so as it does not lose its structural integrity and it maintains a residual load carrying capacity after the earthquake. At the same time, the structure should also fulfill the “damage limitation requirements”, according to which the structure should survive an earthquake having a larger probability of exceedance (typically of 10% in 10 years, corresponding to a return period of 95 years) without the occurrence of damage and the associated limitations of use, the costs of which would be disproportionately high in comparison with the costs of the structure itself.

According to [1.23] in order to satisfy the Ultimate Limit State, structural systems shall be designed with an appropriate mixture of resistance and energy dissipation, which can be ensured only if ductile behaviour is achieved, and Capacity Based Design philosophy [1.32] is followed. In the definition given by Eurocode 8 [1.31], “Capacity Based Design is the design method in which some elements of the structural system (i.e. mechanical joints for the case of timber structures) are chosen and suitably designed and detailed for energy dissipation under severe deformations while

all other structural elements are provided with sufficient strength (i.e. timber elements for the case of timber structures) so that the chosen means of energy dissipation can be maintained”.

As it is well explained in 2.2.2 2(P) of Eurocode 8 [I.31], “The resistance and energy dissipation capacity to be assigned to the structure are related to the extent to which its non-linear response is to be exploited. As reported in [I.23] in operational terms such balance between resistance and energy-dissipation capacity is characterized by the values of the behaviour factor q and the associated ductility classification, which are given in the relevant Parts of EN 1998”. The behaviour factor q is defined as the “factor used for design purposes to reduce the seismic actions in a linear static or modal analysis in order to account for the non-linear response of a structure, associated with the material, the structural system and the design procedures” [I.31].

I.2.1.1 Specific rules for timber structures

Section 8 is the part of the Eurocode 8 related to the specific rules for timber buildings, which are considered as additional to those given in Eurocode 5 [I.33]. The current version of Section 8 is divided into seven different parts, listed in the following:

General: contains general information about this part of Eurocode 8, the specific terms related to timber structures and the design concepts.

Materials and properties of dissipative zones: properties for materials and dissipative zones in seismic design are defined, particularly when using the concept of dissipative structural behaviour.

Ductility classes and behaviour factors: the structural types permitted in seismic areas are listed and the relevant ductility class and behaviour factors defined in Table 8.1. (see Fig. I.33).

Table 8.1: Design concept, structural types and upper limit values of the behaviour factors for the three ductility classes.

Design concept and ductility class	q	Examples of structures
Low capacity to dissipate energy - DCL	1.5	Cantilevers; Beams; Arches with two or three pinned joints; Trusses joined with connectors.
Medium capacity to dissipate energy - DCM	2.0	Glued wall panels with glued diaphragms, connected with nails and bolts; Trusses with doveled and bolted joints; Mixed structures consisting of timber framing (resisting the horizontal forces) and non-load bearing infill.
	2.5	Hyperstatic portal frames with doveled and bolted joints (see 8.1.3(3)P).
High capacity to dissipate energy - DCH	3.0	Nailed wall panels with glued diaphragms, connected with nails and bolts; Trusses with nailed joints.
	4.0	Hyperstatic portal frames with doveled and bolted joints (see 8.1.3(3)P).
	5.0	Nailed wall panels with nailed diaphragms, connected with nails and bolts.

Fig. I.33 – Table 8.1 of Eurocode 8 [I.31]

Structural analysis: in this section general information regarding the slip of joints, the Young modulus to be used in the analyses and the detailing rules in order to consider horizontal diaphragms as rigid are given.

Detailing rules: detailing rules for connections and horizontal diaphragms are given. Provisions for both carpentry and mechanical joints are also provided. However for horizontal diaphragms only light-frame floors are considered.

Safety verifications: provisions for the k_{mod} and γ_M values to be used in the safety verifications are given for structures designed in accordance respectively with the concept of low dissipative and dissipative structural behaviour. In addition provisions are also given for the structural elements to which overstrength requirement applies in order to ensure the development of cyclic yielding in the dissipative zones, even though no value of the overstrength factor is given. Also detailing rules for carpentry joints to avoid brittle failure are given.

Control of design and construction: This section gives provisions on how the structural elements should be clearly detailed and identified in the design drawings and how they should be checked during the construction process.

1.2.1.2 Comments and notes

Eurocode 8 [I.31] is an advanced seismic code but the timber section presents some incongruities and lacks mainly due to the recent development of new building systems and wood-based products.

According to [I.23] the first critical issue concerns with the definition and identification of the different structural systems for timber buildings. However, particularly for widely used structural systems such as Cross Laminated Timber and log house systems, it is hard to find the proper description in Table 8.1 of Eurocode 8 (Fig. I.33) [I.31]. This aspect is not irrelevant if we consider the importance of a correct choice of the ductility class and the correspondent behaviour factor q according to the Capacity Based Design.

As reported in [I.23] analyzing the structural types listed in Table 8.1 of Eurocode 8 (Fig. I.33) [I.31] it can be noticed that some of them are structural components of buildings, such as large span glulam roofs or timber buildings roofs (e.g. trusses with nailed, doweled or bolted joints); some others refer to structural systems used for old buildings (e.g. mixed structures consisting of timber framing and nonload bearing infill) but no longer used for new buildings; and only few of them clearly refer to residential buildings, which are the nowadays most commonly used type of construction.

Another critical aspect is the ductility provisions given for the dissipative zones which are based on simplified rules on the diameter of dowel type fasteners and on the thickness of connected members. According to [I.23] such rules on the characteristic of joints should be superseded by requiring a failure mode characterized by the formation of one or two plastic hinges in the mechanical fastener, which can be easily checked using the Johanssen equations prescribed by the Eurocode 5 Part 1-1 [I.33].

Furthermore some values of the behaviour factor q reported in Table 8.1 of Eurocode 8 [I.31] result unrepresentative of the reliable ductility and dissipative capacity of various building systems. As an example the q -factor equal to 2 imposed for the CLT structure seems to be excessively precautionary. The recent research activities performed in order to identify the seismic behaviour of the CLT structures suggest a q -value up to 3 (see [I.34] and [I.35]). Otherwise for Timber Frame structure is proposed a q -factor equal to 5. Such value is adequate for the traditional light timber

frame structure but results excessive for the new developed heavy frame shearwall systems which exhibit low dissipative capacity.

Moreover no design rules are given for tall buildings. For these specific building typologies it would be desirable the development of a correlation between the q-factor value and the building features such as slenderness, storeys number, design criteria and type and arrangement of connectors. Finally, for each structural system, it should be clearly stated the capacity design criteria and the specific design rules, as well as the overstrength factors.

Some proposals for revision of the current timber part of Eurocode 8 [I.31] are summarized in [I.23] and developed in this thesis work.

1.2.2 Extra - European seismic regulations

The main Extra-European regulations on timber structure are reported in this section. Concept and application limits are briefly described and discussed. The reference countries were chosen based on the widespread of wooden buildings.

1.2.2.1 Canadian regulations

Canada is the country where the wooden constructions are most common. Consequently Canadian regulations are the most comprehensive and detailed in the world for both static and seismic conditions. The most common constructive system used in Canada for residential building is the Platform Frame. Such typical building can be designed according to two different procedures in relation to the dimension, storeys number and building importance. The design can be performed respecting simply design rules when:

- the storeys number is lower than three;
- the maximum in plant area is lower than 600mq;
- the structure is realized by repeated use of modular structural elements;
- the service load is lower than 2.4 kN/mq;
- the usage of the building is limited to residential, directional or industrial.

Buildings that respect the previously defined characteristics can be built up only respecting the constructive rules provided by the chapter 9 of the National Building Code of Canada (NBCC) [I.5] without any structural design. Such rules are based both on engineering design and constructive practice. The adequateness of such system is confirmed by the optimal behaviour of buildings realized respecting such constructive rules, under severe earthquakes. Buildings that not respect previously defined limitations must be specifically design both for static and seismic actions according to the part 4 of the NBCC [I.5].

It should be noticed that the Canadian standards are advanced in design of traditional Platform Frame and Heavy Frame house and medium-rise buildings but no provisions are given for massive CLT system. Such lack was filled by enacting guidelines that summarize the results of the latest research on CLT system under static and seismic actions [I.36].

I.2.2.2 U.S. regulations

In the United States wooden structures are largely spread both for residential houses and medium-rise buildings. The US regulation is strictly similar to the Canadian one. For small timber houses no specific design are necessary while important and multi-storey building must be design according to the International Building Code (IBC) [I.37]. In detail the seismic design of timber structure is reported in the chapter 16 of the IBC[I.37].

In the U.S. the more common and widespread constructive technique is based on the Platform Frame system. Current codes regulate only this building typologies and no information are given about the more recent constructive technique based on the usage of massive wooden panel such as CLT.

I.2.2.3 Japanese regulations

The current Japanese seismic code is the Building Standard Low [I.38] firstly published in 1998. Such codes imposed a design method based on two different steps. The 1st one consists in a preliminary design of the wooden structure against to the seismic action while the 2nd one provides an accurate definition of the strength and the ductility of the entire building according to the modern Limit States Methods. Similarly to the American codes for in plant and in height regular timber house a simplified design is required. Nowadays no specific standards for CLT system are available.

I.2.2.4 Chinese regulations

China is one of the most important potential markets for wood structures. Despite the modern timber constructions are not very common in China, recently it has been developed specific regulations for wooden structures. Such regulations provide specific rules for multi-storey building (GB50005:2003 “Code for Design of Timber structures” [I.39]) based on the Canadian ones. Furthermore the Chinese seismic codes (GB50001:2001 “Code for Seismic Design of Buildings” [I.40]) was upgraded introducing a specific section for the seismic design of wood frame multi storey building. Similarly to the other countries no specific rules are provided for CLT buildings yet.

I.3 Objectives and Scope

The present thesis work aims to pave the development of realistic and reliable procedure for the definition of the seismic behaviour, ductility and dissipative capacity of modern timber structures. This is achieved by bringing together current know-how in the areas of structural wood engineering, numerical modelling and seismic design. Once reviewed the state of art some innovations and scientific findings are carried out referring to the following specific objectives:

1. Development of an hysteretic model suitable to reproduce the specific behaviour of typical wooden connections and reproducible using standard nonlinear element of commercial Finite Element codes so as to be adopted by engineers and designers to perform nonlinear static and dynamic analyses on timber buildings.
2. Development of an expeditious procedure for a direct estimation of the behaviour q-factor of any timber system using as input parameter the load-slip curve obtained from experimental quasi static tests.
3. Characterization of the seismic behaviour of Cross Laminated Timber buildings and definition of the reliable effects of some specific building features such as slenderness, storey numbers, mechanical connection density and arrangement, design criteria etc.. on the q-factor value.
4. Development of an analytical formulation suitable to define the most reliable q-factor value of a CLT buildings starting from the geometrical characteristics of the structure, the typology and arrangement of mechanical connectors and the design criteria.
5. Development and seismic characterization of a new high ductility building system obtained coupling a standard platform-frame shear walls with an external concrete shelter.

The achievement of these objectives provides relevant scientific results about the wooden seismic engineering giving new techniques for the study of the seismic behaviour of timber buildings.

However the main scope of this thesis work is to carry out findings and innovations suitable for updating the current seism code especially with regards to those building typologies which are currently not include in any calculation standard but that at the meantime are largely spreading in the construction practice. Although the present work is limited to specific topic of the modern wood engineering it provides a methodological approach suitable for the scientific research about the seismic behaviour of modern timber structures. This is in itself one of the main scopes of this dissertation.

I.4 Dissertation overview

A preliminary overview on the basic terms and concepts used in structural modeling and nonlinear analysis of timber structures are provided in the Chapter 1 of this dissertation. The specific behaviour of wood joint under cyclic actions and therefore under earthquakes is described with regard to the pinching effect and strength and stiffness degrading. A literature review on the main

numerical models proposed to reproduce the hysteretic load-slip curve of single fasteners, joints and whole wooden elements is presented and discussed.

Chapter 2 reports a proposal for a new wood joint numerical model implementable into standard commercial Finite Element code. The reliability of such new developed model to reproduce the fasteners hysteresis behaviour is presented and critically discussed in comparison with experimental results.

Chapter 3 of this thesis work is based on the evidence that the growing spread of the use of timber structures has led to the development of numerous innovative construction systems but at the same time remains a lack of norms in seismic field, in particular about the ductility or reduction factor to be used for the design of different timber system. In this Chapter 3 the definition given for the q-factor in the scientific literature and its relevance in the design of seismic resistant structures is analyzed. Furthermore the traditional methods for estimating the q-factor are investigated and their main advantages and limitations are critically discussed.

Chapter 4 extensively describes the proposal of a expeditious procedure for the direct estimation of the behaviour q-factor of any timber system using as input parameter the load-slip curve obtained from experimental quasi static tests. The theoretical aspects of this new analytical-experimental procedure are reported with regard to its main advantages and limitations. The validation of this new developed procedure is also reported and an extensively utilization of the proposed procedure to a number of different wooden building system is presented. Furthermore some considerations about the criteria adopted for the definition of the yielding limit are given and the most suitable procedure for the bi-linearization of the load-slip curve is assessed.

Chapter 5 investigate the seismic behaviour of the Cross Laminated Timber structures and the influence of some significant building characteristics, such as building methodology, storeys number, slenderness, design criteria etc., on the q-factor value. Such influence is studied referring to a numbers of building configuration by means of nonlinear analyses carried out using specific hysteretic spring lap-mass model.

Based on the preliminary studies carried out in the Chapter 5, a proposal for an analytical formulation suitable to calculate the q-factor of CrossLam building is developed in Chapter 6. Such procedure requires as input parameters the building geometrical characteristics, the typology and arrangement of mechanical connectors and the design criteria. The validation and the applicability limits of the proposed formulation are presented and critically discussed.

The Chapter 7 of this dissertation investigates from the structural point of view the innovative idea of using an external concrete shelter to improve the performance of standard platform-frame shear walls to realize a high ductility building system. The outcomes from the experimental tests performed in order to define the structural response of this shearwalls are reported. The influence of such concrete skin on the seismic response of the shearwall is also evaluated by means of numerical analysis and the assured ductility factor “q” is estimated.

Structural details, constructive concepts, analytical calculation of the lateral stiffness and load bearing capacity of this newly developed high ductility building system are summarized in Appendix A.

References - Introduction

- [I.1] *Touliatos P.G. Seismic disaster prevention in the history of structures in Greece". Proceeding of Timber building system – COST E5 Workshop on Seismic behaviour of Timber Structures. September 28- 29 2000 Venice Italy.*
- [I.2] *Cóias V., Silva E. Using advanced composites to retrofit Lisbon's old seismic resistant timber framed buildings," in C.Bertolini Cestari, J.Amorim Faria, A.Soiikkeli, editors, European Timber Buildings as an Expression of Technological and Technical Cultures, Elsevier, p109-124.*
- [I.3] *Aytun, A. "Earthen buildings in seismic areas of Turkey," Proceedings of the International Workshop on Earthen Buildings, Vol. 2, Albuquerque, NM, 1976:352.1.*
- [I.4] *Karacabeyli, E. Performance of North American platform frame wood construction in earthquakes. COST E5 Workshop on Seismic behaviour of Timber Structures. September 28- 29 2000 Venice Italy.*
- [I.5] *NBCC. 2005. National Building Code of Canada. Institute for Research in Construction, National Research Council of Canada, Ottawa, Ontario.*
- [I.6] *Ceccotti A., Follesa M., Lauriola M.P. 2007. "Le strutture di legno in zona sismica 2^a edizione" ISBN: 9788879922418*
- [I.7] *Kuklik P., Hansen A.S. Handbook 1 - Timber Structures. Educational Materials for Designing and Testing of Timber Structures, Leonardo da Vinci Pilot Project. 2008*
- [I.8] *Sakamoto I., Fujita K. Structural analyses on traditional timber buildings in Japan. Proceeding of Conservation of the ancient timber load bearing structures meeting, Florence March 2000.*
- [I.9] *Ceccotti A., Follesa M. Seismic behavior of multi-storey XLam buildings. Proc. International Workshop on "Earthquake Engineering on Timber Structures" Coimbra, Portugal, 2006.*
- [I.10] *Toratti T. Seismic Design of Timber Structures. Technical Research Centre of Finland, 2001*
- [I.11] <http://www.strongtie.com>
- [I.12] *Maison B., Bonowitz D., Kornfield I., and McCormick d. Adjacency Issues in Soft-Story Wood-Frame Buildings. report to Structural Engineers Association of Northern California. April 2011*
- [I.13] *Fujita K., Hanazato T., Sakamoto I. Earthquake response monitoring and seismic performance of five-storied timber pagoda. 13th World Conference on Earthquake Engineering Vancouver, B.C., Canada August 1-6, 2004 Paper No. 54*
- [I.14] *Akan A. Some Observation on the seismic behaviour of traditional timber structures in Turkey. Ph.d. thesis, June 2004*
- [I.15] <http://www.frenchimmersion.wordpress.com/2012/10/15/house/colombage-house/>
- [I.16] <http://www.old-fachwerk-house-in-wolfenbuttel--niedersachsen-germany>
- [I.17] http://www.academia.edu/703037/la_casa_antisismica_casa_baraccata_ad_intelaiatura_di_legno
- [I.18] *Langenbach, R. Survivors amongst the rubble: traditional timber-laced masonry buildings that survived the great 1999 earthquakes in Turkey and the 2001 earthquake in India, while modern buildings fell," Proceedings of the First International Congress on Construction History, Instituto Juan de Herra, Escuela Técnica Superior de Arquitectura, Madrid, Vol. 2, 2003: 1257-1268.*
- [I.19] <http://horneinsweden.blogspot.it/2007/02/kiruna.html>

- [I.20] Mohammad M., Gagnon S., Karacabeyli E., Popovski M. *Innovative Mid-rise Timber Structures Offer New Opportunities for Designers*. SEAOC convention proceedings. 2011
- [I.21] <http://www.holzbau.rubner.com/it/strutture-in-legno/1-0.html>
- [I.22] Palermo A., Pampanin S., Calvi G. M. (2005). "Concept and Development of Hybrid Solutions for Seismic Resistant Bridge Systems." *Journal of Earthquake Engineering*, 9(5): 1-23.
- [I.23] Follesa M., Fragiacomio M., Lauriola M. P. a proposal for revision of the current timber part(section 8) of eurocode 8 part 1. Meeting 44 of the Working Commission W18-Timber Structures, CIB. Alghero, Italy, 2011 paper CIB-W18/44-15-1.
- [I.24] Pei, S., van de Lindt, J.W., Pryor, S.E., Shimizu, H., and Isoda, H. 2010. *Seismic testing of a full-scale sixstorey light-frame wood building: NEESWood Capstone test*. NEESWood Report NW-04
- [I.25] Vessby J. *Shear walls for multi-storey timber buildings*. PhD thesis Växjö university, 2008
- [I.26] <http://designbuildsource.com.au/plans-for-worlds-tallest-timber-skyscraper-revealed-in-melbourne>
- [I.27] <http://www.servicelegno.it/>
- [I.28] http://www.progettosofie.it/index_eng.html
- [I.29] *Heavy Timber Construction*. Wood construction data. American Forest & Paper Association. 2004
- [I.30] Birgit Östman B., Källsner B. *National building regulations in relation to multi-storey wooden buildings in Europe*. Reports, No. 60 School of Technology and Design Växjö University. Växjö, Sweden 2011
- [I.31] European Committee for Standardization (CEN). *Eurocode 8 - design of structures for earthquake resistance, part 1: General rules, seismic actions and rules for buildings*. 2004.
- [I.32] Pauley T., Priestley M.J.N. *Seismic design of reinforced concrete and masonry buildings*. Wiley Ed., 1992.
- [I.33] European committee for standardization (CEN). *Eurocode 5 – design of timber structures – part 1-1: general rules and rules for buildings*. 2004.
- [I.34] Ceccotti A. *New technologies for construction of medium-rise buildings in seismic regions: the XLAM case*. IABSE Struct Eng Internat 2008;18:156–65. *Tall Timber Buildings (special ed.)*.
- [I.35] Pozza L., Scotta R., Vitaliani R. *A non linear numerical model for the assessment of the seismic behaviour and ductility factor of X-Lam timber structures*. Proceeding of international Symposium on Timber Structures, Istanbul, Turkey, 25-27 June 2009, 151-162.
- [I.36] *CLT Handbook: Cross-Laminated Timber* Sylvain Gagnon and Ciprian Pirvu. FPInnovation 2011
- [I.37] *International Building Code 2009*. International Code Council
- [I.38] *Building Standard Law of Japan - 2009*
- [I.39] GB 50005:2003 (2005 Version) "Code for Design of Timber Structures"
- [I.40] GB50001:2001 (2007 Version) "Code for Seismic Design of Buildings"

Chapter 1 - Hysteresis models for wood joints

Abstract

This section provides the necessary background on the seismic behaviour of timber buildings. Basic terms and concepts used in structural modeling and nonlinear analysis are presented.

The specific behaviour of wood joint under cyclic actions and therefore under earthquakes is described with regard to the pinching like response and strength and stiffness degrading due to the physical phenomena of wood bearing and steel plasticization.

A literature review on the main numerical models proposed to reproduce the hysteretic load-slip curve of single fasteners, joints and whole wooden elements is presented and discussed. The specific applications of these numerical models are reported especially with regard their usage in CLT or shearwall system modeling.

1.1 Wood fasteners hysteretic characteristic

Timber building is made by assembling wooden elements by means of metal connectors. The knowledge of the specific behaviour of the fasteners under cyclic actions is a fundamental requisite to understand the response of an entire building under earthquake. According to EN 1998-Eurocode 8 part 1-1 [1.1] in timber building the dissipative capacity is exclusively due to the fasteners because the wooden elements remain in elastic field during a seismic event. The connection elements show good ductility and dissipation capacity thank to the simultaneous phenomenon of steel plasticization in the metal connectors (nails or screws) and the localized wood bearing failure due to the concentrated action of the connectors. According to Fragiaco et al.[1.2] a connection is regarded as ductile when at least one plastic hinge is formed in the fasteners or in the screws (see Fig. 1.1). Using the notation proposed by EN 1995-Eurocode 5 Part 1-1 [1.3] and reported in Fig. 1.1 failure modes “b”, “d” and “e” are ductile for steel-timber connections (e.g. angle bracket and hold-down) while failure modes “d”, “e” and “f” are ductile for timber-timber connections (e.g. in plane panel to panel joint). Failure modes that don't present plastic hinge formation are regarded as brittle and must be avoided.

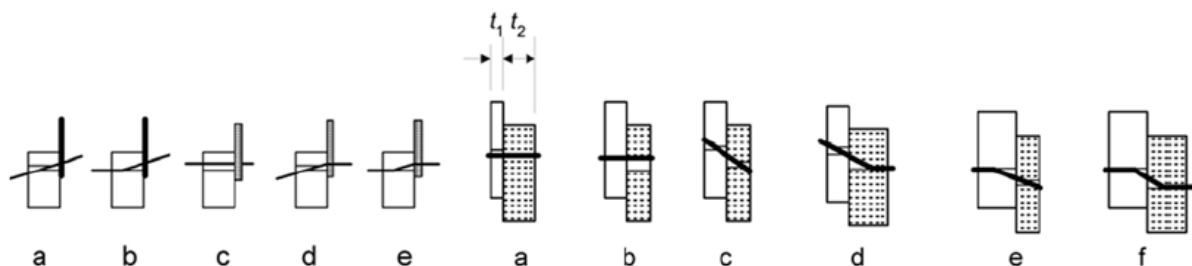


Fig. 1.1 - Failure modes for steel-timber (left) and timber-timber (right) connections according to EC5 [1.3].

According to Judd et al.[1.4] the overall behavior of a wood joint is dominated by the individual features of wood elements and of metal connector as depicted in the following Fig. 1.2.

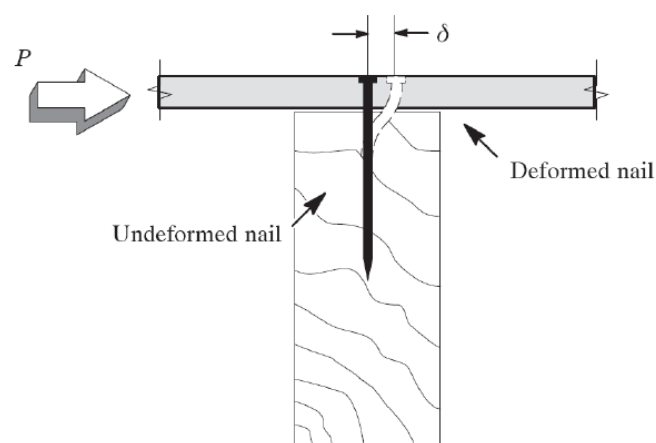


Fig. 1.2 - Example of nailed wood-panel connection [1.4]

A critical aspect in the structural analysis is the model used to describe and idealize the behavior of the connections. The process for idealizing connections is two-tiered: first, idealize the monotonic

response (envelope curve) and second, idealize the cyclic response (hysteresis) during reversed loading.

As depicted in Fig. 1.3 the typical monotonic response of a mechanical connection to a lateral load is initially linear, where an incremental load increase is proportional to the corresponding incremental increase in displacement (initial stiffness). Here wood fibers and fasteners are essentially elastic. Nonlinearity arises as wood fibers crush and/or fasteners begin to yield (deform). Depending on the connection materials and configuration, a nearly plastic plateau may be reached (secondary stiffness). Just prior to failure, the load capacity of the specimen decreases with increasing displacement (a negative tertiary stiffness).

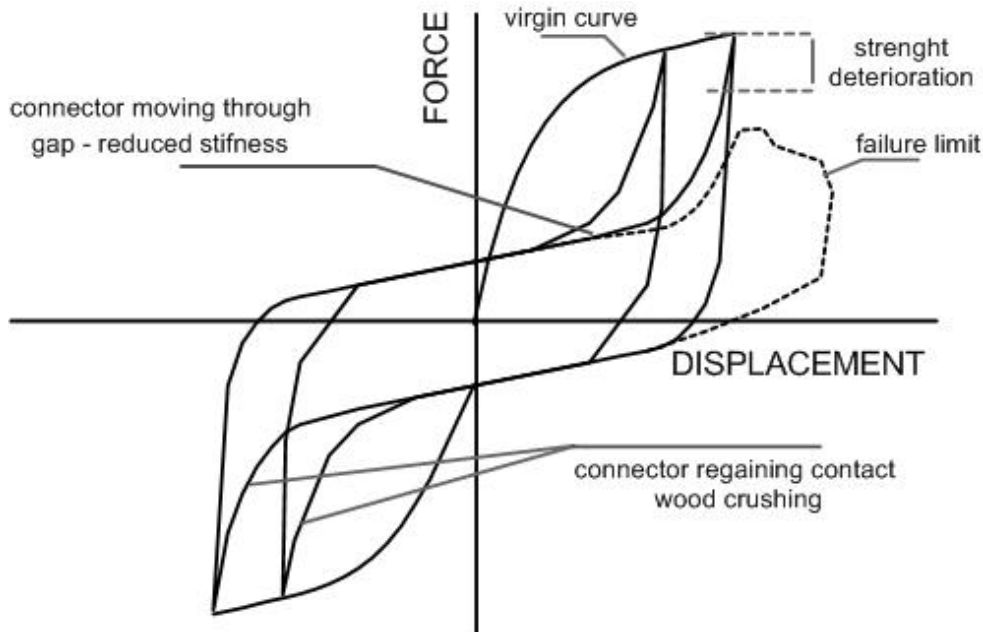


Fig. 1.3 -Typical hysteretic behaviour of a ductile timber connection, suitable for energetic dissipation [1.4].

As described in [1.4] the cyclic response of mechanical connections (see Fig. 1.3) is complex and exhibits pronounced hysteresis loops, indicative of the nonlinear, nonconservative, and time-dependent nature of the connections. Initially, as the connectors displace the force-displacement relationship is linear. The wood fibers, and connector all remain elastic. As loading progresses, the displacement of the connection increases, the wood fibers crush, and the nail may yield. If the loading is reversed, the connectors move through the gap formed by the crushed wood fibers and the connection exhibits low stiffness and strength until the connector again comes into contact with the wood. A further description of the behaviour of a timber joint under cyclic load is proposed by Dujic et al.[1.5] where the main characteristic features of connection cyclic response are summarized as follows:

1. *Nonlinear inelastic* load-displacement relationship without a distinct yield point
2. Progressive loss of stiffness in each loading cycle (will be referred to as *stiffness degradation*)
3. Degradation of strength when cyclically loaded to the same displacement level (will be referred to as *strength degradation*)
4. *Pinched* hysteresis loop
5. *Presence of a failure condition*

As reported in [1.4] stiffness degradation and hysteresis pinching are attributed to slackness caused by initial or previous cyclic loadings. The pinching effect is primarily due to slipping during force reversal. Strength degrading is mainly due to the wood crushing. Furthermore a very important feature, not observed in the previous Fig. 1.3, is that the response of a steel-wood joint at a given time depends not only on instantaneous displacement but also on its past history [1.4]. This is known as memory. Any hysteresis or constitutive model for timber fasteners should incorporate the majority of these experimentally observed characteristics as shown by models reported below.

1.2 Hysteresis models

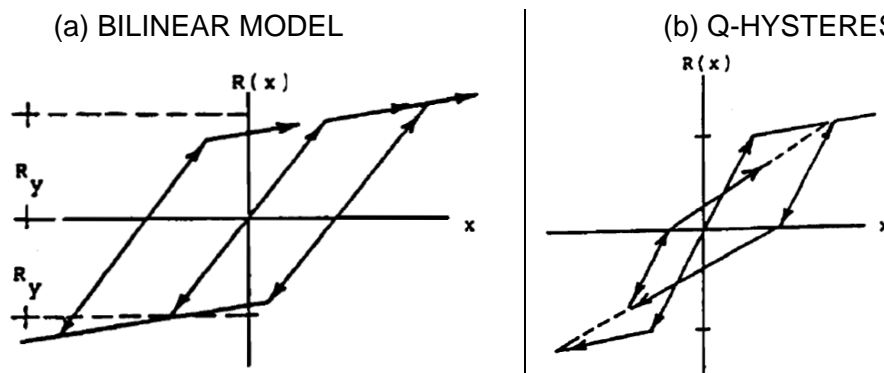
Hysteresis models have been developed for a variety of wood structural systems, including for bolted connections [1.6], moment resisting connections [1.7], as well as for wood shear walls and diaphragms [1.8]. A comprehensive discussion of hysteresis models for sheathing-to-framing connections and other connections in wood-frame structures is discussed by Foliente [1.9] and more recently by van de Lindt [1.10].

In this section the main hysteresis models used to reproduce the specific behaviour of timber structure are presented. A preliminary overview on the general models used for the more common R.C. or steel structure modeling is reported and the applicability of these models to wooden building is discussed. Finally an extensive investigation on the available models capable to reproduce the wood structures pinching like behaviour and the strength and stiffness degradation phenomenon is reported.

1.2.1 General hysteresis models

Analytical modeling of a wooden structure under seismic actions requires a force-displacement relation that can reproduce the true behaviour of the structure at all displacement levels and strain rates. As reported in [1.9] to obtain a simplified modeling of timber structures linear hysteresis models that were originally developed for reinforced concrete and steel structures have also been used in seismic analyses. Some of these models incorporate stiffness degradation and pinching in an attempt to more accurately represent actual system behaviour.

A summary of some general models that can be used for an approximate reproduction of the hysteretic behaviour of wood structures is reported in [1.4] and showed in the following Fig. 1.4.



[1.16] can be used to model an entire connection elements regarding to the specific features of wood or fasteners. Finally models developed by Dolan [1.17], Folz [1.18] and Stewart [1.19] are based on an entire structural element such as wood shearwall or diaphragm. The 2nd way that can be used to classify the hysteresis model is based on the specific usage of the model: as an example the Dolan [1.17] and Folz [1.18] models are suitable only for modeling sheeted wood frame structure, the Ceccotti and Vignoli model can be used for modeling semi-rigid moment resist joint but also the connections usually adopted in CLT structure. Finally the Rinaldin [1.16] model is specific for CLT structure.

This section reports some of the main hysteresis models specifically developed for a suitable reproduction of the wooden structure features. The basic hypothesis and equations that define the hysteresis model are reported and the consequent limitations are discussed. The main applications to specific building structure are also reported.

1.2.2.1 Foschi hysteresis model

The majority of models used to reproduce the behaviour of timber joints are obtained by interpolation of experimental data. Foschi in 1977 [1.20] proposed an analytical formulation to define the hysteresis response of nailed joints typically used in shearwall and horizontal diaphragm. According to [1.4] this model is obtained using basic material properties of the connector and the embedment characteristics of the surrounding wood medium. The approach considers the connector as an elasto-plastic beam in a nonlinear medium which only acts in compression, permitting the formation of gaps between the beam and the medium. The model automatically adapts to any input history, either for force or displacement, and develops pinching as gaps are formed. In 1999 the originally developed model was updated and implemented into a specific dowel connector program called FRAME [1.21] suitable for simulate the dynamic response of ductile timber connections using only material properties as input. As reported in [1.22] the model is characterized by six independent parameters (K , Q_0 , Q_1 , Q_2 , Q_3 , D_{max}) and reproduces the strength and stiffness degradation once the maximum displacement D_{max} is exceeded according the following equations.

$$p(w) = (Q_0 + Q_1 w) \left[1 - \exp\left(\frac{-Kw}{Q_0}\right) \right] \quad w \leq D_{max} \quad \text{Eq. 1.1}$$

$$p(w) = p_{max} \exp[Q_4 (w - D_{max})^2] \quad w > D_{max} \quad \text{Eq. 1.2}$$

Where:

K = initial stiffness

Q_0 = residual force of the asymptote AB (see Fig. 1.5 left)

Q_1 = gradient of the asymptote AB (see Fig. 1.5 left)

Q_2, Q_3 = coefficient that define the degradation phenomena

$$Q_4 = \log(Q_2) / [D_{max}(Q_3 - 1)]^2 \quad \text{Eq. 1.3}$$

$$p_{max} = (Q_0 + Q_1 D_{max}) \left[1 - \exp\left(\frac{-K D_{max}}{Q_0}\right) \right] \quad \text{Eq. 1.4}$$

In the following Fig. 1.5 the pushover curve (left) and the typical hysteresis loop given by the Foschi model (right) [1.23] are depicted.

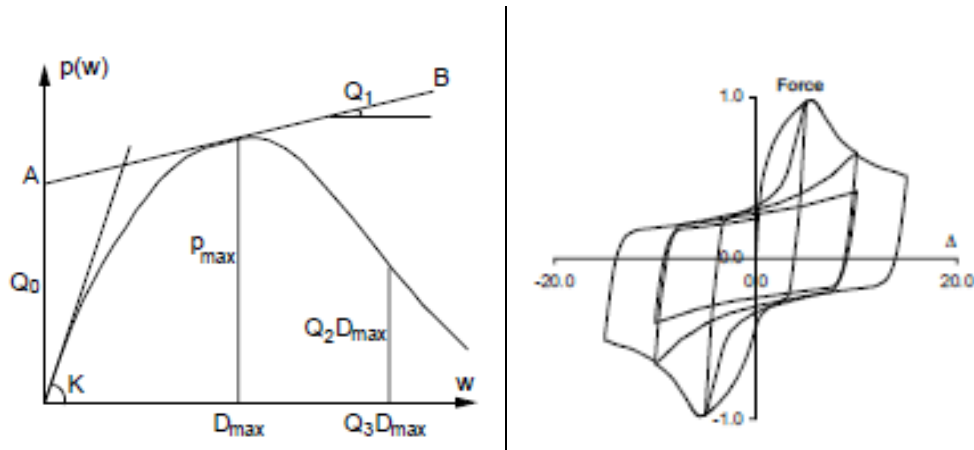


Fig. 1.5– Typical pushover (left) and hysteresis (right) curve defined by Foschi model [1.23]

As reported in Fig. 1.5 (right) the hysteresis response defined using the Foschi model faithfully reproduce the pinching and the strength and stiffness degradation phenomena. The main usage of this model involves the modeling of single connection elements, timber joints as reported in [1.9] but there are no significant examples of usage of the Foschi model to reproduce the cyclic behaviour of entire structures. However the formulation proposed by Foschi for the initial monotonic branch of the joint load slip curve (still to the maximum strength) was largely used to define further numerical model of timber joints as reported in the following paragraphs.

1.2.2.2 Dolan hysteresis model

The hysteresis model proposed by Dolan [1.24] is based on the formulation defined by Foschi [1.22] for the monotonic curve still to the maximum strength before the failure of the connection (see Eq. 1.5). The formulation of the softening branch is specifically defined by Dolan [1.24] as stated in the following Eq. 1.6.

$$|F_u| = (P_0 + K_2|\Delta|) \left[1 - \exp\left(\frac{-K_0|\Delta|}{P_0}\right) \right] \quad |\Delta| < |\Delta_{max}| \quad \text{Eq. 1.5}$$

$$|F_u| = (P_0 + K_2|\Delta_{max}|) \left[1 - \exp\left(\frac{-K_0|\Delta_{max}|}{P_0}\right) \right] - K_3(|\Delta| - |\Delta_{max}|) \quad |\Delta| > |\Delta_{max}| \quad \text{Eq. 1.6}$$

Where:

- Δ is the connection displacement;
- P₀ is the intersection between the hardening branch and the y axis;
- K₀ is the initial stiffness;
- K₂ is the hardening stiffness;
- Δ_{max} is the maximum displacement before the softening branch;
- K₃ is the stiffness of the softening branch.

The following Fig. 1.6 reports the pushover curve defined by the Dolan formulation.

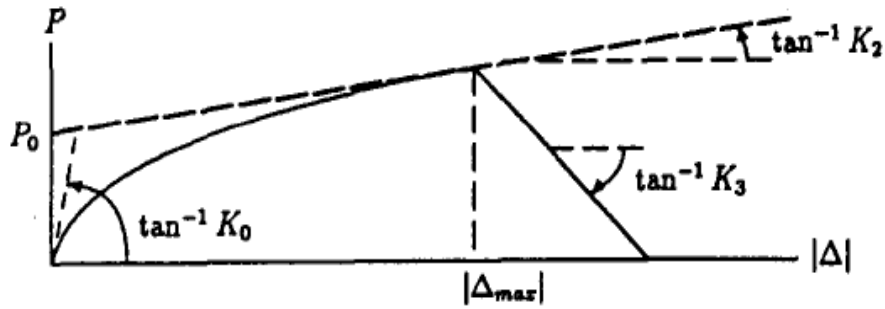


Fig. 1.6 – Pushover curve defined by Dolan model [1.24]

The curve developed by Dolan [1.17] is broken into four different sections as depicted in Fig. 1.7. The sections are governed by the following relations (the subscripts indicate the section number):

$$F_{1u} = -P_1 + K_4\Delta + [\exp(a_1\Delta) - 1] \quad \text{with} \quad a_1 = \frac{\ln(F_1 + P_1 - K_4u_1 + 1)}{u_1} \quad \text{Eq. 1.7}$$

$$F_{2u} = -P_1 + K_4\Delta + [\exp(a_2\Delta) - 1] \quad \text{with} \quad a_2 = \frac{\ln(-P_1 - F_2 + K_4u_2 + 1)}{|u_2|} \quad \text{Eq. 1.8}$$

$$F_{3u} = P_1 + K_4\Delta - [\exp(a_3\Delta) - 1] \quad \text{with} \quad a_3 = \frac{\ln(P_1 - F_2 + K_4u_2 + 1)}{|u_2|} \quad \text{Eq. 1.9}$$

$$F_{4u} = P_1 + K_4\Delta + [\exp(a_4\Delta) - 1] \quad \text{with} \quad a_4 = \frac{\ln(F_1 - P_1 - K_4u_1 + 1)}{u_1} \quad \text{Eq. 1.10}$$

Where:

- Δ is the connection displacement;
- P₁ is the residual force;
- K₄ is the reloading stiffness;
- u₁₋₂ is the maximum displacement achieved during the load history;
- F₁₋₂ is the maximum force achieved during the load history;.

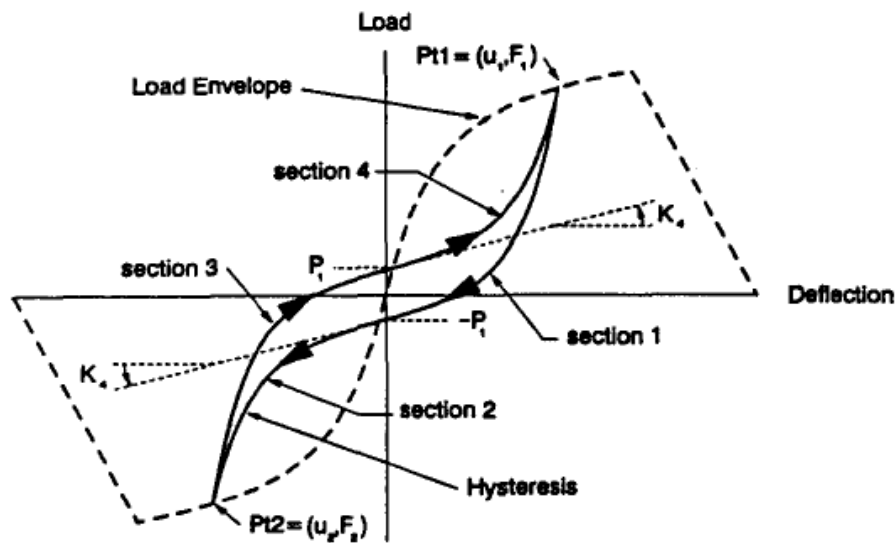


Fig. 1.7 – Hysteresis loop defined by the Dolan model [1.24]

As reported in [1.17] the model is calibrated on the basis of experimental tests which define the global response of the shearwalls. The Dolan model faithfully reproduces the pinching behaviour of the connection but strength degradation phenomena are not reproduced. The validation of the model is given by White [1.25]. The main usages of this model concern the study of the nonlinear response of single shearwall or entire timber frame buildings as summarized in [1.17] and [1.24].

1.2.2.3 Richard & Yasumura hysteresis model

Richard and Yasumura [1.15] proposed a hysteresis model governed by Foschi formulation for the monotonic load still to the maximum force achieved during the load history. The softening and the reloading phases were specifically developed so as to reproduce the strength and the stiffness degradation phenomena. According to the skeleton reported in Fig. 1.8 the pushover curve is defined by the following equations:

$$F(\Delta) = (P_0 + K_1\Delta) \left[1 - \exp\left(\frac{-K_0\Delta}{P_0}\right) \right] \quad 0 \leq \Delta \leq D_1 \quad \text{Eq. 1.11}$$

$$\begin{aligned} F(\Delta) &= F_{max} + K_2(\Delta - D_1) & D_1 \leq \Delta \leq D_2 F(\Delta) \\ F(\Delta) &= F_{max} + K_2(\Delta - D_1) + K_3(\Delta - D_2) & D_2 \leq \Delta \leq D_{max} \\ F(\Delta) &= 0 & \Delta > D_{max} \end{aligned} \quad \text{Eq. 1.12}$$

The cyclic loading rules are based on the four exponential hysteretic curves proposed by Dolan [1.17] to describe the pinching zone. These equations are modified by taking into account the load decrease by cyclic loading at the same displacement due to the damage of wood and sliding.

$$F(\Delta) = F_{dA} + (K_4\Delta + P_2 - F_{dA}) \left\{ 1 - \exp\left[\frac{K_0(U_A - \Delta)}{(2P_2)}\right] \right\} \quad \text{part 1} \quad \text{Eq. 1.13}$$

$$F(\Delta) = F_{dB} + (K_4\Delta + P_2 - F_{dB}) \left\{ 1 - \exp\left[\frac{K_y(U_B - \Delta)}{(2P_2)}\right] \right\} \quad \text{part 2} \quad \text{Eq. 1.14}$$

$$F(\Delta) = F_{dB} + (K_5\Delta + P_1 - F_{dB}) \left\{ 1 - \exp\left[\frac{K_0(U_B - \Delta)}{(2P_1)}\right] \right\} \quad \text{part 3} \quad \text{Eq. 1.15}$$

$$F(\Delta) = F_{dA} + (K_5\Delta + P_1 - F_{dA}) \left\{ 1 - \exp\left[\frac{K_y(U_A - \Delta)}{(2P_1)}\right] \right\} \quad \text{part 4} \quad \text{Eq. 1.16}$$

Were K_4 is equal to P_2/U_A , K_5 to P_1/U_B and K_y to $F(D_y)/D_y$. D_y is the yield displacement determined from the experiment, and $F(D_y)$ is its corresponding force computed with the monotonic loading equation. U_A (or U_B) is the maximum (or minimum) slip reached during the previous loading history. Parts 1 to 4 represent the decreasing and reloading curves 1–4 in Fig. 1.8. It is assumed that the decrease in strength by the second cycle loading in one direction (determining F_{dA} or F_{dB}) is proportional to the maximum load reached in the other direction F_{UB} (or F_{UA}) corresponding to U_B (or U_A) according the following equations:

$$F_{dA} = F_{UA} - \alpha_A [F_{UA} - (P_1 + K_5 U_A)] \quad \text{con} \quad \alpha_A = k \left| \frac{F_{UB}}{F_{max}} \right| \quad \text{Eq. 1.17}$$

$$F_{dB} = F_{UB} - \alpha_B [F_{UB} - (P_2 + K_4 U_B)] \quad \text{con} \quad \alpha_B = k \left| \frac{F_{UA}}{F_{max}} \right| \quad \text{Eq. 1.18}$$

The envelope curve is modified considering the decreased strength due to nail withdrawal. The postpeak monotonic strength ($|\Delta| > D_1$) is obtained by multiplying parameter.

$$\beta_A = \gamma \left[\frac{U_A - D_1}{D_{max} - D_1} \right] \quad e \quad \beta_B = \gamma \left[\frac{U_B + D_1}{D_{max} - D_1} \right] \quad \text{Eq. 1.19}$$

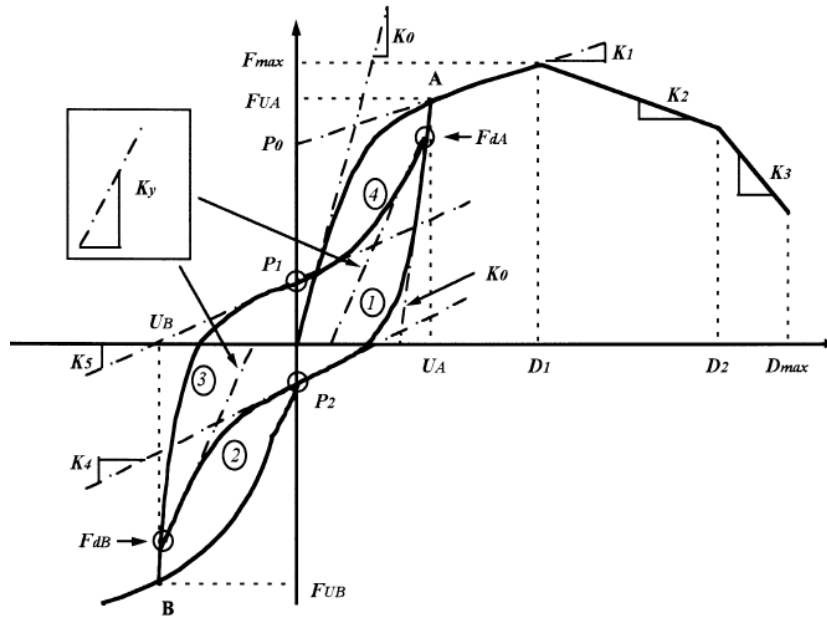


Fig. 1.8 – Richard & Yasumura model [1.15].

There are five more parameters to complete the cyclic rules: P_1 , P_2 , D_y , k e γ . All the parameters were determined from the reversed cyclic loading tests of the nailed joints. The main applications of this hysteresis model concern the simulations of experimental tests on simple wood shearwalls and the consequent investigation of the dynamic response of entire wood shearwall buildings as reported in [1.15].

1.2.2.4 CUREE hysteresis model

In the context of the CUREE-Caltech Wood framed Project, a numerical model capable of predicting the load-displacement response and energy dissipation characteristics of wood shear walls under arbitrary quasi static cyclic loading has been developed by Folz and Filiatrault [1.18] The model has been incorporated into the computer program CASHEW: Cyclic Analysis of SHEar Walls. As discussed below, this model is well suited to study wood shear walls but can also be applied at the structural system level. The basic equation of the model for the monotonic branch is reported below:

$$F = \begin{cases} \text{sgn}(\delta)(F_0 + r_1 K_0 |\delta|) \left[1 - \exp\left(-\frac{K_0 |\delta|}{F_0}\right) \right] & |\delta| \leq |\delta_u| \\ \text{sgn}(\delta_u) F_u + r_2 K_0 [\delta - \text{sgn}(\delta) \delta_u] & |\delta_u| < |\delta| \leq |\delta_F| \\ 0 & |\delta| > |\delta_F| \end{cases} \quad \text{Eq. 1.20}$$

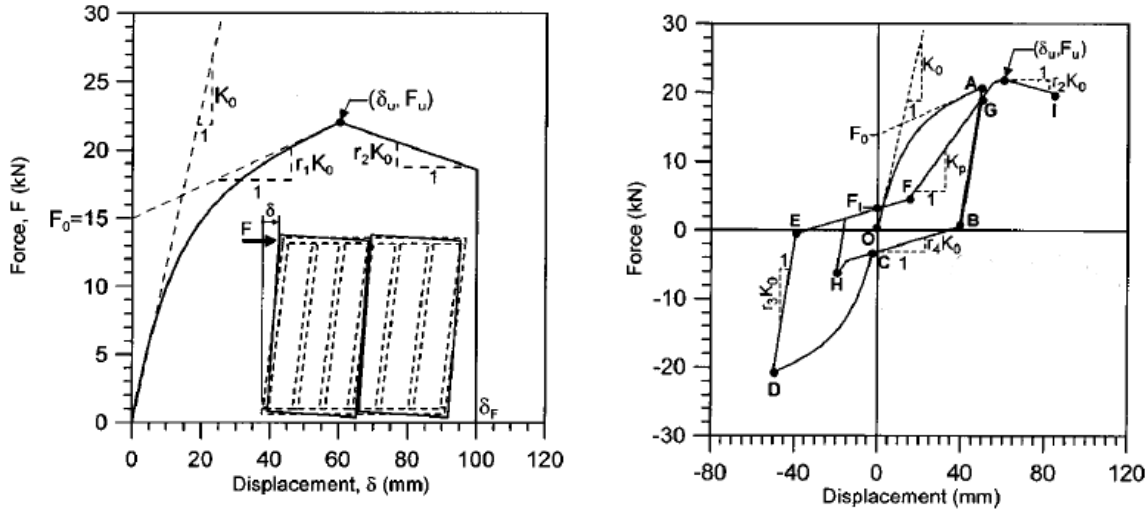


Fig. 1.9 – Monotonic curve (left) and hysteretic loop (right) of CUREE model [1.18]

This connector model, originally proposed by Foschi [1.6], is characterized by six parameters that must fit the experimental data: F_0 , r_1 , r_2 , δ_u and d_f . Under cyclic loading, the load-displacement paths OA and CD follow the monotonic envelope curve as expressed by Eq. 1.20. All other paths are assumed to exhibit a linear relationship between force and deformation. Unload branch of the envelope curve follows a path such as AB with stiffness $r_3 K_0$. Here, both the connector and wood are unloading elastically. Under continued unload the response moves onto path BC, which has reduced stiffness $r_4 K_0$. Along this path, the connector loses partial contact with the surrounding wood because of permanent deformation that was produced by previous loading, along path OA in this case. The slack response along this path characterizes the pinched hysteresis displayed by dowel connections under cyclic loading. Load branch in the opposite direction for the first time forces the response onto the envelope curve CD. Unloading off this curve is elastic along path DE, followed by a pinched response along path EF, which passes through the zero-displacement intercept F_l , with slope $r_4 K_0$. Continued re-loading follows path FG with degrading stiffness K_p , as given by the following Eq. 1.21:

$$K_p = K_0 \left(\frac{\delta_0}{\delta_{max}} \right)^\alpha \quad \text{Eq. 1.21}$$

With $\delta_0 = (F_0/K_0)$ and α = hysteretic model parameter which determines the degree of stiffness degradation. These parameters are obtained from fitting the model to connection test data. Note from Eq. 1.21 that K_p is a function of the previous loading history through the last unloading displacement δ_{un} so that:

$$\delta_{max} = \beta \delta_{un} \quad \text{Eq. 1.22}$$

Where β is another hysteretic model parameter. A consequence of this stiffness degradation is that it also produces strength degradation in the response. A total of 10 parameters are necessary to completely define the CUREE model.

1.2.2.5 Ceccotti & Vignoli hysteresis model

This model was developed in 1989 at the University of Florence by Ceccotti and Vignoli [1.14] to enable the simulation of connections with nonlinear fasteners connecting wood members in drain-2DX Finite Element code. The model was originally developed to reproduce the hysteresis behaviour of moment-resisting semi-rigid joints largely spread in glulam portal frames in Europe. This specific hysteresis behavior of connections was reproduced using different loading and unloading slopes. Parameters for the skeleton curves were found through the load slip curve obtained by means of experimental cyclic tests. A four slope model was first developed in 1989: the outside envelope was defined by two loading slopes: K_1 and K_2 as depicted in the following Fig. 1.10. The unloading slope was equal to the initial loading slope K_1 . A return slope k_6 was defined and an inner slope K_4 was used to model the pinching loops for subsequent cycles. A more accurate six-slope model was later developed in 1991 [1.26], which included a third loading slope, K_3 , and the option of an unloading slope, K_5 , which is different from K_1 . As an example the following Fig. 1.10 reports the skeleton of the four-slope and the six slope model:

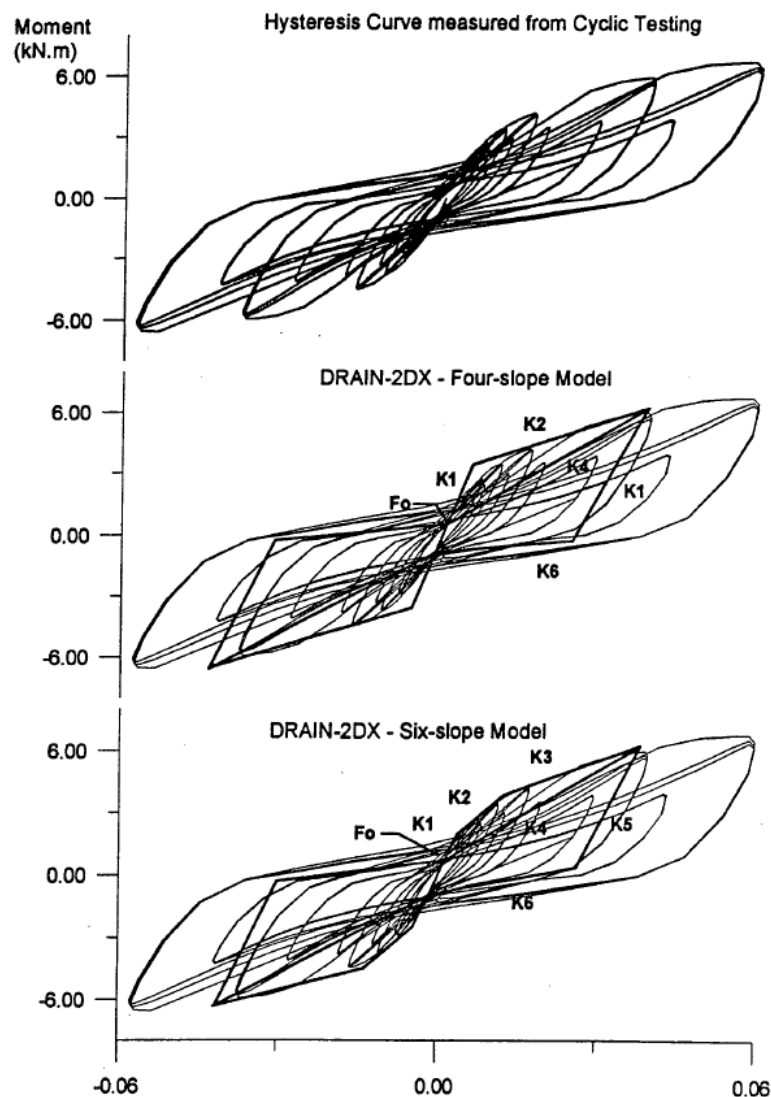


Fig. 1.10 – Slope parameters for the Ceccotti & Vignoli model [1.27]

The equations that define the hysteresis loop are extensively reported in [1.14]. According to [1.7] the accuracy of these curves was limited to certain amplitude rotations because the model was only capable of producing a limited number of slopes. Typically, the slope parameters were chosen to best represent the maximum outside loops because the smaller amplitude loops did not significantly affect the overall shape of the response curve. The calibration of the model is based on experimental cyclic tests on single connection elements or on representative structural elements.

The initial usage of these models was limited to semi-rigid moment resist joints of glulam frame. Then the usage of the six parameters model was extended to modeling any mechanical connection used in wooden structure as largely described in [1.9]. The last applications of the model concern the modeling of the typical connections used in CLT structure such as the wood-steel and wood-wood connections (e.g. angular bracket, holdown and in plane panel to panel joint). In Ceccotti [1.28] is reported the modeling of an entire three storeys CLT building using the Ceccotti & Vignoli model properly calibrated on the outcomes from experimental tests on entire walls elements.

1.2.2.6 Rinaldin hysteresis model

This hysteresis model was specifically developed by Rinaldin et al.[1.16] in order to reproduce the seismic response of CLT structures. In this approach, each connector (angle bracket, hold-down, screw) is schematized with a non-linear spring characterized by a hysteretic behaviour. The model has been implemented in a widespread software package such as Abaqus using an external user subroutine.

The actual curves of the connectors have been approximated with piecewise linear laws, more specifically tri-linear curves, which have been parameterized to allow the user to fully control their shape. Three different types of curve have been developed: for angle brackets, for screws between adjacent vertical panels, and for hold-downs. Each curve is made of several branches composing the backbone curve and the hysteretic cycle.

The formulation proposed for connections made by nailed steel angle or screws is depicted in the following Fig. 1.11 and has the following features:

- It is made of 16 branches, with 4 additional branches for the elastic cycles;
- The four elastic branches represent the cyclic behaviour before plasticization with a high unloading stiffness until the spring plasticization;
- The backbone curve is made of three branches: an elastic, a plastic with hardening, and a softening branch before failure;
- The curve is symmetric; if an unloading occurs, branch #4 is followed until a given percentage (chosen by the user) of the maximum force on the backbone curve is reached. Branch #6 models the slip effect, and branch #40 takes to the backbone curve with a degraded elastic stiffness;
- Branches #1 to #6 are positive with respect to the force and branch #7 is for reloading between pinching branches; branches #10, #20, #30, #40, #50, #60 are negative and branch #70 are for unloading between pinching branches;
- Branches #8 and #80 are used to obtain a better fit with the experimental data for the angle brackets. These are not needed if the spring is used to model screws; otherwise the user has to set two additional parameters for the inclination and starting (or arrival) point of branch #8 (and #80);

1.2.2.7 K. Elwood hysteresis model

This model was defined by k. Elwood [1.29] to represent a 'pinched' load-deformation response and degradation under cyclic loading for RC structure. Currently this model is implemented into the open source research like code OpenSEES [1.30] and can also be used to reproduce the hysteretic behaviour of the connection elements characterized by the pinching and cyclic degradation phenomena. In this model cyclic degradation of strength and stiffness occurs in three ways: unloading stiffness degradation, reloading stiffness degradation, strength degradation. The envelope curve of the connectors have been approximated with piecewise linear laws, more specifically tri-linear curves as depicted in the following Fig. 1.12.

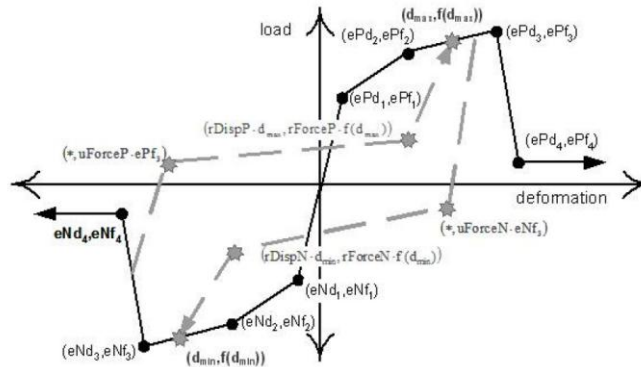


Fig. 1.12 - Definition of Elwood K. hysteresis model [1.30]

A total of 22 input parameters are necessary to define the model:

- ePf₁, ePf₂, ePf₃, ePf₄ force points on the positive response envelope;
- ePd₁, ePd₂, ePd₃, ePd₄ deformation points on the positive response envelope;
- eNf₁, eNf₂, eNf₃, eNf₄ force points on the negative response envelope;
- eNd₁, eNd₂, eNd₃, eNd₄ deformation points on the negative response envelope;
- rDispP (rDispN) defining the ratio of the deformation at which reloading occurs to the maximum (minimum) historic deformation demand;
- rForceP (rForceN) defining the ratio of the force at which reloading begins to force corresponding to the maximum (minimum) historic deformation demand;
- uForceP (uForceN) defining the ratio of strength developed upon unloading from negative (positive) load to the maximum (minimum) strength developed under monotonic loading;
- gK₁, gK₂, gK₃, gK₄ e gK_{lim} defining the unloading stiffness degradation;
- gD₁, gD₂, gD₃, gD₄ e gD_{lim} defining the reloading stiffness degradation;
- gF₁, gF₂, gF₃, gF₄ e gF_{lim} defining the strength degradation;
- gE defining the energy degradation

The basic equations that define the stiffness and strength degradation are:

stiffness degradation:

$$k_i = k_0(1 - \delta k_i) \quad \text{Eq. 1.25}$$

Where k_i is the unloading stiffness at time t , k_0 is the initial unloading stiffness (for the case of no damage), and δk_i (defined below) is the value of the stiffness damage index at time t_i .

$$d_{\max i} = d_{\max 0}(1 + \delta d_i) \quad \text{Eq. 1.26}$$

Where $d_{max\ i}$ is the deformation demand that defines the end of the reload cycle for increasing deformation demand, $d_{max\ 0}$ is the maximum historic deformation demand (which would be the deformation demand defining the end of the reload cycle if degradation of reloading stiffness is ignored), and δd_i (defined below) is the value of reloading stiffness damage index at time t .

strength degradation:

$$(f_{max})_i = (f_{max})_0 (1 - \delta f_i) \quad \text{Eq. 1.27}$$

Where $(f_{max})_i$ is the current envelope maximum strength at time t , $(f_{max})_0$ is the initial envelope maximum strength for the case of no damage, and δf_i (defined below) is the value of strength value index at time t .

The damage indexes, δk_i , δd_i e δf_i may be defined to be a function of displacement history only or displacement history and energy accumulation. For either case, all of the damage indexes are computed using the same basic equations. As an example if the damage indexes are assumed to be a function of displacement history and energy accumulation, the unloading stiffness damage index, δk_i , is computed as follows:

$$\delta k_i = \left[gK_1 (\tilde{d}_{max})^{gK_3} + gK_2 (Cycle)^{gK_4} \right] \leq gK_{lim} \quad \text{Eq. 1.28}$$

$$\tilde{d}_{max} = \max \left[\frac{d_{max\ i}}{def_{max}}, \frac{d_{min\ i}}{def_{min}} \right] \quad \text{Eq. 1.29}$$

With Cycle equal to the number of cycles accrued in the loading history, def_{max} e def_{min} the positive and negative deformations that define failure. The other damage indexes, δd_i and δf_i , are computed using the same equations with degradation model parameters gK^* replaced by gF^* and gD^* , as is appropriate. Further information about the model formulation can be found in [1.30]

The main application of this model is about the RC structure but recently this model is also used to reproduce the hysteresis behaviour of fasteners. Examples of usage of this model are reported in [1.31] for shearwall system and in this thesis work to investigate both CLT and wood shearwall structures.

1.3 Comments

The available models for wood systems described in this chapter use a complex set of force-history rules or limited empirical relations. Some of these models satisfied specific features of joints or structural systems but may be inappropriate for joints or systems with different configurations and material components. Since: (1) there are a lots of combinations of materials and joints in wooden system, (2) wood base products, fasteners and construction methodology continue to evolve, a general model is preferred over models derived from specific configurations. Finally it should be noted that currently the wooden structure can be faithfully modeled only using research-oriented code such as: Drain 3D, OpenSEES, Abaqus etc.. while the standard commercial Finite Element codes are not suitable for wooden systems. This represents a relevant lack for the engineering practice concerning with the seismic design of timber building.

References - Chapter 1

- [1.1] European Committee for Standardization (CEN). *Eurocode 8 - design of structures for earthquake resistance, part 1: General rules, seismic actions and rules for buildings*. 2004.
- [1.2] Fragiaco M, Dujic B, Sustersic I. *Elastic and ductile design of multy-storey crosslam wooden buildings under seismic actions*. *Engineering Structures* 33, 2011, 3043-3053.
- [1.3] European committee for standardization (CEN). *Eurocode 5 – design of timber structures – part 1-1: general rules and rules for buildings*. 2004.
- [1.4] Judd, J. P., and Fonseca, F. S. (2005). “Analytical model for sheathing-to-framing connections in wood shear walls and diaphragms.” *Journal of Structural Engineering, American Society of Civil Engineers*, Vol. 131, No. 2, 345–352.
- [1.5] Dujic B, Hristovsky, Zarnic R. *Experimental investigation of massive wooden wall panel system subject to seismic excitation. Proceeding of the First European Conference on Earthquake Engineering*. Geneva, Switzerland, 2006
- [1.6] Heine, C. P., and Dolan, J. D. (2001). “A new model to predict the load–slip relationship of bolted connections in timber.” *Wood and Fiber Science, Society of Wood Science and Technology*, Vol. 33, No. 4.
- [1.7] Ceccotti, A., and Vignoli, A. (1990). “Engineered timber structures: An evaluation of their seismic behavior.” *Proceedings, 1990 International Timber Engineering Conference*, Vol. 3, 946–953.
- [1.8] Pang, W. C., Rosowsky, D. V., Pei, S., and van de Lindt, J. W. (2007). “Evolutionary parameter hysteretic model for wood shear walls.” *Journal of Structural Engineering, American Society of Civil Engineers*, Vol. 133, No. 8, 1118–1129.
- [1.9] Foliente, G. C. (1995). “Hysteresis modeling of wood joints and structural systems.” *Journal of Structural Engineering, American Society of Civil Engineers*, Vol. 121, No. 6, 1013–1022.
- [1.10] van de Lindt, J. W. (2004). “Evolution of wood shear wall testing, modeling, and reliability analysis: Bibliography.” *Practice Periodical on Structural Design and Construction, American Society of Civil Engineers*, Vol. 9, No. 1, 44–53.
- [1.11] Loh, C., and HO, R., (1990). “Seismic damage assessment based on different hysteretic rules”. *Earthquake engineering and structural Dynamics* 19:753-771
- [1.12] Saiidi, M. (1982). “Hysteresis models for reinforced concrete,” *Journal of the Structural Division, American Society of Civil Engineers*, Vol. 108, No. 5, 1077-1087.
- [1.13] Clough, R. W. (1966). “Effect of stiffness degradation on earthquake ductility requirements,” *Technical Report No. SESM 66–16, University of California, Berkeley, California*.
- [1.14] Ceccotti, A., and Vignoli, A. (1989). “A hysteretic behavioral model for semi rigid joints.”, *European Earthquake Engineering*, Vol 3-3-9
- [1.15] Richard, N., Yasumura M. and Davenne, L., (2003) “Prediction of seismic behavior of wood-framed shear walls with openings by pseudodynamic test and FE model.” *J Wood Sci* 49:145–151
- [1.16] Rinaldin, G., Amadio, C. and Fragiaco, M., (2011), “A component approach for non-linear behavior of cross-laminated solid timber panels” *Proceeding of ANIDS 2011, Bari Italy, 2011, CD*.
- [1.17] Dolan, J.D. (1991). “A numerical model to predict the dynamic response of timber shear walls.” *Proc.*,

Int. timber Engrg. Conf., Vol. 4, 267-274

- [1.18] Folz, B., and Filiatrault, A. F., (2001). "Cyclic analysis of wood shear walls." *Journal of Structural Engineering, American Society of Civil Engineers*, Vol. 127, No. 4, 433-441.
- [1.19] Stewart, W. G. (1987). "The seismic design of plywood sheathed shearwalls." *Ph.D. thesis, University of Canterbury, Christchurch, New Zealand.*
- [1.20] Foschi, R. O., (1977) "Analyses of wood diaphragms and trusses. Part I: diaphragms." *Canadian J. Civ. Engrg.*, 4(3), 345-352 Foschi, R. O., (1977) "analyses of wood diaphragms and trusses. Part I: diaphragms." *Canadian J. Civ. Engrg.*, 4(3), 345-352
- [1.21] Foschi, R. O., (1999) "FRAME, Analytical Hysteresis Model for Dowel-type timber connections, Computer Program, Department of Civil Engineering, University of British Columbia, Canada
- [1.22] Foschi, R. O. (2000). "Modeling the hysteretic response of mechanical connections for structures." *Proceedings, World Conference on Timber Engineering, Department of Civil Engineering, Department of Wood Science, and School of Architecture, University of British Columbia, Vancouver, British Columbia, Canada.*
- [1.23] He, M., Lam, F., and Foschi, R. O. (2001). "Modeling three-dimensional timber light-frame buildings." *Journal of Structural Engineering, American Society of Civil Engineers*, Vol. 127, No. 8, 901–913.
- [1.24] Dolan, J.D. (1989). "The dynamic response of timber shear walls." *PhD thesis, Univ. of British Columbia, Vancouver, B.C., Canada*
- [1.25] White, M. and Dolan, J. (1995). "Nonlinear Shear-Wall Analysis." *J. Struct. Eng.*, 121(11), 1629–1635. doi: 10.1061/(ASCE)0733-9445(1995)121:11(1629)
- [1.26] Ceccotti, A., (1994). "Modeling timber joint, timber structures in seismic regions: RILEM state of art report" *Material and Structures*, 27, 177-178
- [1.27] Frenette C.D., (1996) "Dynamic behaviour of timber frame with dowel type connections." *Proceeding of the international Wood Engineering Conference, New Orleans, USA, Vol. 4, 89-96*
- [1.28] Ceccotti A. New technologies for construction of medium-rise buildings in seismic regions: the XLAM case. *IABSE Struct Eng Internat 2008;18:156–65. Tall Timber Buildings (special ed.)*.
- [1.29] Elwood, K.J., and Moehle, J.P., (2006) "Idealized backbone model for existing reinforced concrete columns and comparisons with FEMA 356 criteria", *The Structural Design of Tall and Special Buildings*, vol. 15, no. 5, pp. 553-569.
- [1.30] Fenves G.L., 2005, *Annual Workshop on Open System for Earthquake Engineering Simulation, Pacific Earthquake Engineering Research Center, UC Berkeley, <http://opensees.berkeley.edu>*.
- [1.31] Pozza L., Scotta R., Polastri A, Ceccotti A. 2012. Seismic behaviour of wood concrete frame shear-wall system and comparison with code provisions. Meeting 45 of the Working Commission W18-Timber Structures, CIB. Växjö, Sveden, 2012, paper CIB-W18/45-15-2.

Chapter 2 – Proposal and validation of a new hysteresis model for wooden joints

Abstract

In this section a proposal for a wood joint numerical model that involves the usage of commercial Finite Element code is reported. The proposed numerical model based on a specific set of nonlinear springs is able to reproduce the load-displacement hysteretic response of steel-wood and wood-wood joints.

The reliability of the devised model to reproduce the connections hysteretic behaviour is presented and critically discussed in comparison with experimental results.

The validation of the model was firstly performed on experimental cycles of single connections, and then verified with reference to shearwalls and whole three-storey buildings behaviour. The results from the SOFIE project experimental tests have been used for the validation of the new developed numerical model.

2.1 Introduction

The recent spread of innovative wooden building systems imposes to civil engineers to investigate the timber structure by nonlinear numerical models able to reproduce the hysteresis behaviour of the connectors. The hysteresis models described in the previous chapter are implemented into complex research-oriented codes that not represent tools generally used by engineers in the design practice.

Currently a requisite necessary to reproduce and analyze the nonlinear seismic response of a timber building is to dispose of a simplified hysteretic model of the connection, which has to be adequately reliable and effective to guarantee the quality of the results.

The purpose is to develop a model of the timber joints which combines the ability of reproducing the main aspects of the actual behaviour of the connections, maintaining an adequate level of complexity and using any finite element codes including commercial ones.

2.2 Proposal for a simplified hysteresis model for wood connections

In this thesis work the behaviour of the connections used in timber structure are reproduced by properly combining springs and uni-directional links in the complex macro-element shown in Fig. 2.1. The developed hysteresis model can be easily reproduced using the standard nonlinear element of a commercial Finite Element code. In this application the Finite element code Strand 7 [2.1] was used.

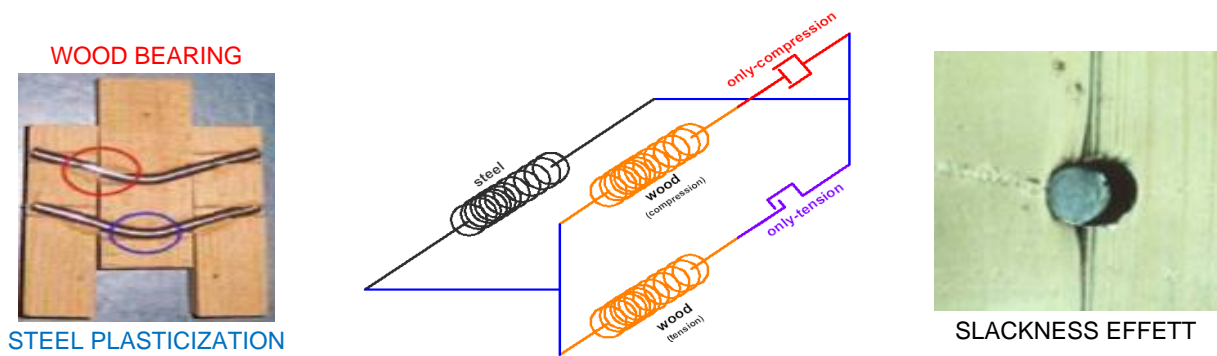


Fig. 2.1 - Connection macro-element.

In detail an elastoplastic spring providing the stiffness of the steel connector (nails or screws) is linked in parallel with an equivalent spring representing the wood behaviour. The wooden part is composed by two elastic-plastic springs in parallel: one accounting only for compressive stress state being connected in series with a compression-only element, the other one oppositely working only for tensile loads being in series which a tension-only element. The compression-only and tension-only elements allow the reproduction of the slackness effect of the hole, and the subsequent formation of gap between steel and wood.

The developed model reproduces the typical pinched behaviour in the load-displacement curves, and the reduction in stiffness for the reloading cycles, but it is unable to reproduce the strength degradation and the softening response after the failure of the connection. These drawbacks perhaps have to be paid when low-demand numerical models with standard finite element springs are required.

Some considerations concerning the different features characterizing the behaviour of the connection have to be carried out in order to select which one could be neglected or reproduced in a simplified way. According to Foliente G. [2.2] pinching behaviour and reloading stiffness degrading cannot be neglected, as they are responsible for the energy dissipation capacity of the connection element. This remark is also confirmed by the numerical simulation conducted by Judd et al.[2.3] on an entire timber frame shearwall. As depicted in Fig. 2.2 the nonlinear time history response of the wall was investigated referring to six different model of the connections: linear and nonlinear elastic models, bilinear model, Clough model [2.4], Q-hysteresis model [2.5] which reproduces only the strength degradation phenomena and finally the modified Stewart hysteresis model [2.6] which reproduces both the pinching behavior and the degradation phenomena (strength and stiffness).

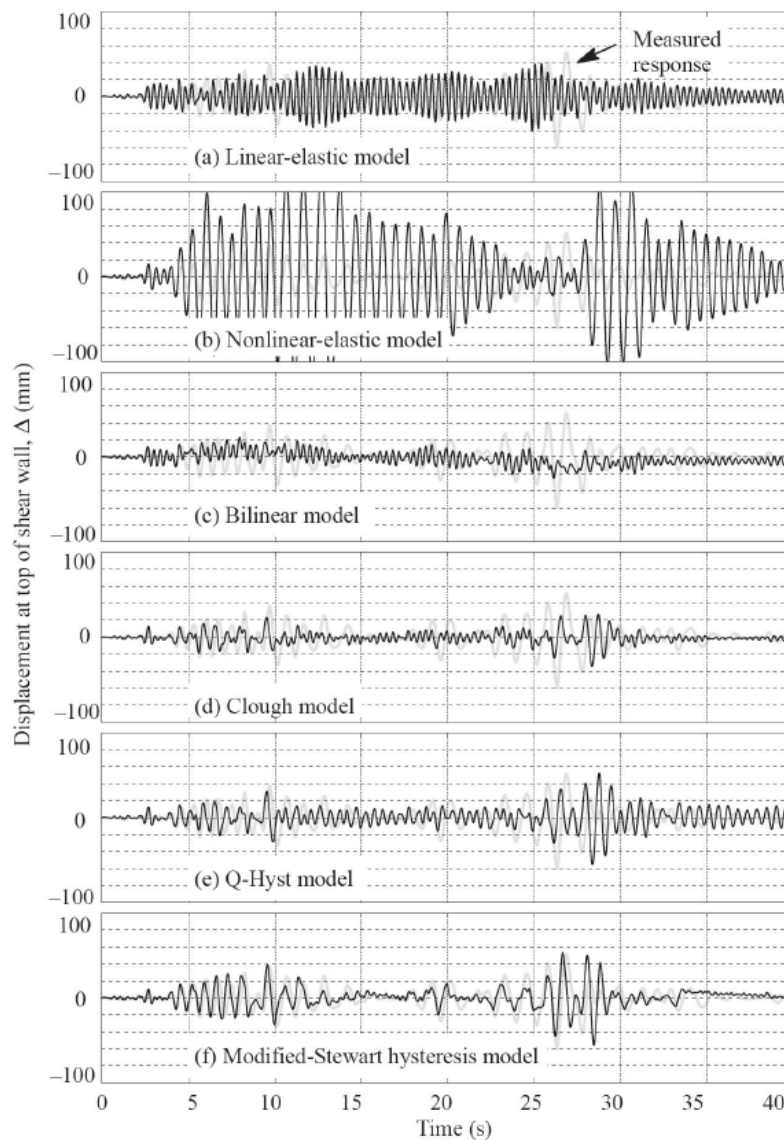


Fig. 2.2 – Sensitivity of different hysteresis model to reproduce the behaviour of wood joints [2.3]

The results obtained from this study clearly shows that the pinching and the reloading stiffness degrading are the most important features to take into account for a faithfully reproduction of the wood joints hysteresis behaviour.

According with Dolan [2.7] the effect of the strength degradation phenomena can be neglected without relevant effects on the global response, if it affects the last phase of the load slip curve before the failure. Otherwise when the strength degradation affects the small amplitude cycle after the yielding limit the degradation phenomena can't be neglected because it strongly influences the connection response in terms of energy dissipation capacity.

Since the strength degradation is not accounted by the model, it can be applied within a range of deformation for which such strength degradation is not relevant, that is the difference between the energy dissipation provided by the model is quite in agreement with that from the actual behaviour. Undoubtedly there are situations which require the implementation of a more complex hysteretic model than the one here proposed: in this case, a specific research-oriented numerical code needs to be used.

With an appropriate choice of the spring parameters, the described macro-element allows to reproduce both the symmetrical pinched hysteretic cycles (e.g. angular bracket and in plane wood to wood joint) and the asymmetrical ones that typically show higher stiffness for compression loads than for tensile ones (e.g. holdown bracket).

2.3 Model calibration procedure

This paragraph reports the general procedure for the calibration of each nonlinear component spring of the developed macro-element. This calibration of the macro-element springs is based on a proper linearization of the experimental load slip curve.

As summarized in Jorissen A. et al.[2.8] available methods for the definition of the yielding limit refer to a bi-linearization of the experimental curves while in this work a trilinear approximation of the load-displacement curves is adopted (see Fig. 2.3).

For monotonic loading the definition of the trilinear skeleton starts with the choice of the first yielding point (δ_{y1} ; F_{y1}) at the end of the experimental linear phase and of the experimental hardening stiffness k_3 . Then $k_1 = F_{y1}/\delta_{y1}$ represents the initial elastic stiffness while k_2 , that is the post-elastic stiffness, and the second yielding point (δ_{y2} ; F_{y2}) are obtained by imposing the equality of the deformation energy.

The hysteretic behaviour of the connections is completed by assuming an kinematic hardening model for both wood and steel springs and by assigning the values of the reloading stiffness k_4 and of the residual force F_0 at unloading, depending mainly on the properties of the steel connectors, that can easily be derived from experimental cycles.

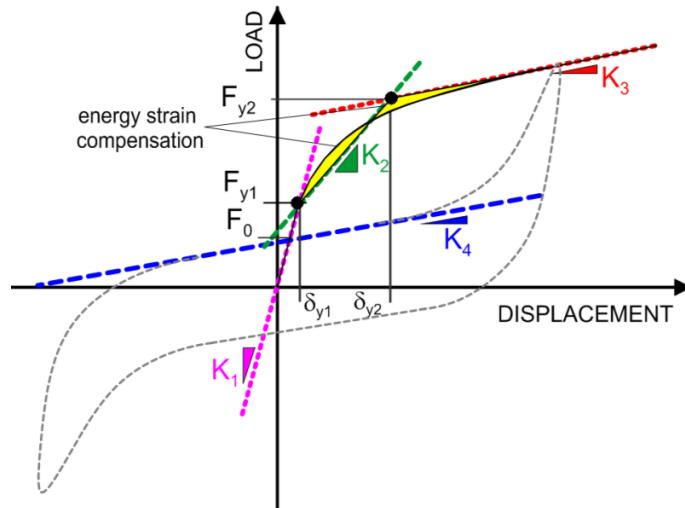


Fig. 2.3 - Characteristic parameters of the connection hysteretic cycle for typical symmetrical connectors

The correlation between the parameters from the whole complex model of the connection and those from the single parts representing the wood and steel contribution are given in Fig. 2.4.

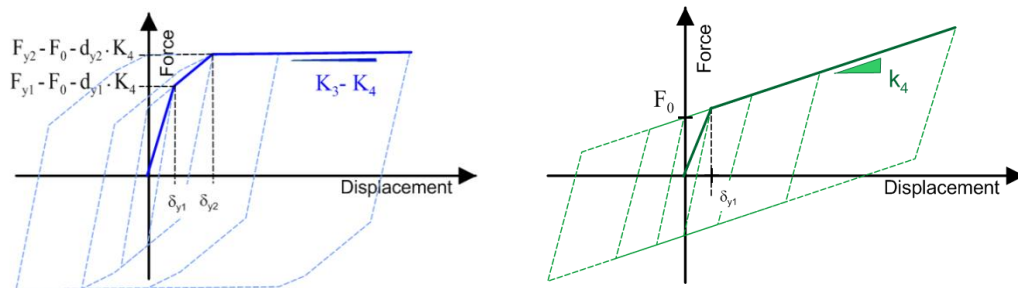


Fig. 2.4 - Skeleton curve of wood (left) and of steel (right) springs for symmetrical hysteretic cycle

The calibration of the asymmetrical connection elements was carried out with the same criteria, only considering the different stiffness and strength of the wood springs in tension and compression.

2.4 Test Simulation on a Single Connection Element

The validation of the devised macro-element was firstly performed on the basis of the experimental load slip curves of single fasteners carried out by means of experimental cyclic test during SOFIE project. In detail this section takes as reference the experimental load slip curve related to angular bracket and holdown reported in [2.9] and that of panel to panel joint reported in [2.10]. The usage of such reference experimental load slip curves is strictly dependent to the numerical reproduction of the shaking table test on the three storeys CLT building. It must be noted that the reference load slip curves for holdown and angular bracket used by Ceccotti A. [2.9] are derived from experimental tests on entire CLT walls and not on single connection elements as confirmed by the maximum strength of the connections which are greater than those obtained by Gavric [2.11] from experimental tests on single connection elements. On the other hand, according to Ceccotti A. [2.9]

the reproduced load slip curves represent the global shear resistance (fasteners strength + friction contribute) and rocking resistance of a representative CLT wall.

The following Fig. 2.5 shows the comparison between the results of the experimental cyclic tests on angle bracket, hold-down and panel to panel connection elements and the respective numerical simulations. The parameters of each macro-element spring used to reproduce the experimental results are also reported.

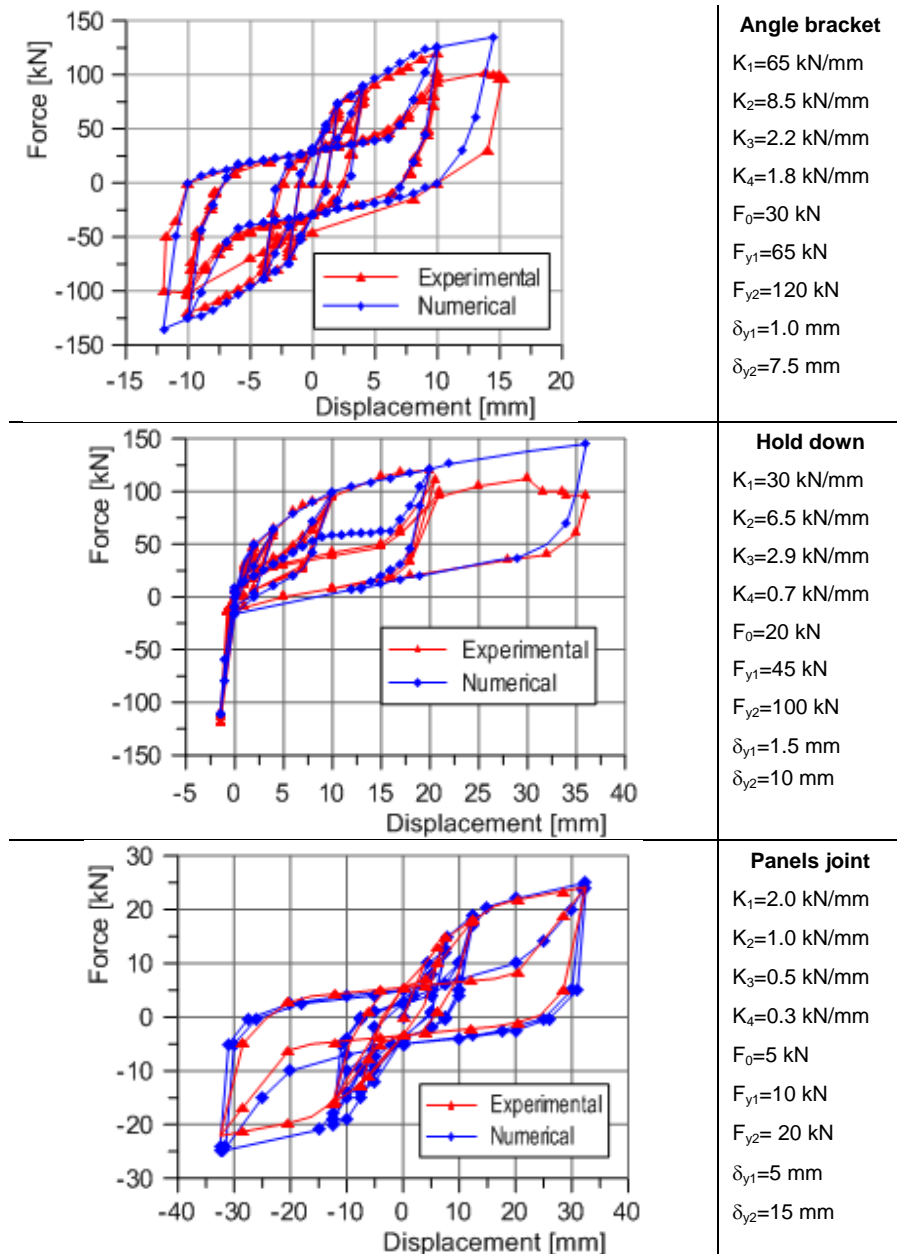


Fig. 2.5 – Comparison between experimental and numerical load-displacement curve of angle bracket, hold-down and panel to panel connection. Parameters of numerical models are listed on the side of plots. For holddown parameters are relative to the tensile branch of the cyclic curve.

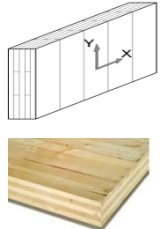
The proposed model fits well the experimental test also in terms of energy dissipation, with differences of 7% for angle bracket, 6% for hold down and 8% for panel to panel connection (percentage value are referred to hardening branch before the failure of the connections).

2.5 Test Simulation on a Single Wall Panel

In order to assess the wall panel-basic joints interaction and the effect of the vertical load, the complete cyclic test in the A-3 configuration described in [2.12] has been simulated. The model is based on the hypothesis that the nonlinear behaviour of the wall is concentrated in the connectors, whereas the timber panel remains in its elastic field. Therefore the macro-elements above described were used to represent the nonlinear behaviour of the connections, and the CrossLam panel was simulated with shell elements as thick as the panel (85mm).

The complex panel layout can be modeled using an orthotropic, homogenized orthotropic or homogenized isotropic material. Blass and Fellmoser [2.13] proposed the **H**omogenized, **O**rthotropic plane stress **B**lass reduced cross **S**ection (HOBS) method, which is based on the reduction of a multilayer to a single layer section using some corrective coefficients. In this work the multilayer CrossLam panel was modeled using a homogenized isotropic material with an averaged elastic-modulus, considering that the assumption of an orthotropic behaviour would slightly affects the global response of the wall. The main characteristics of the CrossLam panel are summarized in Table 2.1.

Table 2.1 - Mechanical characteristics of the CrossLam panel.

Young Modulus X direction [MPa]	E_x	6'800	
Young Modulus Y direction [MPa]	E_y	10'000	
Average Young modulus [MPa]	$E_{average}$	8'400	
Poisson Ratio	ν	0.35	
Density [kg/m^3]	ρ_{med}	530	

The cyclic test has been simulated by imposing a horizontal displacement to the node located on the upper part of the wall. The vertical load of 18.5 kN/m was reproduced applying a distributed force on the top of the wall. The numerical model used in the analysis is reported in Fig. 2.6.

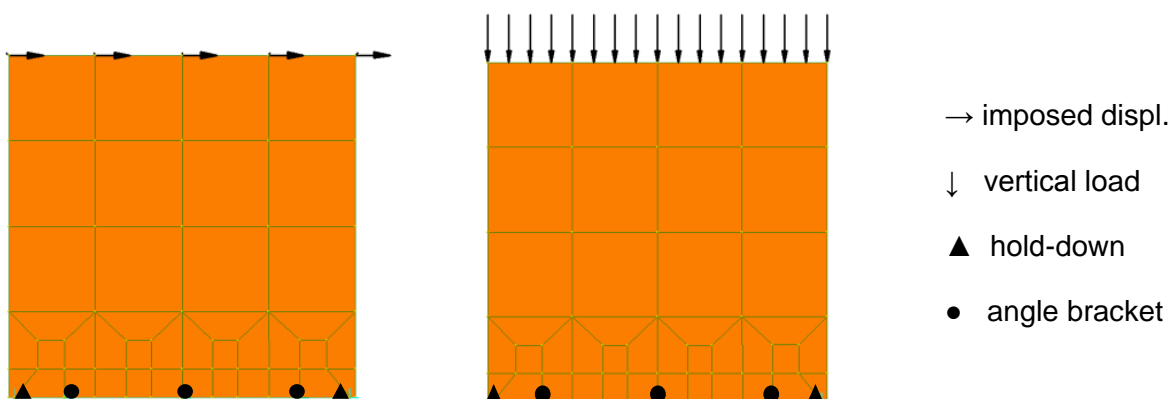


Fig. 2.6 – Numerical model of tested CrossLam wall with indication of connectors, horizontal imposed displacement (left) and applied vertical load (right).

The load-displacement curve, reported in Fig. 2.7, shows the good correspondence between the results of the experimental test and the numerical simulation at each cycle.

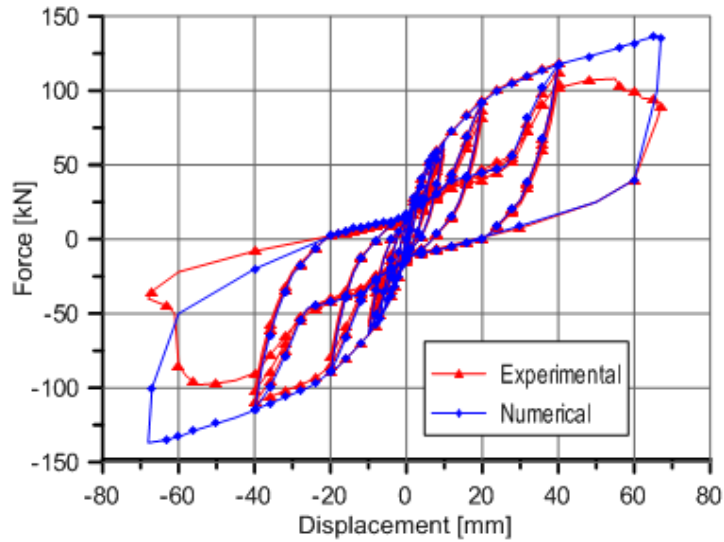


Fig. 2.7 - Comparison between the results of the complete experimental cyclic test and the numerical simulation.

The adequateness of the model is further confirmed by the assessment of the dissipated energy: Fig. 2.8 shows the difference in terms of dissipated energy per cycle between the experimental test and the numerical simulation.

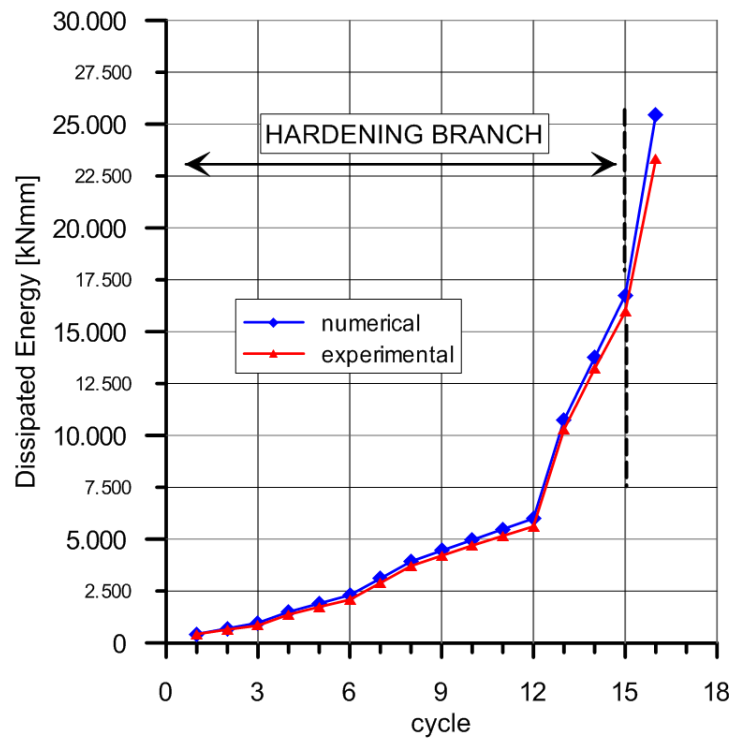


Fig. 2.8- Comparison between accumulation of dissipated energy per cycle between experimental cyclic test and the numerical simulation.

The correspondence is very good until the behaviour of the wall remain in the hardening phase (up to 15th cycle). The maximum difference at the end of the hardening branch is 8.5%. Then the difference increases because the proposed formulation is unable to reproduce the strength reduction and softening phase of the connections.

2.6 Simulation of shaking table tests of whole buildings

To assess the capacity of the macro-element to reproduce the behaviour of a whole building subjected to an earthquake, the numerical reproduction of the experimental shaking table tests of a three-storey building described in [2.9] has been carried out. In particular the so-called “C configuration” with asymmetrical openings at the ground floor has been investigated. The numerical model has been obtained with the same criteria as for the single wall panel cyclic test:

- 85 mm thick walls are represented by means of equivalent isotropic elastic shell with the characteristics already given in 2.5;
- base and across-storey connections are described through the proposed nonlinear macro-elements;
- in plane panel to panel connection joints are obtained by coupling a symmetrical macro-element for the vertical direction and an asymmetrical macro-element for the horizontal direction;
- floors and roof are represented as rigid diaphragms by means of 142 and 85 mm respectively thick isotropic elastic shell elements, analogous to that used for the wall;
- storey masses are applied as equivalent floor masses.

Fig. 2.9 shows the Finite Element model used for analyses of the building. The model of the building has been calibrated on the basis of the shaking table tests using the Kobe (PGA=0.82g) and the Nocera Umbra (PGA scale up to 1.2g) seismic recordings applied along the direction of major openings at the ground floor. The dynamic equilibrium equations have been integrated with a time step equal to 0.001 sec, by adopting an equivalent viscous damping of 2%, according to the Rayleigh model. The results of the dynamic analysis, under Kobe and Nocera Umbra signals, have confirmed that the proposed model is able to reproduce the nonlinear behaviour of the entire building.

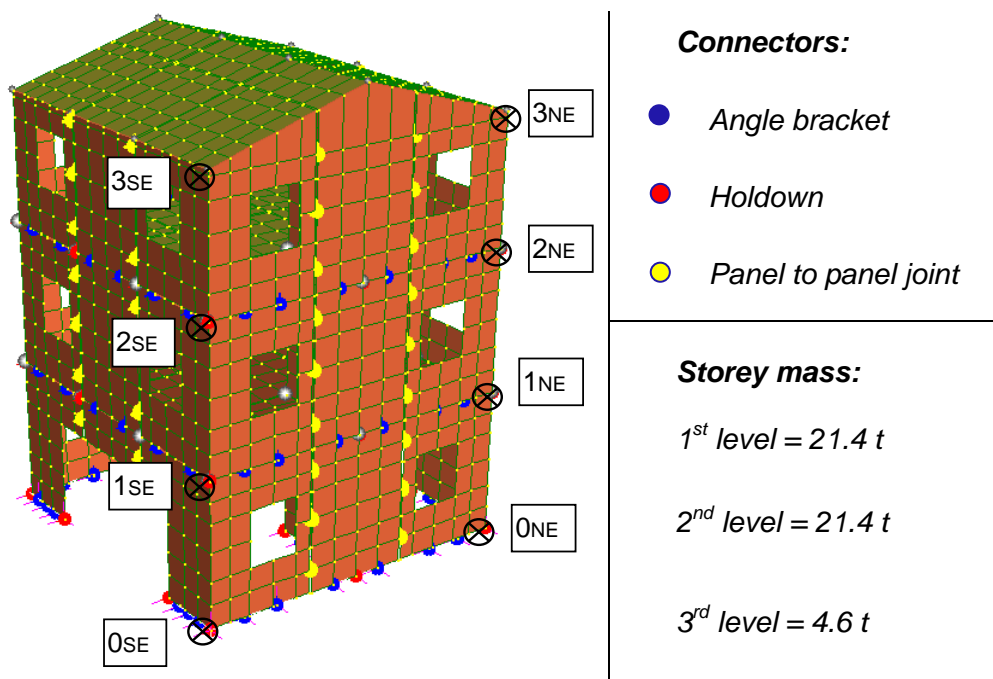


Fig. 2.9 - Views of the model of the entire building with indications of the connections, storey masses and displacement measurement points.

Table 2.2 compares the results of experimental test and of the numerical simulation in terms of maximum storey displacements and hold down uplift in the assessment points reported in [2.9] showing that the maximum difference is below 5%.

Table 2.2 – Comparison between test and model results

	Maximum displacement [mm]						Maximum uplifting [mm]	
	1NE	1SE	2NE	2SE	3NE	3SE	0NE	0SE
Kobe 0.82g								
Test	26.0	29.5	51.5	56.1	58.9	62.2	10.6	7.4
Model	27.2	28.7	49.7	53.5	56.9	59.7	11.4	7.7
Difference	4.7%	2.5%	3.4%	4.6%	3.3%	4.6%	4.6%	4.9%
Nocera Umbra 1.2g								
Test	35.6	37.1	61.5	65.2	71.7	78.7	10.5	9.6
Model	34.2	36.3	63.2	67.8	74.2	81.6	10.9	10.0
Difference	3.9%	2.2%	2.8%	4.0%	3.5%	3.7%	3.8%	4.2%

Fig. 2.10 reports the comparison between the test results and the model prediction in terms of displacement time history of the assessment point 3NE under the Nocera Umbra earthquake scaled up to 1.2g.

It can be observed that a quite good agreement was achieved in particular with regard to the maximum displacement due to acceleration peaks.

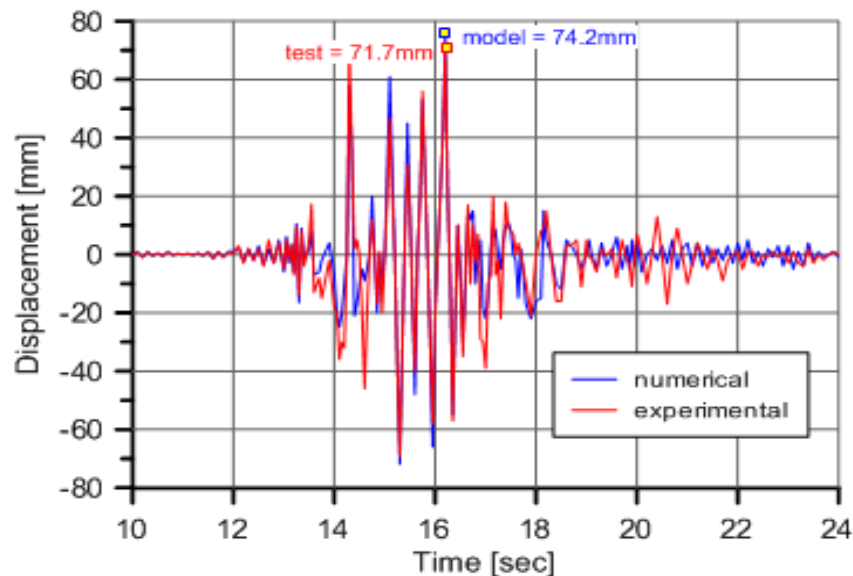


Fig. 2.10 - Test results versus model prediction at point 3NE under Nocera Umbra earthquake scaled up to 1.2g

It can be observed that a quite good agreement was achieved in particular with regard to the maximum displacement due to acceleration peaks.

2.7 Conclusions

The developed numerical model conjugates the need of reproducing the main aspects of the actual hysteretic behavior of the connection (such as pinching behavior and reloading stiffness degradation) with the requirement of maintaining an adequate level of complexity in order to be suitable for the time history analysis of modern timber buildings.

The main advantage of the proposed model consists in the possibility of reproduce with a suitable level of approximation the hysteresis behavior of wood joints using nonlinear spring available on any finite element code such as commercial ones. Consequently the developed model can be adopted by engineers in the design practice for modeling timber buildings.

A proper usage of the developed model must be limited to connections characterized by small strength degradation phenomena or when these phenomena affect only the last phase of the load slip curve before the failure.

The correct calibration of the complex spring in comparison with experimental tests, is a basic requirement for the reliable simulation of the actual behavior of each single connection and consequently of an entire building. Therefore as first step, the experimental results of monotonic and cyclic tests on single connector, wall panels and also on a three-storey cross laminated wooden building tested on the shaking table during SOFIE project, were reproduced with the adoption of the proposed numerical model. The numerical results fit well with the experimental ones, both in terms of shape and greatness of hysteretic load-displacement cycle and of dissipated energy.

Finally this work demonstrates the possibility and the efficacy of reproducing the seismic response of CrossLam structures by assuming a linear elastic behavior for timber panels and using a specifically developed complex spring to reproduce the nonlinear behavior of connectors.

References - Chapter 2

- [2.1] *Theoretical Manual - Theoretical background to the Strand 7 finite Element analysis system. Edition 1 – January 2005*
- [2.2] Foliente, G. (1995). "Hysteresis Modeling of Wood Joints and Structural Systems." *J. Struct. Eng.*, 121(6), 1013–1022. doi: 10.1061/(ASCE)0733-9445(1995)121:6(1013)
- [2.3] Judd, J. P., and Fonseca, F. S. (2005). "Analytical model for sheathing-to-framing connections in wood shear walls and diaphragms." *Journal of Structural Engineering, American Society of Civil Engineers*, Vol. 131, No. 2, 345–352.
- [2.4] Clough, R. W. (1966). "Effect of stiffness degradation on earthquake ductility requirements," *Technical Report No. SESM 66–16, University of California, Berkeley, California.*
- [2.5] Saiidi, M. (1982). "Hysteresis models for reinforced concrete," *Journal of the Structural Division, American Society of Civil Engineers*, Vol. 108, No. 5, 1077-1087.
- [2.6] Stewart, W. G. (1987). "The seismic design of plywood sheathed shearwalls." *Ph.D. thesis, University of Canterbury, Christchurch, New Zealand.*
- [2.7] Dolan, J.D. (1989). "The dynamic response of timber shear walls." *PhD thesis, Univ. of British Columbia, Vancouver, B.C., Canada*
- [2.8] Jorissen A., Fragiaco M. 2011. General notes on ductility in timber structures. *Engineering Structures* 33, 2011, 2987-2997.
- [2.9] Ceccotti A. New technologies for construction of medium-rise buildings in seismic regions: the XLAM case. *IABSE Struct Eng Internat* 2008;18:156–65. *Tall Timber Buildings (special ed.)*.
- [2.10] Sandhaas C, Boukes J, Kuilen JWG, Ceccotti A. Analysis of X-lam panel-topanel connections under monotonic and cyclic loading. Meeting 42 of the Working Commission W18-Timber Structures, CIB. Dübendorf, Switzerland, 2009, paper CIB-W18/42-12-2.
- [2.11] Gavric I, Ceccotti A, Fragiaco M. Experimental tests on cross-laminated panels and typical connections. *Proceeding of ANIDS 2011, Bari Italy, 2011, CD.*
- [2.12] Ceccotti A, Lauriola M.P, Pinna M, Sandhaas C. SOFIE Project – Cyclic Tests on Cross-Laminated Wooden Panels. *World Conference on Timber Engineering WCTE 2006. Portland, USA, August 6-10, 2006, CD.*
- [2.13] Blass HJ, Fellmoser P. Design of solid wood panels with cross layers. *8th World Conference on Timber Engineering WCTE 2004. Lahti, Finland, June 14–17, 2004, p. 543–8.*

Chapter 3 - Procedures for determining the behaviour q-factor of timber building systems

Abstract

This part of dissertation gives the basic background about the available definitions of the q-factor in literature and their relevance in the design of seismic resistant structures. The specific provisions given by current standards for the seismic design of timber structures are reported and critically discussed.

Some considerations about the development of new load-bearing timber systems and the consequently lack of norms for their seismic design, in particular as regarding the appropriate q-factor to be used for the design of different wooden structure are given.

The traditional methods used by the researchers for estimating the q-factor are described and classified into experimental and numerical methods. The main advantages and limitations of the various proposal are reported and critically discussed both in terms of precision of the q-factor estimation and of cost and time-consuming efficiency.

3.1 Background on q-factor definition

The European approach for a simplified seismic design of building using linear static or dynamic analyses is traditionally force-based. Available seismic codes for Europe area [3.1] and for Italy [3.2] refer to the FMD method [3.3] which requires the evaluation of the so-called behaviour q-factor.

According to the definition given by Eurocode 8 [3.1] this behaviour q-factor is introduced to reduce “the forces obtained from a linear-elastic analysis, in order to account for the non-linear response of a structure, associated with the material, the structural system and the design procedures”. Once the elastic seismic actions are reduced by q, designers are allowed to verify stresses on structural elements and connections in comparison with the same capacity design values adopted for static action through the pertinent codes (e.g. Eurocode 2 [3.4] for R.C., Eurocode 3 [3.5] for steel, Eurocode 5 [3.6] for wood, etc.). Based on such definition the q-factor represents the ability of the structure to dissipate energy and to withstand large deformations without ruin.

According to Fajfar P. [3.7] the reduction factor R (i.e. q –factor) used in the available seismic codes is composed by two different contributions: the first contribution R_{μ} takes into account the ductility and therefore the energy dissipation capacity of the structure while the factor Ω_d is the so-called overstrength. Based on such definition the behaviour factor q is defined by the following Eq. 3.1 [3.7]:

$$R = R_{\mu} \Omega_d \quad \text{Eq. 3.1}$$

R_{μ} is the ductility factor and represents the effective dissipative capacity due to the hysteretic behaviour of the material in a ductile structure. According to Fajfar P. [3.7] an excellent overview about the definition of the ductility factor R_{μ} is reported in Miranda E. et al.[3.8]. In detail such paper gives the basic definition of the strength reduction factor and reports the specific elements with influence on its value. The factor R_{μ} depends firstly on the ductility of the structure but it is also influenced by the principal elastic period of the structure and by the soil type. The most common relationship between the strength reduction factor R_{μ} and the principal elastic periods of the structure is given by Vidic et al.[3.9]. Otherwise the influence of the soil type over the strength reduction factor is given by Miranda E. et al.[3.8].

The definition of the strength reduction factor R_{μ} given by Fajfar P. [3.7] for a Single Degree Of Freedom system summarized in the following Eq. 3.2 and Eq. 3.3:

$$R_{\mu} = (\mu-1) T/T_0 + 1 \quad \text{if } T < T_0 \quad \text{Eq. 3.2}$$

$$R_{\mu} = \mu \quad \text{if } T > T_0 \quad \text{Eq. 3.3}$$

In the previous equation μ is the ductility of the system defined as the ratio between the maximum displacement and the yielding displacement (see Fig. 3.1), T is the principal elastic period of the structure and T_0 is the transition period for which the constant acceleration part of the response spectrum transforms to the constant velocity portion of the spectrum. Generally the transition period T_0 is fixed equal to T_c [3.7].

Research on the performance of buildings exposed to severe earthquakes indicated that structural overstrength plays a very important role in protecting buildings from collapse. According to [3.10]

the overstrength factor (Ω_d) may be defined as the ratio of the actual to the design lateral strength of the structure according to the following Eq. 3.4:

$$\Omega_d = V_y / V_d \tag{Eq. 3.4}$$

The component of the ratio are depicted in Fig. 3.1 and termed the ‘observed’ overstrength factor.

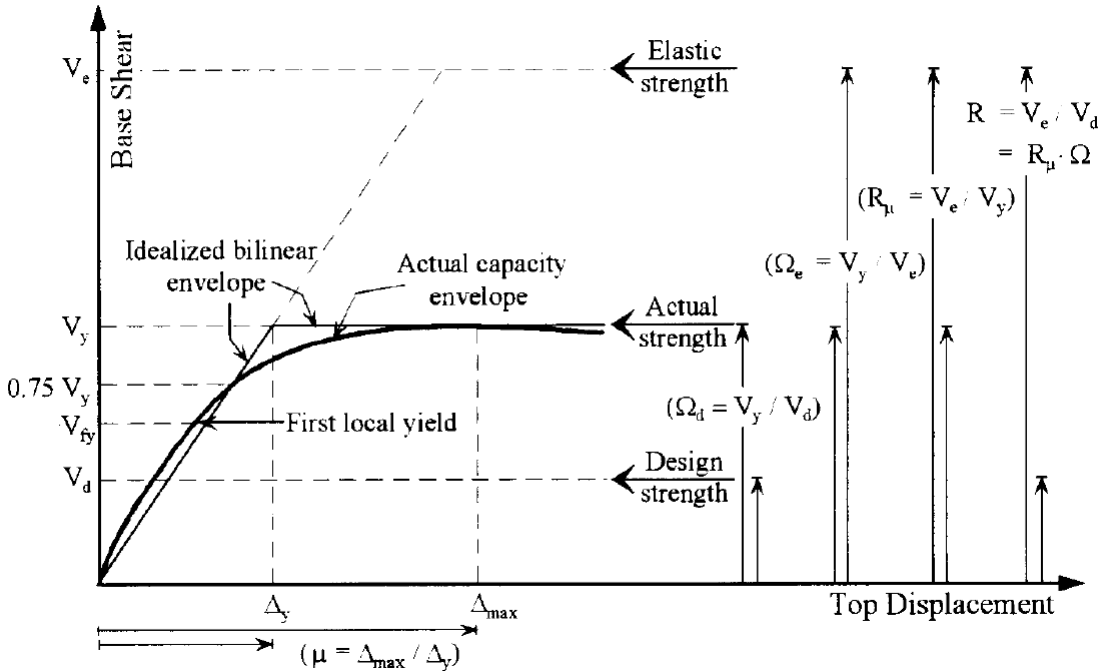


Fig. 3.1 – Relationships between the force reduction factor, R , structural overstrength, Ω , and the ductility reduction factor, R_μ [3.10]

According to [3.10] quantification of the actual overstrength can be employed to reduce the forces used in the design, hence leading to more economical structures. The main sources of overstrength are reviewed in studies performed by Uang [3.11], Mitchell and Paulter [3.12], Humar and Ragozar [3.13] and Park [3.14]. These studies focus on the difference between the actual and the design material strength; the conservatism of the design procedure and ductility requirements [3.11] and [3.13]. Furthermore the effects of the participation of nonstructural elements and of structural elements not considered in predicting the lateral load capacity are taken into account [3.12]. Finally these studies give some insight about the structural redundancy, the strain hardening and the use of the elastic period to obtain the design forces [3.14].

The results of researches reported above are implemented into the currently seismic codes such as Eurocode 8 [3.1], FEMA [3.15] etc... In detail the definition of the q -factor used in the Eurocode 8 [3.1] takes into account the effects of the overstrength ratio according the following Eq. 3.5

$$q = q' \Omega \tag{Eq. 3.5}$$

Where q' represent a basic value of the q -factor, dependent on the type of structural system and its regularity, while Ω represents a general overstrength factor.

The factor q' substantially gives the reduction of the forces obtained from a linear-elastic analysis, in order to account for the non-linear response of a structure [3.1]. In addition this factor q' takes

into account the effects of the plant and high regularity on the dissipative capacity of the building. in EC8 [3.1] this dependence is explained by a specific relation as the following Eq. 3.6

$$q' = K_R q_0 \quad \text{Eq. 3.6}$$

where the coefficient $K_R \leq 1$ takes into account the effects of the building regularity and decreases with the increasing of the building irregularity [3.1].

In a design situation governed by seismic strength demand, the considered overstrength Ω is equivalent to the α_u/α_1 factor defined by EC8 [3.1]. According to the notation reported in Fig. 3.1 α_1 is the multiplicative factor of the seismic design action leading to the first yield in whatever structural member ($V_{f,y}$), and α_u is the multiplicative factor of the seismic design action leading to the failure mechanism of the structure (V_y), while keeping constant all other loads.

A proper definition of these parameters represents a fundamental issue for a suitable seismic design of the building using the FMD method [3.3]. Generally these parameters are well defined by the standards for the more common building systems using traditional material such as steel, R.C. and masonry.

3.2 Overview on timber constructive system q-factor

Wood has been used for a long time to realize roof or floor elements supported by steel or R.C. structure suitably braced against the horizontal forces (i.e. wind and earthquake). The seismic design of these kinds of structure focuses on the vertical and bracing steel or R.C. elements, considering the wooden part only as a structural mass [3.16].

In the last years it has become more and more common the utilization of timber to realize whole seismic resistant structures, therefore a proper seismic design became necessary. According to [3.16] the seismic codes have adapted their provisions to the new technologies but the seismic design of timber structure is not as well detailed as the other more common materials yet.

3.2.1 Q-factor for timber buildings

The reference seismic code for timber structure in European area is the Eurocode 8 [3.1] which gives the guide-lines for all the other national standards. According to Fragiaco et al. [3.17] such timber section focuses on two different issues for a proper seismic design of wooden structure. The 1st issue is about the general rules to ensure an adequate ductility level to the structure while the 2nd one give some indication about the dissipative capacity of the structural typologies and therefore about the most suitable behaviour q-factor [3.1].

Regarding to the ductility the importance of a proper design of the dissipative zones is well highlighted and some specific indications about the wood elements and the fasteners characteristics are given. According to these general ductility criteria it is possible to define three different ductility classes for timber structures: Low Ductility Class (DCL), Medium Ductility Class (DMC) and High Ductility Class (DHC).

If a structure is designed so that it remains in the linear elastic field under earthquake loading and plastic behaviour is not taken into account, it should be assigned to ductility class “DCL” according to Eurocode 8 [3.1]. Structures in this ductility class are structures without or with only a few joints with mechanical fasteners, like cantilevers, beams, arches with two or three pinned joints or trusses joined with connectors. For these structures behaviour factor q cannot exceed $q = 1.5$.

As reported in [3.18] structures can resist stronger earthquakes if the capability of plastic deformations is taken into account. In the design concept “dissipative structural behaviour”, “...the capability of parts of the structure (dissipative zones) to resist earthquake actions above their elastic range is taken into account”. Then “... the behaviour factor q may be taken as being greater than 1.5” (Eurocode 8 [3.1]). In the design concept “Medium capacity to dissipate energy” (Ductility class DCM) e.g. glued wall panels with glued diaphragms, connected with nails and bolts; Mixed structures consisting of timber framing (resisting the horizontal forces) and non-load bearing infill should be assigned. Then a behaviour factor $q = 2$ should be used.

For hyperstatic portal frames with dowelled and bolted joints $q = 2.5$ should be used. Using design concept “High capacity to dissipate energy” (Ductility class DCH), a behaviour factor $q = 3$ should be used for nailed wall panels with glued diaphragms connected with nails and bolts and for trusses with nailed joints. In the same design concept and ductility class are also classified hyperstatic portal frames with doveled and bolted joints for these a behaviour factor $q = 4$ can be assigned. Using the same design concept and ductility class the maximum value $q = 5$ can be adopted for buildings with nailed wall panels with nailed diaphragms connected with nails and bolts.

The q -factors proposed to each building typology are summarized in the prospect 8.1 reported in the following Fig. 3.2.

Table 8.1: Design concept, Structural types and upper limit values of the behaviour factors for the three ductility classes.

Design concept and ductility class	q	Examples of structures
Low capacity to dissipate energy - DCL	1,5	Cantilevers; Beams; Arches with two or three pinned joints; Trusses joined with connectors.
Medium capacity to dissipate energy - DCM	2	Glued wall panels with glued diaphragms, connected with nails and bolts; Trusses with doveled and bolted joints; Mixed structures consisting of timber framing (resisting the horizontal forces) and non-load bearing infill.
	2,5	Hyperstatic portal frames with doveled and bolted joints (see 8.1.3(3)P).
High capacity to dissipate energy - DCH	3	Nailed wall panels with glued diaphragms, connected with nails and bolts; Trusses with nailed joints.
	4	Hyperstatic portal frames with doveled and bolted joints (see 8.1.3(3)P).
	5	Nailed wall panels with nailed diaphragms, connected with nails and bolts.

Fig. 3.2 – Q-factor values for each ductility class and for each building typology according to EC8 [3.1]

It has to be remarked that differently from the other structural typologies the definition of the dissipative capacity for the timber structures is given independently the overstrength factor (i.e. α_u/α_1 ratio [3.1]).

Furthermore the current standards define the dissipative capacity of the more common timber building systems but no indications are given about the recently devised innovative building systems made with solid wood (e.g. CLT structure) or heavy frame structures.

As described in [3.18] the dissipative capacity of these innovative wooden structures should be verified by means of cyclic tests carried out according to the available test protocol and results interpretation (e.g. EN 594 [3.19], EN 12512 [3.20] and ISO standard 16670 [3.21]) but no standard procedure for a suitable definition of the most reliable behaviour q-factor able to take into account the main geometrical and mechanical building characteristics is provided.

3.3 Basic procedure for q-factor evaluation

A proper definition of the most suitable q behaviour factor for the available timber building systems is a fundamental issue of the codes for structural seismic design. According to [3.22] currently the q-factor is mainly evaluate by means of experimental methods based on quasi static tests on single wall specimens or on entire building shaking table tests. As reported in [3.22] another procedure that can be used for the q-factor evaluation is based on numerical methods.

The standard experimental and numerical methods for the q-factor evaluation are summarized in the following scheme (Fig. 3.3).

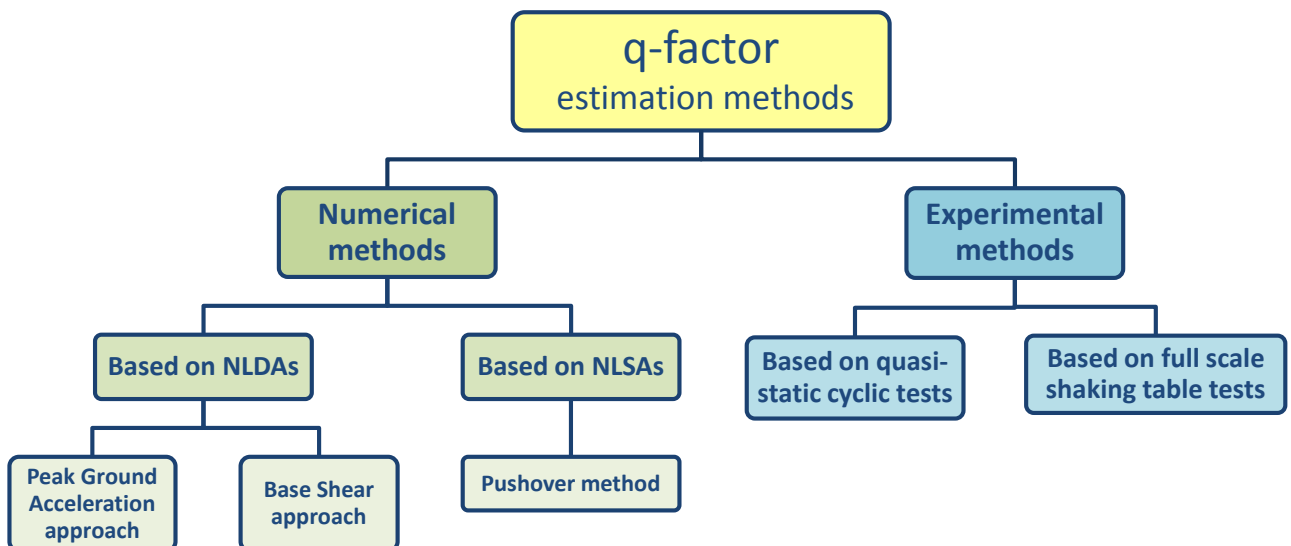


Fig. 3.3 - Scheme of the actual method for the building system q-factor evaluation.

Below are reported the main features and the theoretical approaches of these standard experimental or numerical methods used for the q-factor evaluation.

3.3.1 Conventional methods based on experimental tests

As described in the previous chapter 1, timber building systems show specific pinching like behaviour due to the assembling of wooden elements by means of mechanical connectors. According to Ceccotti [3.16] the definition of the hysteresis behaviour is very complex and can't be based only on the code provisions but experimental tests are necessary.

These experimental tests can be performed to define the hysteresis behaviour of the single fasteners use to assembling the wooden elements. These tests ensure a complete definition of the behaviour of single connectors but give no information on the global response of the construction system. In order to obtain a more accurate definition of the hysteresis behaviour of the building system, cyclic tests on entire wall specimens should to be performed. These experimental cyclic tests are generally carried out respecting the EN 12512 [3.21] provisions and allow to define the following characteristic features: ductility ratio, strength degradation at each ductility levels, equivalent viscous damping.

In the last years the construction of increasing biggest and powerful shaking tables has allowed to carry out shaking test on full scale multi-storeys buildings. The most representative full scale tests on timber buildings are those conducted in Japan on a three [3.23] and on a seven storeys [3.24] CLT buildings (SOFIE research project) and that conducted in Canada on a six storeys wood frame building [3.25] (NEES Wood research project). The shaking table tests define the dynamic response of an entire building under earthquake.

According to Ceccotti et al.[3.22] both the quasi-static tests on single wall specimen and the dynamic tests on entire building allow to obtain an estimation of the q-factor as defined below.

3.3.1.1 Q-factor definition by means of quasi-static cyclic tests

A first attempt to define the behaviour q-factor was related to the concept of static ductility as the ratio of ultimate displacement over yield displacement. In EC8 [3.1], construction typologies are assigned to ductility classes. Three ductility classes exist: Low Ductility Class with a correspondent upper limit value of $q=1.5$; Medium Ductility Class with a correspondent upper limit value of $q=2.5$; High Ductility Class with a correspondent upper limit value of $q=5$.

The three different classes must fulfill certain requirements of static ductility ratio in order to ensure that the given q-factors may be used. For instance, in Medium Ductility Class: "the dissipative zones shall be able to deform plastically for at least three fully reversed cycles at a static ductility ratio of 4" [3.1]. Otherwise in High Ductility Class, "the dissipative zones shall be able to deform plastically for at least three fully reversed cycles at a static ductility ratio of 6" [3.1]. For both the ductility classes the strength degradation between first and third cycles should not exceed 20%.

However, this concept is difficult to use in timber constructions as typical load-displacement curves do not present a well-defined yield point. As an example Fig. 3.4 reports the typical load slip curve of a shearwall and the correspondent ductility levels evaluated according different bi-linearization criteria (EN 12512 [3.21]; and Equivalent Energy Strain Approach [3.26])

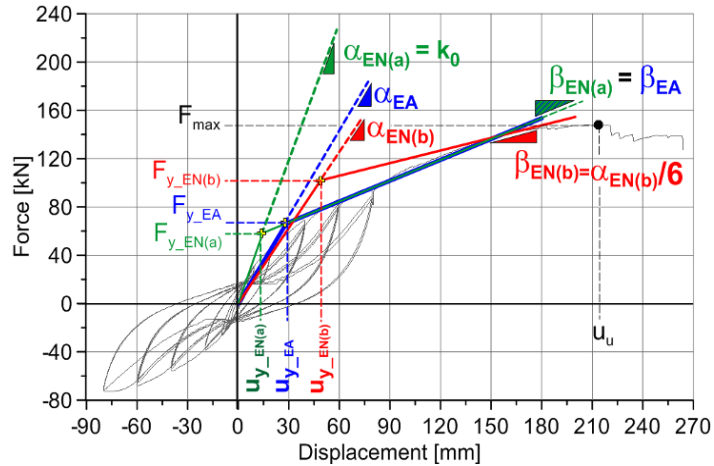


Fig. 3.4 – Shearwall load-slip curve and correspondent ductility levels - EN_a (b) stands for EN12512 a (b) approach while E.A. stands for Equivalent Energy Strain Approach [3.26]

As shown in Fig. 3.4 there is a substantial variability between the yielding limits defined by the different bi-linearization criteria. As the ductility concept is very sensitive to the location of the yield point, the troubles deriving from the uncertainty in its definition are evident. Finally it should be pointed out that this procedure only allow to define the belonging of the investigated building system to a specific ductility class characterized by a q-factor range, but the exact definition of the q-values is not possible.

3.3.1.2 Q-factor definition by means of shaking table test

This method is based on an extensive experimental program setting up with full-scale earthquake tests. As reported in [3.1] and [3.23] this approach involves the following steps:

- design the building with $q=1$ (elastic) and a chosen PGA_{design} value according to the available seismic code (e.g. EC8-1 [3.1]) . According to this design criteria the PGA_{design} corresponds to the PGA that leads the structure to the achievement of the 1st yielding of the structure;
- undertake full-scale shaking table tests on the building increasing the seismic intensity until a previously defined near-collapse criterion is reached;
- note the $PGA_{near\ collapse}$ value for which the near-collapse state is reached during the test;
- evaluate q_{test} as the ratio $PGA_{near\ collapse}$ over PGA_{design} ;
- q_{test} is the experimentally established behaviour factor q.

The thusly established behaviour factor q is only valid for the tested building and the chosen earthquakes. Furthermore the q-factor values is strictly dependent on the seismic code used to design the case study building and therefore to establish the PGA_{design} . In order to generalize the q-factor, more tests on different buildings (same construction technology, different geometry and masses) using different earthquakes should be done. This of course is very costly and time-consuming and rather a theoretical approach as it is not practicable.

3.3.2 Conventional methods based on numerical simulations

According to [3.1] instead of undertaking full scale shaking tests, numerical model of buildings can be used to establish their behaviour when subjected to earthquake loading. The main requirement for the applicability of this method is the availability of a numerical model suitable for reproducing the seismic response of an entire case study building.

As reported in the previous chapter 1 the modeling can take place at many different levels; each level requiring test results as input parameters. As reported in [3.1] the 1st model degree is at “material level”, then material tests must be undertaken to establish the mechanical properties necessary for numerical modeling. This may include material tests on timber and on fasteners. Example of this specific kind of model is that proposed by Foschi [3.27]. The 2nd hierarchical model degree is starting at the scale of “structural element level” (e.g. complete wall specimens). The majority of the hysteresis models used to investigate the response of timber buildings refer to this modeling level (e.g. Dolan model [3.28], CUREE model [3.29] etc..).

However, due to computational limitations, whole buildings can hardly be modeled starting at “material level”. More simplified models, such as wall-level models, calibrated on connection and element tests are more promising. Therefore, the most profitable approach seems to be that with higher-level element testing such as cyclic testing (for instance according to EN 12512 [3.21]) of wall elements combined with numerical modeling using the test results as input parameters for complete building models.

Testing is necessary to establish system properties under fully-reversed cyclic loading. The complex loading conditions typical of an earthquake are thus simplified using cyclic loading protocols. A number of simplified numerical models of entire building validated on the output of experimental cyclic tests on wall specimens are reported in this thesis work and e.g. in [3.18], [3.22] and [3.23].

Once provided the suitable model the numerical procedure based on the following steps:

- choice of a representative case study building;
- design of the building with $q=1$ (elastic) and a chosen PGA_{design} value according to the available seismic code (e.g. EC8-1 [3.1]). As states for the experimental approach based on shaking table tests the PGA_{design} corresponds to the PGA that leads the structure to the achievement of the 1st yielding of the structure;
- building modeling using test results as input parameters;
- execution of NonLinear Dynamic or Static Analyses to define the seismic response of the building.

The seismic response carried out with the nonlinear analyses allows assessing the most reliable q -factor of the investigated case study building. Two different independent procedures can be performed to define the q -factor: the 1st one based on the output from the NLDAs, the 2nd one on the building load-displacement curve obtained by means of NLSAs. Below the main features of these two procedures are described.

3.3.2.1 Q-factor definition by means of NLDAs

The definition of the building seismic response using NonLinear Dynamic Analyses appear to be the most performing and suitable for timber structures because it is independent from the yielding limit definition and refers only to the 1st yielding condition (defined by PGA_{design}) and to the ultimate condition (defined by $PGA_{near\ collapse}$) respectively for an elastic and an inelastic response.

According to [3.16] the NLDAs allow to define both the global building response and the local response of each fasteners or wood elements. The global building response involves the storey displacements and shears while the local response is based on the hysteresis cycle of each fastener. The capability to faithfully reproduce the hysteretic response of each fastener allows catching also the dissipated energy during the shakes. The energy dissipation capacity joined to the concept of ductility is a basic aspect of seismic design.

It should be noted that the dissipative and displacement capacity of the building are strictly connected with the damping coefficient because the numerical models are sensitive to the assumed damping rate. However damping is difficult to evaluate on a global scale, usually a viscous damping in the range between 2% to 5% is estimated [3.22].

A further parameter that affects the building seismic response is the choice of earthquakes. According to [3.22] in order to represent one specific seismic region, geologically possible earthquakes for this seismic region should be chosen. This may include the use of artificially generated earthquakes. Furthermore, in order to generalize the building seismic behaviour, a large variety of earthquakes must be selected and their frequency content has to cover a broad range.

Regarding to the usage of the dynamic building response for the q-factor evaluation two different procedures can be used. The first one is based on a PGA approach while the second one on a Base Shear one. Both the procedures start with the definition of a conventional near collapse condition of the building. Some notes about the choice of the most suitable “near collapse” condition are reported in the following paragraph 3.3.3.

Once define the near collapse condition a series of NLDAs are performed with growing levels of PGA starting from the design condition to the near collapse one. The outputs from the dynamic analyses at each levels of PGA represent the input parameters for the q-factor evaluation as described below.

3.3.2.1.1 PGA-based approach

The Peak Ground Acceleration approach is strictly similar to that used to define the q-factor from the output of the shaking table tests. In fact it refers to the PGA values used for the elastic seismic design of the building (i.e. PGA_{design}) and that one for which it is effectively achieved the near collapse condition (i.e. $PGA_{near\ collapse}$). In the previously defined experimental method the $PGA_{near\ collapse}$ is obtained by shaking table tests while in the numerical one by means of nonlinear analyses performed on the numerical building models. The q-factor is then defined as the ratio between the $PGA_{near\ collapse}$ and the PGA_{design} according to the following Eq. 3.7.

$$q = PGA_{near\ collapse} / PGA_{design} \quad \text{Eq. 3.7}$$

According to [3.7] such definition of the reduction factor q already includes the overstrength corrective factor, defined as the factor between the actual strength to the design strength of the structure.

The main limitation of this approach is that it is based on the hypothesis that the building reaches its first yielding condition under the PGA_{design} and it is constantly independent of the earthquake frequency content. While the near-collapse PGA, determined through a nonlinear analysis, is function of the vibration period and of specific earthquake time history.

The yielding PGA could be defined with a series of nonlinear analyses once the yield condition is reached, but in reality there is no a universally acknowledged definition for first yield condition for an entire building in dynamic conditions. Even in quasi static pushover analyses the yielding condition depends on the criteria used for bi-linearization of the performance curve which is not univocally defined.

Furthermore this q -factor definition is code dependent because it represents a conventional q -value based on the building seismic design according to a specific seismic code.

3.3.2.1.2 BASE SHEAR-based approach

Due to such drawbacks of PGA-based method, an alternative Base Shear-based method can also be used to define the most suitable q -factor using NLDAs results. This method refers to the formulation in terms of forces and defines the ductility factor q' (see Fig. 3.1) as the ratio of the Base Shear obtained from a dynamic linear elastic response of the structure and the base shear obtained from a nonlinear one, using the same earthquake scaled up to $PGA_{near\ collapse}$ according to the following Eq. 3.8.

$$q' = V_{u-elastic} / V_{u-inelastic} \quad \text{Eq. 3.8}$$

Despite it requires higher computational efforts, this second approach proved to be more consistent since both the linear and nonlinear dynamic analyses conducted to obtain the respective shear values take into account in a common way the earthquake frequency content in relation with the building characteristics. Furthermore this q -factor definition is code independent because refers to the actual elastic and inelastic building response and do not need the definition of a conventional yielding limit.

It should be pointed out that this procedure doesn't provide the actual q -factor but only the q' -value (i.e. q -factor ratio due to the ductility [3.7], see Eq. 3.5). No indications are given about the overstrength ratio Ω_d . Based on these considerations the Base Shear approach provide the actual q -factor only when the 1st yielding condition matches with the failure condition, i.e. $\Omega_d = 1$.

3.3.2.2 q -factor definition by means of NLSAs

A proper application of the pushover method [3.7] allows defining the maximum earthquake compatible with the displacement capacity of the building obtained by means of NLDAs. Then the q -factor can be defined as the ratio between the maximum compatible earthquake and the design one according to Fig. 3.5.

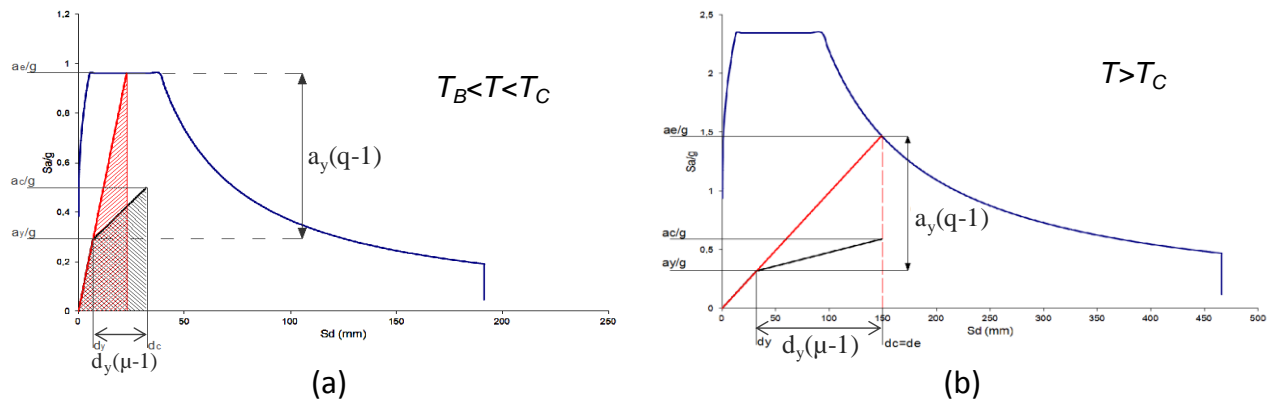


Fig. 3.5 – Q-factor definition according to the pushover procedure [3.30].

The pushover procedure defined by Fajfar [3.30] with the so called N2 method is specific for an elastic perfectly plastic bi-linearization of the behaviour of the building. Timber buildings generally present an hardening post elastic behaviour therefore the procedure described in Albanesi et al.[3.31] for hardening system appears to be more suitable to investigate wooden structures.

The definition of the q-factor using the pushover procedure can be affected by the bi-linearization criteria used to switch from the actual building pushover curve to the equivalent bi-linear curve. It should be noted that the bi-linearization procedure affects mainly the elastic branch of the pushover curve and therefore only the elastic period while the displacement capacity is not affected by the bi-linearization criteria. Perhaps normally timber buildings presents a principal elastic period in the plateau range of the elastic plateau range (see Fig. 3.5 a) therefore the dependency of the elastic stiffness on the bi-linearization procedure doesn't affect significantly the q-factor estimation. As a final remark, the q-factor defined according to the pushover procedure is coherent to that obtained to the PGA approach because both definitions are based on the design earthquake.

3.3.2.3 Summary of numerical methods

The numerical methods defined above provide efficient and reliable procedures for the estimation of the q-factor value. Below are reported some general remark about the various procedures pointing out their applicability limits.

- The reliability of the numerical procedures is strongly dependent on the capacity of the numerical model to faithfully reproduce the seismic response of the building. The choice of an adequate and effective model is a crucial aspect. Its accuracy has to be enough to account for the phenomena really affecting the seismic performance of the building without leading to excessively onerous numerical efforts. Furthermore an accurate calibration of the numerical model coherent with the selected experimental results is necessary.
- The obtained q-factor values are only valid for the specific case study building. It is not possible to extend and generalize the obtained results to the building system because the q-factor is strongly affected by the geometrical building characteristic such as slenderness, plan and elevation regularity etc..
- The numerical approach based on the pushover procedure seems to be less expensive in computational terms. Its applicability is strictly connected with the possibility to represent the global building response through its pushover curve.

- A combined application of the PGA based approach and of the Base Shear one allows the estimation of the overstrength factor Ω_d .

A systematic and repeated use of numerical methods for the analysis of different configurations (made with the same construction technology but having different geometries and masses) with the aim to obtain a general comprehensive definition of the q-factor values for a specific building system (not that of the single building) is applied in this thesis work.

3.3.3 Comments about the “near collapse” condition

The experimental methods based on shaking tests and the numerical methods based on the use of NLDAs refers to the so called “near collapse” condition to define the most suitable q-factor of the investigated structure. According to Ceccotti [3.1] this “near collapse” condition defines the abort criterion for the tests or for the numerical simulations.

The fundamental requirement for structures in seismic regions according to Eurocode 8 [3.1] is the no-collapse requirement. According to [3.1] “the structure shall be designed and constructed to withstand the design seismic action [...] without local or global collapse, thus retaining its structural integrity and a residual load-carrying capacity after the seismic events.

Based on these recommendations and according to [3.18] the “near collapse” condition is not representative of the effective collapse of the structure but it should be defined as the condition that ensure a residual strength and stiffness despite of a certain acceptable structural damage level. For timber buildings the definition of the near collapse condition is not unique because it is dependent on the constructive system. Generally this failure condition match with the collapse of connectors previously defined by means of experimental tests. Several researches on the seismic behaviour of timber structures have been carried out in order to define the most suitable near collapse condition.

As reported in [3.23] for solid CLT shearwall the near collapse condition can be defined as the failure of the connection elements (i.e. holdown and steel angle) used to join the structural CLT panels at the base and at the inter-storeys. The failure of a connection is seen as the achievement of a limit slip of the joint to be defined by means of experimental tests. As an example Ceccotti [3.23] suggested a maximum uplift of the base holdown of about 25mm. In traditional Platform Frame structures the most suitable near collapse condition normally is related to a maximum allowable inter storey drift. Shädle [3.18] proposed a maximum inter-storey drift equal to 2.5% of the storey height.

3.4 Conclusions

The growing spread of the use of timber structures also in seismic regions, has led to the development of numerous innovative construction systems based on solid wall (CLT) or framed (platform frame and heavy frame) techniques. Despite this relevant development of timber building systems a lack of regulations in seismic field remains, in particular concerning the q-factor to be used for their seismic design.

Available seismic codes provide the q-factor only for the standard building typologies and refers to the outcomes from specific experimental cyclic tests to give an estimation of the ductility class and therefore of the most suitable q-factor range. According to Ceccotti et al.[3.22] the urge of developing proposals for an effective procedure for the q-factor evaluation became more and more important

From the research point of view there are substantially two different methods for the q-factor evaluation: the experimental and the numerical methods. Both these methods can provide a more accurate q-factor evaluation respect to the code provisions but both of them present some drawbacks. High costs, high time-consuming, and hardly replay the first; numerical difficulties and high computational effort the second. It has to be stressed that the estimation of the q-factor cannot be limited to that single specific building, but has to be generalized to entire constructive system. To this aim numerical methods are surely more appropriate, but experimental tests are necessary for the preliminary validation of numerical models.

References – Chapter 3

- [3.1] European Committee for Standardization (CEN). Eurocode 8 - design of structures for earthquake resistance, part 1: General rules, seismic actions and rules for buildings. 2004.
- [3.2] Italian Ministry for the Infrastructures. New technical regulation for construction. Decree of the Ministry for the Infrastructures, Ministry of Interior, and Department of the Civil Defence. 2008.
- [3.3] Chopra AK. Dynamics of structures—theory and applications to earthquake engineering. Upper Saddle River: NJ: Prentice Hall; 1995.
- [3.4] European committee for standardization (CEN). ENV 1992-1-1 Eurocode 2 - Design of concrete structures Part 1-1: General rules and rules for building. 2004
- [3.5] European committee for standardization (CEN). ENV 1993-1-1 Eurocode 3 – Design of steel structures Part 1-1: General rules and rules for building. 2005
- [3.6] European committee for standardization (CEN). ENV 1995-1-1 Eurocode 5 – design of timber structures – part 1-1: general rules and rules for buildings. 2009.
- [3.7] Fajfar P. Design spectra for new generation of code. Proceeding 11th World Conference on Earthquake Engineering, Acapulco, Mexico, 1996, paper No. 2127.
- [3.8] E. Miranda and V. V. Bertero, 'Evaluation of strength reduction factors for earthquake resistant design', *Earthquake Spectra* 10, 357-379 (1994).
- [3.9] T. Vidic, P. Fajfar and M. Fischinger, 'Consistent inelastic design spectra: strength and displacement', *Earthquake Engng. Struct. Dyn.* 23, 502-521 (1994).
- [3.10] Elnashai, S. and Mwafy, A. M., (2002), 'Overstrength and force reduction factors of multi-storey reinforced-concrete buildings' *Struct. Design Tall Build.* 11, 329–351 (2002) DOI:10.1002/tal.204
- [3.11] Uang CM. 1991. Establishing R (or R_w) and C_d factors for building seismic provisions. *ASCE* 117(1): 19–28.
- [3.12] Mitchell D, Paulter P. 1994. Ductility and overstrength in seismic design of reinforced concrete structures. *Canadian Journal of Civil Engineering* 21: 1049–1060.
- [3.13] Humar JL, Ragozar MA. 1996. Concept of overstrength in seismic design. In *Proceedings 11th WCEE. IAEE, Acapulco, Mexico. Paper 639.*
- [3.14] Park R. 1996. Explicit incorporation of element and structure overstrength in the design process. In *Proceedings 11th WCEE. IAEE, Acapulco, Mexico. Paper 2130.*
- [3.15] FEMA (Federal Emergency Management Agency). 1997. NEHRP provisions for the seismic rehabilitation of buildings. Report FEMA 273 (Guidelines) and 274 (Commentary). FEMA, Washington, DC.
- [3.16] Ceccotti A., Follesa M., Lauriola M.P. 2007. "Le strutture di legno in zona sismica 2^a edizione" ISBN: 9788879922418
- [3.17] Fragiaco M, Dujic B, Sustersic I. Elastic and ductile design of multi-storey crosslam wooden buildings under seismic actions. *Engineering Structures* 33, 2011, 3043-3053.
- [3.18] Schädle, P., Hans Joachim Blaß, H.J., (2010) "Earthquake behaviour of modern timber construction systems" *Proceeding of the 11th World Conference on Timber Engineering WCTE 2010. Riva del Garda, Italy, June 20–24, 2010, CD.*

- [3.19] EN 594, 1996. *Timber Structures – Test methods – Racking strength and stiffness of timber frame wall panels.*
- [3.20] EN 12512, 2001. *Timber Structures – Test methods – Cyclic testing of joints made with mechanical fasteners.*
- [3.21] ISO Standard 16670, 2003. *Timber Structures – Joints made with mechanical fasteners – Quasi-static reversed-cyclic test method.*
- [3.22] Ceccotti A., Sandhaas C. *A proposal for a standard procedure to establish the seismic behaviour factor q of timber buildings. Proceeding of the 11th World Conference on Timber Engineering WCTE 2010. Riva del Garda, Italy, June 20–24, 2010, CD*
- [3.23] Ceccotti A. *New technologies for construction of medium-rise buildings in seismic regions: the XLAM case. IABSE Struct Eng Internat 2008;18:156–65. Tall Timber Buildings (special ed.).*
- [3.24] Dujic B, Strus K, Zarnic R, Ceccotti A. *Prediction of dynamic response of a 7-storey massive XLam wooden building tested on a shaking table. World Conference on Timber Engineering WCTE 2010. Riva del Garda, Italy, June 20–24, 2010, CD.*
- [3.25] Pei, S., van de Lindt, J.W., Pryor, S.E., Shimizu, H., and Isoda, H. 2010. *Seismic testing of a full-scale sixstory light-frame wood building: NEESWood Capstone test. NEESWood Report NW-04.*
- [3.26] Pozza L., Scotta R., Polastri A, Ceccotti A. 2012. *Seismic behaviour of wood concrete frame shear-wall system and comparison with code provisions. Meeting 45 of the Working Commission W18-Timber Structures, CIB. Växjö, Sveden, 2012, paper CIB-W18/45-15-2.*
- [3.27] Foschi, R. O., (1977) “Analyses of wood diaphragms and trusses. Part I: diaphragms.” *Canadian J. Civ. Engrg.*, 4(3), 345-352 Foschi, R. O., (1977) “analyses of wood diaphragms and trusses. Part I: diaphragms.” *Canadian J. Civ. Engrg.*, 4(3), 345-352
- [3.28] Dolan, J.D. (1991). “A numerical model to predict the dynamic response of timber shear walls.” *Proc., Int. timber Engrg. Conf.*, Vol. 4, 267-274
- [3.29] Folz, B., and Filiatrault, A. F., (2001). “Cyclic analysis of wood shear walls.” *Journal of Structural Engineering, American Society of Civil Engineers*, Vol. 127, No. 4, 433-441.
- [3.30] P. Fajfar and P. Gaspersic, “The N2 method for the seismic damage analysis for RC buildings’, *Earthquake Engng. Struct. Dyn.* 25, 23-67 (1996)
- [3.31] Albanesi, T., Nuti, C., Vanzi, I. (2002). “State of the art of non linear static methods,” *Proc. of the 12th European Conf. on Earthquake Engrg.*, London, United Kingdom, Paper. 602, Oxford: Elsevier Science.

Chapter 4 – Proposal and validation of a procedure for the q-factor estimation of timber buildings

Abstract

This chapter proposes a new procedure for the q-factor evaluation based on a proper application of the pushover method to the load-displacement curve obtained by means of experimental quasi static test on representative wall specimens. The theoretical aspects of the developed analytical-experimental method are reported and the main advantages and limitations are presented and critically discussed.

The new developed procedure is validated in comparison with the q-factor estimation by means of full scale shaking table tests and numerical simulations of a CLT building.

An extensively utilization of the proposed procedure to a number of different wooden building system tested at the CNR IVALSA laboratory (TN) is presented to obtain a reliable estimation of their q-factors. It results out that the criteria adopted for the definition of the yielding limit could largely affect relevant variability of the q factor value. Some considerations about this issue are given and the most suitable procedure for the bi-linearization of the load-displacement curve is assessed.

4.1 Introduction

The traditional experimental and numerical methods described in the previous chapter allow an accurate q-factor evaluation but at the same time demand for high time-consuming, high computational effort and of course are very expensive.

As highlight by Ceccotti et al.[4.1] the urge of developing proposals for the q-factor evaluation became more and more important.

In this chapter a newel developed innovative approach for expeditious q-factor estimation is presented. It is based on a suitable analytical interpretation based on the well-known and universally accepted pushover procedure, of the load-displacement capacity curve obtained from quasi-static monotonic or cyclic test performed on representative wall specimens.

4.2 Description of the analytical-experimental proposal

The conventional procedures for the q-factor evaluation show some critical aspects such as high time-consuming, high computational effort and high economical costs. Due to these drawbacks a more expeditious and less costly procedure for the q-factor evaluation has been developed in this work.

Such innovative procedure is a mixed analytical-experimental method based on the direct application of the pushover procedure to the capacity curve carried out by means of quasi-static experimental tests on representative wall elements. This innovative procedure considers a representative wall specimen as a Single Degree Of Freedom system.

The main step of this new developed procedure are depicted in Fig. 4.1 and listed as follow:

- choice of a wall element representative of the investigated building system;
- execution of a quasi-static pushover test under constant vertical load applied to the top of wall to obtain the capacity curve, that is the plot of the applied shear load versus the horizontal top displacement of the wall;
- schematization of the wall as a SDOF system characterized by its capacity curve and mass corresponding to the constant vertical load applied during the push-over test;
- bi-linearization of the capacity curve with consequent definition of the yielding limit and therefore of the elastic stiffness and ductility [4.2];
- application of the pushover method to define the maximum earthquake spectra compatible with the displacement capacity of the wall (ultimate spectra) [4.3];
- definition of the q-factor as the ratio between the PGAs of ultimate spectra and the yielding spectra [4.3].

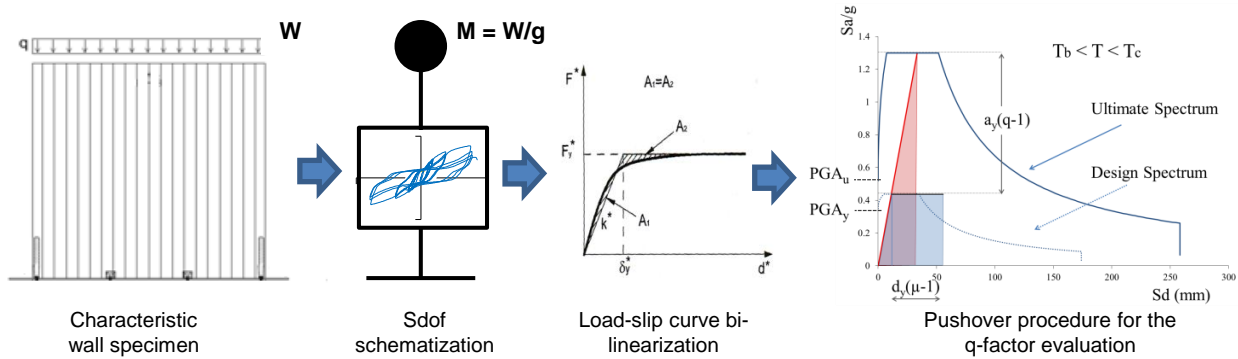


Fig. 4.1 - Main steps of the new developed procedure.

The choice of a wall element representative of the timber building system is a crucial aspect for a proper estimation of the suitable q -factor. This choice should satisfy the following criteria:

- height and more in general geometrical dimension strictly similar to those effective used in the building structure;
- fasteners typology and arrangement as in the typical construction methodology used for composing entire buildings;
- applied constant vertical load of the same magnitude of that due to the floors and roof dead and live loads in reality.

Only respecting these criteria for the choice of the wall specimen the q -factor obtained with the developed procedure can be assumed as the representative value of the building system and can be used for the seismic design.

A further relevant aspect of the developed procedure is the execution of the experimental tests in order to obtain the capacity curve of the wall. This capacity curve can be carried out directly by means of a monotonic ramp test performed e.g. according to the EN 594 [4.4] test protocol. Otherwise the capacity curve can be defined as the envelope of the hysteresis curve carried out with a cyclic test performed e.g. according to the EN 12512 [4.5] test protocol. The envelope curve can be defined as example using the analytical formulation proposed by Foschi [4.6] so as to fit the trend defined by each first load-slip cycle.

As stated for the pushover method also the result from the proposed procedure is dependent on the criteria used for the bi-linearization of the capacity curve. An extensive dissertation about this issue and its effect on the building ductility and q -factor value is given in the next paragraph 4.3.

Finally the application of the pushover method should respect the general rules defined by Fajfar et al.[4.7] for Elastic Perfectly Plastic system and by Albanesi et al.[4.8] for Elasto Plastic Hardening system. As described in the previous paragraph 3.3.2.2 the definition of the q -factor using the pushover method provides values already including the overstrength effect Ω_d [4.3] of the wall.

Based on these remarks it is possible to affirm that the newly developed method provides a reasonable estimation of the q -factor value although it is specific of the considered wall configuration and affected by the same drawback previously defined for the numerical methods. However this procedure results more expeditious, consistent and loss costly if compared to the traditional numerical and full scale experimental ones. Perhaps adequately tuned nonlinear numerical models can be profitably used to extend the results from the experimental tests on single walls.

4.3 Bi-linearization criteria

The capacity curve of a real structure is normally irregular and doesn't show a well-defined yielding limit. Otherwise the failure condition can be clearly defined: as an example as achievement of the maximum strength and the correspondent displacement. However are still available other failure criteria as defined in the previous chapter.

The definition of some characteristic properties of a structure such as the yielding limit, the elastic stiffness, the post elastic stiffness and the ductility is strongly dependent on the criteria used for the by-linearization of capacity curve. According to [4.3] the definition of such parameters and consequently of the ductility represents a crucial issue for the application of the pushover method. More in detail:

- The initial elastic stiffness and the equivalent mass define the principal first mode period of the structure (T^*);
- The yielding and the failure displacements define the ductility (μ) and therefore the displacement capacity of the structure;
- The post elastic stiffness define the specific applicability condition of the pushover methods for Elastic Perfect Plastic systems (i.e. N2 method [4.7]) or for Elastic Plastic Hardening systems (i.e method proposed by Albanesi et al.[4.8])

An extensively overview over the effect of the bi-linearization criteria used to defined the ductility for standard RC ad steel structures can be found in [4.9]. Furthermore in [4.10] it is discussed the adequacy of different by-linearization criteria in relation to the specific shape of the capacity curve.

For timber structures some indications about the effect of the by-linearization criteria over the definition of the ductility are given by Munoz et al.[4.2].It has to be highlighted that for wooden structures the Eurocode 8 [4.3] clearly describes the relevance of ductility for the structural behaviour under seismic actions and gives several clauses dealing with ductility in relation to energy dissipation. Despite the relevance of such item, an unambiguous by-linearization criterion is not available yet and the scientific discussion about the definition of the ductility of a wooden structure is still open.

Regarding this, several suggestions have been given by Stehn et al.[4.11] which reported twelve different ductility definitions (i.e. absolute and relative ductility). Such definitions derive from different choice of the yielding point and of the shape of the bi-linear curve.

It is possible to classify these bi-linearization methods into three different groups:

Stiffness-based methods

- Methods that fit the elastic (hardening) stiffness of the equivalent bi-linear curve to the initial (hardening) stiffness of the capacity curve;
- Methods that impose the elastic and hardening stiffness respecting pre-defined rules specific for each building typologies;

Bi-linear curve shape-based methods

- Methods that fit the bi-linear curve shape to the capacity one;

- Methods that define a priori the shape of the bi-linear curve;

Energy strain-based methods

- Methods that ensure the equality of the energy strain between the equivalent bi-linear curve and the capacity one;
- Methods that do not respect the equivalent energy criteria.

It is possible to combine these methods obtaining some hybrid methods, like that adopted by the modern Italian standards [4.12]. It is a hybrid method where the initial stiffness and the shape of the bi-linear curve are imposed a priori but the yielding limit is defined so as to meet the equivalent energy strain requirement. The ultimate displacement capacity is assumed that corresponding to a residual strength equal to 85% of the maximum load F^*_{bu} (see Fig. 4.2).

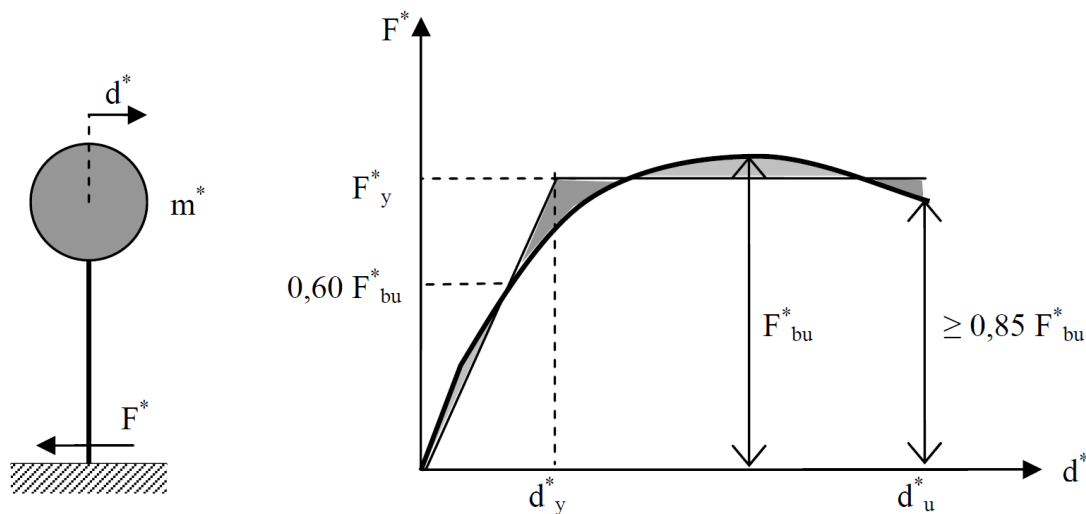


Fig. 4.2 – Bi-linearization criteria proposed by NTC 2008 [4.12]

Since the definition of the bi-linearization criteria and therefore of the ductility ratio are strictly dependent on the methods used to define the yielding and the failure limit of the pushover curve below are summarized the general procedures for a proper definition of such relevant parameters for wooden structure are hereafter summarized.

4.3.1 Yielding point definition

For timber structure the definition of the yielding limit is generally made with reference to the EN 12512 [4.5] which proposes a bi-linearization of the experimental curves using the following two different criteria:

- method (a): adequate for load-slip curve with two well-defined linear branches: yield point is directly determined by the intersection of these two lines.
- method (b): has to be applied for a load-slip curve not presenting two well defined linear branches. In this case the yield point is defined by intersection of the following two lines: the first line will be determined as that drawn through the point on the load-slip curve corresponding to $0.1 F_{max}$ and the point and the load-slip curve corresponding the $0.4 F_{max}$; the second line is the tangent having an inclination of $1/6$ of the first line.

When the pushover curve presents a strongly nonlinear behaviour and/or a relevant hardening phase the two EN 12512 [4.5] methods should not provide sound estimation of the yielding limit and therefore of the ductility.

According to Piazza et al.[4.13] and Jorissen et al.[4.14] an alternative method to demining the yielding limit is adopt an energetic approach. In literature the most common bi-linearization approach based on energy strain balance is the so called Equivalent Energy Elastic Plastic (EEEEP) method [4.15].

In this work a refinement of this method is proposed in order to obtain an elasto-hardening approximation that ensures the equivalence of the energy strain between the envelope and the bilinear curves. This criteria requires the preliminary definition of the analytical envelope load displacement curve proposed by Foschi [4.6] and modified by Bonac [4.16] given in Eq. 4.1. It is define by accurate fitting of the experimental load slip curve. It depends on three parameters that are the stiffness $r_1 k_0 = \beta$ of the hardening branch, the initial stiffness k_0 and the residual force F_0 .

$$F=(r_1 k_0 d+F_0)\left(1-e^{-\frac{k_0 d}{F_0}}\right) \quad \text{Eq. 4.1}$$

where:

- F = actual value of the force
- d = actual value of the displacement
- k_0 = initial stiffness
- $r_1 k_0 = \beta$ = hardening stiffness
- F_0 = residual force

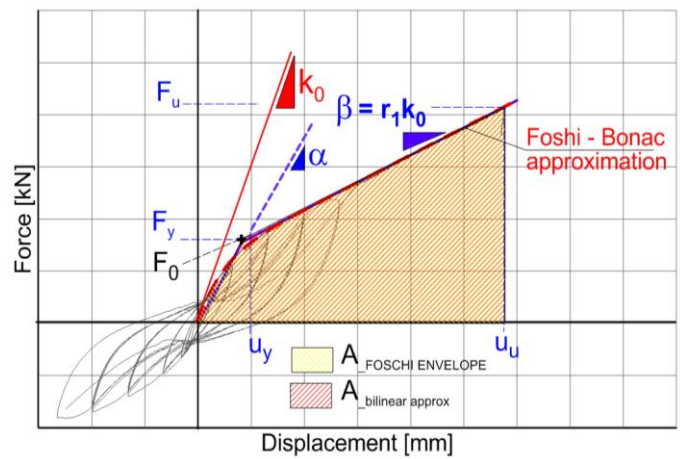


Fig. 4.3 - Identification of yielding and failure limit according to the proposed energetic approach.

The gradient β of the hardening branch is imposed equal to that defined by the Foschi envelope.

The stiffness α of the elastic branch of the bi-linearized law is obtained by imposing the conservation of the strain energy between the analytical envelope and the bilinear law, as depicted in Fig. 4.3.

Known the analytical expression for the envelope and bilinear load-displacement curve it is possible to integrate the strain energy through Eq. 4.2 and Eq. 4.3.

$$A_{\text{FOSCHI ENVELOPE}} = \int_0^{u_u} \left[(r_1 k_0 u + F_0) \left(1 - e^{-\frac{k_0 u}{F_0}} \right) \right] du = \frac{1}{2} r_1 k_0 u^2 + F_0 u - e^{-\frac{r_1 u}{F_0}} \left(k_0 F_0 u - \frac{(k_0 - 1) F_0^2}{r_1} \right) \Big|_0^{u_u} \quad \text{Eq. 4.2}$$

$$A_{\text{BILINEAR APPROX.}} = \frac{1}{2} \left[(F_u + F_y)(u_u - u_y) + F_y u_y \right] = \frac{1}{2} \left[(F_0 + \beta u_u + \alpha \frac{F_0}{\alpha - \beta})(u_u - \frac{F_0}{\alpha - \beta}) + \frac{\alpha F_0}{\alpha - \beta} \right] \quad \text{Eq. 4.3}$$

By imposing the equality of the strain energy the elastic stiffness α is obtained. Once defined the values of the elastic stiffness α and of the hardening stiffness β , the yielding point (u_y, F_y) is given by the intersection between the elastic and the hardening branches.

4.3.2 Failure limit definition

The definition of the failure limit is not unique because it may refer to the maximum load point (F_{max} , u_u) reached during the test or to a specific point (F_u , u_f) along the softening branch of the load slip curve. According to this the EN 12512 [4.5] defines the failure limit both as the maximum load point (F_{max} , u_u) and as the displacement value corresponding to the $0.8 F_{max}$ on the softening branch of the load slip curve. It is clear that different definitions of the failure limit generate different ductility values. In this work reference has been made to first definition of the failure limit since such choice leads to a conservative evaluation of the ductility and of the q-factor..

4.3.3 Bi-linearization methods for timber structures

A total of four different methods for a proper bi-linearization of the capacity curve and for a suitable estimation of the ductility ratio have been investigated in this work. Two of these criteria are based on the provisions given by the EN 12512 [4.5], the other two ensure the energy strain balance between the bi-linear and the capacity curves. The adopted criteria are summarized in the following Fig. 4.4.

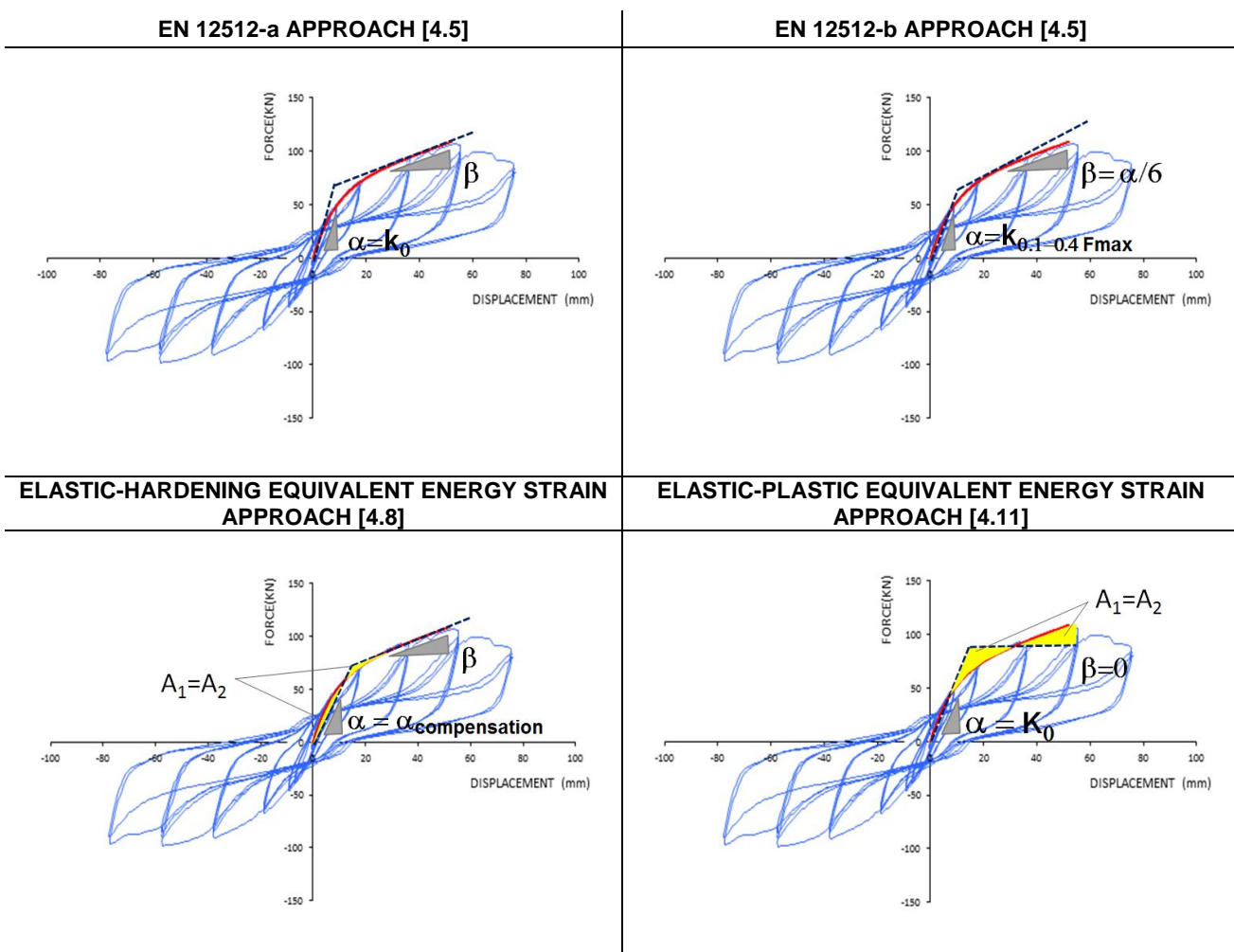


Fig. 4.4 – Bi-linearization criteria.

Such bi-linearization procedures differ for the elastic and hardening stiffness and therefore for the definition of yielding limit. Otherwise a common definition of the failure condition was considered for all of them. In a specific case the different results obtained with the four alternative solutions are depicted in the following Fig. 4.5

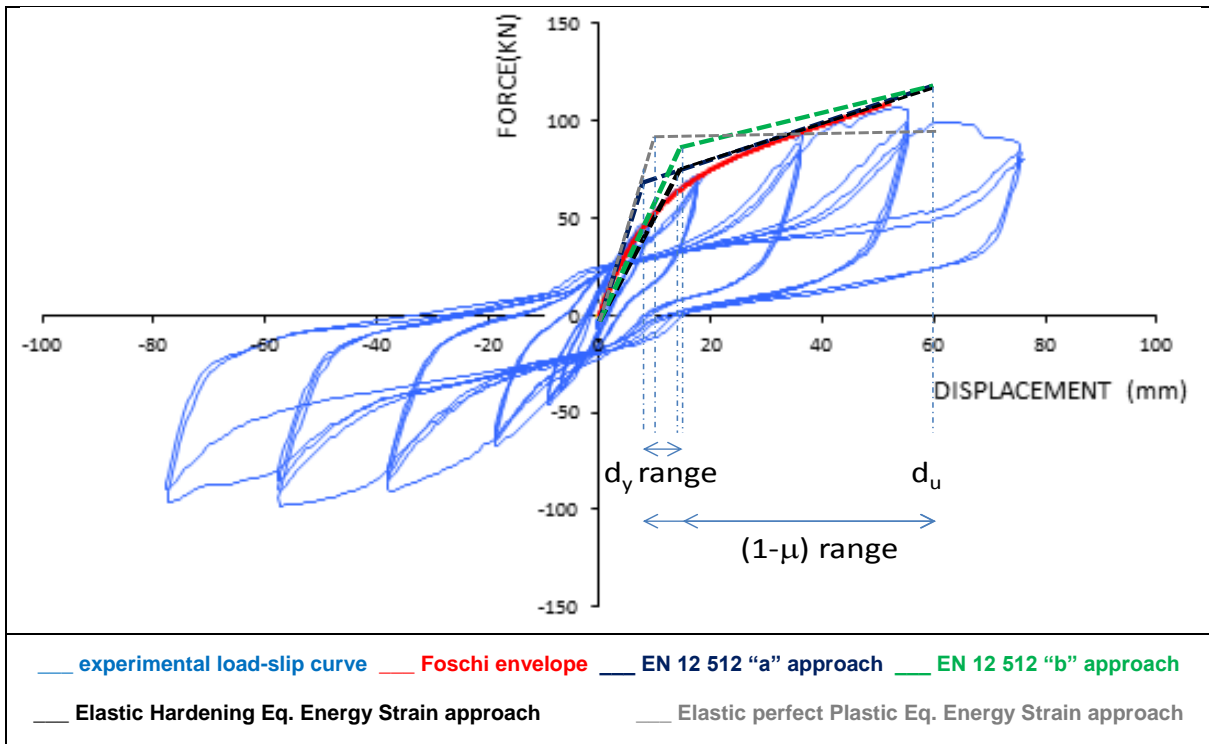


Fig. 4.5 – Yielding limit and ductility given by each considered bi-linearization criteria.

According to Jorissen et al.[4.14] the combined usage of these four different criteria determinates reliable ductility range for all the wooden structures. Furthermore the derivation of different elastic stiffness allows to investigate the influence of the structural principal elastic period T^* on the q -factor value.

4.4 Validation of the proposed procedure

Aim of this section is to verify the capability of the developed procedure to give a reliable evaluation of the q -factor for the wooden building systems. The procedure is validated against the output from the experimental shaking table tests performed on the three storeys building represented in Fig. 4.6 [4.17].

The experimental tests were accompanied by numerical simulations carried out by Ceccotti et al.[4.17] using a spring lamp-mass 3 dimensional model.

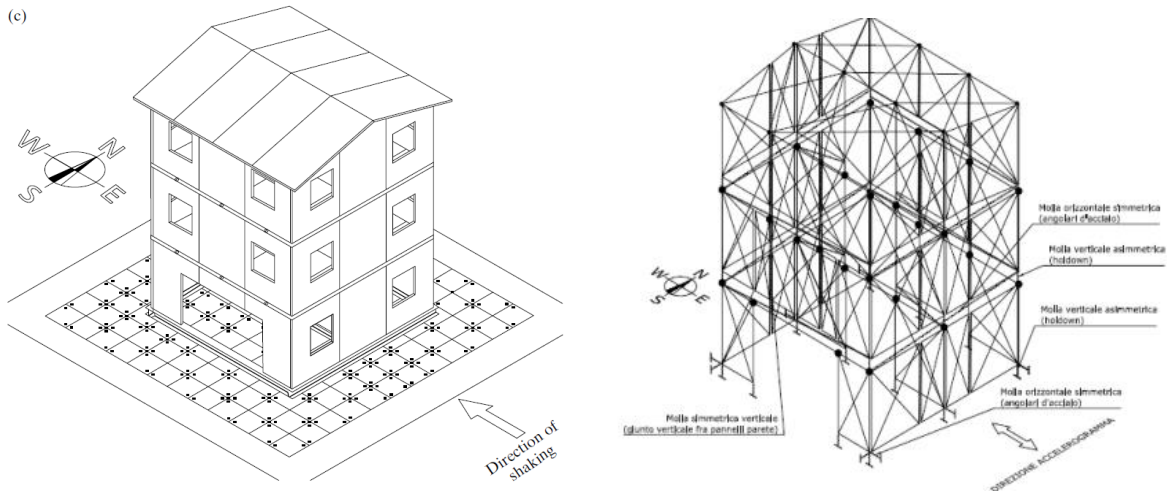


Fig. 4.6 – Reference CLT building tested on shaking table (left) and 3D numerical model (right) [4.17]

The q-factor evaluation for this specific three was made according to the previously defined experimental and numerical methods. Numerically the PGA approach was adopted on the basis of the output from NLDAs applying several natural earthquake signals. The obtained q-factor values are summarized in the following Fig. 4.7.

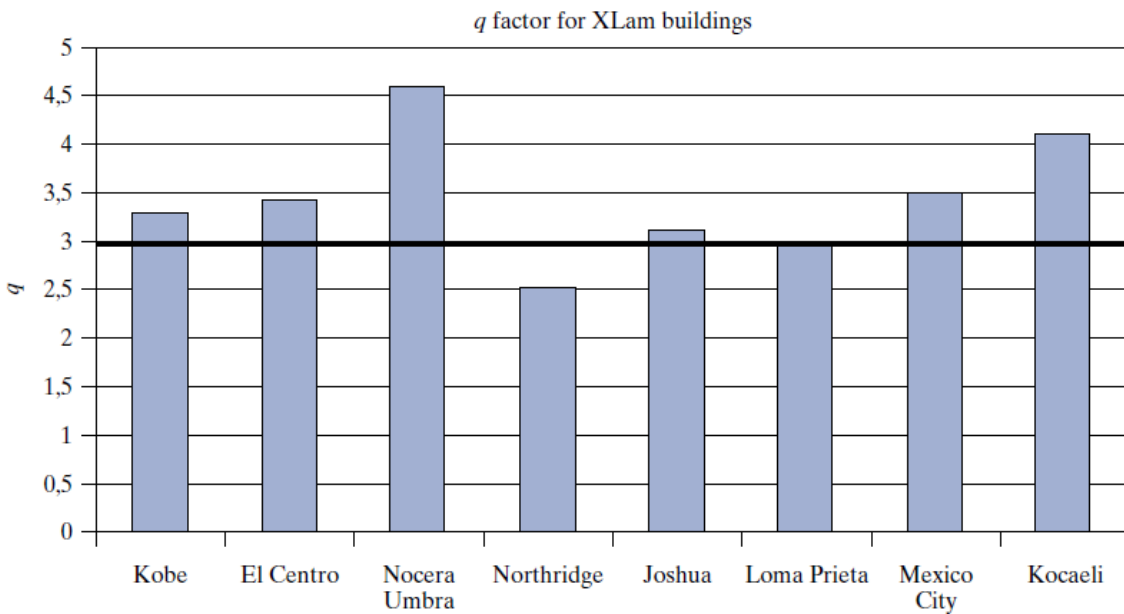


Fig. 4.7 – q-factor estimation for the tested three storeys CLT building [4.17].

According to Fig. 4.7 the q-factor settled on the value of about 3 with a variability range from 2.5 to 4.6.

The developed procedure must be applied to wall specimens representative of the investigated three storeys CLT building. As depicted in Fig. 4.6 each wall that composes the building is made by assembling three CLT panels. The suitable walls specimens for applying the developed procedure have to represent the specific building constructive technique. To this purpose two walls tested at CNR IVALSA laboratory (TN) by means of quasi-static cyclic tests were considered and analyzed using the developed procedure (see walls 1.A and 1.B of Table 4.1). The 1st case study wall 1.A was made by a whole CLT panel while the 2nd case study wall 1.B by two vertically

connected CLT panels. These two walls adequately reproduce the specific construction characteristics and fasteners arrangement and typology of the investigated three storey building as depicted in the following Fig. 4.8.

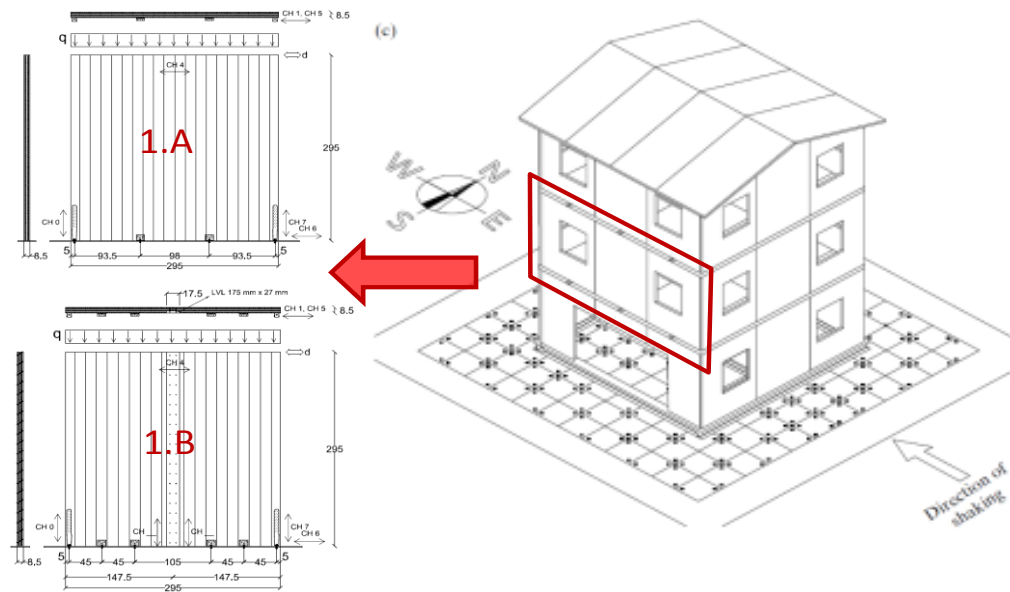


Fig. 4.8 – Choice of the wall elements representative of the investigated building system [4.17].

Furthermore the vertical load applied on the top of the tested wall is about 18.5 kN/m and corresponds to the weight sustained by a base wall of the investigated building. The hysteresis load-slip curve obtained from the experimental tests and the correspondent monotonic envelopes defined using the formulation proposed by Foschi [4.6] are summarized in Table 4.2. The 1st step of the developed procedure consists on the bi-linearization of the envelope curve according to the four methods defined in the previous paragraph 4.3. These bi-linearization curves are reported in Table 4.2 for both wall 1.A and wall 1.B. The application of the pushover method to the bi-linear capacity curve gives the q-factor estimation reported in Table 4.3 for both the case study walls.

The obtained q-factor values using the different bi-linearization criteria span between 2.65 to 4.1. This range fits very well with that obtained by Ceccotti [4.17] ($2.5 < q < 4.6$). The small difference should be due to the 3 dimensional overstrength effects that with this simplified procedure couldn't be taken into account. However these results confirm that the use of the developed procedure provides an estimation of the q-factor as reliable as that obtained by the traditional numerical and full scale experimental methods.

According to this validation results the developed procedure is suitable to produce an expeditious estimation of the most appropriate q-factor of a constructive system without having to perform complex nonlinear numerical analysis or expensive full scale experimental shaking tests. Obviously the adequacy of the results depends on the choice of the reference wall specimens which must be more representative as possible of the building constructive technique.

As a final remark it should be noted that the average q-factor related to the wall 1.A is lower than that of wall 1.B. Such difference is mainly due the connections arrangement: wall 1.B presents a greater number of joints than 1.A and therefore a greater dissipative capacity. Such influence of the connection numbers over the dissipative capacity of the CLT building will be investigated in detail in the next Chapter 5.

4.5 Assessment of the q-factor of various building systems

Once validated, the developed procedure can be applied to a several timber systems in order to obtain an expeditious and reliable estimation of their behaviour q-factor. Hereafter the new developed procedure is used to define the most suitable q-factor of seven different timber building systems tested at the CNR IVALSA laboratory – TN Italy.

A preliminary description of the investigated building system is given both with regard to the wall geometrical characteristics and to the connection typologies. Then the hysteresis load displacement curves obtained with the experimental tests are reported and the correspondent envelopes are defined according to the Foschi formulation [4.6]. Then the bi-linear approximations of the envelope curve are carried out with the criteria defined in the previous paragraph 4.3. Once defined the bi-linear curve the application of the developed procedure allows the evaluation of the q-factor values. A final discussion about the obtained results is given.

4.5.1 Case study wall specimens

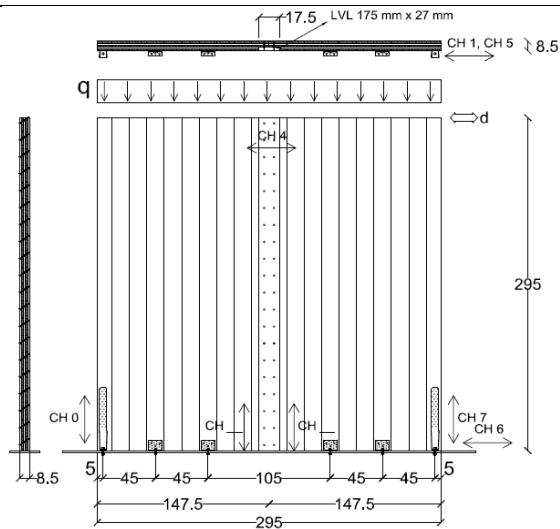
Seven different case study wall specimens have been considered: three solid CLT shearwalls (1.A, 1B, 1C), one heavy wood frame shearwall (2) and three special wooden walls (3, 4, 5). The geometrical characteristics and the connection properties are reported in the following Table 4.1.

For secrecy reason some specific characteristics of the investigated walls 2, 3 and 5 are here omitted. This doesn't represent a limitation for the applicability of the developed procedure since the only parameters necessary for its implementation, i.e. equivalent mass and the capacity curve, are known.

Table 4.1 – Geometrical characteristic of the case study wall specimens.

1.A – CLT wall made with whole panel	
	<p><i>Test Protocol: EN12512 [4.6]</i></p> <p><i>Vertical Load: 18.5 kN/m – Global Mass 5.45 t</i></p> <p><i>Wall dimension: b=2.95m; h=2.95m</i></p> <p><i>Wooden elements: CLT panel 85mm thick</i></p> <p><i>Connection type:</i> 2 holdwon simposn HTT22 with 12 ϕ 4x60 anular ringed nails 2 angle BMF 90x48x3x116 with 11 ϕ 4x60 anular ringed nails</p>

1.B - CLT wall made with two vertically jointed panel



Test Protocol: EN12512 [4.6]

Vertical Load: 18.5 kN/m – Global Mass 5.45 t

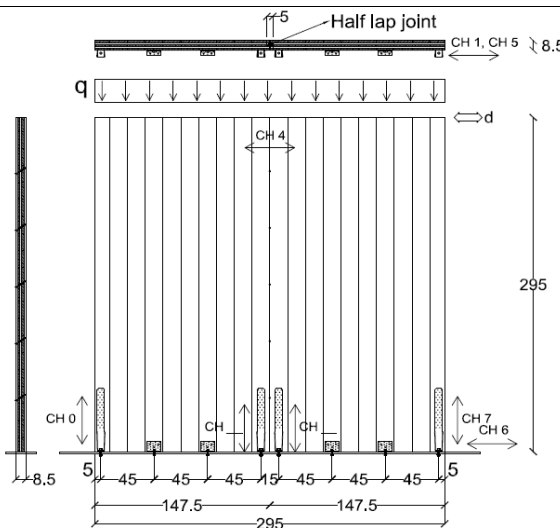
Wall dimension: $b=2.95\text{m}$; $h=2.95\text{m}$

Wooden elements: CLT panel 85mm thick

Connection type:

- 2 holdwon simposn HTT22 with 12 ϕ 4x60 anular ringed nails
- 4 angle BMF 90x48x3x116 with 11 ϕ 4x60 anular ringed nails
- 2x20 screws HBS ϕ 8x100 – spacing 150mm - inclination 35°

1.C - CLT wall made with two base jointed panel



Test Protocol: EN12512 [4.6]

Vertical Load: 18.5 kN/m – Global Mass 5.45 t

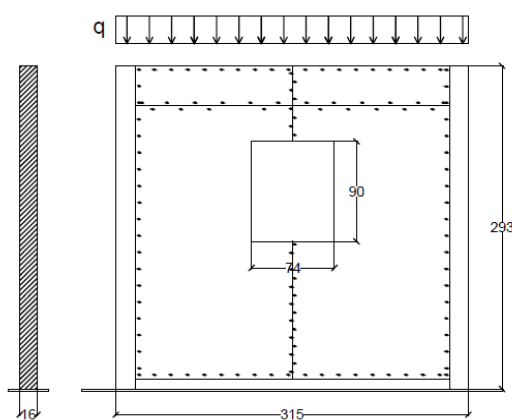
Wall dimension: $b=2.95\text{m}$; $h=2.95\text{m}$

Wooden elements: CLT panel 85mm thick

Connection type:

- 4 holdwon simposn HTT22 with 12 ϕ 4x60 anular ringed nails
- 4 angle BMF 90x48x3x116 with 11 ϕ 4x60 anular ringed nails
- 10 screws HBS ϕ 8x100 – spacing 500mm - inclination 35°

3 - Heavy frame shearwall



Test Protocol: EN12512 [4.6]

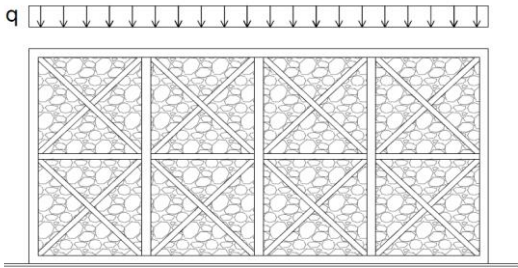
Vertical Load: 18.5 kN/m – Global mass 5.90 t

Wall dimension: $b=3.13\text{m}$; $h=2.95\text{m}$ – window 0.74m x .90m

Wall characteristic:

The primary structure of the wall is a timber frame made by 100mm x 160mm glulam elements. the elements of the frame is connected by means of self-drilling screws. The wall is braced by a special multy-layer wood panel screwed to the frame. The wall is fixed to the steel base using standard angle brackets and holddown.

3 – X timber frame filled with masonry - Haity walls



Test Protocol: EN12512 [4.6]

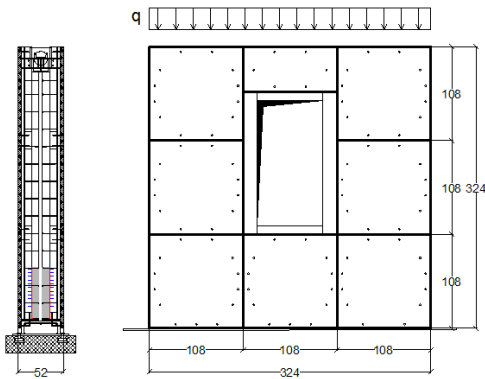
Vertical Load: 10 kN/m – Global mass 7.15 t

Wall dimension: $b=4.4m$; $h=2.2m$

Wall characteristic:

primary wall structure is made by 110mm x 110mm frame composed with 40mm x 200mm timber elements. bracing system made by timber elements and natural rock masonry.

4 – Mixed wood-concrete frame shearwall



Test Protocol: EN12512 [4.6] + EN 594 [4.5]

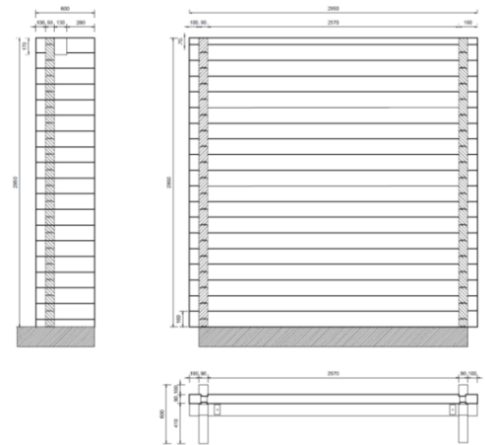
Vertical Load: 20.0 kN/m – Global Mass 7.36 t

Wall dimension: $b=3.40m$; $h=3.24m$ – window 0.82m x 1.60m

Wall characteristic:

Heavy timber frame braced by special external concrete slab. Special homemade holdown and screws used to fixed the RC slab to the frame. For an exhaustive description of this innovative construction system see Chapter 7 and Appendix A.

5 – Blockbau wall



Test Protocol: EN12512 [4.6]

Vertical Load: 10.0 kN/m – Global Mass 2.45 t

Wall dimension: $b=2.95m$; $h=2.95m$

Wall characteristic:

90mm x 160mm x 2950mm crosspiece lay to obtain the main wall. Orthogonally to the wall elements are disposed short elements 90mm x 160mm x 600mm to simulate the effect of two walls orthogonal to the main tested wall. The wall is fixed to the steel base using standard angle brackets and a ϕ 10mm cable to prevent the uplift.

4.5.2 Capacity curves

The seven wall configurations were tested at the CNR IVALLSA laboratory – S. Michele all’Adige TN by means of cyclic tests performed according to the protocol defined by the EN 12512 [4.5]. The maximum top displacement imposed to the wall during the cyclic tests was equal to 80mm. If at such deformation level the walls did not show any failure an additional monotonic ramp test [4.4] was applied until the breaking of the wood elements or the fasteners.

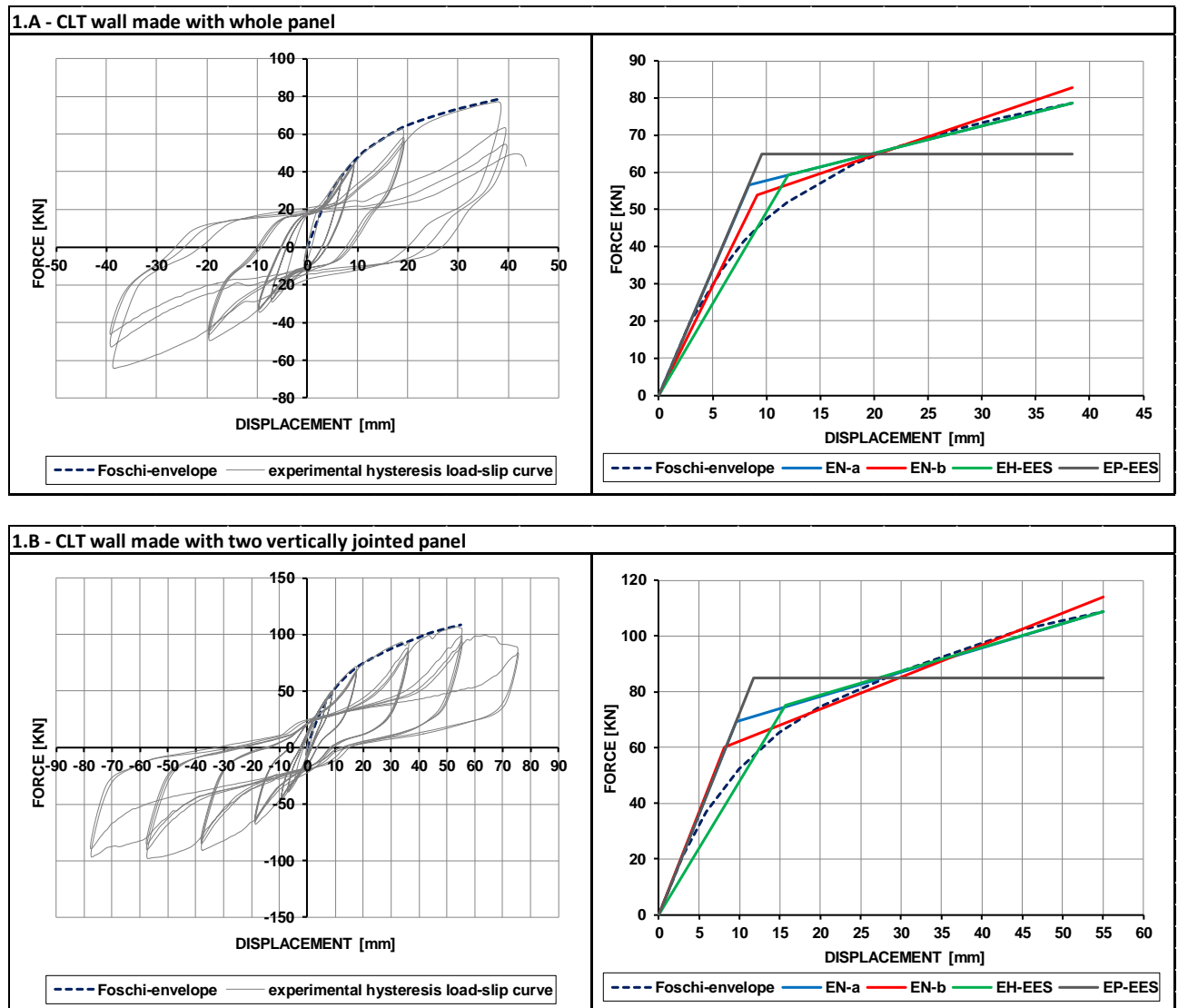
The experimental hysteresis load-slip curves are approximated by means of envelop curve obtained by using the formulation proposed by Foschi [4.6] for the monotonic branch of the wooden systems. Four different bi-linearization criteria of the envelope curve have been used:

- EN-a criteria is based on the method “a” given by EN 12512 [4.5] provisions for the interpretation of the results from cyclic tests;
- EN-b criteria is based on the method “b” given by EN 12512 [4.5] provisions for the interpretation of the results from cyclic tests;
- EH-EES criteria provides an Elastic Hardening curve defined ensuring the Equivalence of the Energy Strain between the bi-linear curve and the envelope one [4.8].
- EP-EES criteria provides an Elastic perfect Plastic curve defined ensuring the Equivalence of the Energy Strain between the bi-linear curve and the envelope one [4.11].

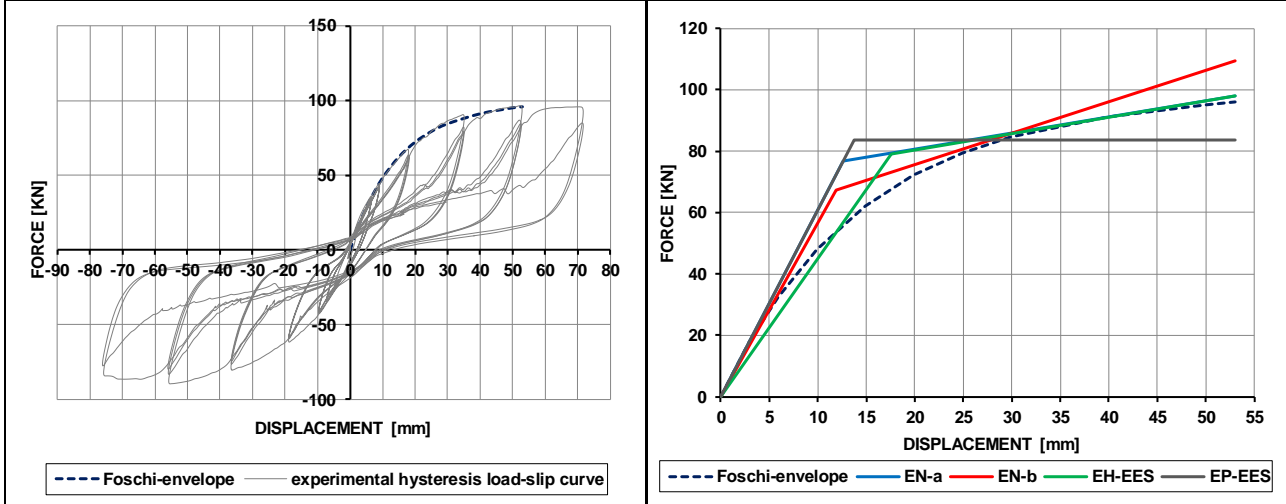
The following Table 4.2 reports for each case study wall the hysteresis loop, the Foschi [4.6] envelope and the four different capacity curves obtained with the so defined bi-linearization criteria.

The specific force, displacement and stiffness values that characterize each bilinear capacity curve are summarized in the next Table 4.3.

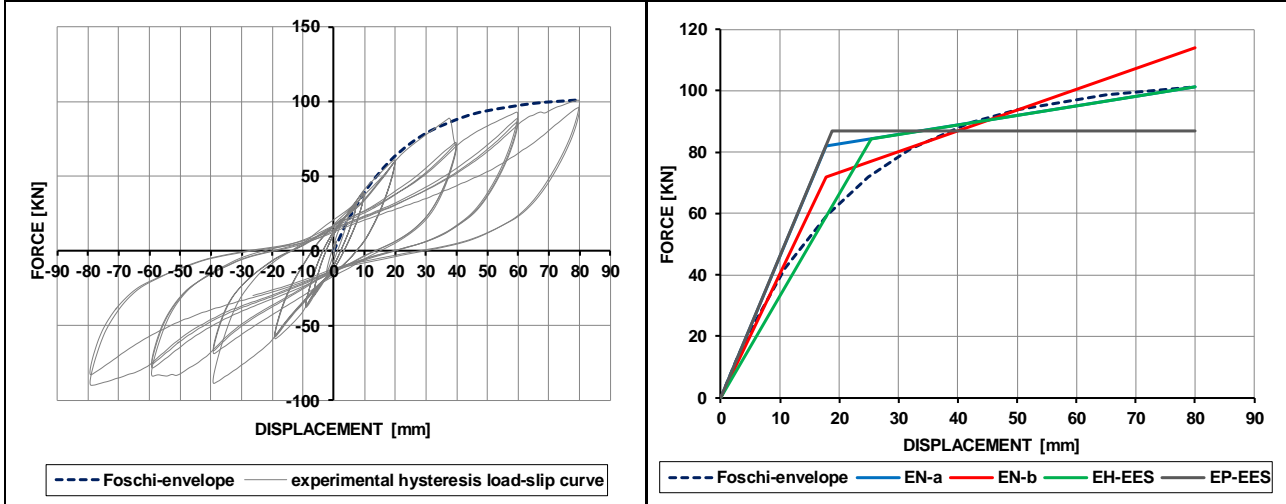
Table 4.2 – Hysteresis loop and correspondent bilinear approximation of the case study wall specimens.



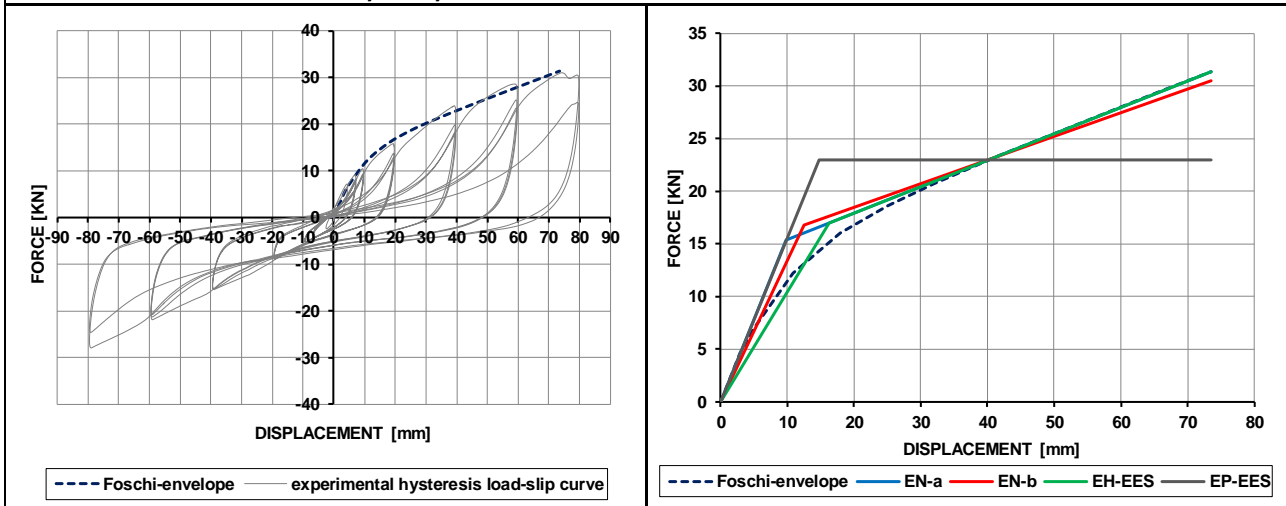
1.C - CLT wall made with two base jointed panel



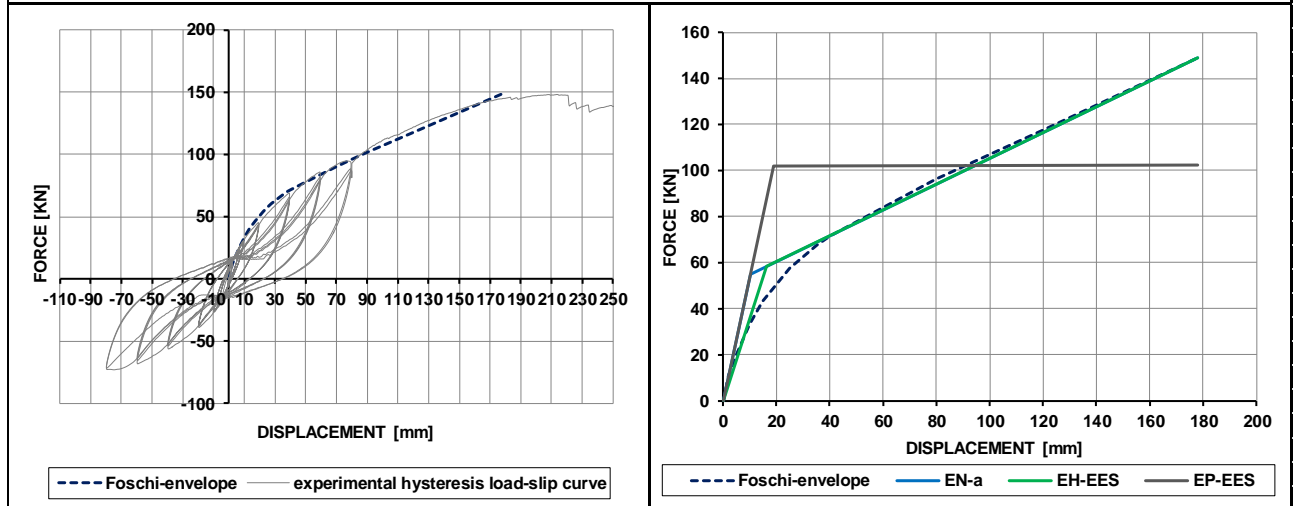
2 - Heavy frame shearwall



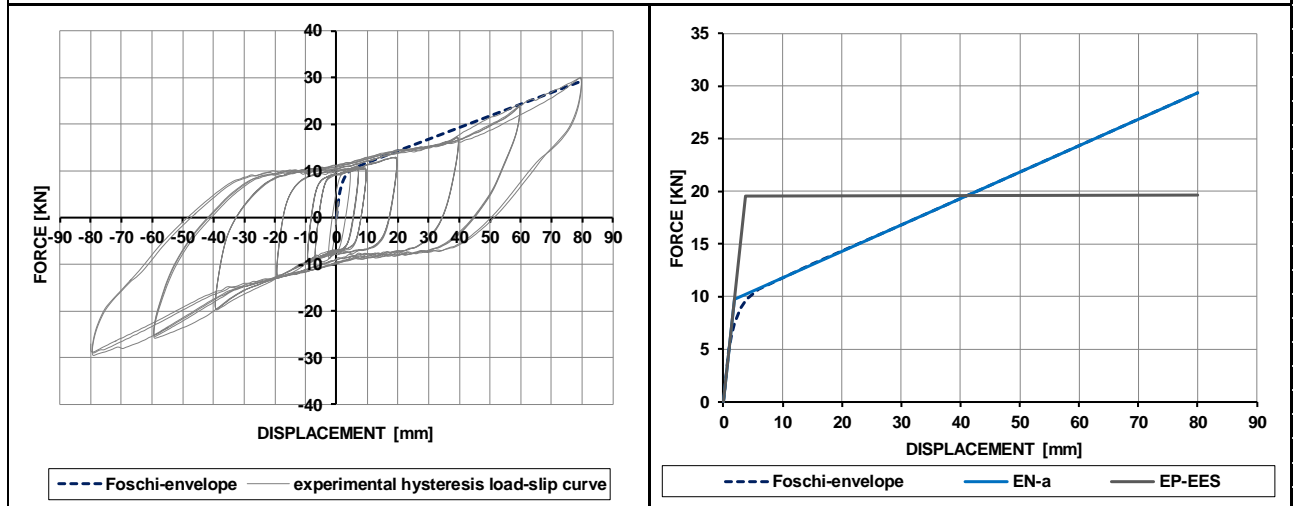
3 - X timber frame filled with masonry - Haity walls



4 – Mixed wood-concrete frame shearwall



5 – Blockbau wall



As shown in Table 4.2 the adopted bi-linearization criteria provide different yielding limits and consequently different ductility ratios. It should be noted that for the case studies 4 and 5 some bi-linearization criteria are not applicable. In detail the EN-b approach cannot be used for “Wall 4” and “Wall 5” because the tangency condition between the hardening branch (defined by imposed gradient) and the envelope curve is not verified. These limitations of applicability of some bi-linearization criteria highlight that the specific shape of the envelope load slip curve has a direct influence on the bi-linearization approach. In detail load-slip curves characterized by high elastic and hardening stiffness generally can be hardly approximated by means of bi-linear curve with fixed gradient of the elastic and post-elastic branch.

4.5.3 q-factor estimation

Once defined the bilinear capacity curves and known the global mass of each case study the correspondent SDOF system is completely defined. It is possible to apply the pushover method in order to define the maximum spectra compatible with the displacement capacity of the wall and therefore the correspondent q-factor [4.3]. For each case studies and bi-linearization methods Table 4.3 reports the following parameters:

- Force at the failure limit F_u
- Displacement at the failure limit d_u
- Force at the yielding limit F_y
- Displacement at the yielding limit d_y
- Initial stiffness of the Foschi [4.16] envelope curve K_0
- Post elastic stiffness of the Foschi [4.16] envelope curve K_{pl}
- Elastic stiffness of the bilinear capacity curve α
- Hardening stiffness of the bilinear capacity curve β
- Ductility ratio $\mu = d_u/d_y$
- Behaviour factor q

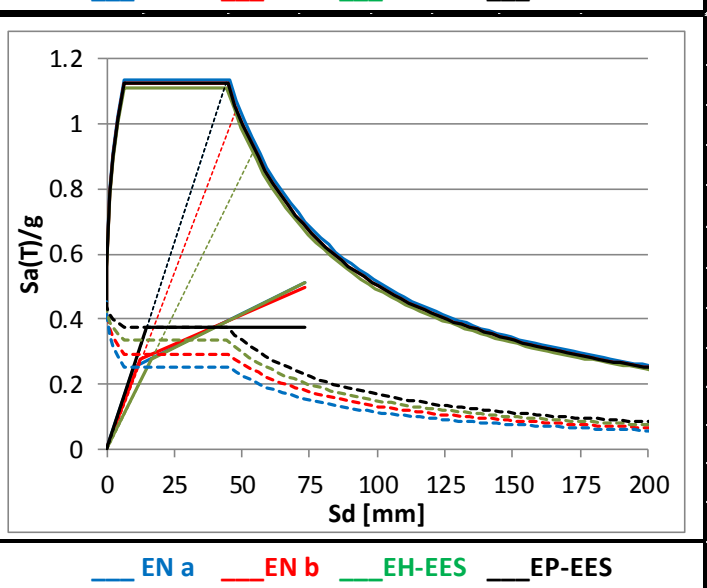
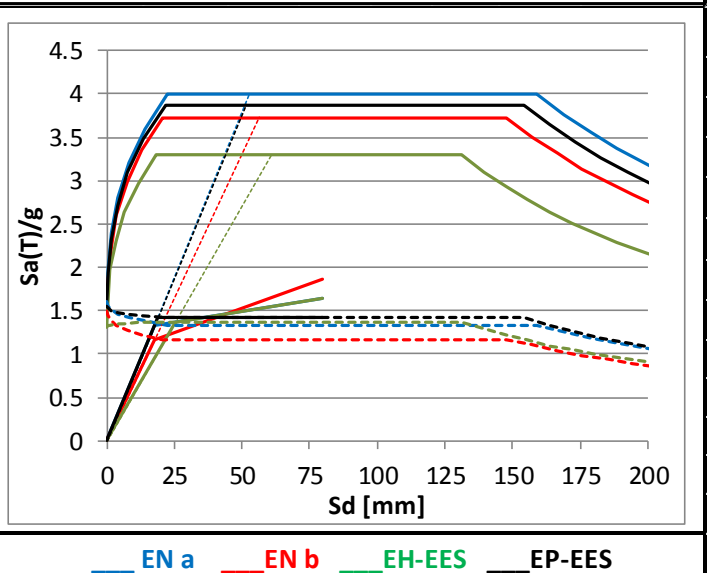
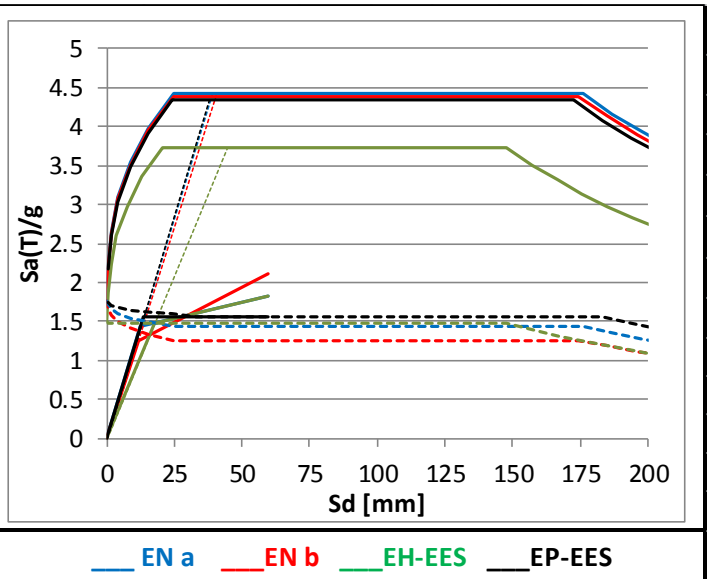
The ductility class is also evaluated according to the criteria based on the ductility ratio defined by the Eurocode 8 [4.18]. The average q-factor value is also reported. Furthermore on the right side of the table the elastic and the design spectra compatible with each capacity curves are plotted in the ADRS format [4.3].

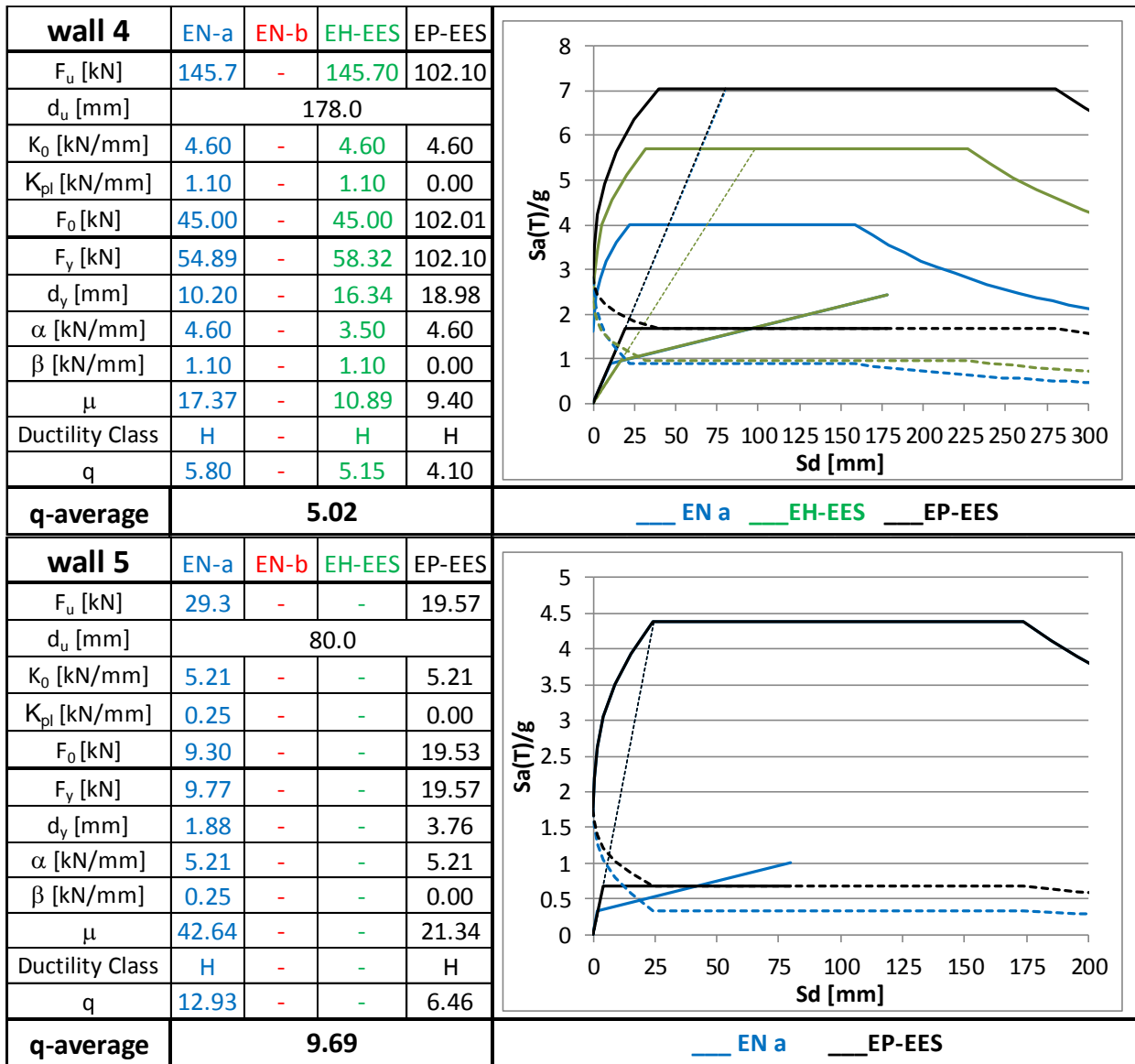
Table 4.3 – q-factor definition for each case studies and bi-linearization criteria

wall 1.A	EN-a	EN-b	EH-EES	EP-EES
F_u [kN]	78.72	82.79	78.72	64.80
d_u [mm]	38.40			
K_0 [kN/mm]	6.77	5.90	6.77	6.77
K_{pl} [kN/mm]	0.73	0.98	0.73	0.00
F_0 [kN]	50.58	45.00	50.58	64.78
F_y [kN]	56.71	54.00	59.38	64.80
d_y [mm]	8.37	9.15	12.01	9.57
α [kN/mm]	6.77	5.90	4.94	6.77
β [kN/mm]	0.73	0.98	0.73	0.00
μ	4.58	4.19	3.19	4.00
Ductility Class	M	M	L	M
q	3.09	3.01	2.46	2.65
q-average	2.80			

wall 1.B	EN-a	EN-b	EH-EES	EP-EES
F_u [kN]	108.6	114.1	108.62	84.95
d_u [mm]	51.9			
K_0 [kN/mm]	7.25	7.41	7.25	7.25
K_{pl} [kN/mm]	0.93	1.23	0.93	0.00
F_0 [kN]	60.43	50.00	60.43	84.92
F_y [kN]	69.31	60.00	75.02	84.95
d_y [mm]	9.56	8.10	15.72	11.72
α [kN/mm]	7.25	7.41	4.77	7.25
β [kN/mm]	0.93	1.23	0.93	0.00
μ	5.42	6.41	3.30	4.43
Ductility Class	M	H	M	M
q	3.51	4.08	2.57	2.80
q-average	3.24			

wall 1.C	EN-a	EN-b	EH-EES	EP-EES
F_u [kN]	97.9	112.4	97.88	83.60
d_u [mm]	59.9			
K_0 [kN/mm]	6.10	5.65	6.10	6.10
K_{pl} [kN/mm]	0.45	0.94	0.45	0.00
F_0 [kN]	71.07	56.00	71.07	83.56
F_y [kN]	76.70	67.20	78.94	83.60
d_y [mm]	12.58	11.90	17.59	13.71
α [kN/mm]	6.10	5.65	4.49	6.10
β [kN/mm]	0.45	0.94	0.45	0.00
μ	4.76	5.03	3.40	4.37
Ductility Class	M	M	L	M
q	3.08	3.49	2.52	2.78
q-average	2.97			
wall 2	EN-a	EN-b	EH-EES	EP-EES
F_u [kN]	101.2	114.0	101.19	86.88
d_u [mm]	80.0			
K_0 [kN/mm]	4.62	4.05	4.62	4.62
K_{pl} [kN/mm]	0.31	0.67	0.31	0.00
F_0 [kN]	76.50	60.00	76.50	86.84
F_y [kN]	81.98	72.00	84.35	86.88
d_y [mm]	17.74	17.79	25.44	18.80
α [kN/mm]	4.62	4.05	3.32	4.62
β [kN/mm]	0.31	0.67	0.31	0.00
μ	4.55	4.52	3.17	4.26
Ductility Class	M	M	L	M
q	3.00	3.18	2.40	2.74
q-average	2.83			
wall 3	EN-a	EN-b	EH-EES	EP-EES
F_u [kN]	31.4	30.5	31.37	22.97
d_u [mm]	73.5			
K_0 [kN/mm]	1.57	1.34	1.57	1.57
K_{pl} [kN/mm]	0.25	0.22	0.25	0.00
F_0 [kN]	12.84	14.00	12.84	22.96
F_y [kN]	15.30	16.80	16.94	22.97
d_y [mm]	9.78	12.49	16.27	14.68
α [kN/mm]	1.57	1.34	1.04	1.57
β [kN/mm]	0.25	0.22	0.25	0.00
μ	7.51	3.84	3.31	5.02
Ductility Class	H	L	L	M
q	4.56	3.84	3.31	3.01
q-average	3.68			





As shown in Table 4.3 there is a quite good correspondence between the estimated q factor and their range suggested by Eurocode 8 [4.18] on the basis of the ductility class. The estimated q -factors are always in the range defined by the correspondent Ductility Class for each case study wall specimens and bi-linearization criteria. Below are reported some consideration specific for each case study wall specimens.

- 1.A, 1B, 1C - CLT wall specimens: the effect of the different bi-linearization criteria over the q -factor value is not so relevant. The variability of the elastic stiffness with the bi-linearization criteria is very small and the elastic principal period T^* is always in the plateau range. The bi-linearization criteria based on the energy balance (i.e. EH-EES and EP-EES) provide the lower estimation of the q -factor.
- 2 - Heavy frame shearwall specimen: as state for the CLT walls the variability of the elastic stiffness with the bi-linearization criteria is very small and the elastic principal period T^* is always in the plateau range. Again the bi-linearization criteria based on the energy balance (i.e. EH-EES and EP-EES) provide the lower values of the q -factor.
- 3 - X timber frame filled with masonry (Haity wall): this constructive systems shows low value of initial stiffness therefore the bi-linearization criteria used to define the capacity curve strongly affects the elastic stiffness. The principal elastic periods T^* of the various

bilinear curves therefore is not always in the plateau range. Consequently a wide variability of the q-factor values is obtained. Again the bi-linearization criteria based on the equivalence of the strain energy provide the lower q-factor estimation.

- 4 - Mixed wood-concrete frame shearwall: the variability of the elastic stiffness due to the bi-linearization criteria is not so relevant since all the principal elastic periods T^* of the SDOF systems are comprised in the plateau range. The bilinear capacity curve obtained using the energetic approach provide the lower q-factor estimations.
- 5 - Blockbau wall: this wall is characterized by a specific rigid-plastic behavior due to the friction effects and by large displacement before failure. Consequently the ductility ratio and the q-factor result to be very high. It should be noted that this constructive systems is realized without mechanical connections and the lateral load bearing capacity is only due to the friction effects between the overlapped wood elements and to the carpentry joints at the corner of the wall.

According to Eurocode 8 [4.18] this wooden system is precautionary classified as a system with low dissipative capacity and must be design in elastic field. Therefore the evaluated q-factor contrasts with the code provision. This discrepancy between the code provisions and the experimental evidence highlights on one hand that the dissipative capacity due to the friction effects can be relevant, on the other hand that the q-factor estimation based on the ductility ratio overestimate the actual behaviour factor of this constructive typology.

As a final remark it should be noted that according to the available seismic code (e.g. [4.18] and [4.12]) the friction effects couldn't be considered in the seismic design. With such assumption it is evident that the q-factor given by the code provisions represents a conservative estimation of the reliable dissipative capacity of this building typology.

The results of the bi-linearization criteria used to define the capacity curve over the q-factor value are reassumed in Fig. 4.9.

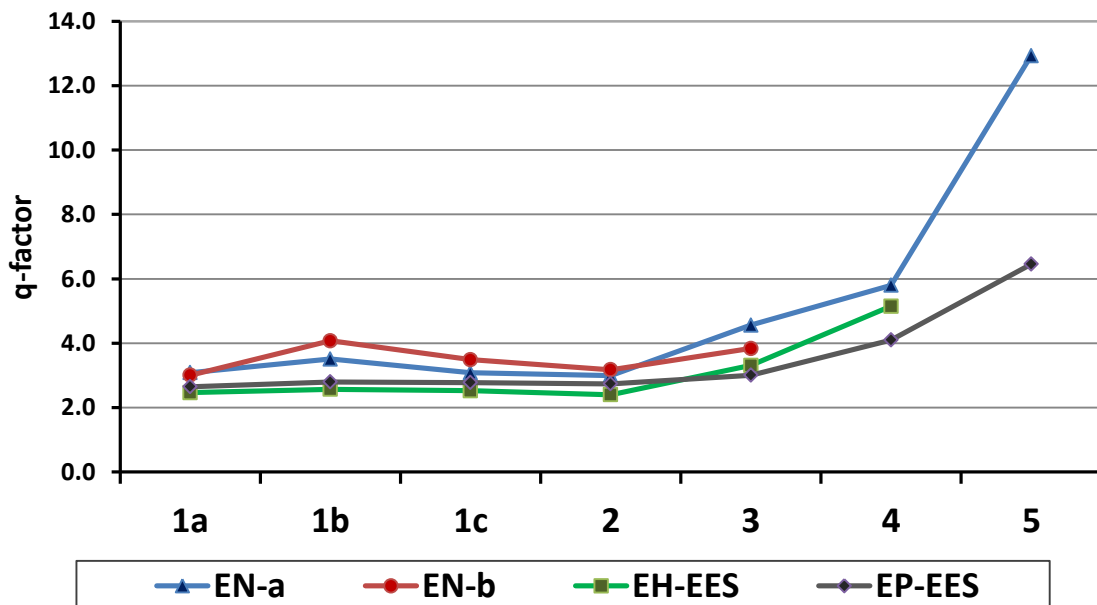


Fig. 4.9 – Influence of the bi-linearization criteria over the q-factor value.

Fig. 4.9 make evident that the criteria based on the equivalence of the strain energy provide the more precautionary and stable estimation of the behaviour q-factor. Adoption of the criteria based

on the EN 12512 [4.5] gives the highest estimations of the q-factor and with a greater variability. Therefore their utilization is not conservative.

It appears that the Elastic perfect Plastic bilinear capacity curves provides the more reliable estimation of the nonlinear response and ductility of the building constructive system and therefore of their respective q-factor. Furthermore such bi-linearization criteria can be applied independently the specific shape and nonlinear behaviour of the capacity curve like the EN 12512 “a” approach [4.5]. The criteria based on the Elasto Hardening Energetic and the EN 12512 “b” [4.5] approaches could present some applicability limits due to the imposition of the elastic and hardening stiffness.

Finally it should be pointed out that according to [4.2] the q-factor range defined using the developed procedure applied to the EN-a and the EP-EES capacity curve provide the most reliable estimation of the real dissipative capacity and of the effective ductility of the investigated building system.

4.6 Conclusions

The new procedure proposed in this chapter demonstrated to be a viable alternative to traditional numerical and full scale experimental methods, being really expeditious and efficient.

It is based on the same experimental tests required for example by the Eurocode 8 [4.18] for the definition of the Ductility Class, but allows the analytical evaluation of the q-factor through a suitable application of the well-known pushover method [4.3]. Consequently this new developed procedure overcomes the critical aspects of the traditional numerical and experimental methods such as the high time-consuming, the high computational effort and the high economical costs.

The points that are crucial for the a trustable q-factor estimation are substantially two: (1) the choice of an adequate wall specimens really representative of the building technology and (2) the use of a sound bi-linearization criteria to switch from the nonlinear load-displacement curve to the bi-linear capacity one. Regarding to this second aspect the exhaustive validation phase of the procedure allowed to individuate the most suitable approaches for a proper bi-linearization of the wooden structure load-slip curve between all that proposed in the scientific literature.

References – Chapter 4

- [4.1] Ceccotti A., Sandhaas C. *A proposal for a standard procedure to establish the seismic behaviour factor q of timber buildings. Proceeding of the 11th World Conference on Timber Engineering WCTE 2010. Riva del Garda, Italy, June 20–24, 2010, CD.*
- [4.2] Munoz W., Mohammad M., Slaenikovich A., Quenville P. 2008. *Need for a harmonized approach for calculations of ductility of timber assemblies. Meeting 41 of the Working Commission W18-Timber Structures, CIB. St. Andrews, Canada, 2008, paper CIB-W18/41-15-1.*
- [4.3] Fajfar P. *Design spectra for new generation of code. Proceeding 11th World Conference on Earthquake Engineering, Acapulco, Mexico, 1996, paper No. 2127.*
- [4.4] EN 594, 1996. *Timber Structures – Test methods – Racking strength and stiffness of timber frame wall panels.*
- [4.5] EN 12512, 2001. *Timber Structures – Test methods – Cyclic testing of joints made with mechanical fasteners.*
- [4.6] Foschi, R. O., (1977) "Analyses of wood diaphragms and trusses. Part I: diaphragms." *Canadian J. Civ. Engrg.*, 4(3), 345-352 Foschi, R. O., (1977) "analyses of wood diaphragms and trusses. Part I: diaphragms." *Canadian J. Civ. Engrg.*, 4(3), 345-352
- [4.7] P. Fajfar and P. Gaspersic, "The N2 method for the seismic damage analysis for RC buildings', *Earthquake Engng. Struct. Dyn.* 25, 23-67 (1996)
- [4.8] Albanesi, T., Nuti, C., Vanzi, I.(2002). "State of the art of nonlinear static methods," *Proc. of the 12th European Conf. on Earthquake Engrg.*, London, United Kingdom, Paper. 602, Oxford: Elsevier Science.
- [4.9] Costa A., Romão X., Oliveira C. S. 2009. *A methodology for the probabilistic assessment of behaviour factors. Bull Earthquake Eng (2010) 8:47–64 DOI 10.1007/s10518-009-9126-5*
- [4.10] Mitchell D, Paulter P. 1994. *Ductility and overstrength in seismic design of reinforced concrete structures. Canadian Journal of Civil Engineering 21: 1049–1060.*
- [4.11] Stehn L., Björnfot A. 2002. *Comparison of different ductility measurements for a nailed steel-to-timber connection. Proceeding of the 7th World Conference on Timber Engineering WCTE 2002. Shah Alam, Selangor Darul Ehsan, Malaysia, 12th-15th August 2002.*
- [4.12] *Italian Ministry for the Infrastructures. New technical regulation for construction. Decree of the Ministry for the Infrastructures, Ministry of Interior, and Department of the Civil Defence. 2008.*
- [4.13] Piazza M., Polastri A., Tomasi R. 2011. *Ductility of timber joints under static and cyclic loads. Proceedings of the Institution of Civil Engineer published online, doi: 10.1680/stub. 10.00017*
- [4.14] Jorissen A., Fragiaco M. 2011. *General notes on ductility in timber structures. Engineering Structures 33, 2011, 2987-2997.*
- [4.15] Foliente GC. 1996. *Issues in seismic performance testing and evaluation of timber structural systems. In: Proceedings of the 1996 international timber engineering conference. vol. 1. p. 1.29 –.36.*
- [4.16] Foschi RO., Bonac T. 1977. *Load slip characteristic for connections with common nails. WOOD SCI Technol 1977;9(3):118-23*
- [4.17] Ceccotti A. *New technologies for construction of medium-rise buildings in seismic regions: the XLAM*

case. IABSE Struct Eng Internat 2008;18:156–65. Tall Timber Buildings (special ed.).

[4.18] *European Committee for Standardization (CEN). Eurocode 8 - design of structures for earthquake resistance, part 1: General rules, seismic actions and rules for buildings. 2004.*

Chapter 5 – Numerical evaluation of the q-factor for various CLT building configurations

Abstract

This section provides the necessary background on the Cross Laminated Timber building technique. Basic terms and concepts used in structural design and constructive technology are presented.

A literature review on the state of the arte about the research activity on the CLT system is presented especially with regard to the experimental tests performed to define the seismic behaviour, the dissipative capacity and therefore the suitable q-factor.

An extensive study about the influence of some significant characteristics such as building assembly, storeys number, design criteria, density of the joints etc.. on the seismic response and dissipative capacity of the CLT building is presented. Such study has been conducted on a representative number building configurations by means of nonlinear dynamic and static analyses, carried out using suitable hysteretic spring models. A final discussion about the obtained results is presented.

5.1 Introduction

The CrossLam building system is largely spreading out thanks to its optimal characteristics. The sustainability and economic profitability of modern timber buildings are increasingly linked to their being integrated with low-energy-consuming construction devices and solutions at the building management stage, which renders this typology competitive, efficient and safe if compared to other more traditional construction typologies. Moreover the CrossLam buildings show a good seismic behaviour due to their lightness and good energy dissipation capacity. In the construction practice, the massive wooden panels are assembled through metallic connectors (hold-down, angle brackets and screws). These connectors, if correctly designed, show a ductile behaviour, which confers to the “wood+connectors” system an optimal behaviour to cyclic actions and, therefore, to earthquakes. Some criteria for ductile design of CrossLam buildings are presented in [5.1].

Although the CrossLam technology is widespread in the common practice, there are few construction and calculation guidelines in the building codes, such as Eurocode 5 [5.2] and Eurocode 8 [5.3], especially with regard to the seismic design. The well-known and widely used Force-Based Design (FBD) method approach for the seismic design of structures [5.4] is based on the evaluation of the behaviour factor q which is needed to transform the elastic response spectrum into a design spectrum. In this way a nonlinear structure can be designed to resist to seismic action using a linear-elastic static or dynamic analysis, where the structural ductility and dissipation capacity of the structure are implicitly considered into the behaviour factor q value. CrossLam timber structures are not specifically considered by EC8 [5.3] and Italian regulation [5.5] as a building typology. The reduction factor q for buildings with glued timber elements is safely imposed equal to 2 regardless of the slenderness of the building and of the number and arrangements of the connectors in relation to the size and geometry of the structure. The effects of this lack of the available codes are relevant considering that the usage of CLT panels to realize even tall buildings is continuously increasing.

In this part of the dissertation some indications and findings on the most suitable value of the q -factor and on the dissipation capacity for the CrossLam building are critically presented. In detail the influence of some significant characteristics, such as arrangement of the fasteners, number of storey, etc., on the seismic response of the whole building and therefore on the reduction (or behaviour) factor value are examined and studied. Some additional investigations are carried out about the effects of the criteria used to design the mechanical connectors and of the different overstrength factor used for the various typologies of joints. The results obtained from such investigations represent the basis for the development of a proposal for an analytical formulation to calculate the q -factor values starting from building slenderness and wall compositions (i.e. number and arrangements of panel to panel connections).

5.2 Seismic research on CLT building - State of art

The use of CLT building system in the north Europe and Alpine Area is becoming more and more common thanks to its optimal structural robustness and thermic and acoustic insulation performance. In the last year this innovative building system is spreading also in the Mediterranean areas and in North America. These regions are characterized by a medium – high seismic levels therefore the adequateness of the CLT building to efficiently resist earthquakes must be verify. In order to define the behaviour of CrossLam buildings under seismic conditions, researches and specific studies have been carried out in several European countries and in Canada.

The most comprehensive research activity to quantify the seismic behaviour of low- and mid-rise CrossLam construction was part of the SOFIE Project in Italy. This project was undertaken by the Trees and Timber Institute of the National Research Council of Italy (CNR IVALSA) in collaboration with National Institute for Earth Science and Disaster Prevention in Japan (NIED), Shizuoka University, and the Building Research Institute (BRI) in Japan. The testing program included tests on single connectors [5.6] and [5.7]; plane cyclic tests on CrossLam shearwalls with different layouts of connections and openings [5.8]; pseudo-dynamic tests on a one-storey 3-D specimen in three different layout [5.9]; shaking table tests on a three storey building under different earthquakes [5.10]; and finally a series of full-scale shaking table tests on a seven storey CrossLam building conducted at E-Defense facility in Miki, Japan [5.11]. The following Fig. 5.1 reports as an example some representative images of the most relevant experimental tests performed during the SOFIE project.

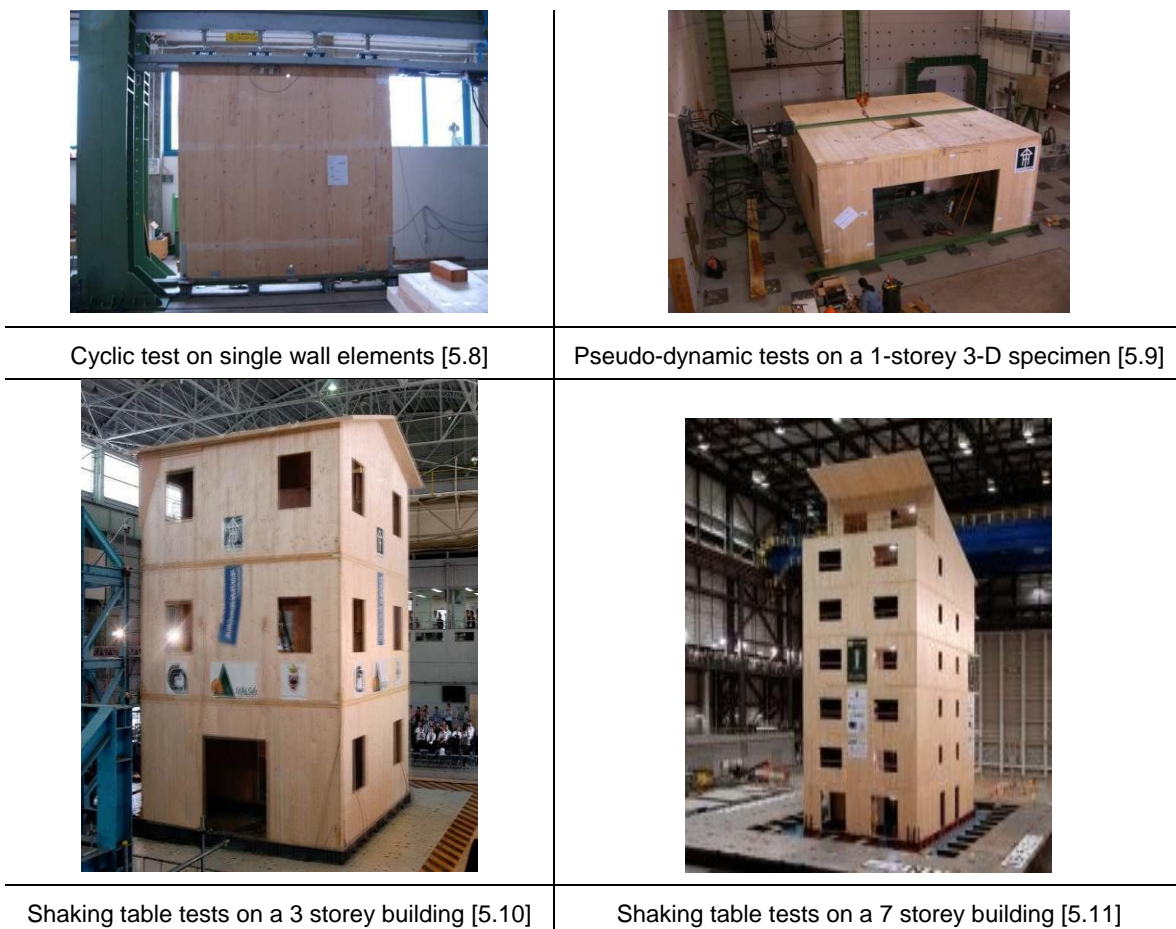


Fig. 5.1 – Main experimental tests on CLT specimen carried out during SOFIE project.

SOFIE project has not only provided experimental tests but also numerical simulations conducted on the 3-storey building with the aim to define its most suitable behaviour q -factor. The following Fig. 5.2 reports the DRAIN 3D spring lamped-mass numerical model used to perform the numerical analyses. In detail the fasteners nonlinear springs were modeled using the “Ceccotti – Vignoli” hysteretic model [5.10].

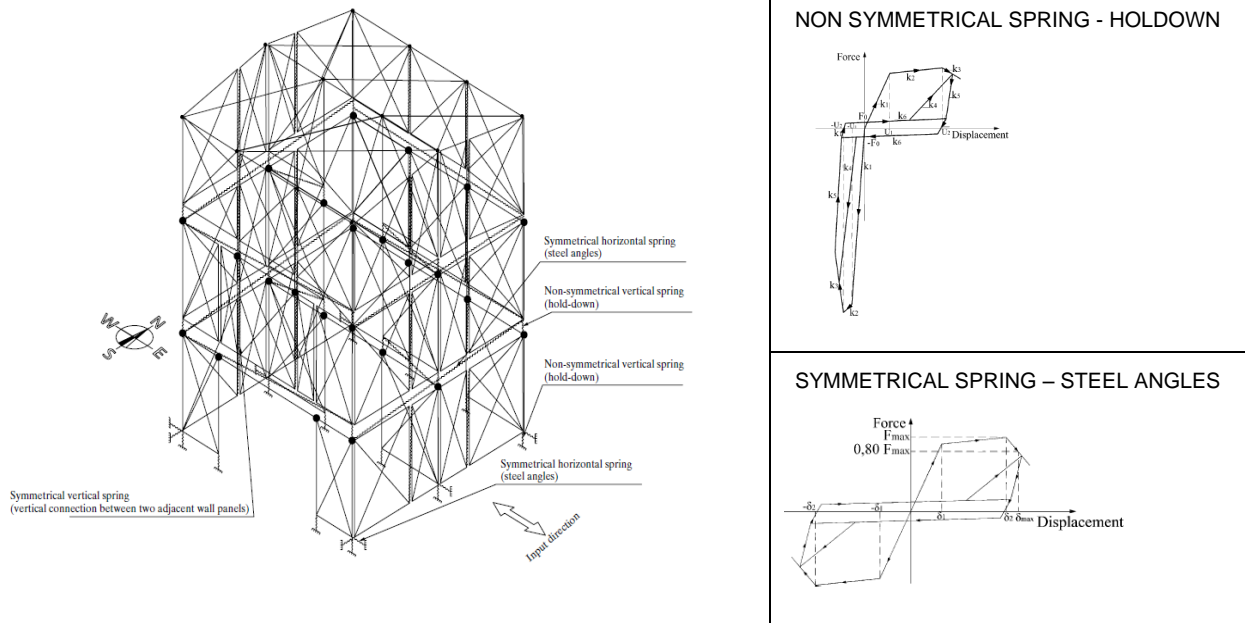


Fig. 5.2 – DRAIN 3D numerical model used to investigate the CLT building seismic response during SOFIE project (left) and “Ceccotti Vignoli” hysteretic model for connectors (right) [5.10].

On the basis of such analytical studies and experimental tests, it has been forwarded that a q -factor equal to 3 was a more reasonable estimation for the CrossLam buildings [5.10].

Other studies were conducted at the University of Ljubljana, Slovenia, to determine the seismic behaviour of 2-D CrossLam shearwalls. Numerous quasi-static monotonic and cyclic tests were carried out on the walls with the aim to investigate the influence of boundary conditions, magnitude of vertical load and anchoring system [5.12] and shaking table tests were conducted on two single-storeys CrossLam box at the Dynamic Testing Laboratory of Institute of Earthquake Engineering and Engineering Seismology (IZZIS) in Skopje, Macedonia [5.13].



Cyclic test on single wall elements [5.12]



Pseudo-dynamic tests on a 1-storey 3-D specimen [5.13]

Fig. 5.3 – Main experimental tests conducted at the University of Ljubljana, Slovenia.

Finally FPInnovations-Forintek in Vancouver has undertaken a research project for determining the structural properties and the seismic resistance of CrossLam structures. A total of 32 monotonic and cyclic tests were performed on various configurations of CrossLam walls [5.14].

The following Fig. 5.4 reports the most significant experimental tests carried out in FPInnovations laboratory.



Fig. 5.4 – Main experimental tests carried out in FPInnovations laboratory – Canada [5.14].

The outcomes from these experimental tests were used by S. Pei et al.[5.15] to calibrate the numerical model successively used to analyze the same six storeys building tested on shaking table during the NEES project [5.16]. This building was redesigned using the CLT building and adopted as reference case study to define the most suitable q-factor for CLT building. A q-factor of about 3.75 was obtained from the performed numerical analyses and given as reasonable estimation for the investigated CrossLam buildings [5.15].

The research activities and experimental test described above focuses on the seismic response of specific CLT elements and buildings characterized by particular geometric features, building methodology, fasteners arrangement. In detail the obtained results in terms of q-factor, are specific of the studied buildings and cannot be extended to the entire building system.

Furthermore no indication are given about the effect of some specific building characteristic such as the slenderness, the wall composition, the in-plan and in-high regularity and the fasteners arrangement, on the seismic response and therefore on the most suitable q-factor to use for seismic design of CLT building.

However the results of the previously defined research activities represent a relevant database on the behaviour of the CLT buildings that can be used as input information to develop more complete studies on the seismic response of this construction technology.

5.3 Overview on the CLT construction practice

As described above, the considerable diffusion of the CLT building system has been accompanied by the development of a numbers of construction methodologies. These methodologies differ mainly on the dimension for the CLT panels used to assemble the walls. In detail walls can be made by an unique CLT panel or by proper assembling of smaller CLT panels. From the construction point of view it is preferred using CLT panel as bigger as possible so as to minimize the in situ joints. Recently it is becoming more common the using of small modular CLT panel. Clearly with this choice the number of in situ joints increases but some advantages are introduced from the point of view of lifting and handling the panels and the modularization of the construction system with consequent reduction of the material waste. Generally these CLT modular panels presents the height equal to the inter storey and base 1.25 m wide.

The constructive technique used to realize the walls strongly affect the displacement capacity and therefore the seismic behaviour of the building. This correlation is also confirmed by the experimental tests carried out during the SOFIE project [5.6]. The following Fig. 5.5 summarized the outcomes from the cyclic tests performed on three different wall elements: the first one is made by a unique CLT panel, the second and the third made with two adjacent CLT panels differently connected. The fasteners arrangement and the load slip derived from each tested walls are reported in the same figure.

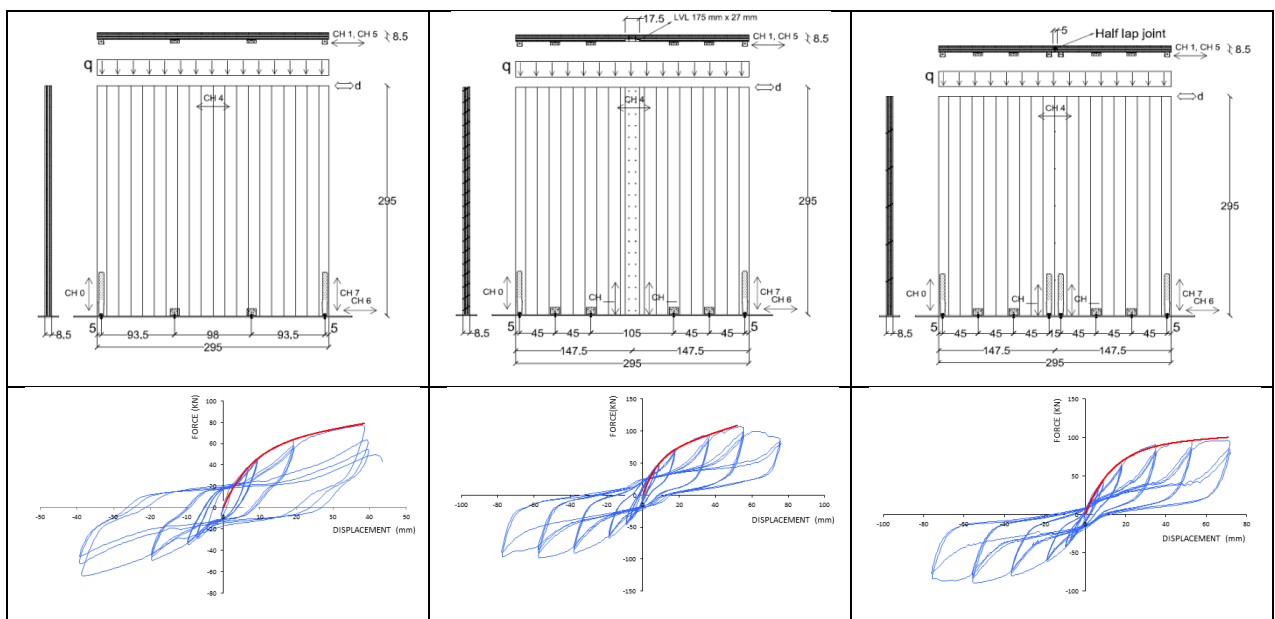


Fig. 5.5 - Fasteners configuration and load slip curve of the tested walls

As shown in Fig. 5.5 the displacement capacity of the jointed walls is greater than that of the wall made by a unique CLT panel. Consequently, according to the conclusion draft in the previous Chapter 4, the q -values of the joint free CLT wall is lower than that of the jointed ones.

Experimental evidence points out the relevance of the wall composition over the seismic response of the CLT building. A proper seismic design of CLT building should take into account the constructive methodology through a suitable choice of the design criteria of the fasteners and of the seismic behaviour factor. Indeed no provisions about this are given by modern seismic codes.

5.4 Parameters influencing the q-factor value

The dissipative capacity of a CLT building is a complex function of a number of parameters according to the scheme in Fig. 5.6.

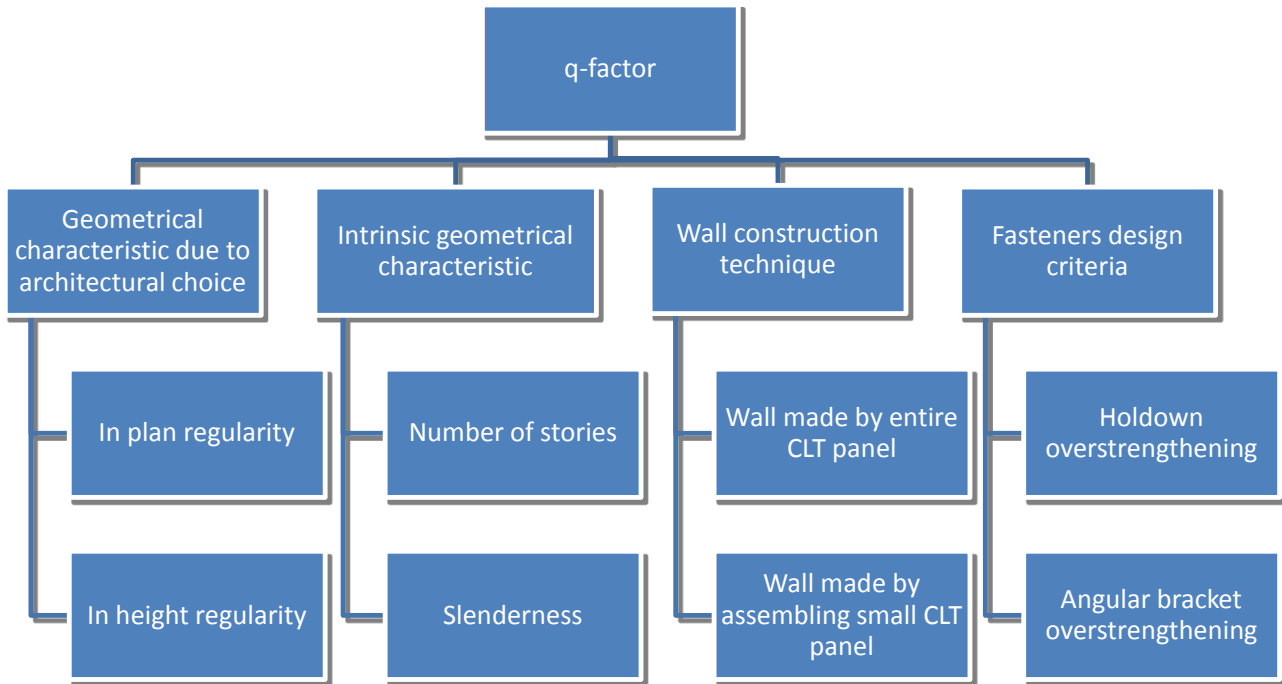


Fig. 5.6 - Parameters with influence over the q-factor.

Such scheme can be resumed with the following Eq. 5.1:

$$q = q(\text{Regularity}, N. \text{ storeys}, N. \text{ wall joints}, \text{Slenderness}, \text{Joint overstrength ratio}) \quad \text{Eq. 5.1}$$

All these parameters influence the seismic response and the dissipative capacity of the CLT building. In detail:

- The *in plan regularity* influences the distribution among the shear wall of the horizontal force introduced by the earthquake in the structure. A symmetric in-plan wall distribution is the optimal configuration which minimizes the torsional effect. On the contrary an unbalanced and irregular in-plan wall distribution causes disequilibria in the seismic force distribution and displacement demand between the shearwalls and a reduction in the seismic performance of the building.
- The *elevation regularity* affects the transmission of seismic forces through the levels of the buildings up to the foundations. It is evident that a building with continuous walls from the foundation to the roof and with regular distribution of the opening performs better in case of seismic event. Noncontinuous walls and irregular opening distribution affect negatively the seismic resistance of the building and requires the horizontal forces follow complex path to be transported to the footings.
- The *storeys number* has a direct effect on the principal elastic period of the building and therefore on the seismic susceptibility of the construction. Increasing the storeys

number the number of panel to panel junctions grows up. Consequently the number of fasteners also increases together with the global dissipative capacity of the building. This trend is reliable only for building up to 7-8 levels, then the additional storeys remains in elastic field without relevant effect on the dissipative capacity.

- The slenderness is defined as the ratio between the height and the base dimension of the building. It determines the response of the building: to low slenderness values a shear like behaviour correspond while high slenderness induces a flexural and rocking like behaviour.
- The wall joints number (i.e. construction methodology) influences strongly the displacement capacity of the building and therefore its ductility. A wall composed by assembling of a numbers of CLT panels is surely more dissipative than a joint free one of equal strength.
- The joints design criteria defines the failure mode of the connection. As reported in [5.1] using a capacity design criteria. i.e. assuring a proper overstrength to fragile failure mechanism, it is possible to guarantee a ductile failure of the connectors and consequently increases the ductility of the building. As an example a rocking like behaviour of the building can be forced by overstrengthening the shear connections respect to the holdowns.

An accurate definition of the q-factor couldn't disregard the influence of those parameters that strongly affect the actual seismic behaviour of the building.

Indeed also the most modern and updated seismic codes [5.3] [5.5] only take into account the dependence of the q-factor from the in plant and elevation regularity, while the influence of all the other parameters is not considered and a unique base q-value is given for all CLT structures.

Aim of the following section is to give some addresses and original findings about the influence of the cited parameters on the q-factor value, summarizing the results from an extensive numerical simulation campaign of different buildings.

5.5 Parametric analyses to assess the influence of slenderness, design criteria, wall composition and joints arrangement on the CLT building q-factor

In this section an extensively investigation on a numbers of different CLT buildings is carried out. Aim of the investigation is to give some indications about the relationship between the q-factor values and some relevant characteristics of CLT building such as the number of storeys, the building slenderness and the wall composition.

The proposed research starts with the choice of a representative case study building of which the numerical simulation and the q-factor evaluation is conduced. The reference case study building was chosen among the buildings erected in L'Aquila during the reconstruction project C.A.S.E. after the 2009 earthquake [5.15]. A total of 24 different configurations of such building were designed varying number of storeys, walls composition and joints arrangement.

These building tests were studied using a 2D plane numerical model with mass lumped springs based on the Elwood [5.18] pinching hysteretic model. Such model is available into the open-source research FEM code Open SEES [5.19]. The numerical model was calibrated on the bases of the experimental cyclic test carried out on CLT wall elements during the SOFIE project.

A numbers of NLSAs and NLDAs were performed in order to investigate the seismic behaviour of the case studies building. The q-factors of each building configurations was evaluated on the basis of the results from the nonlinear analyses using procedures defined in the previous Chapter 3.

5.5.1 Reference CLT building

The building taken as reference to develop all the 24 case studies building has been selected among those built up during the C.A.S.E project for the post-earthquake rebuilding of Abruzzo region – 2009, Italy [5.15], specifically the CLT three storeys building realized by WOOD BETON S.p.a. Company.

Fig. 5.7 gives some views of the considered building.



Fig. 5.7 – Views of the considered three storeys building.

The building is composed by 4 structurally independent portions with rectangular plan as depicted in Fig. 5.8.



Fig. 5.8 – Plant view of the considered three storeys building.

Only the lateral portion of the building having plan dimensions of 17.5 m x 8.75 m was considered. The inter-storey height is equal to 3.05 m. This building portion is made by CLT 160 mm thick

panels used both for perimeter walls and floors. Floor panels are arranged along the shorter dimension and are supported on the perimeter walls and on an intermediate middle beam. Regarding to the seismic aspects the wall distribution is regular in plan with two seismic resistant walls along the longer side and three seismic resistant walls along the shorter one as shown in Fig. 5.9.

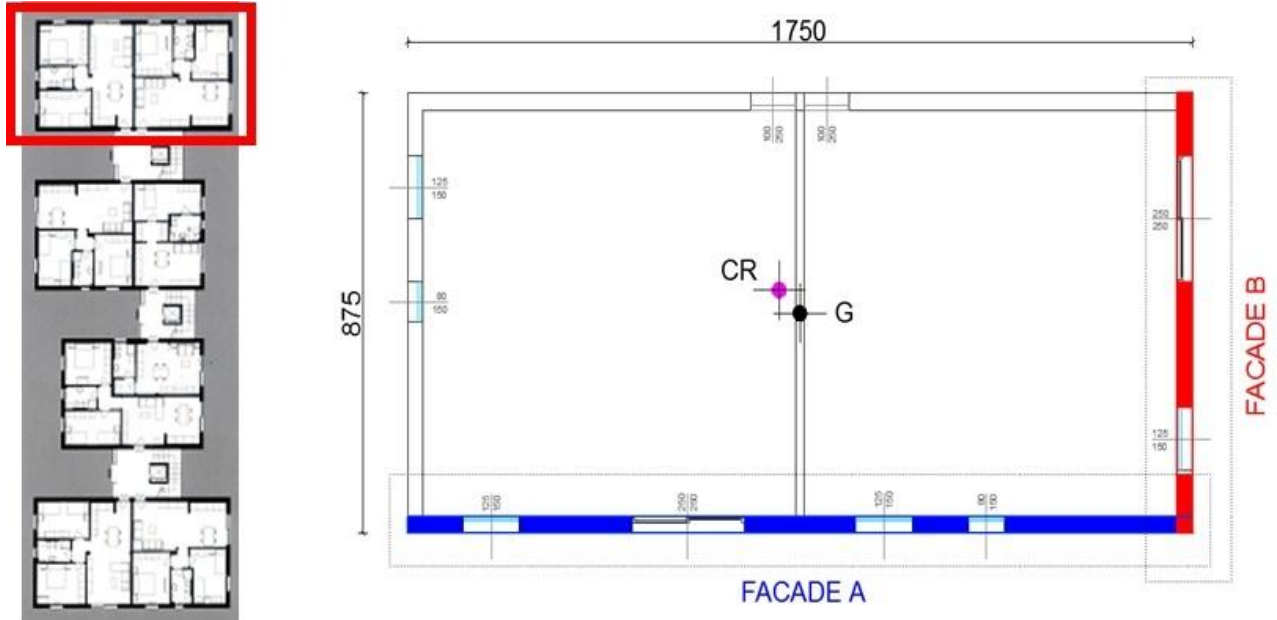


Fig. 5.9 - Seismic resistant walls distribution with evidenced the walls analyzed with a 2D plane model.

The wall distribution is symmetrical in both the directions and also the storey mass distribution is uniform. Hence the mass center G almost coincides with the stiffness center CR and the torsional effects are negligible.

In shake of simplicity, a 2D plane model was used to study the building response, along each principal axe of the building. The two perimeter walls evidenced in Fig. 5.9 having the major number of openings were analyzed. The openings distribution on these façades is regular as depicted in the following Fig. 5.10. For both the two façades various composition of CLT panels assembling and fasteners arrangement were considered and their seismic response analyzed.

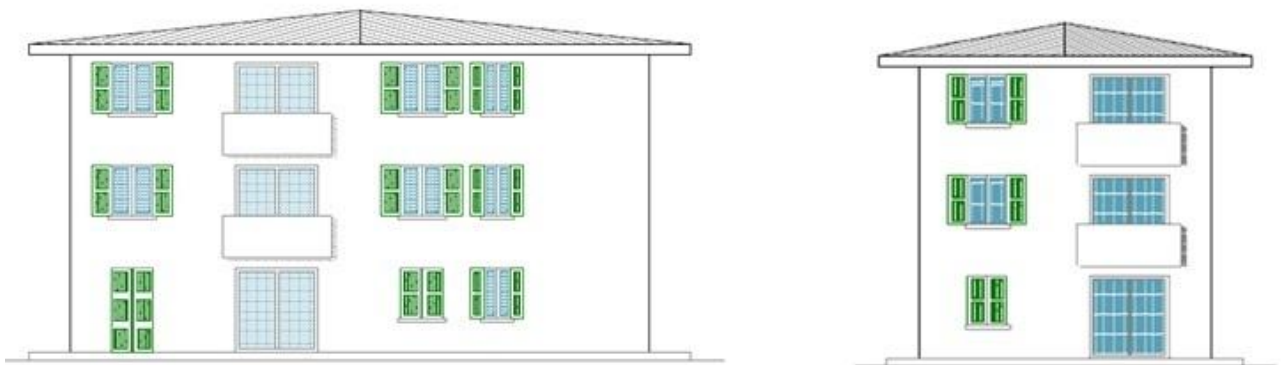


Fig. 5.10 – Perspective view of the examined façade A (left) and B (right).

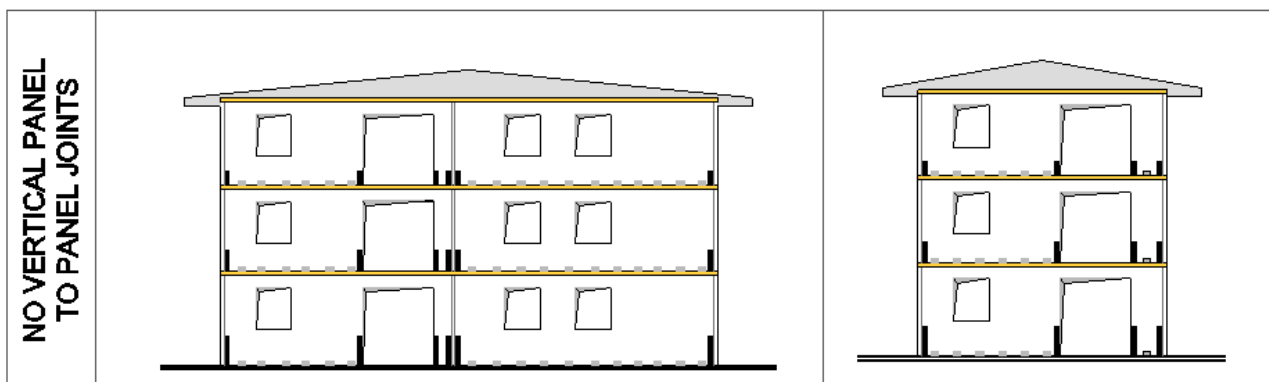
5.5.2 Assessment of building test configurations

The analyzed configurations were defined with reference to the principal geometrical characteristics (i.e. length, inter storey high, opening distribution..) of the reference building and of the two perimetral façade above defined. A total of 24 different configurations (12 for each façade) were set varying the storeys number (from 1 to 7) and the wall composition. Three different wall composition were considered: the 1st one provides walls made by entire CLT panels (no vertical joints), the 2nd one provides walls made by 4 or 2 CLT panels respectively for façade A and B (medium degree of vertical joints), the 3rd one provide walls made by 1.25 wide CLT panels (high degree of vertical joints). All the 24 different configurations are summarized in Fig. 5.11.

	NO VERTICAL JOINTS		MEDIUM DEGREE OF VERTICAL JOINTS		HIGH DEGREE OF VERTICAL JOINTS	
1 STOREY						
3 STOREYS						
5 STOREYS						
7 STOREYS						

Fig. 5.11 – Case study configurations.

The fasteners arrangement depends on the wall composition. Regardless of the examined configuration the holdowns are placed at the extremities of the wall, at the side of the door opening and at the T walls intersections. Some additional holdowns are placed at the side of the vertical panel to panel joints, as depicted in Fig. 5.12. Angle connections for adsorbing shear forces are assumed uniformly distributed along the wall-foundation interface and along the inter-storey joints independently (see Fig. 5.12.)



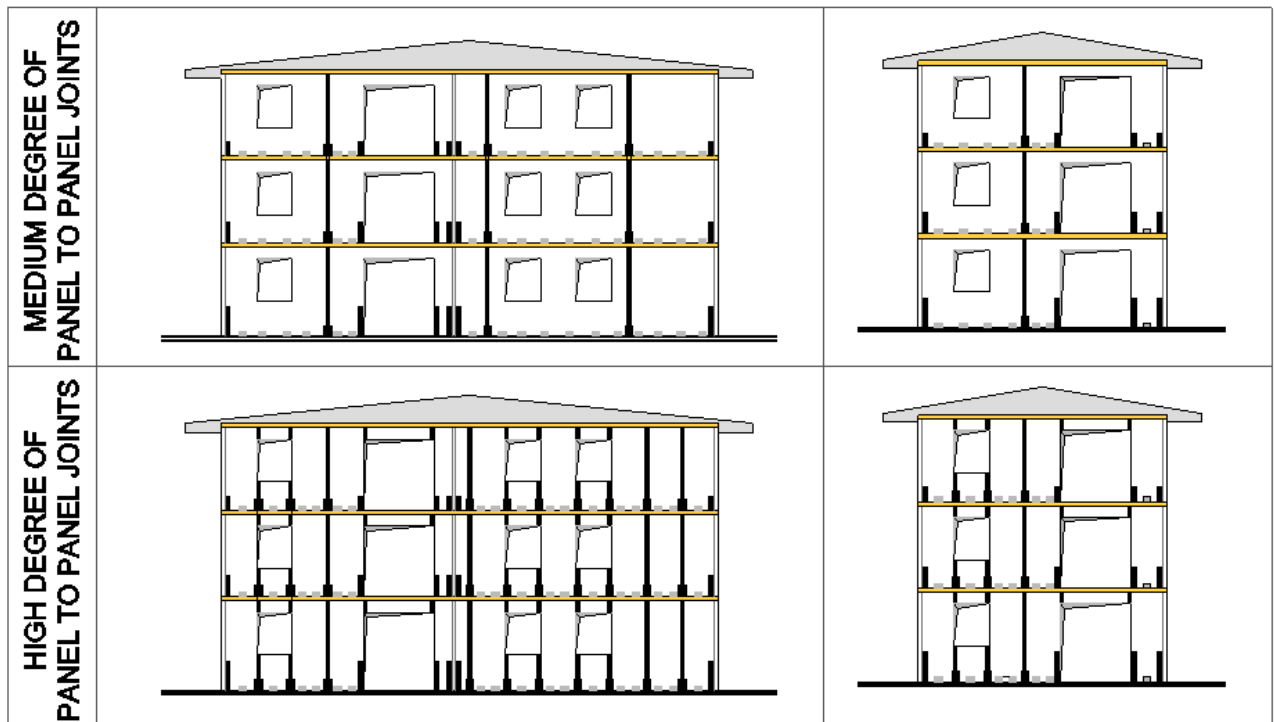


Fig. 5.12 - Fasteners arrangement for each junction levels and reference facades - the three storeys case study was taken as reference.

In CLT building construction an alternative solution is possible and often applied consisting in the substitution of the holdowns in correspondence of the internal joints with strong vertical panel to panel joints made with LVL strips fastened to the CLT panels by means of nails or self-drilling screws (see Fig. 5.13). In order to investigate the influence of such different construction method on the seismic response of the building 8 additional case studies were analyzed. Taking into account these 8 additional configurations a total of 32 case studies were investigated.

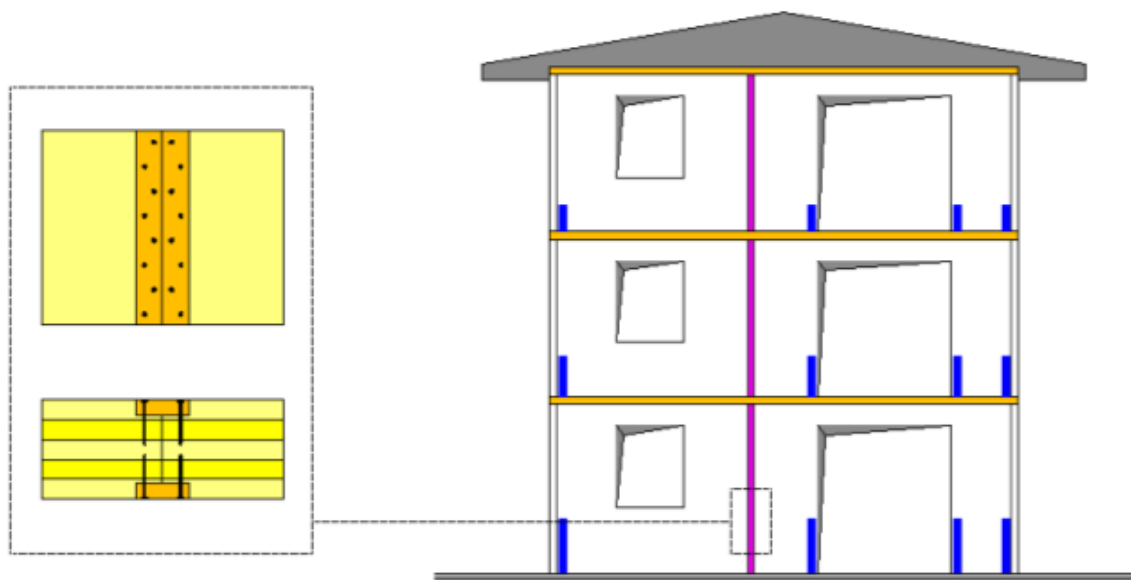


Fig. 5.13 – Detail of LVL panel to panel joints and relative holddown arrangement on the wall - the three storeys case study was taken as reference.

Fig. 5.14 summarizes all the configurations and reports also their respective slenderness $\lambda=H/B$, seismic mass M and principal elastic period T_1 .

	NO VERTICAL JOINTS		MEDIUM LEVEL OF VERTICAL JOINTS			HIGH LEVEL OF VERTICAL JOINTS		
1 STOREY								
	A 1 N	B 1 N	A 1 M	B 1 M	B 1 M*	A 1 H	B 1 H	B 1 H*
	$\lambda=0,17$	$\lambda=0,35$	$\lambda=0,17$	$\lambda=0,35$	$\lambda=0,35$	$\lambda=0,17$	$\lambda=0,35$	$\lambda=0,35$
	M=18,0	M=12,0	M=18,0	M=12,0	M=12,0	M=18,0	M=12,0	M=12,0
	$T_1=0,12$	$T_1=0,14$	$T_1=0,14$	$T_1=0,14$	$T_1=0,15$	$T_1=0,17$	$T_1=0,16$	$T_1=0,19$
3 STOREYS								
	A 3 N	B 3 N	A 3 M	B 3 M	B 3 M*	A 3 H	B 3 H	B 3 H*
	$\lambda=0,52$	$\lambda=1,05$	$\lambda=0,52$	$\lambda=1,05$	$\lambda=1,05$	$\lambda=0,52$	$\lambda=1,05$	$\lambda=1,05$
	M=92,0	M=60,0	M=92,0	M=60,0	M=60,0	M=92,0	M=60,0	M=60,0
	$T_1=0,24$	$T_1=0,28$	$T_1=0,30$	$T_1=0,30$	$T_1=0,32$	$T_1=0,41$	$T_1=0,36$	$T_1=0,41$
5 STOREYS								
	A 5 N	B 5 N	A 5 M	B 5 M	B 5 M*	A 5 H	B 5 H	B 5 H*
	$\lambda=0,87$	$\lambda=1,74$	$\lambda=0,87$	$\lambda=1,74$	$\lambda=1,74$	$\lambda=0,87$	$\lambda=1,74$	$\lambda=1,74$
	M=166,0	M=108	M=166,0	M=108	M=108	M=166,0	M=108	M=108
	$T_1=0,40$	$T_1=0,46$	$T_1=0,47$	$T_1=0,50$	$T_1=0,53$	$T_1=0,58$	$T_1=0,60$	$T_1=0,64$
7 STOREYS								
	A 7 N	B 7 N	A 7 M	B 7 M	B 7 M*	A 7 H	B 7 H	B 7 H*
	$\lambda=1,22$	$\lambda=2,44$	$\lambda=1,22$	$\lambda=2,44$	$\lambda=2,44$	$\lambda=1,22$	$\lambda=2,44$	$\lambda=2,44$
	M=240,0	M=156	M=240,0	M=156	M=156	M=240,0	M=156	M=156
	$T_1=0,59$	$T_1=0,75$	$T_1=0,65$	$T_1=0,78$	$T_1=0,81$	$T_1=0,80$	$T_1=0,97$	$T_1=0,96$
DENOMINATION CRITERIA FOR CASE STUDY CONFIGURATIONS: X Y Z(*) X= REFERENCE FACADE (A; B) - Y=STOREYS NUMBER (1; 3; 5; 7) - Z=JOINTS DENSITY (N; M, H) WALL CONFIGURATION MARKED WITH * STANDS FOR ALTERNATIVE PANEL TO PANEL JOINTS DESIGN CRITERIA								

Fig. 5.14 – Total of case study configuration and indication of the respectively slenderness, storeys mass and principal elastic period

The slenderness values span in the range 0.17-2.44 while the principal elastic periods are comprised between 0.12s. to 0.97 sec. It is worth noting that with the same number of storeys the slenderness of façade B configurations is twice of the corresponding for façade A.

5.5.3 Seismic design criteria of the shear walls

The seismic design of the investigated configurations was carried out by Linear Static Analysis adopting the following common data, according to Eurocode 8 [5.3]: type 1 elastic response spectra and rock foundation (type A soil according to EN 1998-1, corresponding to $S=1.0$, $TB=0.15\text{sec}$, $TC=0.4\text{sec}$, $TD=2.0\text{sec}$), behaviour factor $q=1$, lowest bound factor for the design spectrum $\beta=0.20$. Design PGA was assumed equal to $0.35g$ (the highest value for the Italian territory) with a building importance factor $\gamma_I=1$. The reference design spectra are reported in Fig. 5.22.

The design of each connector was conducted according to the procedure and design guidance reported in [5.10]: the hold-downs prevent the wall uplift due to the rocking effect while the angle brackets prevent the wall slip due to the shear effect.

The storeys shear forces acting on the angular brackets are defined by the horizontal force balance while the forces acting on the holddown are defined by the global moment equilibrium according to Fig. 5.15.

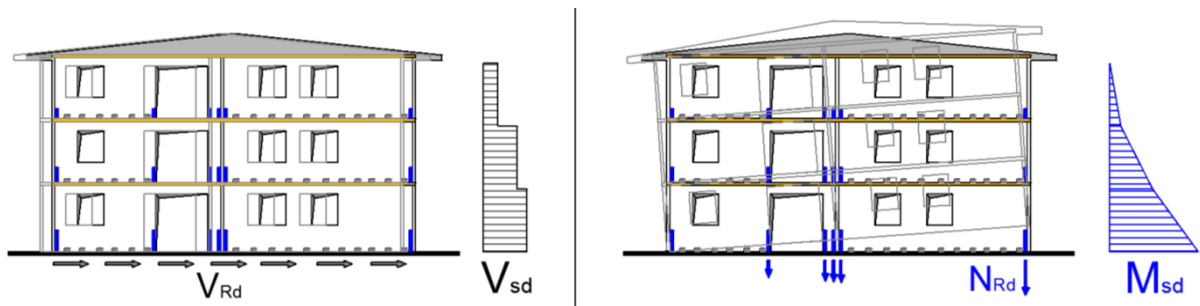


Fig. 5.15 – Force distribution on base angular bracket and holddown under earthquake.

The forces acting on the vertical panel to panel joints were defined considering the average shear forces acting on the boundary of the panel according to the force distribution reported in Fig. 5.16 (a). Otherwise the design of the internal holddown was performed considering the balance between the seismic force acting on each single CLT panel, the stabilization contribution given by the vertical connections and the holddown reaction according to the scheme (b) depicted in Fig. 5.16.

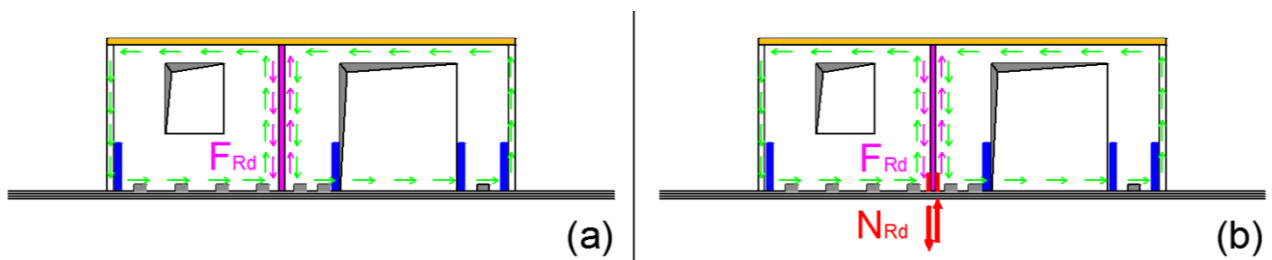


Fig. 5.16 – Force distribution on the vertical panel to panel joints (a) and middle holddown (b) under earthquake.

The design criteria described above provide the force acting in the fasteners but no information are given about the strength definition of the connection elements. In this work the maximum strength and displacement of the fasteners were deduced from the experimental load-slip curve of the holddown, angular bracket and panel to panel joints reported in [5.6]. These load-slip curves were assumed as reference and scaled up to obtain the required resistance, as a suitable number of

connections would be arranged in parallel to bear the applied seismic force. Table 5.1 reports for each kind of fasteners its hysteretic load-slip curve obtained from the experimental tests and the correspondent failure limits. An image of the test setup is also reported.

Table 5.1 – Fasteners failure limit according to experimental tests [5.6]

Holddown					
Property	Unit	Hold-downs tension		Hold-downs shear	
		\bar{x}	COV[%]	\bar{x}	COV[%]
F_y	[kN]	40.46	8.11	3.64	33.85
v_y	[mm]	8.80	21.79	1.25	32.52
F_{max}	[kN]	48.33	5.37	10.13	9.85
v_{max}	[mm]	20.30	14.17	26.89	10.34
F_u	[mm]	38.79	5.31	9.83	8.32
v_u	[mm]	23.75	13.82	30.00	0.00
D	[-]	2.76	16.25	26.78	38.85
k_{el}	[kN/mm]	4.51	14.34	3.16	43.53
k_{pl}	[kN/mm]	0.75	14.37	0.28	7.64

Angular bracket					
Property	Unit	Angle brackets tension		Angle brackets shear	
		\bar{x}	COV[%]	\bar{x}	COV[%]
F_y	[kN]	19.22	2.73	22.98	5.18
v_y	[mm]	7.26	9.03	11.74	5.86
F_{max}	[kN]	23.47	4.32	26.85	3.15
v_{max}	[mm]	17.69	9.62	27.28	12.78
F_u	[mm]	18.74	4.32	26.19	4.47
v_u	[mm]	23.19	6.14	30.00	0.00
D	[-]	3.21	6.81	2.60	5.33
k_{el}	[kN/mm]	2.52	9.76	2.09	16.40
k_{pl}	[kN/mm]	0.42	9.56	0.35	16.27

Panel to panel joint					
Property	Unit	Over-lapped joint		LVL joint	
		\bar{x}	COV[%]	\bar{x}	COV[%]
F_y	[kN]	3.23	11.95	4.85	17.67
v_y	[mm]	2.55	11.99	5.70	22.75
F_{max}	[kN]	5.25	13.18	6.96	8.82
v_{max}	[mm]	23.50	9.81	28.96	8.84
F_u	[mm]	4.61	15.98	6.83	12.66
v_u	[mm]	29.83	1.37	30.00	0.00
D	[-]	12.12	11.01	5.71	21.49
k_{el}	[kN/mm]	1.24	18.59	0.84	16.28
k_{pl}	[kN/mm]	0.11	20.01	0.10	39.81

The design of the fasteners was made without applying any overstrength factor between the external seismic action and the resistance according to the following relationship (Eq. 5.2, Eq. 5.3, Eq. 5.4)

$$\gamma_{O_A} = V_{Rd}/V_{Sd}=1 \quad \begin{matrix} \gamma_{O_A} = \text{angular bracket overstrength factor} \\ V_{Rd} = \text{angular bracket strength} \\ V_{Sd} = \text{seismic shear force on angular bracket} \end{matrix} \quad \text{Eq. 5.2}$$

$$\gamma_{O_H} = N_{Rd}/N_{Sd}=1 \quad \begin{matrix} \gamma_{O_H} = \text{holdown overstrength factor} \\ N_{Rd} = \text{holdown strength} \\ N_{Sd} = \text{seismic tensile force on holdown} \end{matrix} \quad \text{Eq. 5.3}$$

$$\gamma_{O_VJ} = F_{Rd}/F_{Sd}=1 \quad \begin{matrix} \gamma_{O_VJ} = \text{vertical panel to panel joint overstrength factor} \\ F_{Rd} = \text{vertical panel to panel joint strength} \\ F_{Sd} = \text{seismic force on vertical panel to panel joint} \end{matrix} \quad \text{Eq. 5.4}$$

These design criteria guarantee a uniform exploitation of all the building fasteners without any premature failure of some connection. The maximum ductility to the building is also assured. The

design criteria adopted assure the achieving of the maximum shear resistance of the angular bracket without premature failure of both holdown and vertical panel to panel joint. This behaviour has been confirmed by means of pushover analyses of the three storeys building which resulting capacity curves are reported in Fig. 5.17. Such pushover curves were obtained with the configurations A3N, A3M, A3H and adopting the storeys force distribution defined by the LSA.

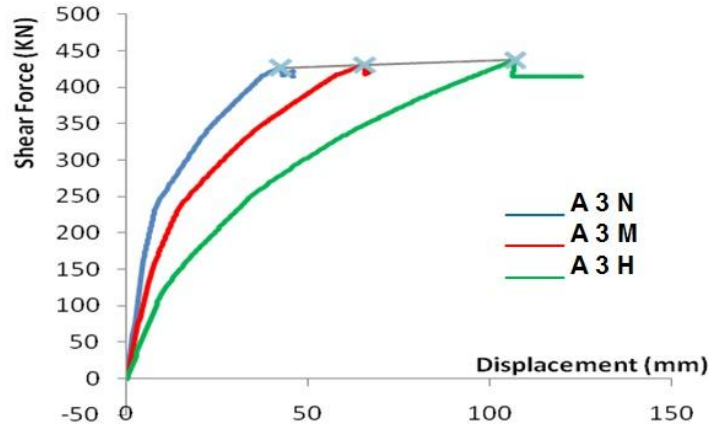


Fig. 5.17 - Pushover curve for three different wall configuration of the three storeys building.

As depicted in Fig. 5.17 the three building configurations fail for the same maximum base shear but with different values of the failure displacement. In detail the building configuration with the maximum number of vertical panel to panel joints (A3H) shows the greatest displacement capacity according to the experimental test [5.6] described in the previous Chapter 4.

Finally three additional design criteria were considered in order to verify the influence of the overstrength (or understrength) of the holdown respect to the angular bracket and vice versa on the seismic response of the building and therefore on the q -factor value. The 1st and the 2nd design criteria provides respectively holdown 10% and 25% stronger than the angular bracket while the 3rd one angular bracket 20% stronger than the holdown. These alternative design criteria were applied only to four building configurations: A3M, B3M, A5M, B5M.

5.5.4 Numerical model of the building

The 32 case study configurations were analyzed by means of 2-Dimensional spring mass-lumped numerical models. The K. Elwood [5.18] hysteretic model implemented into the research code “Open SEES” [5.19] was used to reproduce the pinching like behaviour and strength degrading phenomena of the fasteners. This section reports an extensively description of the numerical model used to investigate the building configurations and details its calibration procedure on the basis of the outcomes from experimental tests.

5.5.4.1 Numerical model of the case studies building

The numerical models used to assess the seismic response of the building configurations assume that the nonlinear behaviour is due to exclusively to the fasteners while the wood elements remains in the elastic field. In the 2D numerical model the CLT panels are modeled as lattice modules composed by stiff elastic truss element. The reliability of the proposed model is justified by actual small shear deformation of the CLT panels. As said before the fasteners are modeled using the K.

Elwood nonlinear springs [5.18], connecting the CLT modules. As an example the following Fig. 5.18 reports the typological numerical model used to assess the seismic response of the building configurations. The three storeys building made with modular CLT panels 1.25 m wide is take as example. In the figure the element typologies are highlighted with different colors.

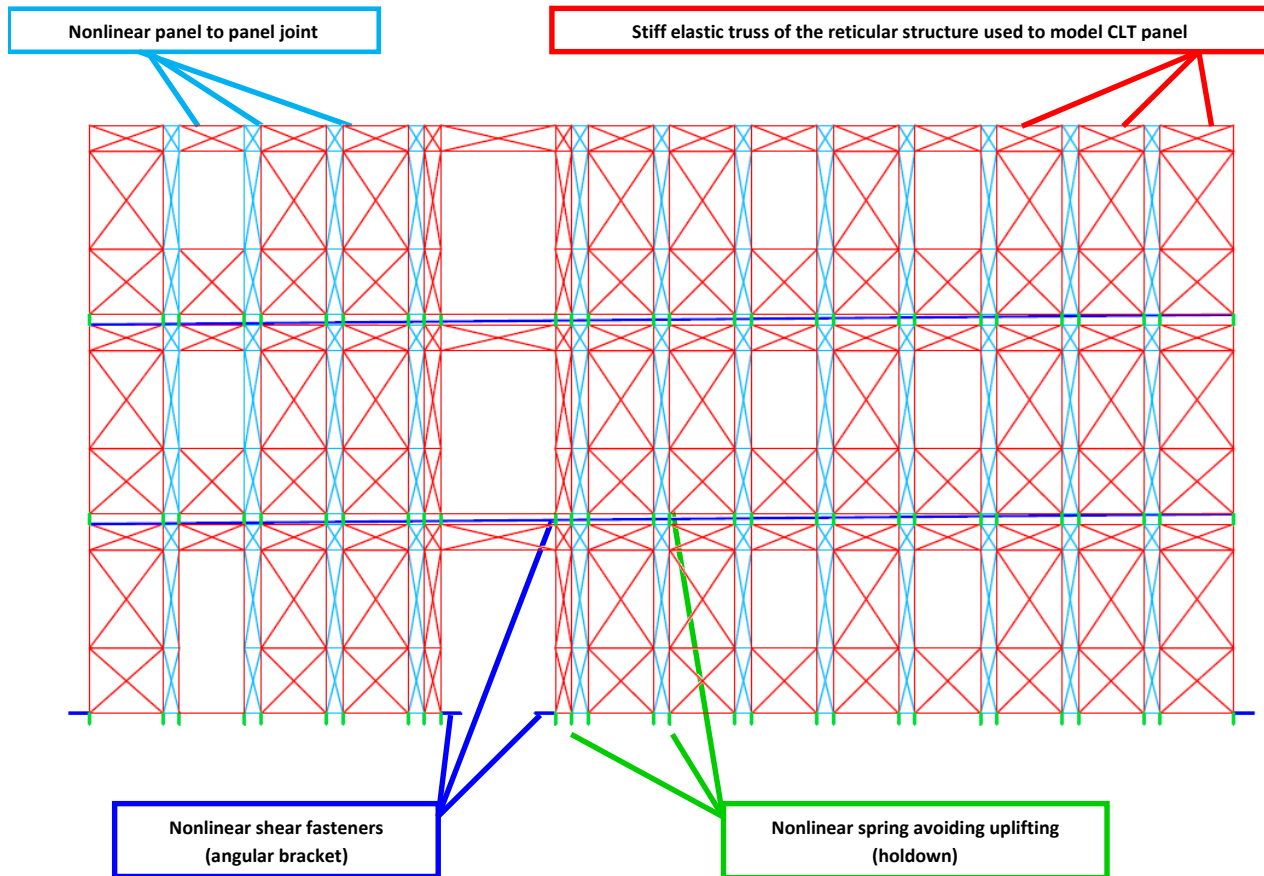


Fig. 5.18 – Scheme of the three storeys building numerical model.

In order to faithfully consider the stabilizing effect of the vertical load on the holddown reaction the storeys masses are uniformly distributed and applied to the nodes of each floor level.

5.5.4.2 Numerical model calibration

The connectors typologies used for assembling the CLT panels are depicted in Fig. 5.19.

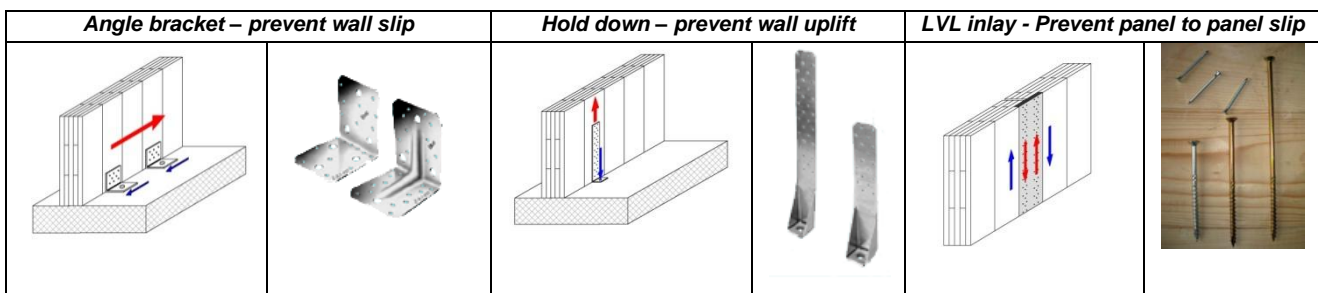


Fig. 5.19 – Example of main fasteners used in CLT building.

These fasteners were tested during the SOFIE research project in the CNR IVALSA laboratory (TN) by means of cyclic test carried out on single connection element [5.6] and on entire wall elements [5.8]. In order to verify the interaction between the CLT lattices model and the fasteners models the experimental tests of various wall specimens were numerically simulated.

Fig. 5.20 reports by an example of comparison between the output from the experimental test and the numerical simulation performed on a CLT wall without vertical joint (i.e. specimens 3a of SOFIE project tst program). The comparison was made with reference to the load -slip curve of the base fasteners and of the entire wall. A comparison in terms of dissipated energy is also given. Fig. 5.20 also gives a sketch of the test setup and a scheme of the numerical model.

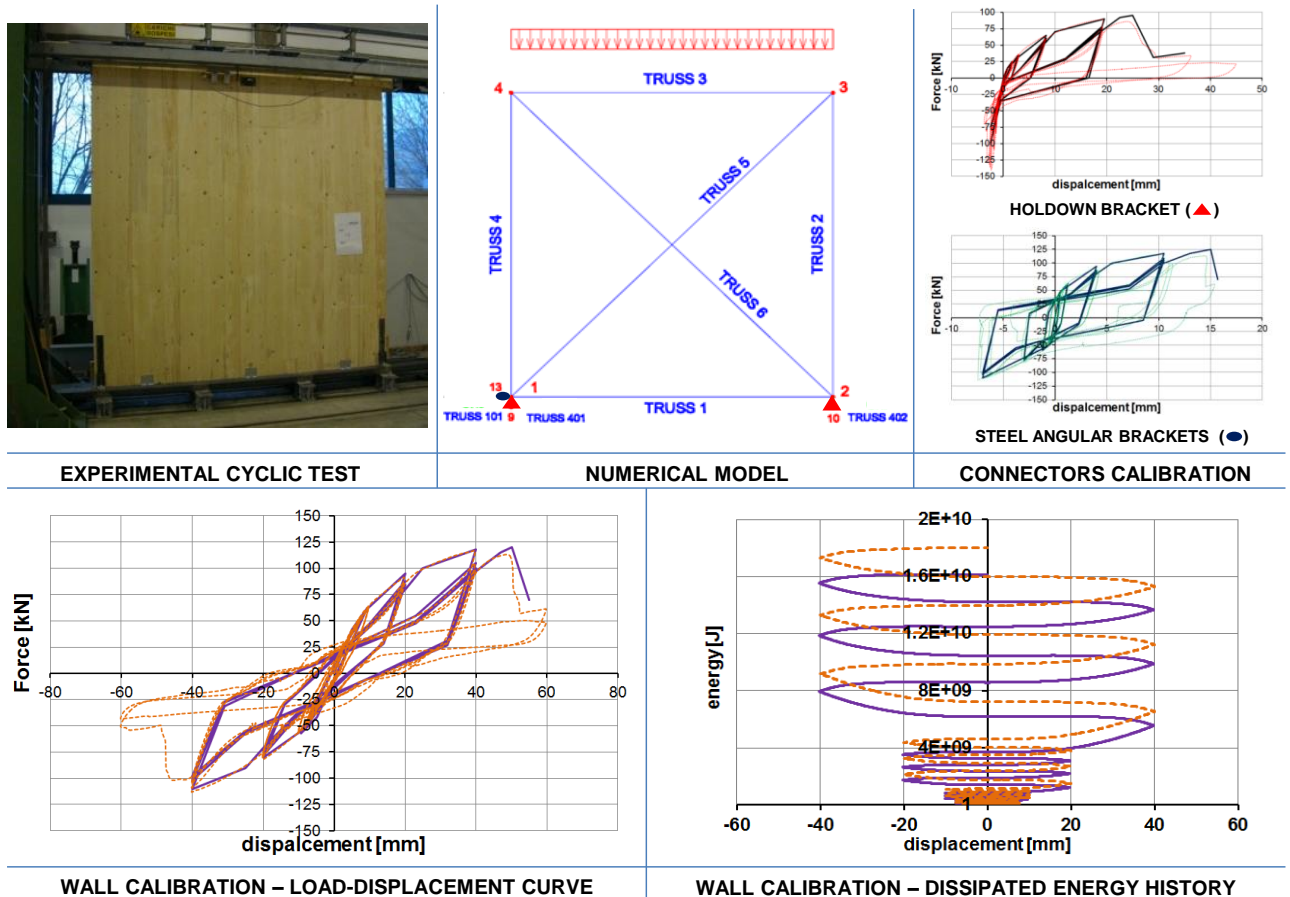


Fig. 5.20 – Example of calibration of the numerical model on the experimental test

The load slip curves obtained from the numerical simulations fit very well those from the experimental tests, both in terms of shape of hysteresis curve and dissipated energy. The difference in terms of dissipated energy is about 10%. The adopted hysteresis model faithfully reproduces the pinching and the strength degradation phenomena. Furthermore the actual failure condition of the connectors is kept.

According to the design criteria above described, the load slip curves obtained from the numerical simulations were scaled up to obtain the strength values required by the seismic design of the building. This procedure corresponds to the constructive practice of installing an adequate number of fasteners to obtain the required resistance.

5.5.5 NonLinear Static and Dynamic Analyses on the buildings

This section focuses on the NonLinear Analyses carried out on the designed building configurations, using the previously described numerical model. Two different types of nonlinear analyses were performed in order to verify the actual response of the examined building configurations. The NonLinear Static Analyses (i.e. NLSAs) allow to obtain the capacity curve of the building giving global information about the yielding and failure limits and therefore about the global ductility of the structure. The NonLinear Dynamic Analyses (i.e. NLDAs) provide the response of the building under dynamic condition simulating the actual building displacement and fasteners force achieved during an earthquake. A final comparison between the results obtained with the two types of analyses is reported and critically discussed.

5.5.5.1 Calibration of NonLinear Static Analyses

The NLSAs were performed according the standard pushover procedure described in the previous paragraph 3.3.2.2 . In order to obtain a more reliable indication about the seismic response of the building tests two different storeys forces configuration were considered. The 1st one provides a force distribution proportional to the displacement of the first elastic modal shape of the building while the 2nd one a force distribution proportional to the storey masses. Fig. 5.21 shows the two force distributions with reference to the three storeys building configurations.

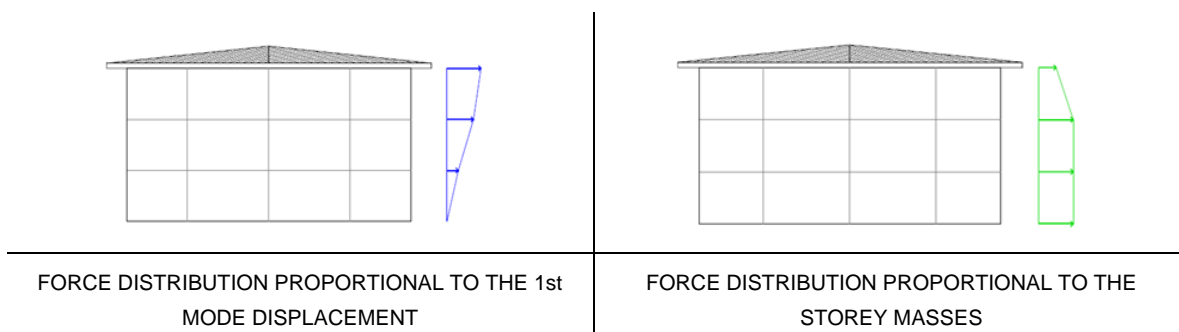


Fig. 5.21 – Example of force distribution used in the NLSAs.

The pushover obtained using these two force distribution delimited an operative zone of the building, as depicted as way as example in Fig. 5.23. The actual building response is intermediate between the two defined with the two force distributions.

The capacity curves obtained by means of the NLSAs represent the input data for the procedure for the q-factor evaluation based on the pushover method. It should be noted that the ultimate condition of the building is clearly defined in the pushover curve: it corresponds to the first achievement of a connection element failure. Because of the hardening behaviour of the buildings the bi-linearization procedure proposed by Albanesi et al.[5.20] was used.

5.5.5.2 Calibration of NonLinear Dynamic Analyses

The NDAs were conducted considering three different seismic signals artificially generated so as to fulfill the compatibility requirement with the design spectrum. (see Fig. 5.22).

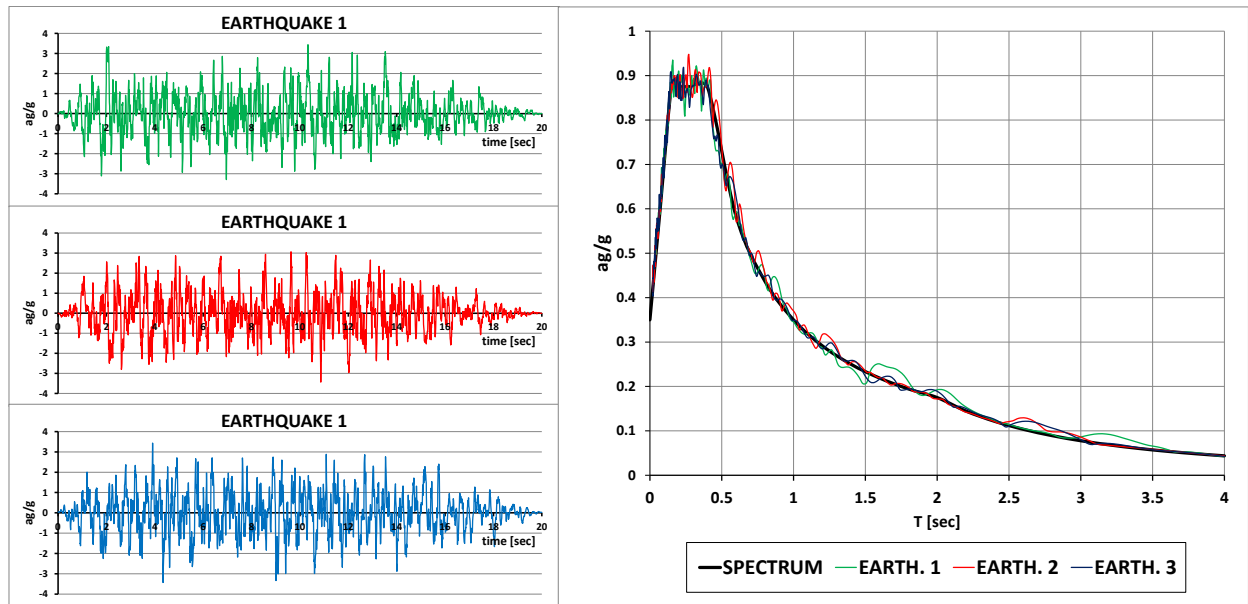


Fig. 5.22 - Seismic signals used in NLDAs (left) and demonstrating of the fulfillment of spectrum-compatibility requirement (right).

The dynamic equilibrium equations have been integrated with a time step equal to 0.001 sec, by adopting an equivalent viscous damping of 2%, according to the Rayleigh model.

In this work the time history analyses were used mainly to define the PGA that leads the structure to the near collapse condition. As stated for the pushover procedure and according to [5.10] the near collapse condition corresponds to the first achievement of a connection element failure. The fasteners failure conditions are summarized in the previous Table 5.1 and are faithfully reproduced by the fasteners numerical models. To individuate the near collapse condition a series of NLDAs were performed with growing levels of PGA starting from the design value.

The main output from NLDAs for each levels of PGA are: (1) the fasteners hysteretic load-slip curve, (2) the time history of storeys displacement and inter storey drifts, (3) the global hysteretic curve of the building obtained by plotting the top displacement versus the correspondent base shear.

5.5.5.3 Analyses results

The output from the NLSAs and NLDAs are reported and compared for each of the 32 examined building configurations. In detail this section reports the following results:

NonLinear Dynamic Analyses:

- the $PGA_{near\ collapse}$ values for each of the three seismic signals;
- maximum top displacements achieved during the shakes for the near collapse condition and the correspondent base shears.

NonLinear Static Analyses:

- the PGA_{max} of the maximum earthquake compatible with the building displacement capacity defined by the pushover curve;

- pushover curves obtained with force distribution proportional to both the displacement due to the 1st eigenfrequency and the storeys masses.

A total of 160 analyses were performed, subdivided into 64 pushover and 96 time history analyses. The obtained results are presented separately.

5.5.5.3.1 Results in terms of near-collapse PGA values

The $PGA_{near\ collapse}$ values obtained using from NLDAs for each of the three earthquake signals are reported in the following Table 5.2 for each building configuration, together with the two values of the maximum allowable PGAs from NLSAs for the two force distribution patterns.

Table 5.2 - PGA_{max} and $PGA_{near\ collapse}$ for each investigated case study building.

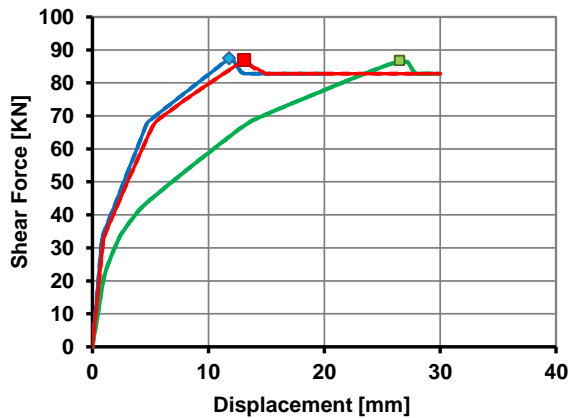
ID	λ	β	push_d	push_m	th1	th2	th3	min	max	average
A1N	0.17	1.00	0.41	0.41	0.45	0.50	0.42	0.41	0.50	0.44
A1M	0.17	1.22	0.44	0.44	0.45	0.55	0.45	0.44	0.55	0.47
A1H	0.17	1.89	0.44	0.44	0.50	0.57	0.46	0.44	0.57	0.48
A3N	0.52	1.66	0.47	0.44	0.52	0.58	0.50	0.44	0.58	0.50
A3M	0.52	2.17	0.53	0.39	0.58	0.62	0.55	0.39	0.62	0.53
A3H	0.52	3.72	0.49	0.39	0.70	0.73	0.68	0.39	0.73	0.60
A5N	0.87	2.07	0.75	0.61	0.55	0.60	0.57	0.55	0.75	0.62
A5M	0.87	2.77	0.75	0.50	0.68	0.76	0.68	0.50	0.76	0.67
A5H	0.87	4.86	0.96	0.81	0.84	0.90	0.80	0.80	0.96	0.86
A7N	1.22	2.35	0.72	0.54	0.70	0.80	0.75	0.54	0.80	0.70
A7M	1.22	3.18	1.03	0.66	0.82	0.90	0.75	0.66	1.03	0.83
A7H	1.22	5.65	1.35	0.90	0.95	1.00	0.95	0.90	1.35	1.03
B1N	0.35	1.00	0.39	0.39	0.40	0.50	0.40	0.39	0.50	0.42
B1M	0.35	1.13	0.39	0.39	0.40	0.50	0.40	0.39	0.50	0.42
B1H	0.35	1.65	0.40	0.40	0.40	0.50	0.40	0.40	0.50	0.42
B3N	1.05	1.49	0.55	0.40	0.57	0.65	0.55	0.40	0.65	0.54
B3M	1.05	1.74	0.53	0.37	0.55	0.62	0.60	0.37	0.62	0.53
B3H	1.05	2.77	0.51	0.39	0.50	0.63	0.62	0.39	0.63	0.53
B5N	1.74	1.73	0.84	0.56	0.75	0.82	0.75	0.56	0.84	0.74
B5M	1.74	2.05	0.88	0.60	0.78	0.85	0.80	0.60	0.88	0.78
B5H	1.74	3.32	0.83	0.72	0.85	0.84	0.75	0.72	0.85	0.80
B7N	2.44	1.87	0.75	0.75	0.70	0.73	0.70	0.70	0.75	0.73
B7M	2.44	2.23	0.87	0.64	0.75	0.80	0.78	0.64	0.87	0.77
B7H	2.44	3.65	1.38	0.96	0.88	0.90	1.10	0.88	1.38	1.04
B1M*	0.35	1.13	0.39	0.39	0.41	0.50	0.41	0.39	0.50	0.42
B1H*	0.35	1.65	0.37	0.37	0.43	0.52	0.42	0.37	0.52	0.42
B3M*	1.05	1.74	0.55	0.39	0.55	0.60	0.60	0.39	0.60	0.54
B3H*	1.05	2.77	0.60	0.43	0.70	0.80	0.62	0.43	0.80	0.63
B5M*	1.74	2.05	0.87	0.60	0.88	0.95	0.84	0.60	0.95	0.83
B5H*	1.74	3.32	0.98	0.70	0.80	0.93	0.80	0.70	0.98	0.84
B7M*	2.44	2.23	0.81	0.60	0.78	0.80	0.78	0.60	0.81	0.75
B7H*	2.44	3.65	1.07	0.83	0.85	1.00	1.00	0.83	1.07	0.95

The building configurations marked with (*) refer to the building technology with vertical panel to panel joint made with strong LVL connection and without internal holdowns. The minimum, maximum and average PGA values reported in Table 5.2 are defined over all the 5 PGA values.

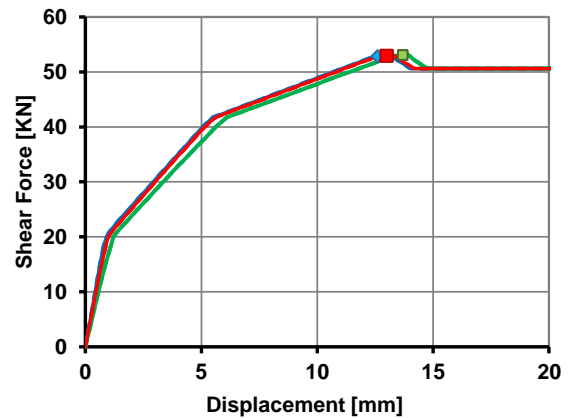
5.5.5.3.2 Results in terms of load-displacement values

The pushover curves obtained for each case study are plotted and superposed to the results from the time history for the near collapse condition. These conditions are represented in the graphs by the points corresponding to the maximum displacement achieved at the top of the building and the corresponding base shear for each shakes investigated. Fig. 5.23 plots the obtained results for the various slenderness λ and junction density of the buildings.

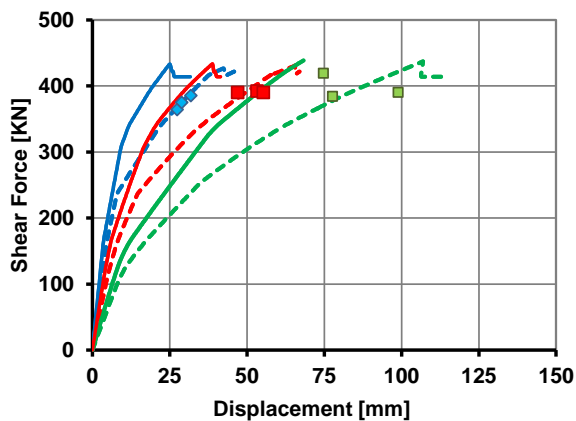
$\lambda = 0.17$



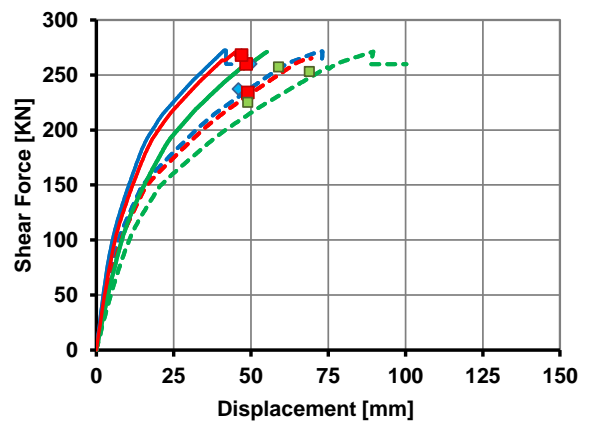
$\lambda = 0.35$



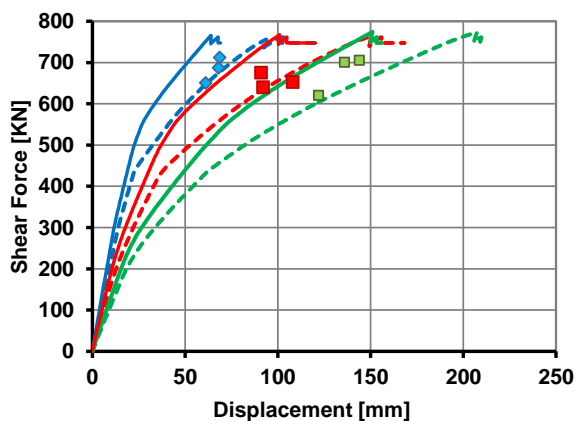
$\lambda = 0.52$



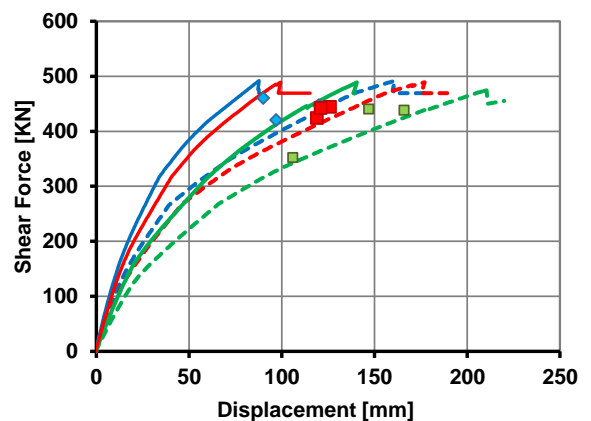
$\lambda = 1.05$

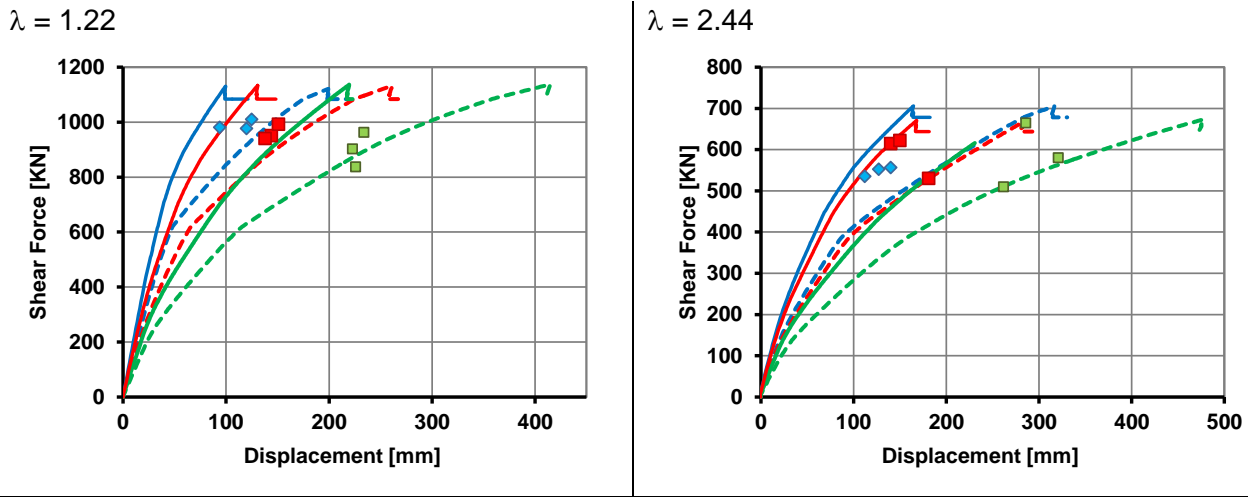


$\lambda = 0.87$



$\lambda = 1.74$

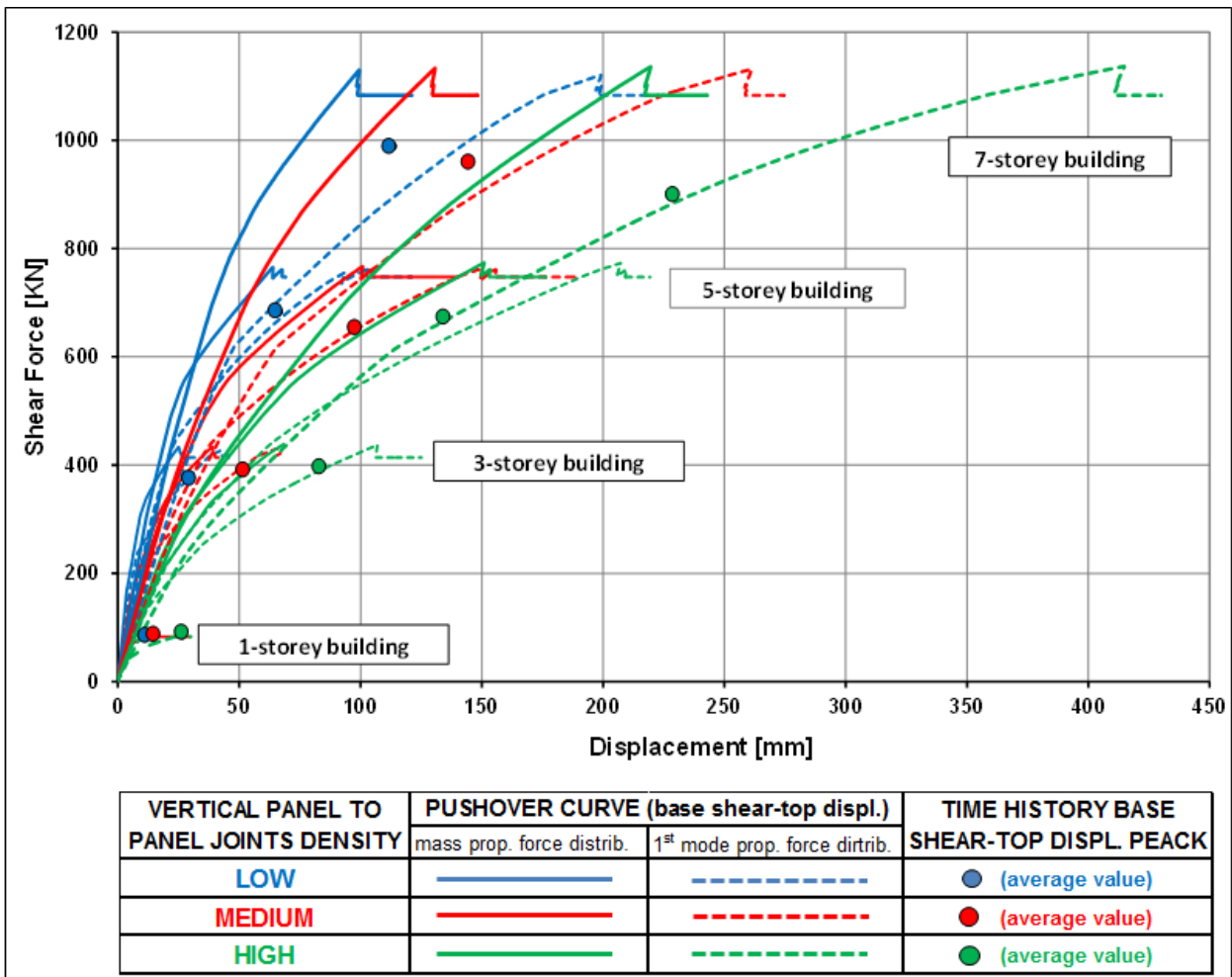




VERTICAL PANEL TO PANEL JOINTS DENSITY	PUSHOVER CURVE (base shear-top displ.)		TIME HISTORY BASE SHEAR-TOP DISPL. PEACK
	mass prop. force distrib.	1 st mode prop. force dirtrib.	
LOW			
MEDIUM			
HIGH			

Fig. 5.23 – Pushover curve and near collapse condition load-displacement values for building configuration with reference to façade A (left) and B (right).

Fig. 5.24 summarized pushover curves and average near collapse load-displacement points for each slenderness, and junction level.



VERTICAL PANEL TO PANEL JOINTS DENSITY	PUSHOVER CURVE (base shear-top displ.)		TIME HISTORY BASE SHEAR-TOP DISPL. PEACK
	mass prop. force distrib.	1 st mode prop. force dirtrib.	
LOW			(average value)
MEDIUM			(average value)
HIGH			(average value)

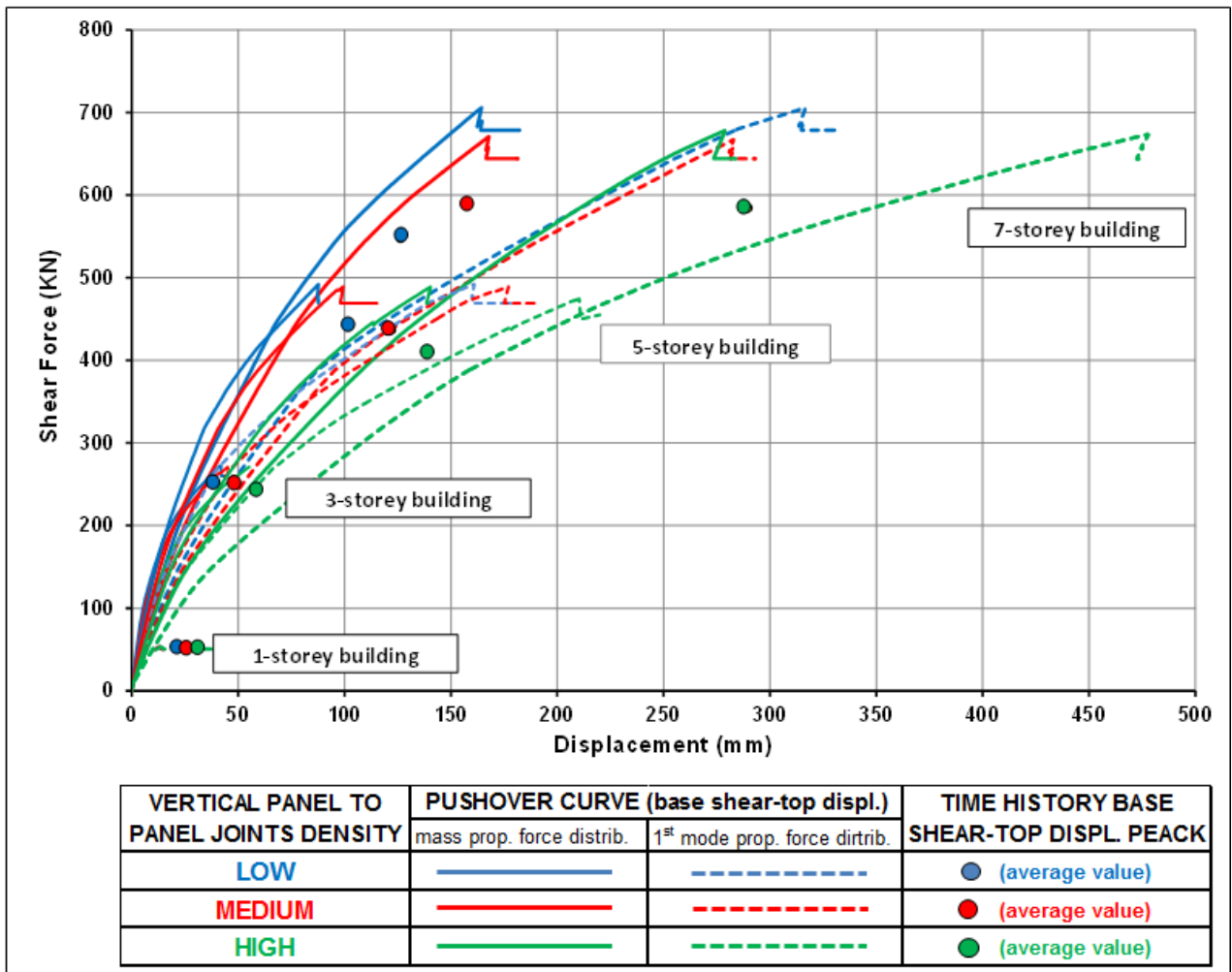


Fig. 5.24 – Summary pushover curve and near collapse condition load-displacement values for building configuration with reference to façade A (top) and B (bottom).

5.5.5.3.3 Final remarks and summary of analyses

The results reported in the previous paragraphs pointed out a similar response of the façade A and façade B. In detail the performed analyses have shown that:

- there is a growing trend of the PGA_{max} and $PGA_{near\ collapse}$ with:
 - the storeys number;
 - the number of vertical panel to panel joints;
 - the slenderness of the building.
- the option between intermediate holdowns or vertical panel to panel joint doesn't affect significantly the building response.

Finally the graphs pointed out a good correspondence between the near collapse conditions given by the NLSAs and the NLDAs. In detail this correspondence is perfect for the 1 storey building since it is assailable to a Single Degree Of Freedom system. For the three and five storeys buildings the near collapse condition defined with the NLDAs seems to be reached with lower base shear values respect to that defined with NLSAs. The seven storeys configurations present the grater differences especially for the configurations with the highest level of vertical joints.

Generally the most relevant differences are in terms of base shear while regarding to the displacement the results from near-collapse NLDAs are always in the range defined by the two pushover curves obtained with the 1st eigenfrequency displacement and the mass proportional force distribution. This confirms that the influence of the dynamic effects and the higher modes in the building response became more and more relevant with increasing number of storeys.

5.5.6 Q-factor evaluation for the different building configurations

Once defined the seismic response of every building configuration in terms of pushover curve and $PGA_{naer\ collapse}$ values it is possible to evaluate the most suitable q-factor applying the procedures defined in the previous Chapter 3. In this section the procedures based on the pushover method and on the PGA approach are used in order to obtain a reliable estimation of the q-factor values. Table 5.3 reports the obtained q-factor values for each building configuration and construction technology. The building configurations marked with (*) refer to the assembling with strong vertical panel to panel joints and no intermediate holdowns. As already done for the values of PGA, the minimum, maximum and average q-factors reported in Table 5.3 are defined referring to all the 5 values obtained with both NLSAs (2) and NLDAs (3).

Table 5.3 – Q-factor estimation for all the investigated building configuration

ID	λ	q-push_d	q-push_m	q-th1	q-th2	q-th3	q_min	q_max	q_av.
A1N	0.17	2.87	2.87	2.06	2.29	1.92	1.92	2.87	2.40
A1M	0.17	3.16	3.16	2.06	2.51	2.06	2.06	3.16	2.59
A1H	0.17	3.75	3.75	2.29	2.61	2.10	2.10	3.75	2.90
A3N	0.52	3.35	3.06	2.80	3.12	2.69	2.69	3.35	3.00
A3M	0.52	3.71	3.33	3.12	3.33	2.96	2.96	3.71	3.29
A3H	0.52	4.31	3.81	3.76	3.93	3.66	3.66	4.31	3.89
A5N	0.87	3.48	2.97	2.96	3.23	3.07	2.96	3.48	3.14
A5M	0.87	3.67	3.92	3.66	4.09	3.66	3.66	4.09	3.80
A5H	0.87	4.63	4.45	4.52	4.84	4.30	4.30	4.84	4.55
A7N	1.22	3.74	3.01	3.76	4.30	4.03	3.01	4.30	3.77
A7M	1.22	4.17	3.68	4.41	4.84	4.03	3.68	4.84	4.23
A7H	1.22	4.90	4.69	5.11	5.38	5.11	4.69	5.38	5.04
B1N	0.35	2.96	2.96	2.29	2.86	2.29	2.29	2.96	2.67
B1M	0.35	2.96	2.96	2.29	2.86	2.29	2.29	2.96	2.67
B1H	0.35	3.30	3.30	2.29	2.86	2.29	2.29	3.30	2.81
B3N	1.05	4.13	3.20	3.26	3.71	3.14	3.14	4.13	3.49
B3M	1.05	4.06	3.09	3.14	3.54	3.43	3.09	4.06	3.45
B3H	1.05	4.22	3.48	2.86	3.60	3.54	2.86	4.22	3.54
B5N	1.74	4.29	3.77	4.29	4.69	4.29	3.77	4.69	4.27
B5M	1.74	4.53	4.03	4.46	4.86	4.57	4.03	4.86	4.49
B5H	1.74	4.84	4.49	4.86	4.80	4.29	4.29	4.86	4.66
B7N	2.44	4.73	4.09	4.00	4.17	4.00	4.00	4.73	4.20
B7M	2.44	4.83	4.15	4.29	4.57	4.46	4.15	4.83	4.46
B7H	2.44	4.82	4.57	5.03	5.14	6.29	4.57	6.29	5.17
B1M*	0.35	3.03	3.03	2.34	2.86	2.34	2.34	3.03	2.72
B1H*	0.35	3.26	3.26	2.46	2.97	2.40	2.40	3.26	2.87
B3M*	1.05	4.47	3.21	3.14	3.43	3.43	3.14	4.47	3.54
B3H*	1.05	4.30	3.26	4.00	4.57	3.54	3.26	4.57	3.93
B5M*	1.74	4.45	3.92	5.03	5.43	4.80	3.92	5.43	4.73
B5H*	1.74	4.95	4.37	4.57	5.31	4.57	4.37	5.31	4.75
B7M*	2.44	4.74	4.29	4.46	4.57	4.46	4.29	4.74	4.50
B7H*	2.44	4.76	4.44	4.86	5.71	5.71	4.44	5.71	5.10

Analyzing the results reported in Table 5.3 it is possible to state that:

- a. The ductility factor $q=2$ proposed by the available seismic codes [5.3] seems to be precautionary and unrepresentative of the actual energy dissipation capacity of the CLT building system. As a confirmation only in one case out of the 160 analyzed was achieved a q -factor lower than 2. Such lowest q -factor values (A1N-th3) has been obtained for the single storeys joint free building characterized by a small number of connections and therefore by a small dissipative capability. Such results are strictly in line with the outcomes reported in [5.21].
- b. The q -factor value is strongly dependent on the specific characteristic of the building. More in detail there is a growing trend of the q factor with the storeys number and the number of the panels used to compose the walls (i.e. with the density of vertical joints).
- c. There is a direct dependence of the q -factor and the slenderness of the building: structures with rocking like behaviour are characterized by greater q -factor values respect those with shear like behaviour.
- d. The adoption of a construction technology characterized by strong vertical panel to panel joints and no internal holdowns (i.e. building configurations marked with ^(*)) does not affect the building response and therefore the q -factor value.

The previously reported remarks evidence that the actual dissipative capacity of the CLT building can't be represented by a unique and constant q -factor value. Univocal definition of the q -factor that disregards the dependence from the storeys number, the slenderness and the wall composition results to be approximate and unrepresentative of the actual seismic behaviour of the building. A more complex correlation between the q -value and such peculiar characteristics of the buildings is needed.

Finally it should be highlight that in this work the effects of the building in plan and in high regularity weren't investigated. To this aim additional analyses would be necessary using more complex 3 Dimensional numerical models.

5.6 Influence of the fasteners overstrengthening on the q -factor value

The analyses and the q -factor estimations provided in the previous paragraphs are based on the analysis of buildings designed under the assumption of no overstrength factors for all the connections and joints. In order to investigate the effects of different design criteria a number of additional analyses were performed on buildings designed providing different levels of overstrengthening between angle brackets and holdowns. These levels are identify by the coefficient γ which is defined as the ratio between the overstrength factor of the angular bracket γ_{O_A} and the overstrength factor of the holdown γ_{O_H} (see the previous Eq. 5.2 and Eq. 5.3) according to the following Eq. 5.5:

$$\gamma = \gamma_{O_A} / \gamma_{O_H} \quad \text{Eq. 5.5}$$

Two of the investigated were for an overstrengthening of the holdown respect to the angular bracket ($\gamma=0.8$ and 0.9), one for an overstrengthening of the angular bracket respect to the holdowns ($\gamma=1.1$).

The effects of these different overstrengthening levels have been assessed on four significant building configurations: both the facades of the three and five storeys building with intermediate joint density configurations were designed according to the various overstrengthening levels and then analyzed by means of NLSAs and NLDAs. Using the output from the nonlinear analyses the most suitable q -factors were evaluated for all the building configurations with the same procedure described in the previous paragraph 5.5.6. Table 5.4 reports the q -factor values obtained with the pushover method and the PGA approach, in comparison with that previously obtained with no overstrengthening ($\gamma=1.0$).

Table 5.4 – q -factors values for the additional case study configurations designed for various fasteners overstrengthening levels





BUILDING ID		$\gamma = \gamma_{O_A} / \gamma_{O_H}$	q_{push_displ}	q_{push_mass}	q_{th1}	q_{th2}	q_{th2}
A 3 M		0.8	2.75	2.60	2.53	2.73	2.05
		0.9	3.45	2.90	2.84	2.93	2.66
		1	3.71	3.33	3.12	3.33	2.96
		1.2	3.84	3.39	3.13	3.21	2.94
A 3 M		0.8	3.22	2.51	2.31	2.67	2.76
		0.9	3.58	2.79	2.92	3.05	3.06
		1	4.06	3.09	3.14	3.54	3.43
		1.2	3.97	3.07	3.08	3.58	3.29
A 5 M		0.8	3.18	2.86	3.04	3.03	3.37
		0.9	3.65	3.49	3.29	3.56	3.37
		1	3.92	3.67	3.66	4.09	3.66
		1.2	3.91	3.74	3.61	4.12	3.57
A 5 M		0.8	3.53	3.06	3.62	4.09	3.90
		0.9	4.27	3.72	3.98	4.19	4.12
		1	4.53	4.03	4.46	4.86	4.57
		1.2	4.50	4.05	4.47	4.71	4.46

Table 5.4 shows that regardless of the procedures used, the q -factor values obtained for case studies with an overstrengthening of holdowns respect to angular brackets are lower than the reference ones (i.e. $\gamma=1$). The overstrengthening of the holdown induces a shear like behaviour of the building with consequent premature failure of the angular brackets. Otherwise the overstrengthening of the angular brackets respect to the holdown seems to not change the q -factor. In fact the rocking like behaviour of the building is maintained and the failure is achieved with the braking of the holdown.

The ratio c between the average values of the actual q -factor and the reference one q_{ref} ($\gamma=1.0$) defined by Eq. 5.6 is plotted in Fig. 5.25 versus the value of the overstrength factor γ .

$$c = q / q_{ref}$$

Eq. 5.6

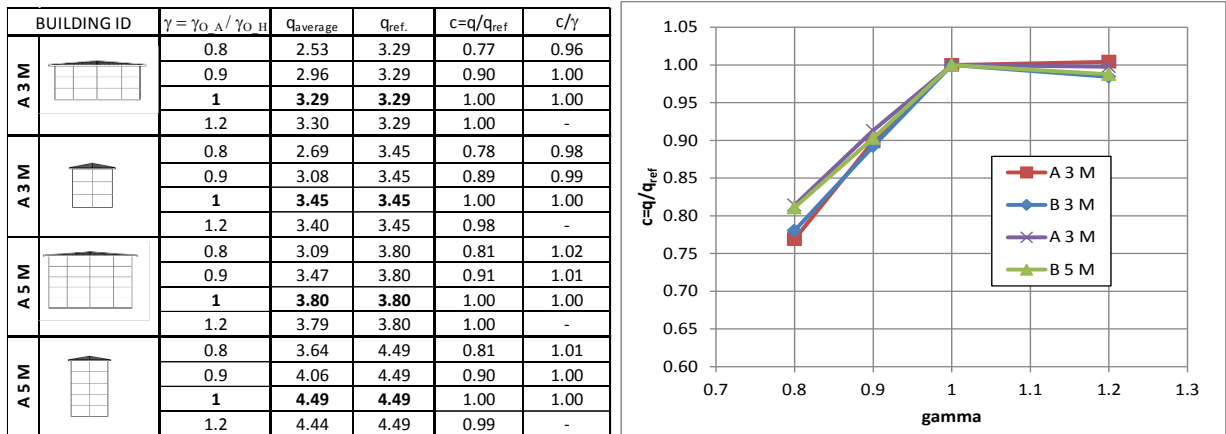


Fig. 5.25 – Modification of the behaviour factor q with the overstrength levels for each examined configurations.

Fig. 5.25 makes evident the proportional diminution of the q -factor with the diminution of the overstrength levels when $\gamma < 1$, that is when holdowns stronger than angular bracket. Otherwise in the opposite condition (i.e. $\gamma > 1$) the q -factors remain equal to those evaluated for the reference building procedure.

5.7 Conclusions

Despite in Europe and Canada research projects which investigate on the seismic behaviour of CLT buildings are ongoing no provisions are given about the correlation between the structural characteristics and their q -factor values.

Studies performed in this part of the dissertation highlight a strong correlation between the q -factor and some specific building characteristics such as slenderness, storeys number, building technology and criteria used for the design of the connectors. The effects of these specific structural features on the building seismic response and on the q -factor value were investigated by means of several nonlinear numerical analyses on a numbers of case studies building. The adopted numerical models faithfully reproduce the specific hysteretic behaviour of the connectors and were calibrated on the results form experimental tests. The obtained results demonstrate that:

1. the q -factor value equal to 2 proposed by the current standards for the CLT structure seems to be too precautionary respect the actual dissipative capacity demonstrated trough the numerical simulations
2. the q -values increase with:
 - a. the building slenderness
 - b. the number of storeys
 - c. the junction density
3. the q -values is dependent on the design criteria used for dimensioning the connectors: overstrength of the holddown causes a proportional reduction of the q -values, while no effects derive from the overstrengthening of the angular bracket.

The last item suggest the introduction of a capacity design criteria for dimensioning the connections in order to assure anticipate rocking (bending) failure in buildings than sliding (shear) failure.

The obtained results represent a crucial issue for the seismic design of CLT buildings. An analytical formulation for the definition of the q-factor value as a function of the parameters varied in the sensitivity analyses above described will be forwarded in the next section.

References – Chapter 5

- [5.1] Fragiaco M, Dujic B, Sustersic I. Elastic and ductile design of multy-storey crosslam wooden buildings under seismic actions. *Engineering Structures* 33, 2011, 3043-3053.
- [5.2] European committee for standardization (CEN). Eurocode 5 – design of timber structures – part 1-1: general rules and rules for buildings. 2004.
- [5.3] European Committee for Standardization (CEN). Eurocode 8 - design of structures for earthquake resistance, part 1: General rules, seismic actions and rules for buildings. 2004.
- [5.4] Chopra AK. *Dynamics of structures—theory and applications to earthquake engineering*. Upper Saddle River: NJ: Prentice Hall; 1995.
- [5.5] Italian Ministry for the Infrastructures. New technical regulation for construction. Decree of the Ministry for the Infrastructures, Ministry of Interior, and Department of the Civil Defence. 2008.
- [5.6] Gavric I, Ceccotti A, Fragiaco M. Experimental tests on cross-laminated panels and typical connections. *Proceeding of ANIDS 2011, Bari Italy, 2011, CD*.
- [5.7] Sandhaas C, Boukes J, Kuilen JWG, Ceccotti A. Analysis of X-lam panel-to panel connections under monotonic and cyclic loading. Meeting 42 of the Working Commission W18-Timber Structures, CIB. Dübendorf, Switzerland, 2009, paper CIB-W18/42-12-2.
- [5.8] Ceccotti A, Lauriola M.P, Pinna M, Sandhaas C. SOFIE Project – Cyclic Tests on Cross-Laminated Wooden Panels. *World Conference on Timber Engineering WCTE 2006. Portland, USA, August 6-10, 2006, CD*.
- [5.9] Lauriola M.P, Sandhaas C. Quasi-Static and Pseudo-Dynamic test on XLam walls and buildings. *COST E29 International Workshop on Earthquake Engineering on timber Structures. Coimbra, Portugal, 2006, pages 119-133*
- [5.10] Ceccotti A. New technologies for construction of medium-rise buildings in seismic regions: the XLAM case. *IABSE Struct Eng Internat* 2008;18:156–65. *Tall Timber Buildings (special ed.)*.
- [5.11] Dujic B, Strus K, Zarnic R, Ceccotti A. Prediction of dynamic response of a 7-storey massive XLam wooden building tested on a shaking table. *World Conference on Timber Engineering WCTE 2010. Riva del Garda, Italy, June 20–24, 2010, CD*.
- [5.12] Dujic B, Aicher S, Zarnic R. Investigation on in-plane loaded wooden elements – influence of loading on boundary conditions. *Otto Graf Journal, Materialprüfungsanstalt Universität. Otto-Graf-Institut, Stuttgart, 2005, Vol. 16*.
- [5.13] Dujic B, Hristovsky, Zarnic R. Experimental investigation of massive wooden wall panel system subject to seismic excitation. *Proceeding of the First European Conference on Earthquake Engineering. Geneva, Switzerland, 2006*
- [5.14] Popovski M, Schneider J, Schweinstreiger M. Lateral load resistance of Cross-Laminated wood panels. *World Conference on Timber Engineering WCTE 2010. Riva del Garda, Italy, June 20–24, 2010, CD*.
- [5.15] Pei, S., Popowski, M., van de Lindt, 2012. “Performance based design and force modification factors for CLT structures. Meeting 45 of the Working Commission W18-Timber Structures, CIB. Växjö, Sveden, 2012, paper CIB-W18/45-15-1.
- [5.16] Pei, S., van de Lindt, J.W., Pryor, S.E., Shimizu, H., and Isoda, H. 2010. Seismic testing of a full-

scale sixstory light-frame wood building: NEESWood Capstone test. NEESWood Report NW-04.

- [5.17] *L'Aquila. Il progetto C.A.S.E., Edid by Iuss Press, 2010, ISBN: 886198052X*
- [5.18] *Elwood, K.J., and Moehle, J.P., (2006) "Idealized backbone model for existing reinforced concrete columns and comparisons with FEMA 356 criteria", The Structural Design of Tall and Special Buildings, vol. 15, no. 5, pp. 553-569.*
- [5.19] *Fenves G.L., 2005, Annual Workshop on Open System for Earthquake Engineering Simulation, Pacific Earthquake Engineering Research Center, UC Berkeley, <http://opensees.berkeley.edu/>.*
- [5.20] *Albanesi, T., Nuti, C., Vanzi, I. (2002). "State of the art of nonlinear static methods," Proc. of the 12th European Conf. on Earthquake Engrg., London, United Kingdom, Paper. 602, Oxford: Elsevier Science.*
- [5.21] *Pozza L., Scotta R. Valutazione numerica del comportamento sismico e del fattore di struttura "q" di edifici in legno con pareti tipo XLam. Proceeding of ANIDS 2011, Bari Italy, 2011, CD*

Chapter 6 – Proposal and validation of an analytical formula for the evaluation of the q-factor of CLT buildings

Abstract

A proposal for a new analytical formulation to calculate the q-factor of CrossLam building is presented in this part of the dissertation. Such procedure is based on a number of preliminary numerical simulations presented in the previous chapter conducted to define the influence of some significant characteristics (e.g. connection arrangement, storeys number, slenderness, design criteria) on the seismic response of the CLT buildings and consequently on the q-factor.

Two different analytical formulations for the q-factor estimation have been developed and calibrated against the output from the numerical simulations. Such formulas are resumed in two abacuses for an immediate q-factor definition using as input parameters the building slenderness and a synthetic index that account for the storeys numbers and wall composition (i.e. density of panel to panel vertical joints). The developed procedure includes specific rules for a proper design of the connectors and of their correspondent overstrength factors.

The validation of the developed procedure is reported. To demonstrate the reliability of the proposed method, it was applied to two different independent case study building.

Some investigations about the relationship between the principal elastic period and the q-factor value are also reported and critically discussed.

Finally some energetic evaluations have been carried out in order to verify the energy dissipation contribution of each CLT building components during a seismic event. Some notes concerning the related findings are hereafter discussed.

6.1 Proposal for an analytic procedure for the CLT building q-factor evaluation

The analyses and the relative q-factor estimations reported in the previous Chapter 5 evidenced a strong dependence of the building dissipative capacity on certain specific characteristics of the structure. This dependence is mainly correlated to the storeys number, building slenderness and number of CLT panels used to assemble the walls (i.e. density of vertical panel to panel joints).

Aim of this section is to formulate an analytical expression able to take into account the relationship between the appropriate q-factor of a CLT building value and suitable parameters summarizing the specified building characteristic and the design criteria. To define the analytical formulation the following steps have been followed:

- a. Proposal of synthetic indexes of the main relevant building characteristics;
- b. verification of the effect of such indexes on the q-factor value by means of data analyses;
- c. identification of suitable relationships between the synthetic indexes and the q-factor;
- d. calibration of the coefficients adopted in such relationships;
- e. definition of specific rules for a proper design of the connectors overstrength (alternatively: proposal of a q-factor correction as a function of a design criteria adopted)
- f. investigation on the effects of the principal elastic period on its q-factor value.

Finally the proposed analytical formulas have been summarized by means of some abacuses useful for an immediate q-factor definition starting from the defined synthetic indexes.

6.1.1 Building synthetic indexes

In wooden buildings the dissipative capacity is strongly dependent on the number of connectors able to dissipate energy, since wood is designed to remain elastic during the earthquake. In the CLT construction practice fasteners are arranged along:

- wall – foundation interface
- wall – floor interface
- wall – roof interface
- wall panel to panel vertical joints

This work proposes the adoption of a specific index α to represent the joint density of the building. This index is defined as the ratio between the façade area \mathbf{A} and the sum of junction lines lengths \mathbf{P} . Once defined the wall dimension (\mathbf{B} and \mathbf{H}), the inter storey height (\mathbf{h}), the facade area (\mathbf{A}), the storeys number (\mathbf{n}) and the vertical panel to panel joints number (\mathbf{m}) it is possible to calculate the coefficient α according to Eq. 6.2.

The so defined coefficient α gives a measure of joints density of the façade; perhaps its direct correlation with the q-factor values is not trivial. It is useful to compare the α value with that corresponding to a reference configuration defined as the ratio between the area (\mathbf{A}) and the perimeter (\mathbf{P}_0) of a hypothetical façade without intermediate junction lines according to Eq. 6.1. Fig. 6.1 helps to understand the meaning of the synthetic indexes α and α_0 for a typical wall.

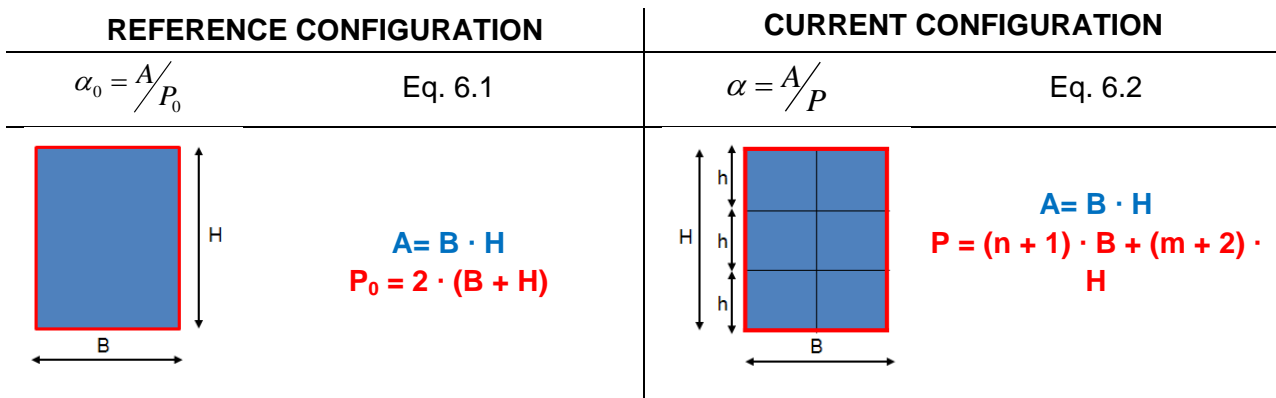


Fig. 6.1 - Definition of the reference (left) and actual (right) junction indexes.

It should be noted the similitude between the definition of the coefficient α the equivalent hydraulic radius of a pipe. The ratio between the two indexes provides the adimensional coefficient β accounting for both the density of vertical panel to panel joints façade and the number of storeys.

$$\beta = \alpha_0 / \alpha \quad \text{Eq. 6.3}$$

Table 6.1 gives the values of the coefficient β for each of the building configuration investigate in the previous chapter 5. In shake of immediacy in the same table the corresponding q-factor range and the slenderness of the façade are reported.

 Table 6.1 – Values of the coefficient β , q-factor range and slenderness for each of the examined facades.

	A1N	B1N	A1M	B1M	A1H	B1H
1 STOREY	$\lambda = 0.17$	$\lambda = 0.35$	$\lambda = 0.17$	$\lambda = 0.35$	$\lambda = 0.17$	$\lambda = 0.35$
	$\beta = 1.00$	$\beta = 1.00$	$\beta = 1.22$	$\beta = 1.13$	$\beta = 1.89$	$\beta = 1.65$
	$q_{\min} = 1.92$	$q_{\min} = 1.00$	$q_{\min} = 2.06$	$q_{\min} = 2.29$	$q_{\min} = 2.10$	$q_{\min} = 2.29$
	$q_{\text{average}} = 2.40$	$q_{\text{average}} = 2.96$	$q_{\text{average}} = 2.59$	$q_{\text{average}} = 2.67$	$q_{\text{average}} = 2.90$	$q_{\text{average}} = 2.81$
	$q_{\max} = 2.87$	$q_{\max} = 2.96$	$q_{\max} = 3.16$	$q_{\max} = 2.96$	$q_{\max} = 3.75$	$q_{\max} = 3.30$
3 STOREYS	A3N	0	A3M	B3M	A3H	B3H
	$\lambda = 0.52$	$\lambda = 1.05$	$\lambda = 0.52$	$\lambda = 1.05$	$\lambda = 0.52$	$\lambda = 1.05$
	$\beta = 1.66$	$\beta = 1.49$	$\beta = 2.17$	$\beta = 1.74$	$\beta = 3.72$	$\beta = 2.77$
	$q_{\min} = 2.69$	$q_{\min} = 3.14$	$q_{\min} = 2.96$	$q_{\min} = 3.09$	$q_{\min} = 3.66$	$q_{\min} = 2.86$
	$q_{\text{average}} = 3.00$	$q_{\text{average}} = 3.49$	$q_{\text{average}} = 3.29$	$q_{\text{average}} = 3.45$	$q_{\text{average}} = 3.89$	$q_{\text{average}} = 3.54$
5 STOREYS	A5N	B5N	A5M	B5M	A5H	B5H
	$\lambda = 0.87$	$\lambda = 1.74$	$\lambda = 0.87$	$\lambda = 1.74$	$\lambda = 0.87$	$\lambda = 1.74$
	$\beta = 2.07$	$\beta = 1.73$	$\beta = 2.77$	$\beta = 2.05$	$\beta = 4.86$	$\beta = 3.32$
	$q_{\min} = 2.96$	$q_{\min} = 3.77$	$q_{\min} = 3.66$	$q_{\min} = 4.03$	$q_{\min} = 4.30$	$q_{\min} = 4.29$
	$q_{\text{average}} = 3.14$	$q_{\text{average}} = 4.27$	$q_{\text{average}} = 3.80$	$q_{\text{average}} = 4.49$	$q_{\text{average}} = 4.55$	$q_{\text{average}} = 4.66$
7 STOREYS	A7N	B7N	A7M	B7M	A7H	B7H
	$\lambda = 1.22$	$\lambda = 2.44$	$\lambda = 1.22$	$\lambda = 2.44$	$\lambda = 1.22$	$\lambda = 2.44$
	$\beta = 2.35$	$\beta = 1.87$	$\beta = 3.18$	$\beta = 2.23$	$\beta = 5.65$	$\beta = 3.65$
	$q_{\min} = 3.01$	$q_{\min} = 4.00$	$q_{\min} = 3.68$	$q_{\min} = 4.15$	$q_{\min} = 4.69$	$q_{\min} = 4.57$
	$q_{\text{average}} = 3.77$	$q_{\text{average}} = 4.20$	$q_{\text{average}} = 4.23$	$q_{\text{average}} = 4.46$	$q_{\text{average}} = 5.04$	$q_{\text{average}} = 5.17$
	$q_{\max} = 4.30$	$q_{\max} = 4.73$	$q_{\max} = 4.84$	$q_{\max} = 4.83$	$q_{\max} = 5.38$	$q_{\max} = 6.29$
	NO VERTICAL JOINTS		MEDIUM DENSITY OF VERTICAL JOINT		HIGH DENSITY OF VERTICAL JOINT	

Table 6.1 evidences a growing trend of the coefficient β with both the storeys number and the vertical panel to panel joints number. For the examined configurations, β spans from 1 to 5.65. The minimum unitary value corresponds to the single storey building without vertical joints, while the maximum one to the tallest buildings with high density of vertical joints.

Table 6.1 also allows to appreciate a growing trend of the q-factor with the coefficient β .

More precisely, assuming as a constant the β value, it appears that a slender building correspond an higher q-factor value. It means that also the building slenderness λ influences the q-factor value. Based on this evidence it has been supposed that the q-factor could be written only as a function of two indexes: the junction level β and the slenderness λ as in the following Eq. 6.4.

$$q = q(\beta, \lambda) \tag{Eq. 6.4}$$

A detailed study was required in order to identify the more suitable relationship between the q-factor value and these adimensional indexes β and λ . A useful tool to investigate on the influences of these parameters is the frequency distribution curves of the q-factor.

Hereafter are reported some frequency histograms of the q-factor grouped with a class amplitude equal to 0.25. The correspondent normal distributions are superposed to the frequency histograms.

A first series of the q-factor frequency histograms was drawn separating the values corresponding to two ranges of slenderness λ : $0 < \lambda < 1$ and $\lambda > 1$. The graph in following Fig. 6.2 has been obtained which clearly shows that the building configuration with higher slenderness correspond greater q-factor values.

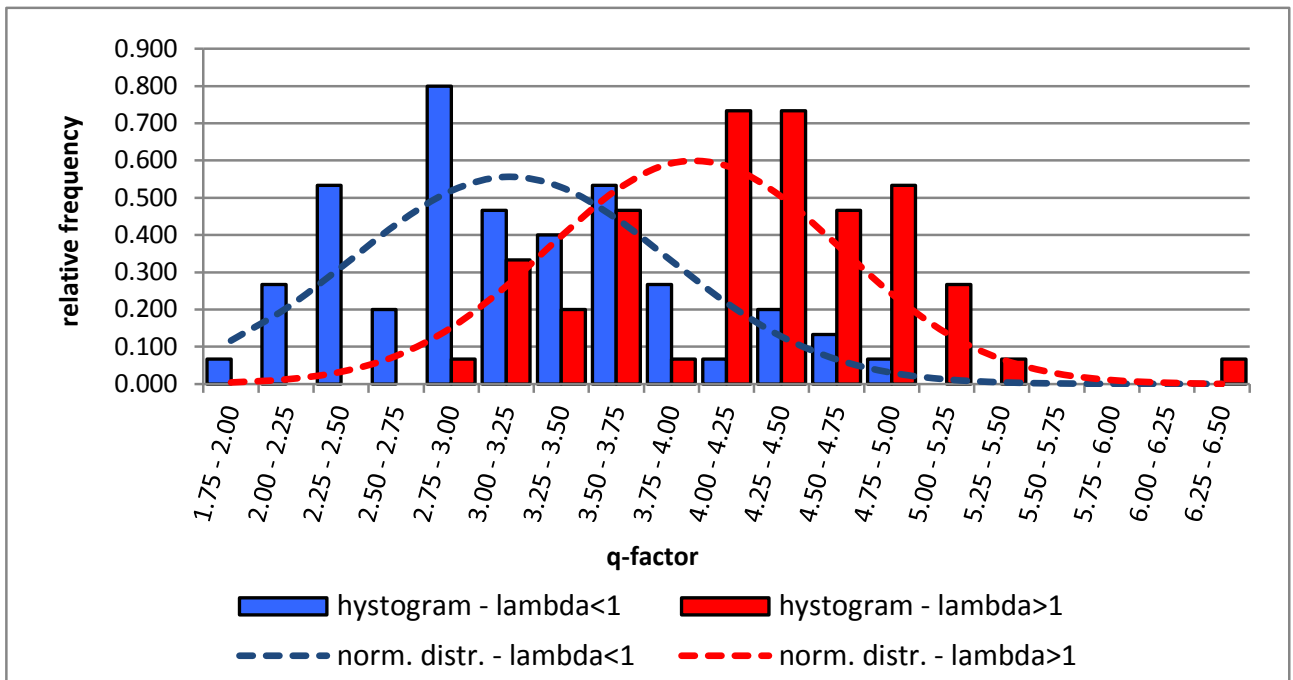


Fig. 6.2 – Histograms and correspondent normal distributions for the two slenderness levels considered

For $\lambda < 1$ the average q-factor is about 3 while for $\lambda > 1$ the q-factor is about 4. This result confirms that the q-factor value is directly related to the building slenderness λ .

Furthermore it is possible to build up the frequency histograms of the q-factor for growing level of the coefficient β . Three different ranges of the coefficient β were considered: $1 < \beta < 2$; $2 < \beta < 3$; $\beta > 3$. The following Fig. 6.3 reports the three histograms and superposed the correspondent normal distributions.

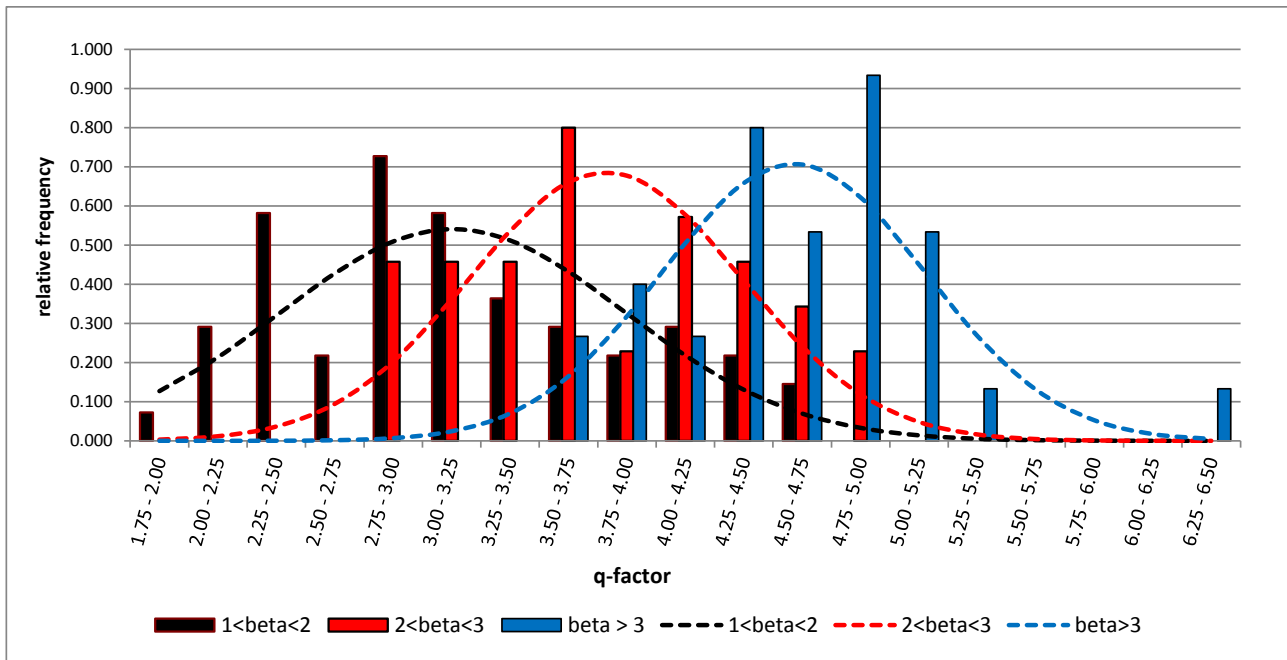


Fig. 6.3 – Histograms and correspondent normal distributions for the three junction levels considered

Such normal distributions highlight a strong dependence of the q-factor on the index β . As shown by the normal distributions the average q-values spans from about 3 for $1 < \beta < 2$ to about 4.5 for $\beta > 3$.

The frequency distributions provided an unambiguous indication on the dependence of the q-factor on the slenderness λ and on the joints density β .

6.1.2 Analytical formulations to assess the q-factor

The next step was finding out the most suitable forms for Eq. 6.4. The proposed analytical relationships between the q-factor value, the slenderness λ and the junction density β are given in this section. They have been calibrated on the basis of the contents of Table 6.1.

Before setting the analytical expressions a preliminary rearrange of the obtained q-factor was carried out in order to focus separately on the effects of the building synthetic indexes β and λ .

To this aim the following Table 6.2 summarizes for each slenderness λ and junction level β the correspondent q-factor range. The average and the 5% and 95% percentile values of q have been calculated according to the criteria defined by EN 14358-2007 [6.1].

Then the characteristic lower and upper percentile values and the average values listed in Table 6.2 are plotted versus the junction density β for each investigated slenderness λ in Fig. 6.4.

Table 6.2 – *q*-factor range for each slenderness and junction level

ID	λ	β	q_{min}	q_{max}	$q_{average}$	$q_{k_{0.05}}$	$q_{k_{0.95}}$
A1N	0.17	1.00	1.92	2.87	2.40	1.95	2.85
A1M	0.17	1.22	2.06	3.16	2.59	2.04	3.14
A1H	0.17	1.89	2.10	3.75	2.90	2.10	3.70
A3N	0.52	1.66	2.69	3.35	3.00	2.74	3.27
A3M	0.52	2.17	2.96	3.71	3.29	3.01	3.57
A3H	0.52	3.72	3.66	4.31	3.89	3.64	4.15
A5N	0.87	2.07	2.96	3.48	3.14	2.92	3.36
A5M	0.87	2.77	3.66	4.09	3.80	3.60	4.00
A5H	0.87	4.86	4.30	4.84	4.55	4.35	4.75
A7N	1.22	2.35	3.01	4.30	3.77	3.29	4.25
A7M	1.22	3.18	3.68	4.84	4.23	3.79	4.66
A7H	1.22	5.65	4.69	5.38	5.04	4.78	5.30
B1N	0.35	1.00	2.29	2.96	2.67	2.32	3.02
B1M	0.35	1.13	2.29	2.96	2.67	2.32	3.02
B1H	0.35	1.65	2.29	3.30	2.81	2.30	3.31
B3N	1.05	1.49	3.14	4.13	3.49	3.06	3.91
B3M	1.05	1.74	3.09	4.06	3.45	3.06	3.84
B3H	1.05	2.77	2.86	4.22	3.54	3.06	4.02
B5N	1.74	1.73	3.77	4.69	4.27	3.94	4.59
B5M	1.74	2.05	4.03	4.86	4.49	4.19	4.79
B5H	1.74	3.32	4.29	4.86	4.66	4.40	4.91
B7N	2.44	1.87	4.00	4.73	4.20	3.89	4.50
B7M	2.44	2.23	4.15	4.83	4.46	4.20	4.72
B7H	2.44	3.65	4.57	6.29	5.17	4.51	5.83

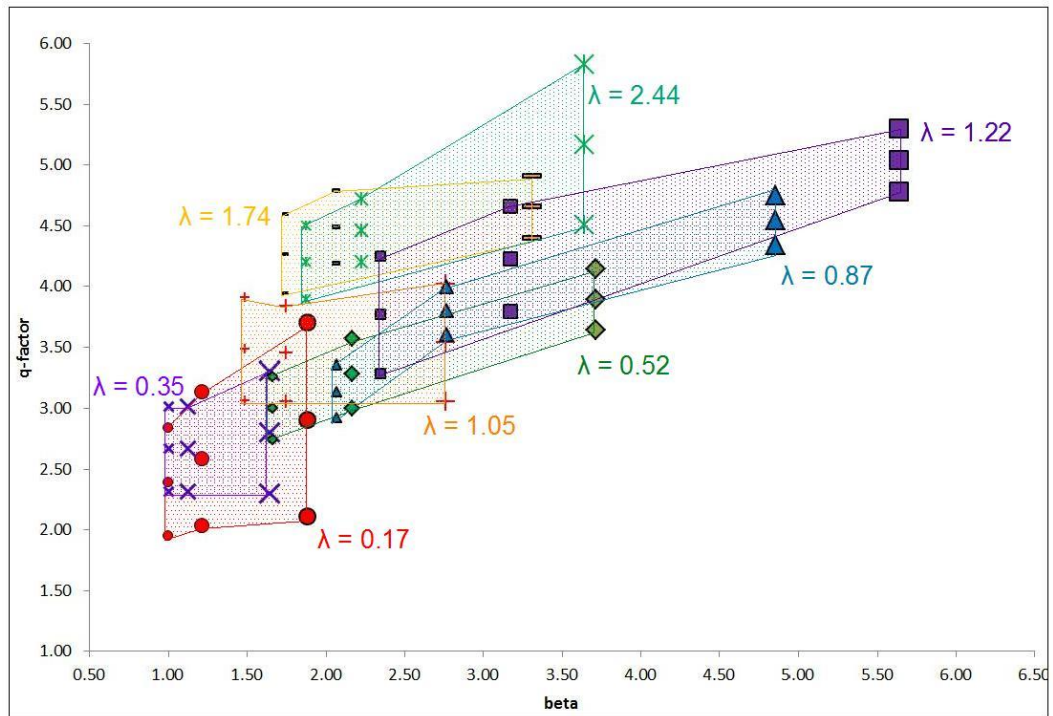


Fig. 6.4 – 5% - 95% characteristic *q*-factor ranges versus junction levels β for each examined slenderness λ

The distribution reported in Fig. 6.4 doesn't allow highlighting clear dependence of the q-factor on the building synthetic indexes β and λ . However the direct separate dependence of the q-factor on slenderness and junction density is evident.

Two different analytical formulas between the q-factor and the two indexes are proposed. The first one provides a linear dependence between the q-factor and the joints density β while the second one is a power expression of β . Both the proposed formulas take into account the effect of the building slenderness λ by means of a correlation coefficient.

6.1.2.1 Linear formulation

The proposed linear formulation correlates the q-factor values with the junction density β through a proportionality coefficient. This coefficient depends on the building slenderness through an exponential function as reported in the following Eq. 6.5.

$$q(\beta, \lambda) = q_0 + (k_0 e^{k_0 \lambda}) \beta \quad \text{Eq. 6.5}$$

The adoption of a variable proportionality coefficient allows to define a specific curve for each slenderness value. The constant parameter k_0 and q_0 have to be calibrated so as to obtain the best fit with the q-values from the numerical simulations.

6.1.2.2 Power formulation

This second analytical formulation proposes a power function of the q-factor to the junction density β according to the following Eq. 6.6.

$$q(\beta, \lambda) = (q_0 + k_1 \lambda) \beta^{k_2} \quad \text{Eq. 6.6}$$

The first factor in the formula accounts for building slenderness, while the second one for the joints density. The coefficients k_1 , k_2 and q_0 are calibrated so as to reach the fit with the numerically estimated q-factors. As in the linear formulation the structure of the proposed analytical law formed by two multiplying factors, one depending on λ , the other on β , allows to put the formulas in form of an abacus for faster q-factor estimations.

6.1.2.3 Calibration of the proposed formulations

The calibration of the proposed formulas is based on the numerical q-factor evaluation of several facades configurations presented in the previous chapter. For a conservative analytical evaluation of the ductility factor q, the calibration of the parameters in Eq. 6.5 and Eq. 6.6 has been done by searching the best fit with the 5% percentile of the q-factor distribution. The fitting of the averaged q-values would have been not conservative, while that of the minimum valued would have been strongly influenced by single anomalous responses to specific seismic spectra. The evaluation of the coefficients has been made so as to minimize the summation of the square difference between the analytical values and the numerical 5% percentile values of the q-factor.

According to this minimization procedure the parameters that allow the best fit are:

- linear formulation: $k_0=0.36$; $q_0=1.98$
- power formulation: $k_1=0.53$; $k_2=0.33$; $q_{0_REF}=1.97$

With such parameters, the comparison of both the linear and power formulation with the numerical 5% percentile q-factors from numerical simulations is given in the following Fig. 6.5. Q-values are plotted versus the parameter β , separately for each of the analyzed slenderness value λ .

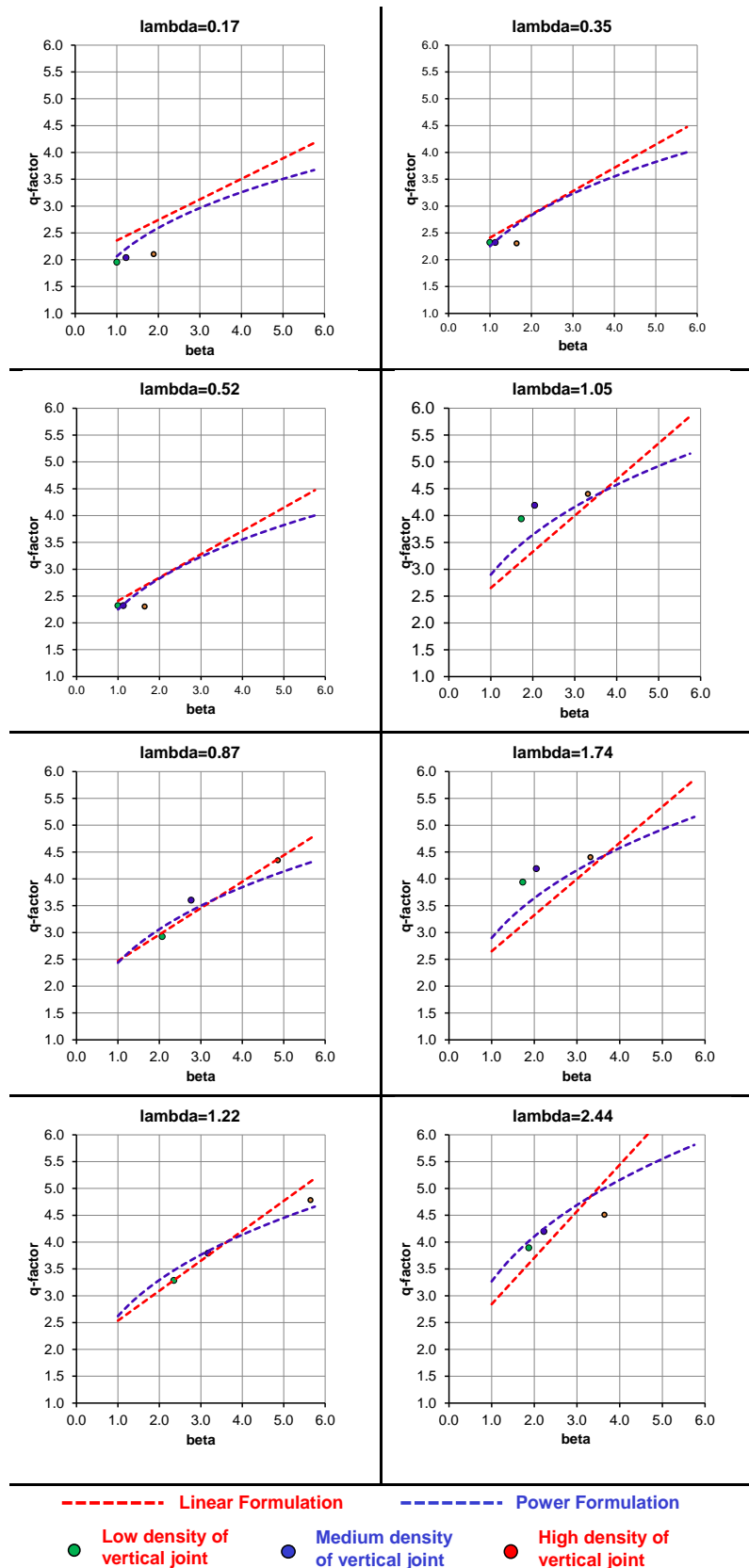


Fig. 6.5 – Comparison between the 5% percentile numerical and analytical q-factors, separately for each analyzed slenderness.

The graphs reported in Fig. 6.5 testify the good correspondence between the numerical and analytical values of the ductility factor, along all the investigated slenderness range. Despite a more complex formulation, the power formulation seems to give a more accurate prediction of the q-factor than the linear one especially for lower slenderness and joints density values.

As a final remark the proposed analytical laws do not provide any limitation of the q-factor for high values of slenderness λ and joint density β . Perhaps it is appropriate to fix an upper value of the q-factor. A reasonable upper limit could be 5, as that stated by standard codes for the high ductility Platform Frame buildings.

The so devised analytical formulas 6.5 and 6.6, with the parameters afore given, lead to the abacus representations in Fig. 6.6. These abacuses allow to achieve an immediate estimation of the most suitable q-factor for a CLT building characterized by a specific slenderness and junction level.

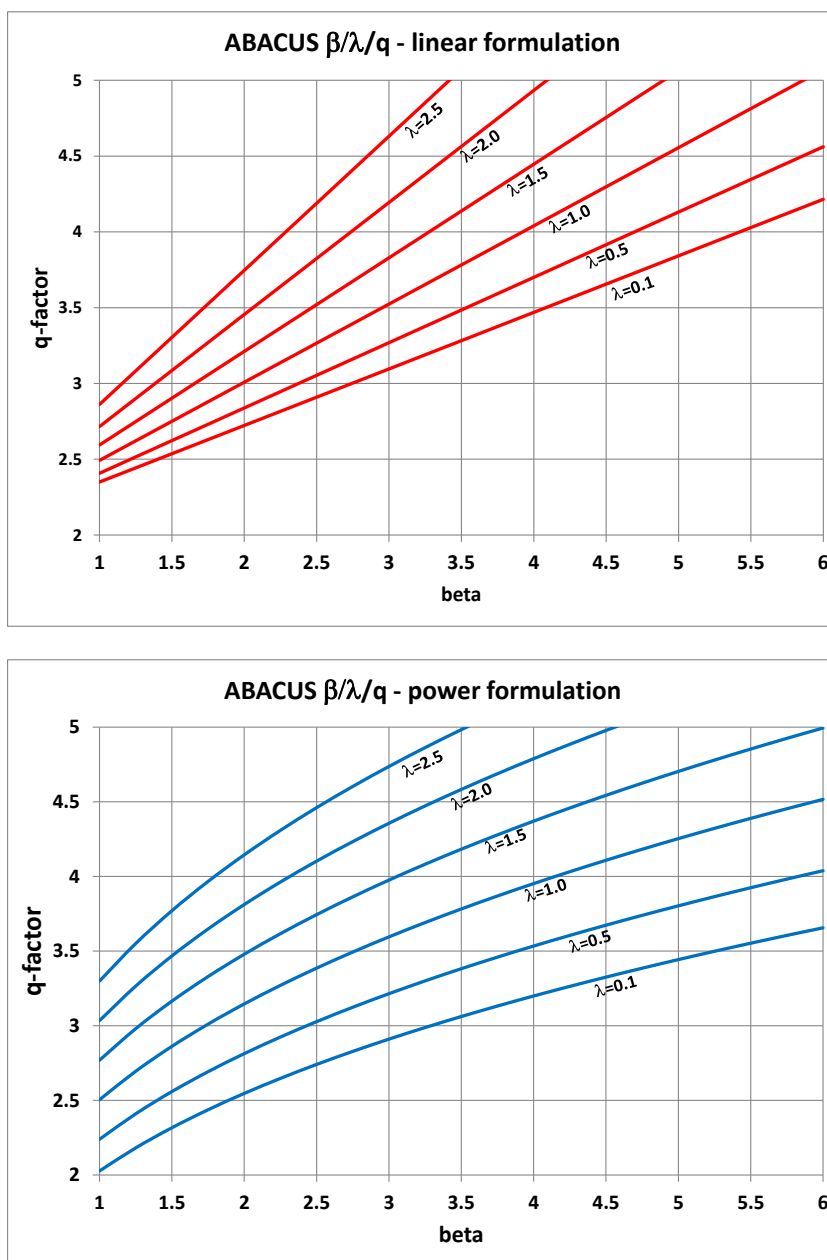


Fig. 6.6 – linear (top) and power (bottom) abacus for the q-factor estimation

As a final consideration it has to be recalled that the so devised formulas for the q-factors evaluation are valid under the following assumptions:

- CLT building is regular in plan and in high;
- Connectors are designed providing a minimum overstrength of the angular brackets respect the other connections, so as to avoid premature failure due to shear loads.

When these two conditions are not met suitable corrections must be applied to the q-factor obtained using the proposed abacuses. Available seismic codes [6.2] give some provisions about the effects of the building irregularity on the seismic response and the correction coefficient of the q-factor suggest there can be applied until more precise findings from 3-D numerical analyses or irregular structures will not be available.

Indeed no guidelines are given concerning the influence of the connectors overstrengthening on the q-factor values.

6.1.3 Effects of the connectors design criteria

Procedures described in the previous paragraphs ensure an accurate estimation of the q-factor only under specific design hypothesis on the connectors strength. Such design criteria require a balanced application of the overstrength factor to the connectors respecting the following Eq. 6.7:

$$\gamma = \gamma_{O_A} / \gamma_{O_H} = (V_{rd} / V_{sd}) / (N_{rd} / N_{sd}) \geq 1 \quad \text{Eq. 6.7}$$

where:

- γ = overstrength ratio
- γ_{O_A} = angular overstrength
- γ_{O_H} =holddown overstrength
- V_{rd} = angular strength
- V_{sd} = seismic action on angular bracket
- N_{rd} = holddown strength
- N_{sd} = seismic action on holddown

Analyses performed in the previous §5.6 with overstrength ratio $\gamma < 1$ have shown that in such condition the q-factor values decrease almost linearly.

Such results suggest the introduction of a correction index K_O modifying the q-factors obtained using the relationships defined in §6.1.2. Such correction index can be defined according the following Eq. 6.8:

$$K_O = (V_{rd} / V_{sd}) / (N_{rd} / N_{sd}) \leq 1 \quad \text{Eq. 6.8}$$

where:

- V_{rd} = angular strength
- V_{sd} = seismic action on angular bracket
- N_{rd} = holddown strength
- N_{sd} = seismic action on holddown

Obviously and alternatively, a coefficient $\gamma \geq 1$ have to be imposed and then the introduction of such correction factor is not needed.

6.1.4 Effects of the principal elastic period on the q-factor value

The formulation and the correction index developed in the previous paragraph takes into account the effects of the building characteristics and of the connectors design criteria, but the influence of the principal elastic period on the q-factor values has not been investigated yet.

This section reports some investigations about the relationship between the principal elastic period of the structure and its q-factor value. They have been conducted with reference to the three storeys SOFIE building[6.3], using the developed numerical model of the fasteners (see Chapter 2). Further investigations on the effect of the wall arrangement are also reported.

6.1.4.1 Case study buildings

The response of a building subjected to earthquake is dependent on its elastic vibration period. To consider this dependency, buildings with the same geometrical features but with different fundamental elastic periods were analyzed. Furthermore in order to verify the influence of the wall assembling analyses have been carried out on two different case study configurations. A total of six test buildings characterized by different principal elastic periods were investigated.

The three storey building tested by means full scale shaking table test was taken as reference [6.3] for the six buildings. A complete description of the geometrical features of such reference building is reported in [6.3].

The two case study configurations differ only in the number of vertical joints between wall panels at each floor: Configuration “A” considered three joined panels, while configuration “B” was joints free.

Such case study buildings were analyzed using a Finite Element Model. The hysteretic behavior of the connections was reproduced using the “macro-element model” described in the previous Chapter 2. Fig. 6.7 reports a sketch of the numerical models with the distribution of the connectors and of the vertical panel-to-panel joints for the two case studies.

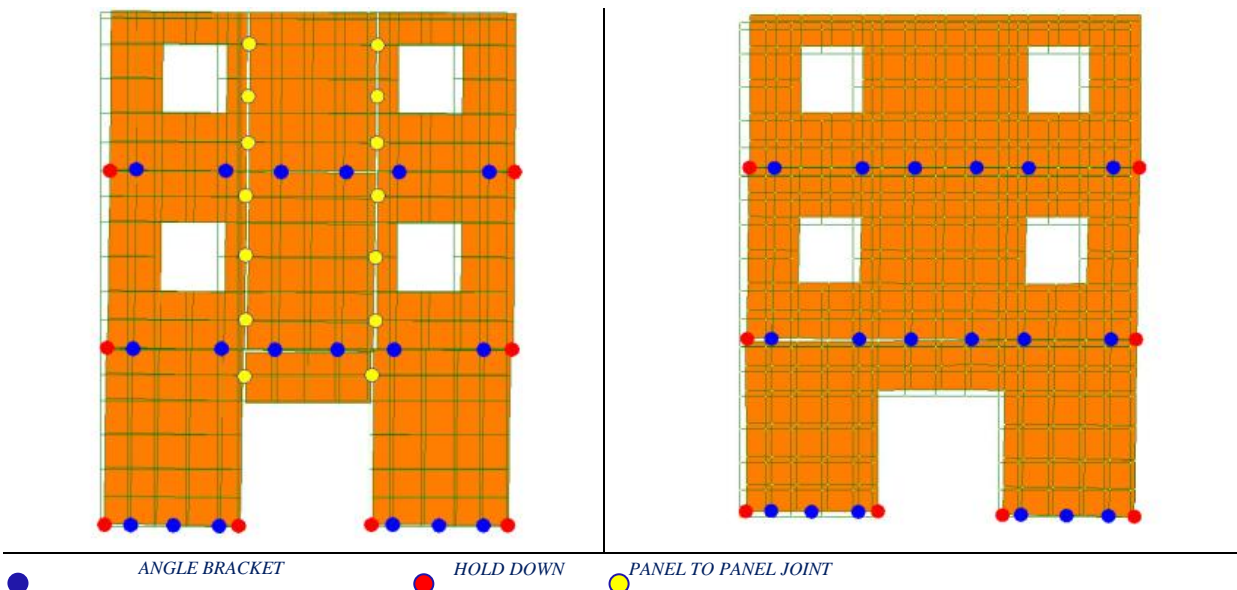


Fig. 6.7 – Deformed numerical models and connectors distribution for configurations “A” (left) and “B” (right).

Table 6.3 reports the storey masses and principal vibration periods for each of the studied buildings. The intermediate period A-configuration building faithfully reproduce the 3-storey building tested at SOFIE project [6.3], while the others had the same geometry but differed in mass and stiffness. The buildings of the B-configuration were the same as the A-configuration, except for the vertical panel-to-panel joints.

Table 6.3 - Storey masses and principal vibration period for each of the investigate buildings. In bold is evidenced the configuration tested on shaking table test with the SOFIE Project [6.3]

CASE STUDY		T ₁ [sec]	STOREY MASS [t]			
			1 st	2 nd	3 rd	Total
A	i	0.16	17.8	17.8	3.6	39.2
	ii	0.21	21.4	21.4	4.6	47.4
	iii	0.26	26.8	26.8	5.8	59.4
B	j	0.14	17.8	17.8	3.6	39.2
	jj	0.18	21.4	21.4	4.6	47.4
	jjj	0.22	26.8	26.8	5.8	59.4

The seismic design of the case study buildings was carried out by Linear Static Analysis adopting the following common data according to Eurocode 8 [6.2]: type 1 elastic response spectra and rock foundation (type A soil according to EN 1998-1, corresponding to $S=1.0$, $T_B=0.15\text{sec}$, $T_C=0.4\text{sec}$, $T_D=2.0\text{sec}$), behaviour factor $q=1$, lowest bound factor for the design spectrum $\beta=0.20$. Design PGA was assumed equal to 0.35g (the highest value for the Italian territory) with a building importance factor $\gamma_I=1$.

The design of each connector was conducted according to the procedure and design guidelines reported in [6.4]: the hold-downs prevent the wall uplift due to the rocking effect while the angle brackets prevent the wall slip due to the shear effect. The distribution and the number of connectors were the same in each building (coincident with that of the three-storey CrossLam building tested on shaking table during SOFIE project) but the number of nails or screws used in each connection varied according to the seismic design force specific of each building.

6.1.4.2 Analysis of q-factor values

The q factor has been calculated according to the approach based on the NLDAs (i.e. PGA-based approach and BS-based approach) considering 7 different artificially generated seismic signals, so as to meet the spectrum compatibility requirement. As stated above the investigated case studies buildings were modeled using the same numerical model adopted to validate the developed macro-element as described in the previous Chapter 2. For a detailed definition of the numerical model refer to § 2.6 while for its the calibration see § 2.4 and § 2.5.

Each building has been subjected to a growing level of seismic intensity, from the design value ($PGA_{u_code}=0.35g$) up to the collapse condition ($PGA_{NEAR\ COLLAPSE}$) stated as the first achievement of the ultimate displacement of a single connection element. The near collapse condition was defined with the same criteria reported in [6.3], e.g. was assumed as uplift equal to 25 mm for the hold-down connections and a slip equal to 20 mm for angle brackets.

The following Table 6.4 reports the PGA values for each building and the type of connectors which firstly reached the near collapse condition.

Table 6.4 - PGA values for the near collapse condition registered in the analysis; letter A near to acceleration value corresponds to failure of the angular brackets while the letter H corresponds to failure of holdowns.

PGA _{NEAR COLLAPSE} [ag/g]		Earthq. 1	Earthq. 2	Earthq. 3	Earthq. 4	Earthq. 5	Earthq. 6	Earthq. 7	Average	
A	i	T1=0.16 sec	1.19 - H	1.10 - H	1.37 - H	0.95 - A	1.33 - H	1.35 - H	1.05 - A	1.19
	ii	T1=0.21 sec	1.35 - H	1.00 - A	1.40 - H	1.08 - A	1.45 - H	1.42 - H	1.23 - H	1.27
	iii	T1=0.26 sec	1.29 - H	1.10 - H	1.37 - H	1.02 - H	1.48 - H	1.29 - H	1.29 - H	1.28
B	j	T1=0.14 sec	0.87 - A	0.98 - A	1.08 - H	0.79 - A	1.05 - A	0.95 - A	1.02 - A	0.96
	jj	T1=0.18 sec	1.05 - A	0.93 - A	0.95 - A	0.82 - A	1.15 - H	1.07 - A	1.10 - H	1.01
	jjj	T1=0.22 sec	1.08 - A	0.96 - A	1.08 - A	0.85 - A	1.12 - H	1.04 - A	1.12 - A	1.04

As shown in Table 6.4 the near collapse condition is mainly reached with the failure of the hold down connectors for the A Configuration: out of 21 cases studied, only 3 present the failure of the angle brackets. Otherwise for the B configuration prevail the failure of the angle brackets which occurs in 16 cases out of 21. This highlights that CrossLam buildings with vertical joints show a rocking-like behaviour under horizontal actions while those without vertical panel to panel joints tend to demonstrate a shearing-like failure, as the deformed shapes of the numerical models reported in Fig. 6.7 demonstrate.

The results in Table 6.4 evidence that the average range of the PGA_{near collapse} spans from 1.19 g to 1.28 g for building test n. 1 and from 0.96 g to 1.04 g for building test n. 2. The variability is very small, about 7%. Furthermore Fig. 6.8 shows no evident correlation between the PGA_{near collapse} and the principal elastic period.

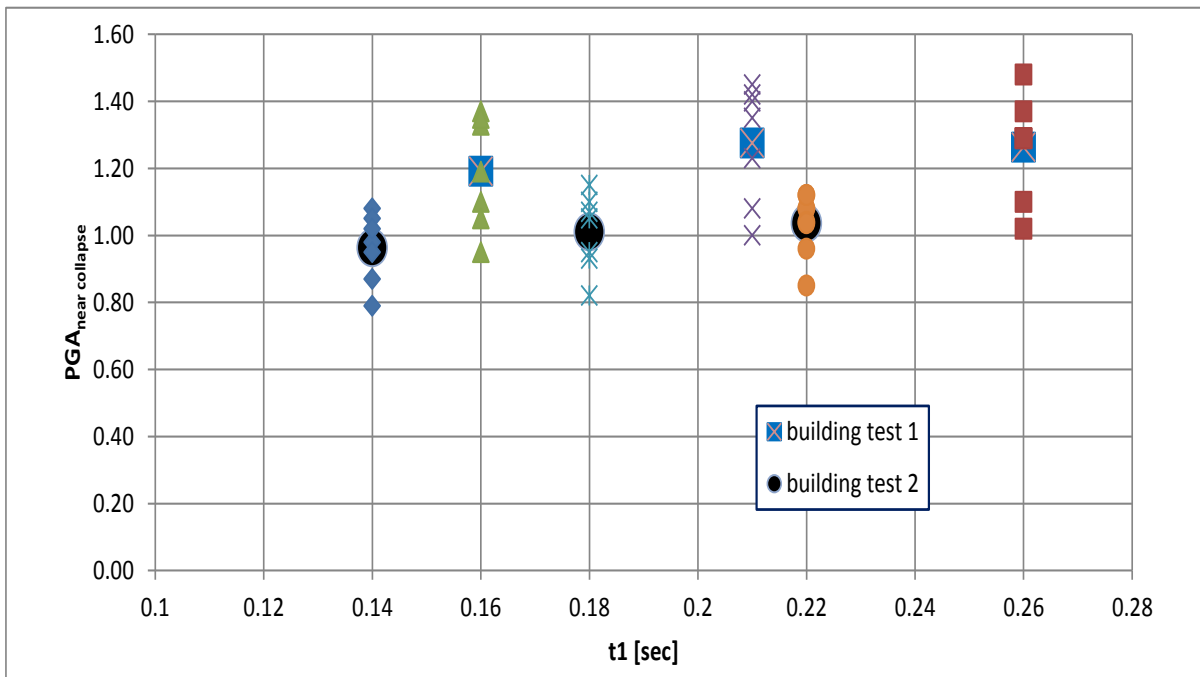


Fig. 6.8 - Relationship between the PGA_{near collapse} values and principal Eigen frequency of the building

Applying the near collapse signals further dynamic analyses have been performed to assess the base shear intensity in the hypothesis of non-dissipative elastic behaviour of the connections. As

an example Fig. 6.9 gives the two time historeys of base shear for the near collapse seismic signal N. 7.

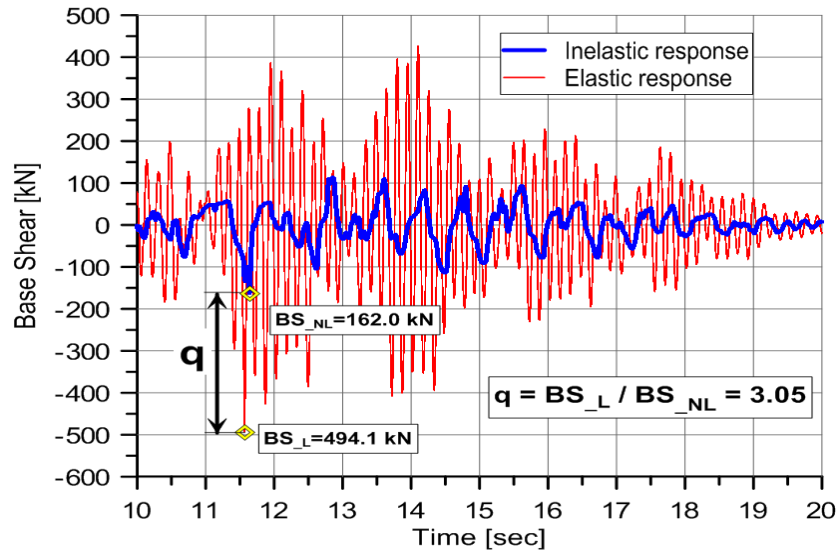


Fig. 6.9 - Time history of base shear for the earthquake N. 7 amplified to near collapse condition for elastic and inelastic connections behaviour

Once defined the $PGA_{NEAR_COLLAPSE}$ and the base shear for both the elastic and nonlinear dissipative behaviour of the building it is possible to apply the conventional methods for the q-factor evaluation defined in the previous paragraph 3.3.2.1. In detail in this application the PGA base approach and the Base Shear-based one were used to define the suitable estimation of the q-factor.

The application of such methods allowed the calculation of the q-factor for each of the six test buildings and for each of the 7 seismic signals. The results are reported in Fig. 6.10 for the configuration “A” and in Fig. 6.11 for the configuration “B”.

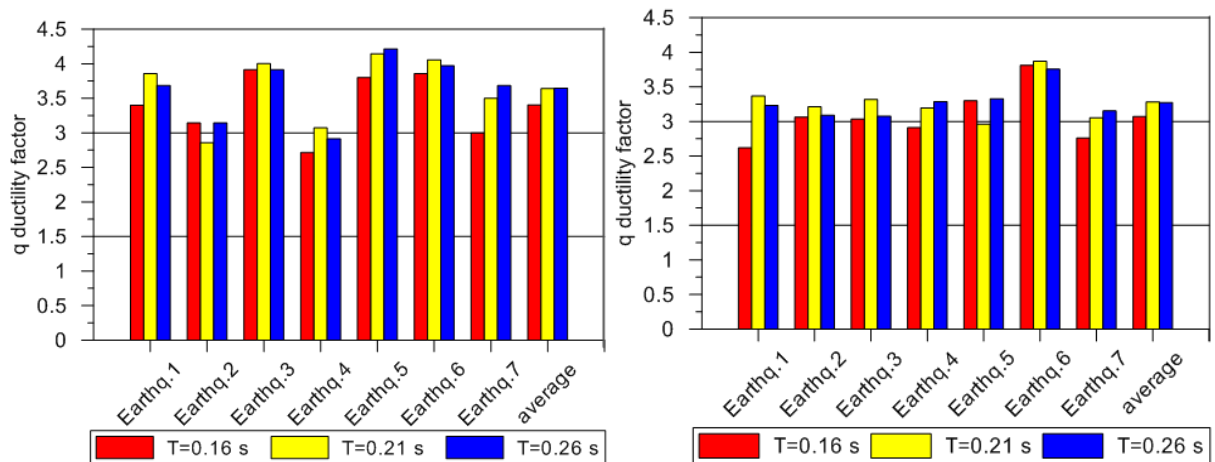


Fig. 6.10 - q-factors for configuration “A” buildings calculated with the PGA-based approach (left) and the base shear based approach (right)

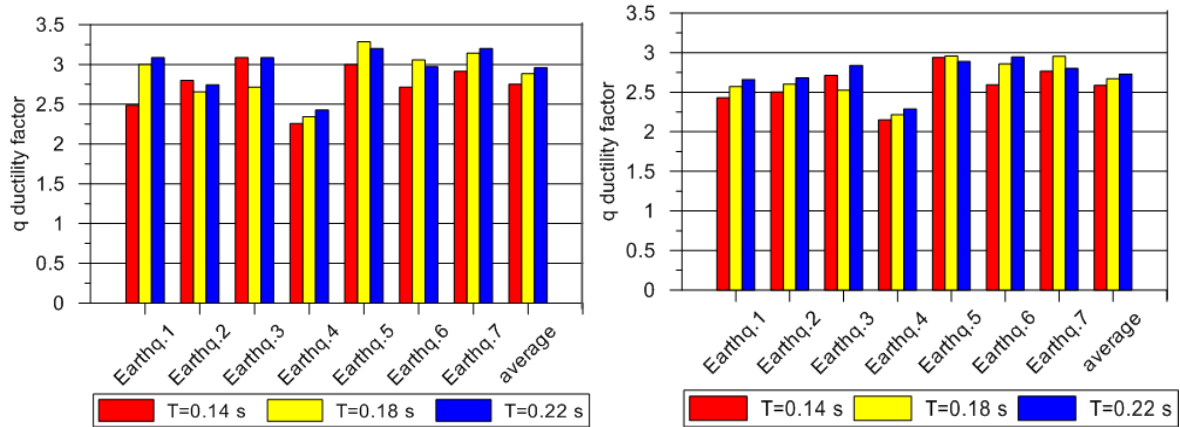


Fig. 6.11 - q-factors for configuration “B” buildings calculated with the PGA-based approach (left) and the base shear based approach (right)

A simple elaboration of the obtained q-factors is summarized in Table 6.5.

Table 6.5 – Statistical analysis of the obtained q-factor values

q factor evaluation approach	Configuration “A”		Configuration “B”	
	Base Shear - approach	PGA-approach	Base Shear - approach	PGA-approach
average value	3.21	3.56	2.66	2.78
maximum value	3.87	4.21	2.96	3.29
minimum value	2.62	2.71	2.15	2.26
Range	1.25	1.50	0.81	1.03
standard deviation	0.31	0.46	0.24	0.36

For the configuration “A” buildings having the vertical panel to panel connections, the q- factor ranges between 2.62 and 4.21 with an average value equal to 3.38, confirming the results obtained by Ceccotti [6.3].

Regarding to the configuration “B” the obtained values of the q factor are consistently lower respect the configuration “A” with a range between 2.15 and 3.29. The following Table 6.6 reports a comparison between the reference q-factor values define by Ceccotti [6.3] and those obtained by the proposed numerical simulations.

Table 6.6 - Comparison between analytical and numerical q-factor values.

		Reference q-value [6.3]	Numerical simulation q- value
Configuration “A”	Min	2.51	2.62
	Average	3.05	3.38
	Max	4.57	4.21
Configuration “B”	Min	-	2.15
	Average	-	2.72
	Max	-	3.29

Independently on the approach used, the average value of the q-factor obtained for the configuration “A” is about 20% greater than that for configuration “B”, demonstrating the relevant effect of the wall arrangement in determining the ductility and dissipation capacity of the CrossLam buildings. Such results are aligned with those obtained in the previous Chapter 5 referring to different building configuration and represent an independent validation of the performed studies about the dependence of the q-factor on the number of vertical panel to panel connections.

From the dynamic analyses with the $PGA_{\text{near collapse}}$ seismic signals it doesn't appear any significant correlation between the principal elastic periods to the q-factor value (see Fig. 6.12) of the buildings.

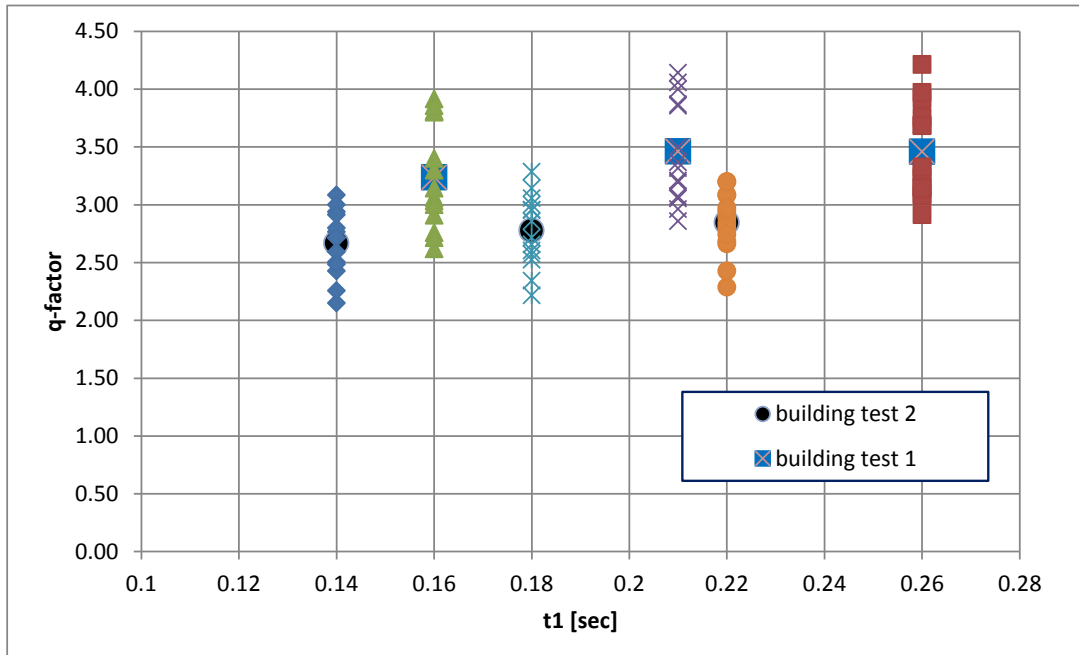


Fig. 6.12 - Relationship between the q-values and principal elastic period of the studied building

It should be pointed out that the examined set of buildings is not exhaustive, since all of them have the principal elastic period range within the plateau limits of the elastic response spectra. In order to obtain a more reliable investigation on the relationship between the main period of the building and the correspondent q-factors further analyses should be performed considering a wider range of the principal elastic period of the building. However on the basis of the results obtained in this work it is possible to affirm that in the plateau range the q-factor values are independent from the principal mode period.

It should be noted that the majority of the CLT buildings present a principal elastic period comprise in the plateau range, as shown in the previous Fig. 5.14. Only for high-rise or very slender buildings that could present greater principal elastic periods, further investigation would be necessary.

6.1.5 Full formulation of the ductility factor

The studies and analyses described in the previous section have allowed to define:

- the analytical formulation suitable to link the specific building features to the q-factor value;
- the correction index to account for the effects of the connectors design criteria;
- the independence of the q-factor value from the principal elastic period of the building (at least for normal CLT buildings).

Such results and findings can be formalized into a proposal of a design formula for the estimation of the most suitable ductility factor for CLT buildings.

$$q_{\text{eff}} = k_R K_O q(\beta, \lambda) \quad \text{Eq. 6.9}$$

where:

k_R = take into account of the building in plan and in high regularity

K_O = take into account of the fasteners overstrengthening criteria

$q(\beta, \lambda)$ = reference q-factor - depends on slenderness and junction level

Regarding to each component of the q-factor expression:

- the coefficient k_R can be assumed 1,0 for regular buildings, 0.8 for irregular buildings, according to available seismic codes provisions;
- the coefficient K_O can be defined according to the previous Eq. 6.8.

The reference q-factor $q(\beta, \lambda)$ is defined by the linear or the power relations respectively given by Eq. 6.5 and Eq. 6.6 by with the of the input parameters λ and β previously given.

The proposed expression for the q-factor of CLT buildings could be considered for a possible implementation into a future review of the seismic codes.

6.2 Validation of the developed analytical procedure

In this section the devised analytical procedure is applied to calculate the q-factor values of two different case studies building. The 1st case study refers to the NEES wood six storeys building [6.6] while the second one to the SOFIE three storey building [6.3]. A detailed description of the investigated building is presented especially with regard to storeys number, fasteners arrangements, geometrical characteristics and walls composition (i.e. number of horizontal and vertical joints, wall area and perimeter etc..) in order to define the input parameters necessary for the q-factor analytical evaluation.

Furthermore an alternative configuration of the SOFIE case study building has been studied. This configuration differs from that tested on shaking table only for the composition of the walls which are made by an unique CLT panel without any vertical panel to panel joint. This additional configuration was investigate in order to obtain a further verification on the influence of vertical panel to panel joint in the seismic response of the building and therefore on the q-factor value.

The q-factor values obtained by Pei et al.[6.5] for the case study 1 and by Ceccotti [6.3] for the case study 2 are compared with those from the analytical procedure. A critically discussion on the obtained results and on the reliability of the devised procedure is reported.

6.2.1 Case study n. 1 - NEES Wood building

The first case study refers to the six-storey wood frame building tested in the final phase of a Network for Earthquake Engineering Simulation (NEES) project in the 2009 [6.6]. This wood frame building was taken as reference by Pei et al.[6.5] and redesigned using CLT panels for the walls and the floors.

The examined building presents a regular and symmetrical rectangular part 18.3 m long e 12.2 m wide as depicted in the following Fig. 6.13. The wall along the longer side is composed by 3 jointed CLT panels 6.10 m wide while that along the shorter side by 5 jointed CLT panels 2.44 m wide.

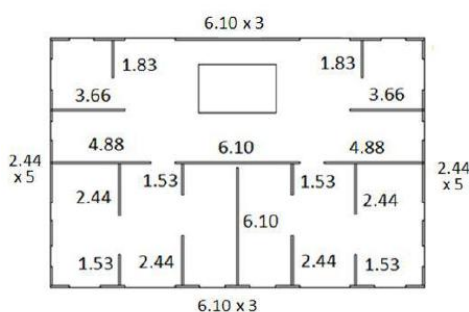


Fig. 6.13 - Building plan (left) and view of the shaken table test (right) [6.6]

In order to define the seismic behaviour and the most suitable Force Modification Factor of this NEESWood building in [6.5] several NLDAs were performed referring to 22 shakes according to FEMA P-695 [6.7]. The dynamic analyses were carried out using a complete 3-dimensional model of the building. The CUREE model proposed by Folz and Filialtrault [6.5] was used to reproduce the hysteretic behaviour of the fasteners. The Force Modification Factor of such CLT building

according to the definition of the National Building Code of Canada [6.9] of this CLT building proposed by Pei et al.[6.5] is:

$$R_{NBCC} = R_d \times R_0 = 2.5 \times 1.5 = 3.75$$

Such definition of the behaviour factor using the NBCC is based on the approach proposed by Fajfar [6.9] which provides the decomposition of the reduction factor into two components: the 1st one due to the ductility while the 2nd one due to the overstrength effects. However the global R-factor defined by the NBCC [6.9] has the same meaning of strictly of the ductility q-factor used into the European code [6.2].

The proposed analytical procedure for the q-factor estimation has been applied to the case study building. The following Table 6.7 summarizes the geometrical characteristics of the NEES Wood building [6.6] which represent the only needed input data for the analytical procedure.

Table 6.7 - Geometrical characteristic of the case study N.1 – NEES Wood building

Length side 1	L1	18.3 m
Length side 2	L2	12.2 m
Height	H	18.0 m
Number of storeys	n	6
Number of vertical panel to panel connection on side 1 wall	m1	2
Number of vertical panel to panel connection on side 2 wall	m2	4

It should be noted that the examined building has different wall composition along the two direction (1 and 2), therefore two different analytical q-factors are evaluated. The following Table 6.8 reports the details of the analytical evaluation of the q-factor.

Table 6.8 - q-factor analytical evaluation of the case study N.1 - NEESWood building

		Direction 1	Direction 2
Building synthetic indexes:			
facade area	$A = L_i \cdot H$	330 m ²	220 m ²
facade perimeter	$P_0 = 2 \cdot (L_i + H)$	72.6 m	60.4 m
jointed lines perimeter	$P = (n + 1) \cdot L_i + (m + 2) \cdot H$	200.0 m	193.4 m
Parameter α	$\alpha = A / P$	1.65 m	1.14 m
Parameter α_0	$\alpha_0 = A / P_0$	4.55 m	3.64 m
Parameter β	$\beta = \alpha / \alpha_0 = P / P_0$	2.76	3.20
slenderness	$\lambda = H / L_i$	0.98	1.48
Power approach			
reference q-factor	q_0	1.97	1.97
coefficient k1	K1	0.53	0.53
coefficient k2	K2	0.33	0.33
q-factor	$q = (q_0 + k1\lambda) \cdot \beta^{k2}$	3.48	4.04
Linear approach			
reference q-factor	q_0	1.98	1.98
coefficient $k_0(\lambda)$	K_0	0.36	0.36
q-factor	$q = q_0 + K_0 e^{k_0\lambda} \beta$	3.39	3.94
Average q-factor	$q_{average}$	3.44	3.99

The q-factor values obtained using the power and the linear formulations are in good agreement with those obtained by Pei et al.[6.5]. In detail the proposed evaluation gives two different q-values for the two wall direction of the building. Along the direction containing walls with fewer panel to

panel joints the lower q-factor is evaluated. The average q-value is about 3.71 and is nearly equal to the R_{NBBC} factor = 3.75 confirming the reliability of the proposed analytical procedure.

6.2.2 Case study n. 2 - SOFIE building

The second case study is the three storeys CLT building tested on shaking table in NIED – Japan during the SOFIE project - 2007. A detailed description of the geometrical characteristic of this building is reported in [6.3]. It has a symmetrical and regular square plant with a side of 7.0 meters. Each wall is composed by assembling three CLT panel as depicted in the following Fig. 6.14.

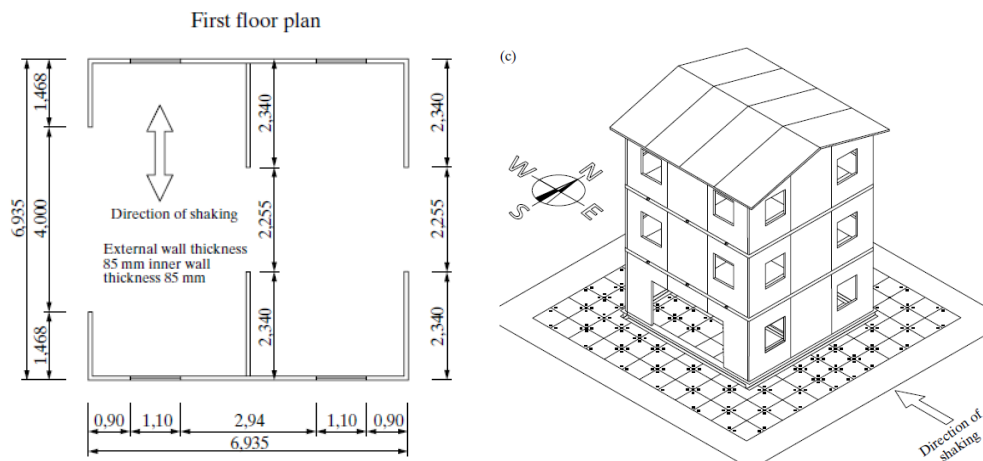


Fig. 6.14 - Building plan (left) and axonometric view of the shaken table test (right) [6.3].

The q-factor assured by the building was evaluated by Ceccotti [6.3] by means of shaking table test and numerical simulations. The numerical simulations were conducted using a spring mass-lumped model and adopting the “Ceccotti – Vignoli” model [6.11] to reproduce the hysteretic behaviour of the fasteners. A sketch of the used numerical model is reported in the following Fig. 6.15.

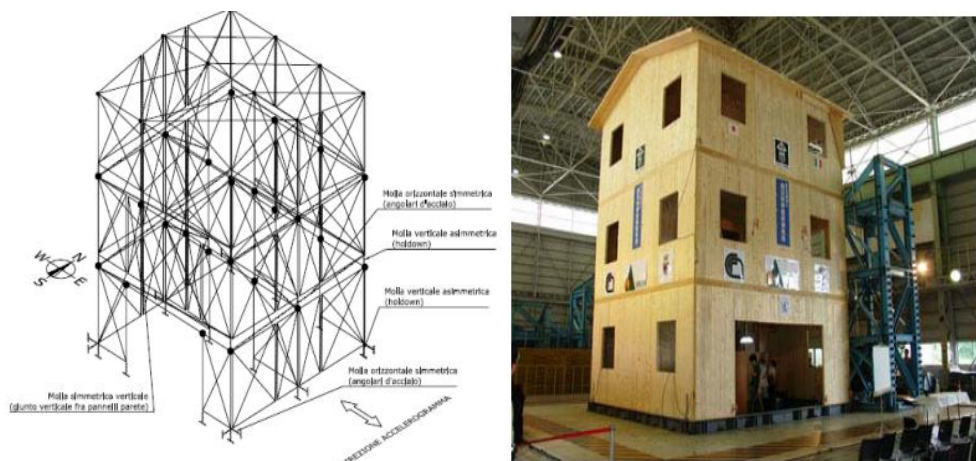


Fig. 6.15 - Sketch of the building model used for the numerical simulation (left) and view of the shaken table test (right) [6.3]

The performed test and analyses gave a q-factor up to 3 for this specific CLT building as reported in [6.3]. Such q-value has been also confirmed by the independent numerical simulation performed using the numerical model for the connectors developed in this thesis work (see § 6.1.4.2).

In order to obtain a further validation of the analytical procedure for the q-factor evaluation and investigate the influence of the panel to panel joint on the building response an alternative panels assembling was examined. In this configuration walls are made by entire CLT panel at each floor. According to the numerical simulation described in the previous § 6.1.4.2, a reduced q-factor equal to 2.70 seems to be adequate for the design of the alternative configuration.

The following Table 6.10 reports the geometrical characteristic of the examined configurations.

Table 6.9 - Geometrical characteristic of the case study N.2 - SOFIE building.

		CONF. 1	CONF. 2
Length side	L	7.0 m	
Height	H	10.0 m	
Number of storeys	n	3	
Number of vertical panel to panel connection on wall	m	3	0

Based on these geometrical input parameters the q-values for both the examined configuration were evaluated with the proposed procedure. The steps of the calculation are found in Table 6.10.

Table 6.10 - Q-factor analytical evaluation of the case study N.2 - SOFIE building.

		Configuration 1	Configuration 2
Building synthetic indexes			
facade area	$A = L_i \cdot H$	70.0 m ²	
facade perimeter	$P_0 = 2 \cdot (L_i + H)$	34.0 m	
jointed lines perimeter	$P = (n + 1) \cdot L_i + (m + 2) \cdot H$	68.0 m	48.0 m
Parameter α	$\alpha = A / P$	1.03 m	1.46 m
Parameter α_0	$\alpha_0 = A / P_0$	2.06 m	2.06 m
Parameter β	$\beta = \alpha / \alpha_0 = P / P_0$	2.00	1.41
slenderness	$\lambda = H / L_i$	1.43	1.43
Powerl approach			
reference q-factor	q_0	1.97	1.97
coefficient k1	K1	0.53	0.53
coefficient k2	K2	0.33	0.33
q-factor	$q = (q_0 + k1\lambda) \cdot \beta^{k2}$	3.43	3.05
Linear approach			
reference q-factor	q_0	1.98	1.98
coefficient $k_0(\lambda)$	K_0	0.36	0.36
q-factor	$q = q_0 + K_0 e^{k0\lambda} \cdot \beta$	3.18	2.82
Average q-factor	$q_{average}$	3.31	2.93

The calculated q-values fit quite well with that proposed by Ceccotti [6.3] for configuration 1 and that obtained in this work for configuration 1 and 2. As show in Table 6.10 for this specific case study the difference between the q-values obtained using power and negligible.

6.3 Energetic evaluations

Aim of the previous sections was the definition of an analytical formulation suitable to provide an accurate q-factor estimation starting from some specific building properties such as the slenderness, wall composition, connectors design criteria and principal elastic period.

The assessment of the most suitable q ductility factor is a fundamental step for the seismic design of CrossLam structures, according to the Force-Based Design (FBD) method [6.12]. The FBD method allows defining the effective forces and displacements induced by an earthquake on a structures keeping into account of its reliable nonlinear behaviour, but gives no information about the amount of dissipated energy by each type of connectors and its distribution at the various levels.

In this section the energy-based seismic behaviour assessment, suggested by Uang and Bertero [6.13], is applied to the studied CrossLam buildings. In this approach attention is paid not to the resistance of the structure to lateral load but on its ability in dissipating the energy inputted from the earthquakes. All the energetic evaluations presented in this section have been carried out considering the previous numerical simulation of the configuration “A” CrossLam building, which corresponds to the sample tested in the SOFIE project having first mode period $T_1=0.21$ s (see paragraph 6.1.4.1).

6.3.1 Energetic balance equation

In sake of clarity the energetic balance is presented for SDOF (Single Degree Of Freedom) structures, the extension to the MDOF (Multi Degrees Of Freedom) being immediate. A more detailed description of the energetic method is reported in [6.13]. Starting from the equation of motion defined in Eq. 6.10 the energy balance is obtained by integrating each term of the dynamic equilibrium balance equation over the entire displacement history.

$$m\ddot{x} + c\dot{x} + kx = m\ddot{x}_g \quad \text{Eq. 6.10}$$

The results of such integration give the energetic balance equation which states that at any instant the energy given by the seismic action must be equal to the sum of kinetic, elastic, viscous energies, as follows:

$$E_k + E_d + E_s = E_i \quad \text{Eq. 6.11}$$

where:

$$E_k = \int m \dot{x} dx = \frac{m\dot{x}^2}{2} \quad \text{Eq. 6.12}$$

$$E_d = \int c \dot{x} dx \quad \text{Eq. 6.13}$$

$$E_s = \int k x dx \quad \text{Eq. 6.14}$$

$$E_i = - \int m \ddot{x}_g dx \quad \text{Eq. 6.15}$$

The individual contributions included on the left side of Eq. 6.11 represent the relative kinetic energy (E_k), the dissipative energy caused by inherent damping within the structure (E_d), and the elastic strain energy (E_s). The sum of these energies must balance the input energy (E_i) inputted in the structure by the earthquake. We can note that each term above defined is actually time dependent [6.13].

It is unrealistic expecting that a structure remains entirely elastic during a severe earthquake; therefore it is acceptable that some damage may occur. In such a case, the energy input (E_i) from the earthquake exceeds the capacity of the structure to store and dissipate energy by the mechanisms specified in Eq. 6.12 to Eq. 6.14. Once this capacity is surpassed, portions of the structure typically yield and crack. The stiffness k is then no longer a constant, and the spring force in Eq. 6.10 must be replaced by a more general functional relation $f_s(x)$, which will commonly incorporate hysteretic effects. More in general, for an inelastic response of structures Eq. 6.14 is rewritten as follows:

$$E_s = \int f_s(x) dx = E_{se} + E_{sp} \tag{Eq. 6.16}$$

E_s is now the sum of two additive contributions, E_{se} and E_{sp} , representing the fully recoverable elastic strain energy and the dissipative plastic strain energy, respectively. Fig. 6.16 provides time history of the energy response for the case study undergoing the seismic excitation scaled up to near collapse conditions.

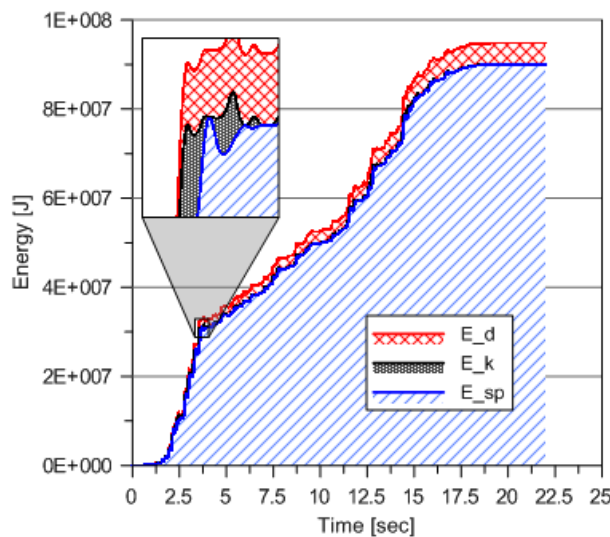


Fig. 6.16 - Time trend of the various energy contributions for the case study building for the seismic signal scaled up to near collapse condition.

Note that the terms E_{se} and E_k represent the contribute of energy returned at the end of the earthquake; the two terms E_d and E_{sp} represent the dissipated energy, which sum must be equal to the input energy by the earthquake (E_i) when the final stable condition is restored. Therefore:

$$E_i(t > t_f) = E_d(t > t_f) + E_{sp}(t > t_f) \tag{Eq. 6.17}$$

In Eq. 6.17 t_f corresponds at the moment at which stable quiet condition is restored after the end of the seismic motion.

6.3.2 Evaluation of the hysteretic energy dissipation

The capacity of the CrossLam buildings to resist to earthquake through plasticizing of connectors can be measured by the capacity of different hysteretic dissipation sources in comparison to seismic input energy.

As mentioned in [6.3] the contributions to hysteretic dissipation are mainly given by angle brackets (E_{Sp_A}), hold downs (E_{Sp_H}) and panel to panel connections (E_{Sp_P}).

$$E_{Sp} = E_{Sp_A} + E_{Sp_H} + E_{Sp_P} \quad \text{Eq. 6.18}$$

These energy components can be evaluated by integration of the hysteretic load-displacement curves of each of the connection elements. Fig. 6.17 shows some examples of such hysteretic loops obtained from the dynamic analysis of the case study.

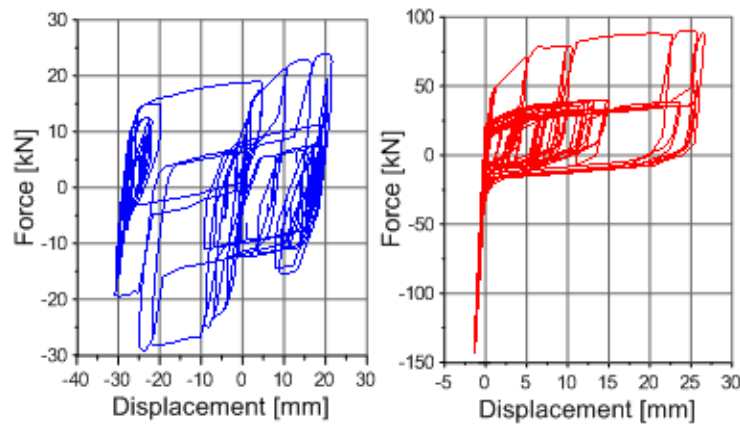


Fig. 6.17 - Examples of hysteretic load displacement curve of angle bracket (left) and hold down (right) from nonlinear dynamic analysis.

The contribution to energetic dissipation of each type of connectors is evidenced in Fig. 6.18 which highlights that, for the case study, the energy dissipated by the angle brackets and hold downs is far greater than that of the panel-to-panel joints.

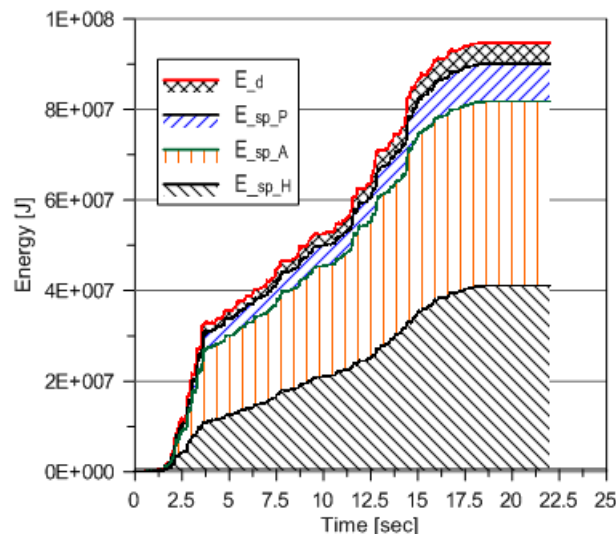


Fig. 6.18 - Time trend of energy dissipated for each specific connection element.

Adopting the same methodology it is also possible to identify the energy contribution dissipated by hysteresis at each level. According to this partition the total hysteretic dissipation can be defined as the sum of the contributions at each of the three levels as follows:

$$E_{Sp} = E_{Sp_1} + E_{Sp_2} + E_{Sp_3} \tag{Eq. 6.19}$$

This subdivision is useful to verify which level gives the most relevant contribution to the energetic dissipation and therefore to the seismic resistance. Knowing the base shear-drift curve at each level of the building (reported in Fig. 6.19), the dissipated energy is equal to the accumulation of the energy strain enclosed within the loops.

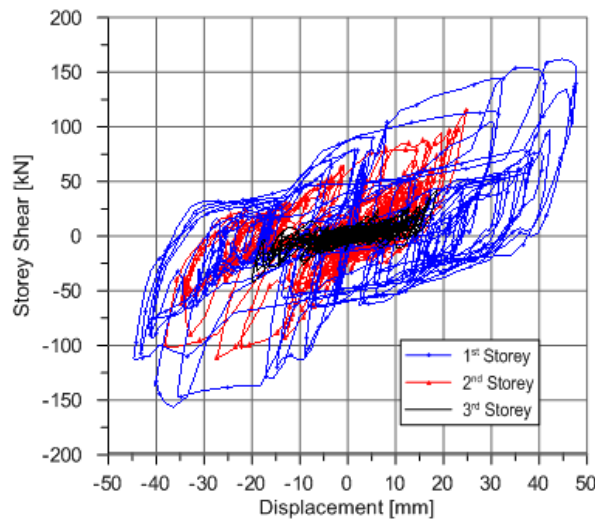


Fig. 6.19 - Shear-drift curves for each level of the case study building in the analyses with the seismic signal scaled up to near collapse condition

The time evolution of the dissipated energy contribution at each level is reported in Fig. 6.20. The first level dissipates most of the energy input due to the earthquake while the upper floors give a minor contribution to the energy dissipation.

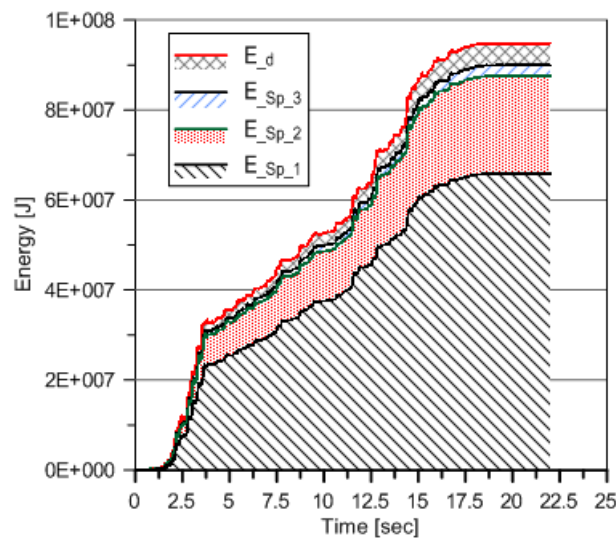


Fig. 6.20 - Energetic response for each level of the case study building –analyses with seismic signal scaled up to near collapse condition

6.3.3 Energy balance for increasing PGA

In the previous section the time histories of energy responses obtained for an earthquake signal scaled up to near failure have been reported. To explore completely the seismic behaviour of the case study CrossLam structure it is useful to trace how the various energy dissipation contributions evolve for growing PGA level. The values of viscous and hysteretic dissipated energy were evaluated for 5 different PGA levels, starting from the design level $\text{PGA}=0.35\text{g}$ up to the near collapse level reached for a $\text{PGA}=1.225\text{g}$. Only the stabilized result, that is for $t > t_f$, are reported. The following Fig. 6.21 and Fig. 6.22 show the viscous and hysteretic dissipated energy contribution for each type of connection, for increasing PGAs. As shown in Fig. 6.21 the absolute value of input energy exponentially increases with PGA intensity. Very significant are the relative results (in per cent) given in Fig. 6.22 which allow some insight about the distribution of the inelastic energy dissipation and then about the overall structural behaviour.

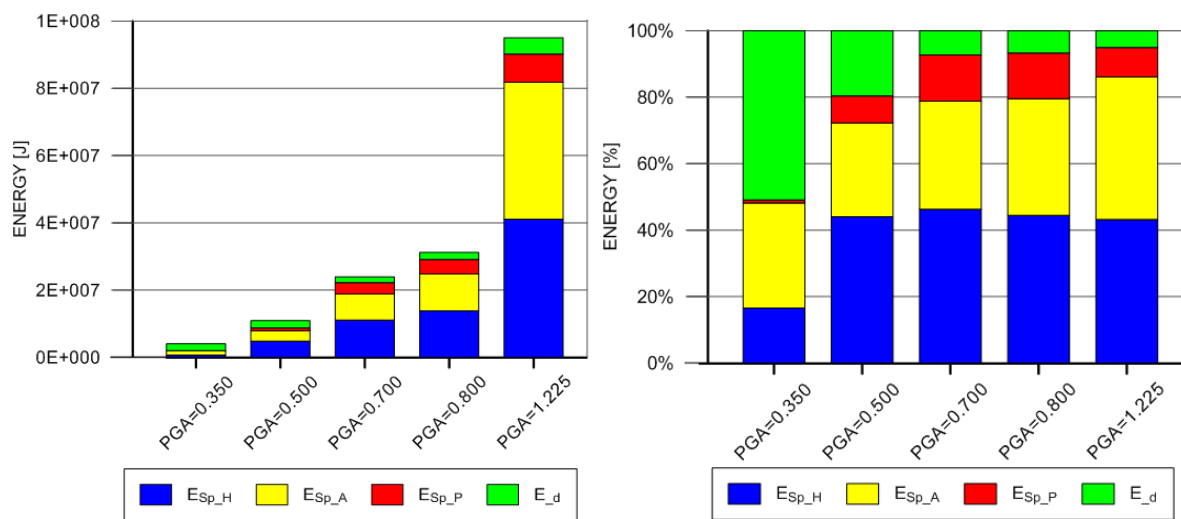


Fig. 6.21 - Absolute (right) and relative (left) values of viscous and hysteretic dissipated energy contributions for each connection type (in this figure: H stands for hold-down, A for angles and P for panel-to-panel joints).

For the yielding PGA value ($\text{PGA}=0.35\text{g}$ – i.e. the design PGA value) the viscous dissipation is relevant if compared to the hysteretic sources since with moderate deformations the connection elements almost remain in their elastic field. In such condition the greater contribution to hysteretic dissipation is given by the angle brackets and the modest contribution imputable to hold downs demonstrates that the rocking effect is reduced. As the seismic motion increase, the hysteretic dissipation becomes more relevant than the viscous damping effect and between the hysteretic dissipation terms that of hold down became the dominant.

The energy dissipated by each connector type was further subdivided into the contributions cumulated at each level of the building and the results are plotted in Fig. 6.22. It is evident that for each connection type the energy dissipated by the elements at the ground floor is always the main part. Such observation testifies that the examined building when subjected to seismic excitation acts as a rigid body, with rocking and sliding deformations localized into the ground floor connections.

With increasing PGA intensity, the dissipated energy contributions of the connection elements positioned at the upper floors assume greater relevance as highlighted by Fig. 6.22 which plots the total hysteretic dissipations at each levels.

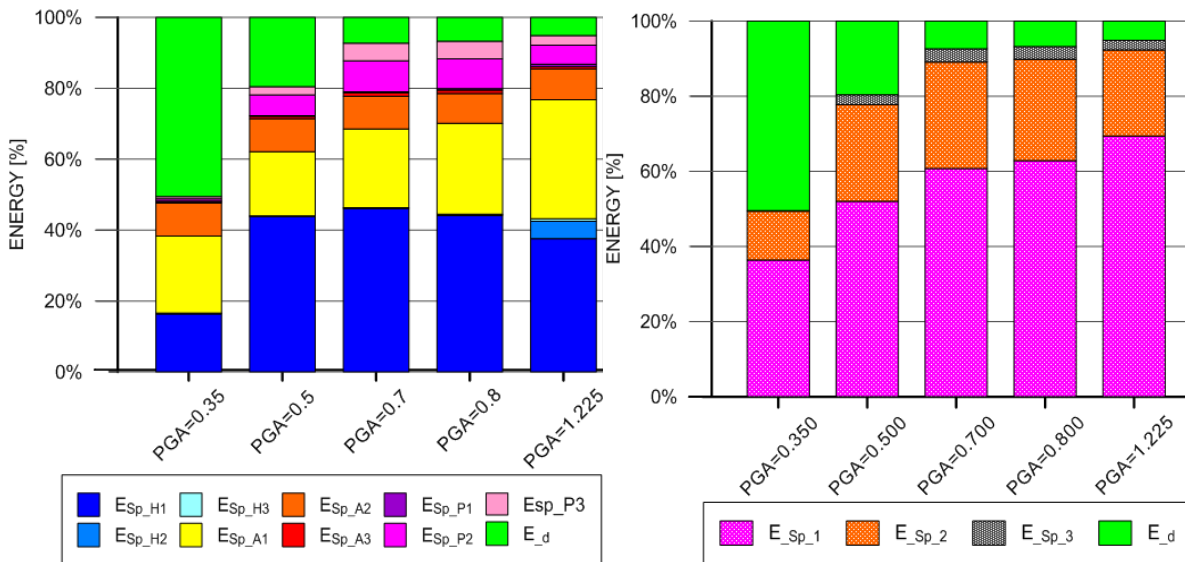


Fig. 6.22 - Relative values of viscous and hysteretic energy dissipation by each connection type at each level (left) and relative values of total dissipated energy contributions at each level. (right)

Finally it should be noted that to obtain a more representative results about the distribution of the dissipated energy among the various connectors and floors it is necessary to consider a larger number of case study configurations. However the investigations performed in this section using the energetic approach provide some relevant guidelines about the dissipative capacity of the connectors typically used into CLT building.

6.4 Conclusions

The main result achieved in this part of dissertation is the definition of analytical formulas for the calculation of the q-factor value of CLT building. The input parameters of such formula are the geometrical characteristics of the building (summarized by specific synthetic indexes that sum up the influence of the storeys numbers and wall composition), the regularity of the building and the design criteria of the connectors. Furthermore specific rules for a proper design of the connectors and of their correspondent overstrength factors are provided. The developed expression for the q-factor estimation of CLT building could be considered for a possible implementation in a future review of seismic codes.

The investigations performed to define the relationship between the principal elastic period and the q-factor value highlight that they are independent at least in the plateau range of the response spectrum that is for almost all the CLT buildings.

The validation of the developed procedure on two different case studies building has confirmed its reliability.

The last part of this section has confirmed the ability of the energetic approach in identifying the dissipative capacity of the various connection elements at the different levels of the building and how the relevance of the different contributions changes as the intensity of earthquakes increases.

References – Chapter 6

- [6.1] EN 14358, 2007. *Timber structures – Calculation of characteristic 5-percentile values and acceptance criteria for a sample*. CEN, Brussels, Belgium.
- [6.2] European Committee for Standardization (CEN). *Eurocode 8 - design of structures for earthquake resistance, part 1: General rules, seismic actions and rules for buildings*. 2004.
- [6.3] Ceccotti A. *New technologies for construction of medium-rise buildings in seismic regions: the XLAM case*. *IABSE Struct Eng Internat* 2008;18:156–65. *Tall Timber Buildings (special ed.)*.
- [6.4] European committee for standardization (CEN). *Eurocode 5 – design of timber structures – part 1-1: general rules and rules for buildings*. 2004.
- [6.5] Pei, S., Popowski, M., van de Lindt, 2012. “Performance based design and force modification factors for CLT structures. Meeting 45 of the Working Commission W18-Timber Structures, CIB. Växjö, Sveden, 2012, paper CIB-W18/45-15-1.
- [6.6] Pei, S., van de Lindt, J.W., Pryor, S.E., Shimizu, H., and Isoda, H. 2010. *Seismic testing of a full-scale sixstory light-frame wood building: NEESWood Capstone test*. *NEESWood Report NW-04*.
- [6.7] FEMA 2009. *FEMA P695 Quantification of Building Seismic Performance Factors*. Federal Emergency Management Agency, Washington, D.C.
- [6.8] Folz, B., and Filiatrault, A. F., (2001). “Cyclic analysis of wood shear walls.” *Journal of Structural Engineering*, American Society of Civil Engineers, Vol. 127, No. 4, 433-441.
- [6.9] NBCC. 2005. *National Building Code of Canada*. Institute for Research in Construction, National Research Council of Canada, Ottawa, Ontario.
- [6.10] Fajfar P. *Design spectra for new generation of code*. *Proceeding 11th Word Conference on Earthquake Engineering*, Acapulco, Mexico, 1996, paper No. 2127.
- [6.11] Ceccotti, A., (1994). “Modeling timber joint, timber structures in seismic regions: RILEM state of art report” *Material and Structures*, 27,177-178
- [6.12] Chopra AK. *Dynamics of structures - theory and applications to earthquake engineering*. Upper Saddle River: NJ: Prentice Hall; 1995.
- [6.13] Uang C.M, Bertero V. *Evaluation of seismic energy in structures*. *Earthquake engineering and structural dynamics* 1990; 19: 77-90

Chapter 7 – Theoretical and experimental development of a high ductility wood-concrete shearwall system.

Abstract

This section investigates from the structural point of view the innovative idea of using an external concrete shelter made of precast slabs to improve the performance of standard platform-frame shear walls. The idea consists of external plating made of thin Reinforced Concrete slabs screwed to the wooden frame of the walls. As a result, the concrete slab acts as a diaphragm against the horizontal forces. It also has thermal and acoustic functions and can be used to create a natural ventilation chamber between the concrete shell and the wooden structure. This results in substantial improvements of overall performance of the shearwall.

The structural response of this shearwalls under monotonic and cyclic loading conditions has been assessed by means of experimental tests. The tests outcomes are presented and compared with those from code provisions. Fulfillment of the requirements given by Eurocode 8 as regards the attribution to the Higher Ductility Class is also verified.

The influence of concrete skin on the seismic response of the shearwall is also evaluated by means of numerical analysis and the suitable “q” ductility factor is estimated.

7.1 Introduction

Structural skins are extensively used in building practice to improve and adjust the mechanical characteristic of existing structural elements or historical buildings. Nowadays it is becoming widespread the application of such structural skins to new structures in particular for wooden buildings.

In north Europe and especially in the UK, the brick-clad timber-framed has been used for a long time but the outer encasement has only aesthetic and protection functions and it doesn't perform any structural functions. As an example Fig. 7.1 reports a five storey brick clad timber frame (Manchester - UK [7.1])



Fig. 7.1 – Crown House, Manchester Five Storey Brick Clad Timber Frame [7.1]

This building typology doesn't appear to be suitably used in seismic areas because the external brick-clad increase the global mass of the building without improving the lateral shear resistance of the structure. Moreover the flexibility and ductility of the two structures, the wooden internal one and the bricks cladding, are definitively different and they would interact with unpredictable effects in case of seismic events.

In order to verify the actual response of this building system and define the specific connection system between the external brick encasement and the inner wooden shearwall a six storeys, TF2000, timber-frame building was tested at BRE Cardington in 2000 [7.1]. The project has been collaboration between government, BRE, TRADA Technology Limited and the timber industry. The following Fig. 7.2 reports the tested six storey building and a detail of the movement joint between the external brick encasement and the inner wooden shearwall.



Fig. 7.2 – Brick Clad Timber Frame at BRE Cardington (left) and Typical Movement Joint (right) [7.1]

In Canada and north America mixed shear walls made of wood frame coupled with gypsum boards to improve the lateral shear resistance are widespread and extensively studied [7.2]. In the Alpine area constructive systems adopting wood frame braced by fiber cement sheets are becoming more common and, in order to verify the structural response of this wood frame walls under horizontal force, many research are being carried out [7.3].

The recent diffusion of the timber buildings in hot climate zone, such as the Mediterranean area, claims the development of new insulation system characterized by high mass and presence of moving air chambers in the outer side of the walls.

This part of dissertation investigates from the structural point of view the implications of the use of an external R.C. skin applied to timber frame structure. Such skin satisfies both the previous cited requirements and improves the summer insulation performance of the wood frame building. First of all, the usage of concrete guarantees high external mass. Moreover a specifically developed structural fastening system of the concrete slab to the wooden shear wall, ensures the presence of a continuous ventilation cavity along the wall. The application of this structural outer R.C. skin improves substantially the lateral shear performance of walls subjected to horizontal actions because the external slabs act as diaphragm. In this new plated wooden shearwall the bracing stiffness and strength assured by the OSB panel nailed to the wooden frame are cumulated with those given by the outer concrete skin which is screwed to the frame by means of large diameter connectors. The use of these specific fastening systems assures a considerable stiffness and, in the meantime, a great capacity of energy dissipation in case of seismic events.

This new developed constructive system is not accounted by the building codes (Eurocode 5, EN 1995 [7.4] and Eurocode 8, EN 1998 [7.5]) yet, therefore there is a lack of guidelines for its seismic design and the choice of the appropriate behaviour q-factor.

The most suitable static and seismic design procedure of this new developed constructive technique is proposed in this part of dissertation imitating the calculation standards normally adopted for the Platform Frame system. Such procedure is based on the method proposed by Piron and Lam 2003 [7.6] and on the theoretical studies performed by Folz and Filaltrout 2004 [7.7] and [7.8]. The outcomes from the developed design procedure are verify against experimental tests and numerical simulations.

7.2 Plated wooden shearwall – Concept

The developed mixed constructive system combines a typical Platform Frame building system with an external thin reinforced concrete slab acting as a diaphragm against the horizontal forces and having also thermal and acoustic functions. Manufacturing limitations combined with common inter storey height imposed a maximum dimension of the concrete slab side equal to 1080 mm. Hence the wood frame differs from the standard platform frame building: the spacing of the vertical stud doesn't depend on the size of the OSB sheets but on that of the external square precast concrete slabs.

These dimensional limitations have inspired the development of a prefabricated modular system for buildings where the mixed wood-reinforced concrete shearwalls are made by connecting single modulus preassembled in the factory. On the construction site the single precast modular panels are connected together by means of screws and to the foundation with mechanical fasteners (nailed holddown and bolts). The structural layout is similar to platform frame system where the walls are made of modular panels with aspect ratio of 3:1 (3.24m high and 1.08m long). The typical modular panel is reported in Fig. 7.5.

The geometry of the panels allows a continuous ventilation chamber from foundation to the roof between the OSB panels and the concrete slabs. The presence of this continuous moving air layer between the two diaphragms guarantees an optimal thermo-hygrometric performance and keeps dry the interface wood-concrete preventing the wood deterioration.

The structural layout of the mixed wood-concrete wall consists of two resistant systems with different structural functions: elements engaged for vertical actions and elements which react to the horizontal actions (wind and earthquake). Below in reason of brevity, is reported a synthetic description of the main geometrical and structural features of this new developed building systems. For a more detailed description of these structural and geometrical characteristic see Appendix A.

The system that supports the gravity loads is the wood frame structure which transfers to the foundation the own weight and the dead and live vertical loads. Two adjacent modular wall panels are jointed together by the superposition of a vertical joint cover screwed to the vertical studs. This joint cover realized the vertical support for the floor and roof beams.

Bracing system reacting to horizontal actions consists of two different kind of rigid diaphragms connected to wood frame. The first bracing system is made by the use of three OSB panel (1080 mm x 1080 mm x 15 mm) connected with staples to the wood frame. The second bracing system consists of three square reinforced concrete slab (1080 mm x 1080 mm x 40 mm) connected to the wood frame with screws. The reinforcement of the slabs is made of wire mesh knitted 60 mm x 60 mm. The concrete slab is fixed to the wood frame using 8 mm diameter screws coupled with a plastic bush. The plastic bush serves important functions: reduces the clearance between the concrete slab and the screw without using sealant products; acts as spacer between the horizontal cross beam of the wood frame and the concrete slab ensuring the ventilation cavity; increases bearing resistance of the screws arranged along the vertical column, Fig. 7.3. For extra details about the fastening system of the RC slabs see Appendix A.

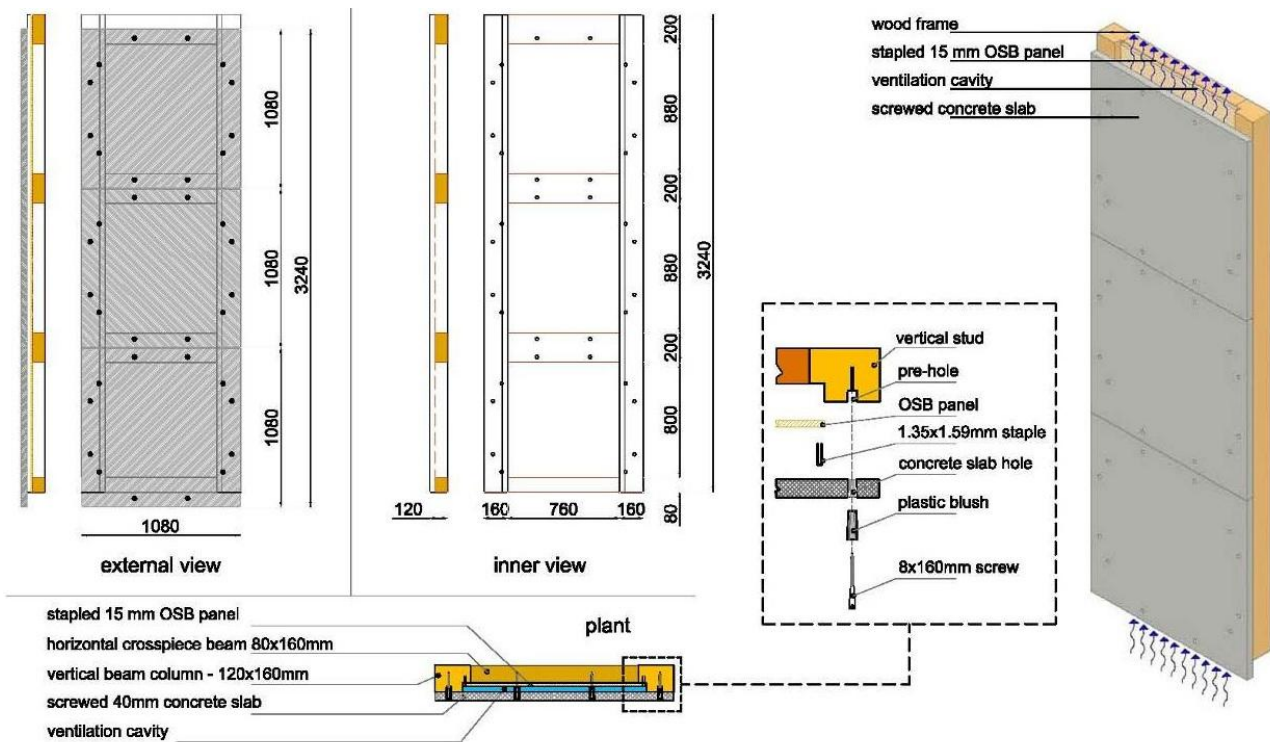


Fig. 7.3 – View of the precast modular panel

The modular wall panel is anchored to foundation using special holdown and bolt which avoid rocking and slip effects respectively. The holdown is made by press-belted L-profile 3 mm thick nailed at the corner formed by the vertical columns and the joint cover element. Such holdown is connected to the concrete foundation with bolts as the standards holdown. The wall panel slip is prevented fixing the bottom horizontal crosspiece beam and the bottom concrete slab to the foundation by bolts. The shear action of OSB bracing is transferred to the foundation by anchoring the bottom horizontal beams (see Fig. 7.4)

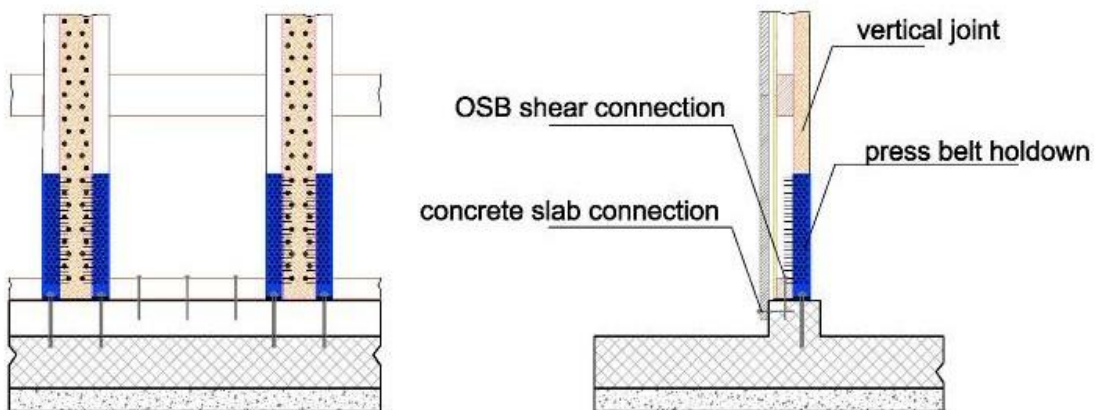


Fig. 7.4 – View of the foundation anchor system.

An extensive description of the connection system and of the structural detail specifically developed for this innovative building system is reported in Appendix A.

7.3 Cyclic and monotonic tests

In order to verify the actual resistant characteristics and the hysteretic behaviour of the investigated constructive system a series of experimental tests were performed. This paragraph describes the structural layout and the main characteristics of tested walls with regards to connectors and bracing system. Test layout, instrumentation, load condition and protocol adopted for the quasi static reversed cyclic tests are also given. The outcomes from such tests are reported.

7.3.1 Test wall configurations

Three different wall configurations were tested: "wall A" aspect ratio of 3:1 (3.24m high and 1.08m long, one modular panel); "Wall B" aspect ratio of 3:2 (3.24m high and 2.16m long made of two adjacent modular panel) "Wall C" presents an opening in the central panel, aspect ratio of 1:1 (3.24m high and 3.24 m long made of three adjacent modular panel). In sake of brevity are presented only the outcomes of the test of "Wall B" and "Wall C", being from "Wall A" completely aligned to the others.

7.3.2 Test setup and instrumentation

"Wall B" and "Wall C" were tested using different setup due to their different geometrical characteristics and load conditions. In order to faithfully reproduce the actual base connection system a base concrete foundation was provided. The test setup used for "Wall B" is presented by Fig. 7.5. Vertical load equal to 20 kN/m was applied using three hydraulic actuators placed at the vertical wood columns. To allow the wall uplift without variance in the vertical load the hydraulic actuators were placed in series with springs. The "Wall C" test was carried out loading two walls arranged specular respect to load axis with the aim to balance the torsional effects and to keep the unidirectional movement of the wall. The setup used for "Wall C" is presented in Fig. 7.5. Lateral guides with rollers in contact to the top horizontal beam were also used to ensure unidirectional movement of the walls. Uniform vertical load equal to 20 kN/m was applied at the top of each wall through actuator and distribution steel beam. The displacements of the wall panel were measured with transducers placed as shown in Fig. 7.5.

7.3.3 Test procedure

The cyclic tests were performed according to EN 12512 [7.9] in displacement control at rate of 0.04 mm/s. The yielding displacement v_y was estimate referring to preliminary test made on single modular panel "Wall A". The collapse of the wall has not been reached during the cyclic tests stopped at 80 mm displacement cycles. To verify the actual lateral load capacity and ductility of the investigated constructive system, a ramp monotonic test on the "Wall C" was performed according to EN 594 [7.10] in displacement control at rate of 0.04 mm/s.

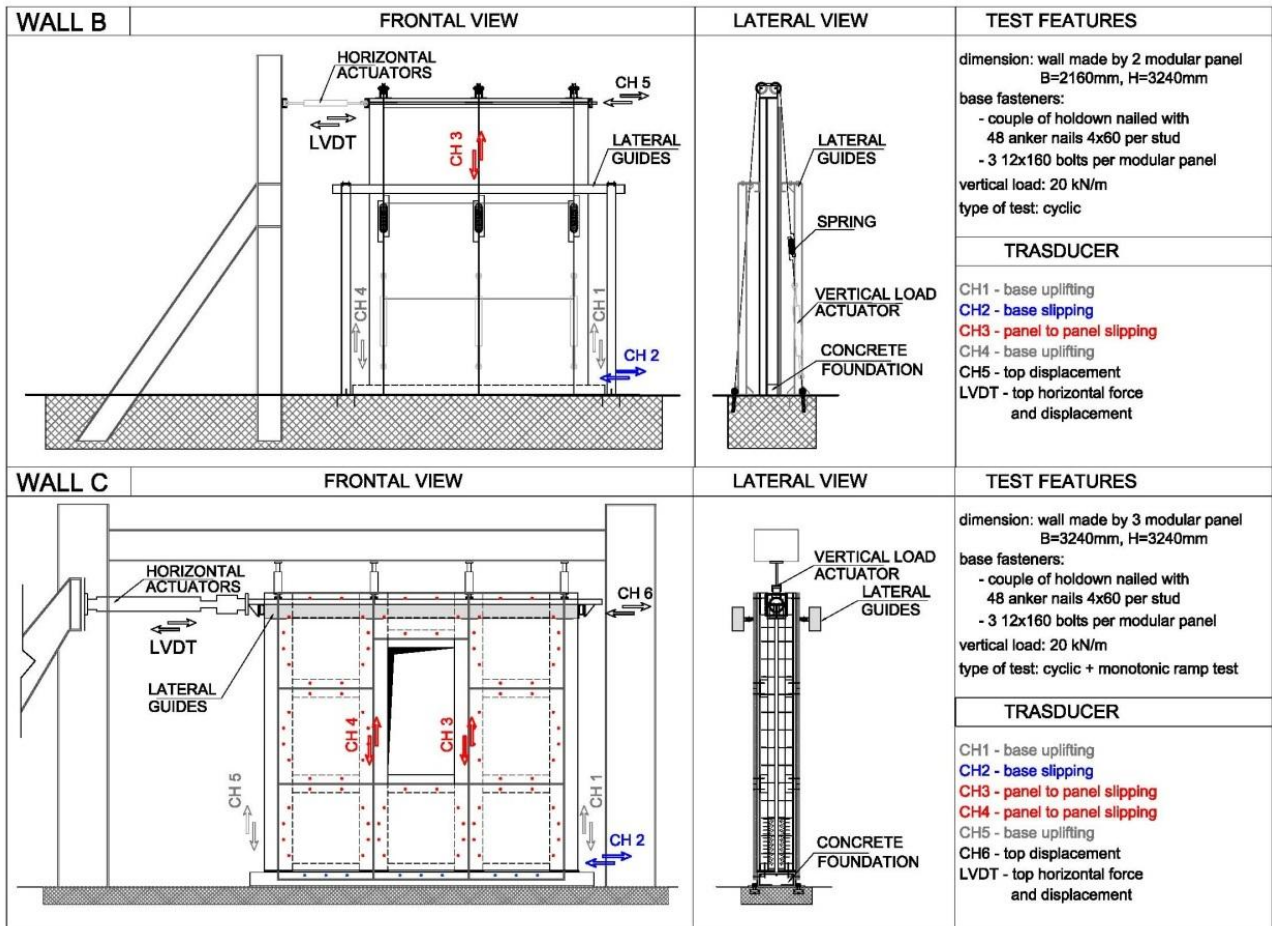


Fig. 7.5 - Sketch of the setup, "Wall B" and "Wall C".

7.3.4 Test outcomes

The performed cyclic tests have allowed to define the hysteretic cycles of the walls obtained plotting the measured top displacement and the force imposed by the actuator, see Fig. 7.6. As shown in Fig. 7.6, the load-slip curve related to "Wall B" is asymmetric because during the pushing phase the lateral guides were unable to prevent the out of plane instabilities of the wall. Due to this problem it has been possible to carry out only the pull cycles at the largest amplitude. The test stopped before the achieving of the ultimate strength of the wall since the maximum elongation of the actuator system (100 mm) was reached.

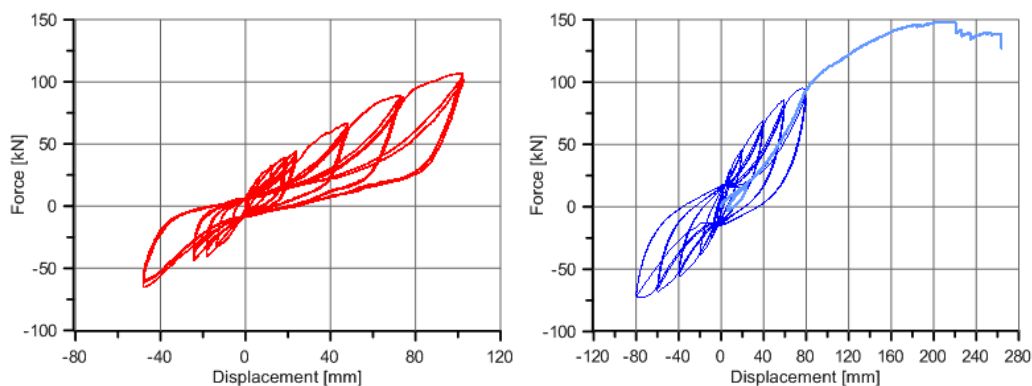


Fig. 7.6 - Load displacement curve, cyclic test for "Wall B" (left) and "Wall C" (right)

During the cyclic phase the “Wall C” has not shown failure or relevant strength degrading phenomena as shown in Fig. 7.7. The collapse condition was achieved only with a final monotonic ramp test performed after the end of the cyclic test as shown in Fig. 7.6 (right). “Wall B” and “Wall C” present the typical hysteretic behaviour of the steel-wood and wood-wood connections characterized by the pinching phenomenon. Moreover the tested walls show a marked hardening phase probably due to the use of large diameter connectors to fix the concrete bracing system to the wood frame.



Fig. 7.7 - Wall configuration at the end of the cyclic test - “Wall B” (left) and “Wall C” (right)



Fig. 7.8 - “Wall C”- configuration at the end of the monotonic ramp test and failure details.

As depicted in the previous Fig. 7.8, the tested “Wall C” has shown a significant shear deformation of the bracing system at the end of the monotonic ramp test with relevant relative sliding between the concrete slabs. Despite this strong shear deformation of the wall, the concrete slabs shown no brittle failures and no relevant cracks in correspondence of the fastening points. This means that the connection system used to fix the concrete slab to the wood frame was adequately designed to ensure a ductile failure of the bracing system with the formation of the plastic hinge in the screws in correspondence of the wood-concrete interface (see Fig. 7.8 – right). Regarding to the base fasteners failure it must be underlined that during the cyclic test their deformation was small and only at the end of the monotonic test some failures occur in the base holdown due to the excessive uplift of the wall (see Fig. 7.8 – bottom).

7.4 Analysis of experimental result

The outcomes from the cyclic tests were analyzed in order to define the main structural characteristics of this new developed plated shearwall. In this section the evaluation of the yielding limit, ultimate conditions, stiffness for the elastic and hardening branch, maximum ductility achieved during the test, equivalent viscous damping and the strength degrading at each level of ductility is reported and critically discussed. A final comparison with the design provision is performed regarding to both static (strength and stiffness) and seismic (ductility class) features.

7.4.1 Estimation of the ductility

Ductility is an important requirement in structural design against seismic actions. An extensive treatment about the implication of the ductility on the building response is reported in the Chapter 4 of this dissertation. Here the available procedures suitable for the ductility estimation are described and examined according to indication given by Munoz et al. [7.11].

The evaluation of the ductility of this new developed construction system is based on the so called EN-a, EN-b, EH-EES and EP-EES criteria summarize in the paragraph 4.3 of this dissertation. These criteria are the more representative for wooden structure as stated by Stehn [7.12]. Furthermore in the paragraph 4.5 is also reported a preliminary calculation of the ductility ratio of the "Wall C" configuration using these four criteria. However below the ductility estimations for both the tested walls using these four bi-linearization criteria are summarized.

Preliminary to the ductility estimation it must be defined the envelope curve that best fit the cyclic experimental hysteresis load-slip curve of each examined wall. As described in the previous paragraph 4.3.1 the Foschi [7.13] three parameters formulation provides the most suitable approximation of the experimental hysteresis curve. The parameters of the Foschi [7.13] envelope curve are reported in Table 7.1.

Once obtained the envelope curve it is possible to define the ductility ratio according to the previously defined criteria. First of all it should be noted that both the experimental load displacement curves of the investigate walls show a well-defined hardening phase while the elastic branch is nonlinear with continuous variation of the stiffness.

Due to these particularities of the experimental load-slip curve some limitations on the applicability of the bi-linearization criteria occur. In fact the method (b) proposed by the EN 12512 [7.9] imposed the value of the hardening stiffness equal to 1/6 of that elastic one without taking into account the actual hardening stiffness of the wall. Due to the specific shape of the experimental load-slip curve the tangency condition between the hardening branch (defined by imposed gradient) and the envelope curve is not realized. Consequently the so called EN-b approach is not applicable therefore the yielding condition is here defined referring only to the other three approaches: EN-a, EH-EES and EP-EES.

As explain in Fig. 7.6, the failure condition wasn't achieved during the cyclic tests therefore for the "Wall B" reference is made to the maximum displacement and force reached during the last cycle of the test. Otherwise for the "Wall C" such failure condition is defined by the displacement corresponding to the maximum force reached during the monotonic ramp test. This choice of the

failure condition gives the lower and most precautionary ductility values. The failure force and displacement values are reported in Table 7.1 for both the investigated walls.

Starting from such definitions of the yielding and failure limits, it is possible to calculate the ductility value. The main outcomes in terms of elastic and hardening stiffness, strength and ductility obtained adopting both the EN 12512 [7.9] procedures and the energetic ones are summarised in Table 7.1.

Table 7.1 - Test results and interpretation according to the energetic and EN 12512 [7.9] approaches

PARAMETERS IDENTIFICATION		WALL B			WALL C		
Initial stiffness	K_0 [kN/mm]	4.4			4.6		
Hardening stiffness	$r_1 K_0$ [kN/mm]	1.1			1.1		
Residual force	F_0 [kN]	30.0			45.0		
Ultimate displacement	V_u [mm]	102.0			182.1		
Ultimate force	F_u [kN]	112.6			145.7		
		EN-a	EH-EES	EP-EES	EN-a	EH-EES	EP-EES
Elastic stiffness	α [kN/mm]	4.4	3.3	4.4	4.6	3.5	4.6
Hardening stiffness	β [kN/mm]	1.1	1.1	0.0	1.1	1.1	0.0
Yielding displacement	V_y [mm]	10.3	13.6	16.8	54.9	58.3	102.1
Yielding force	F_y [kN]	41.4	44.4	68.5	10.2	16.3	19.0
Ductility ratio	$\mu = V_u / V_y$	9.9	7.5	6.1	17.4	10.9	9.4

As reported in Table 7.1 both the tested walls are characterized by ductility estimations always greater than 6 independently from the adopted approach. In detail the approaches based on the equivalence of the energy strain between the envelope and the bi-linear curves provide the lower ductility values. Finally it should be pointed out that the ductility values related to “Wall B” are lower than those to “Wall C”. This difference is due to the definition of the failure condition of the walls. “Wall C” reached the failure at the end of the experimental test unlike “Wall B” didn’t reach the failure condition and probably still had some displacement capacity and therefore a greater ductility. The different bi-linearization criteria related to “Wall C” and the Foschi [7.13] envelope are reported in the previous Fig. 4.5.

7.4.2 Wall equivalent viscous damping

The equivalent viscous damping v_{eq} is an adimensional parameter useful to summarize the hysteretic properties of structural elements. It is defined according to EN 12512 [7.9] referring to the 3rd cycle of each ductility level using the following Eq. 7.1.

$$v_{eq} = \frac{E_d}{2\pi E_p} \quad \text{Eq. 7.1}$$

Where the dissipated energy E_d and the potential elastic energy E_p are identified in Fig. 7.14.

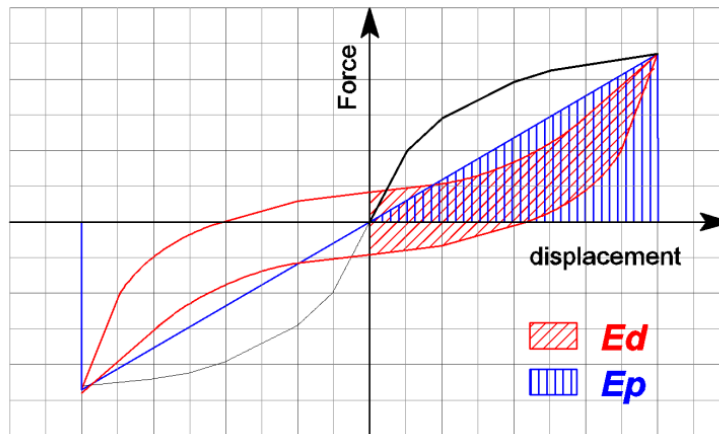


Fig. 7.9 - Dissipated and potential energy used to define the equivalent viscous damping [7.9]

The equivalent viscous damping values calculated for each ductility level and for each wall specimens are reported in the following Table 7.2.

Table 7.2 - Equivalent viscous damping values obtained from the cyclic test

Wall B				Wall C			
Cycle amplitude	Ep [kJ]	Ed [kJ]	V_{eq}	Cycle amplitude	Ep [kJ]	Ed [kJ]	V_{eq}
18mm	436.5	387	14.12%	10mm	304.6	282.0	14.74%
24mm	657.48	574	13.90%	20mm	911.0	721.1	13.60%
48mm	1971.6	1561	12.61%	40mm	2725.2	2395.8	13.27%
72mm	3965.4	2250	9.04%	60mm	5128.8	4154.9	12.9%
102mm	6763.62	3263	7.68%	80mm	7569.6	5561.8	11.7%

For both the investigated walls, the equivalent viscous damping values decrease with the increasing of cycle amplitude. This aspect means a reduction in the dissipative capability with the increasing of the displacement due to the pinching phenomenon.

It should be stressed that the equivalent viscous values related to “wall C” are always greater than those obtained for “wall B”. It means that the middle windowed modular panel of the “wall C” gives relevant contributions on the dissipative capacity of the composed wall despite its strength and stiffness contributions are negligible.

7.4.3 Wall strength degradation

Wooden structures assembled using fastening systems are sensible to the degradation of the connection element characteristics when undergoing to cyclic action. The consequent strength impairment is a relevant parameter to identify the ability of a wooden structure to resist to cyclic action and therefore to earthquake.

According to Eurocode 8 [7.5] such parameter within the ductility ratio defines the Ductility Class of a timber structure. The following Table 7.3 reports the strength degradation recorded at each ductility level of the examined walls.

Table 7.3 - Strength degradations at each cycle amplitude

Wall B		Wall C	
cycle amplitude	impairment strength	cycle amplitude	strength reduction
18mm	4.1%	10mm	2.5%
24mm	4.7%	20mm	5.9%
48mm	6.7%	40mm	7.8%
72mm	6.9%	60mm	8.5%
102mm	7.1%	80mm	9.50%

As show in Table 7.3 the strength impairment values increase with the cycle amplitude but remain always lower than 10% for both the investigated walls. These testify the good behaviour of this plated wooden shearwall under cyclic actions and therefore its adequacy for use in seismic zone.

7.4.4 Comparison with static and seismic design provisions

In this section a comparison between the outcomes of the experimental tests and the design provision is given both with regard to the static and seismic performance. The analytical formulas reported in Eurocode 5 [7.4] were used to estimate the initial stiffness and maximum strength of the investigated walls. Finally the attribution of the proposed plated shearwalls to a suitable ductility class was made referring to the requirements given by Eurocode 8 [7.5].

7.4.4.1 Strength and stiffness evaluation according to Eurocode 5

The calculation of the lateral load bearing capacity and stiffness of each modular panel is made according to the available code provisions and it is detailed in Appendix A. Hereafter are reported the analytical strength and stiffness values of each examined wall obtained by adding the strength and stiffness values related to the single modular wall panel. As reported in Appendix A the modular panel with a window, used in the “Wall C”, was not considered as resistant element because it presents only one entire square R.C. outer slab. Table 7.4 reports a comparison between the analytical estimations and those defined via experimental tests.

Table 7.4 - Comparison between the experimental results and the code provisions

	K0 [kN/mm]	Kser_EC5 [kN/mm]	Δk [%]	Fmax [kN]	Fk_5%_EC5 [kN]	ΔF [%]
“Wall B”	4.40	4.56	3.5	112.6	103.6	8.0
“Wall C”	4.60	4.56	4.0	145.7	103.6	28.8%

As shown in Table 7.4 the actual value of the lateral resistance is always greater than that obtained with the code provision. In detail for the “Wall C” the difference is about 30% and it is in line with the ratio between the 5% percentile and the average value of a typical normal probabilistic distribution for a wood structure (see EN 14358 [7.14]). Otherwise for the “Wall B” the difference is

lower and about 8%. In this case the experimental value doesn't correspond to the maximum strength of the wall because the test was stopped before reaching the failure condition.

Regarding to the initial stiffness the analytical values fit very well with the experimental ones: the differences are always lower than 5%. The design values obtained referring to the Eurocode 5 [7.4] provisions are in good agreement with the outcomes from the experimental test. This confirms the adequacy of the code provisions to define the strength and stiffness of the mechanical fasteners used in this mixed wood-concrete constructive system.

7.4.4.2 Ductility class definition

Eurocode 8 [7.5] and also Italian standard [7.15] provides three different ductility classes (i.e. Lower Ductility Class; Medium Ductility Class and High Ductility Class) depending on the dissipative capacity of the timber building. The parameters used by EC8 [7.5] to classify the belonging to a specific ductility class of a timber structures are the ductility ratio and the strength degrading value. In detail a ductility ratio up to 4 is required for the DCM and up to 6 for the DCH. In both cases the impairment strength must be lower than 20%.

Both the studied walls present ductility ratios always greater than 6 independently from the criteria used for the bi-linearization of the experimental load-slip curves. Furthermore the strength degrading is always lower than 20%. Based on the EC8 [7.5] provisions this constructive system can be considered as a structure with a high level of ductility and therefore belonging to the High Ductility Class. This classification point out the good dissipative capacity of this plated wooden shearwall but doesn't define exactly the most suitable "q-factor" to use for the seismic design because this constructive system doesn't belong to the standard building typologies reported on table 8.1 of EC8 [7.5] although it is similar to the Platform Frame technology. However the q-factor range, correspondent to the highest ductility class spans from 3 to 5 [7.5].

A preliminary estimation of the most suitable q-factor was made referring to the "Wall C" specimen and applying the new developed analytical-experimental procedure for an expeditious q-factor estimation explained in the previous Chapter 4. Such procedure provides for this specific wall specimen a q-factor range from 4.2 up to 5.8 with an average value of about 5. The lower value is obtained using the EP-EES bi-linearization approach while the highest one using the EN-a approach.

However a more accurate study on the seismic response of this building system is needed to define the most appropriate q factor. According to Ceccotti et al.[7.16] a more accurate estimation of the q-factor must involve numerical simulation in order to reproduce by means of finite element model, the hysteretic behaviour of the investigated plated shearwalls.

7.5 Numerical model of the tested modular panel

The numerical procedure based on the usage of the Nonlinear Dynamic Analyses for the q-factor evaluation defined by Ceccotti et al.[7.16] is based on element experimental testing combined with numerical modeling of a complete test building using test results as input parameters. Such numerical model of a complete test building is made referring to the hysteretic response of each connectors used to assembled the plated shearwall and is calibrated by means of experimental

tests. The investigated shearwalls are characterized by four different bearing systems: bracing systems, hold-downs, base bolts and in plane vertical joints between adjacent wall modules as summarized in Fig. 7.10.

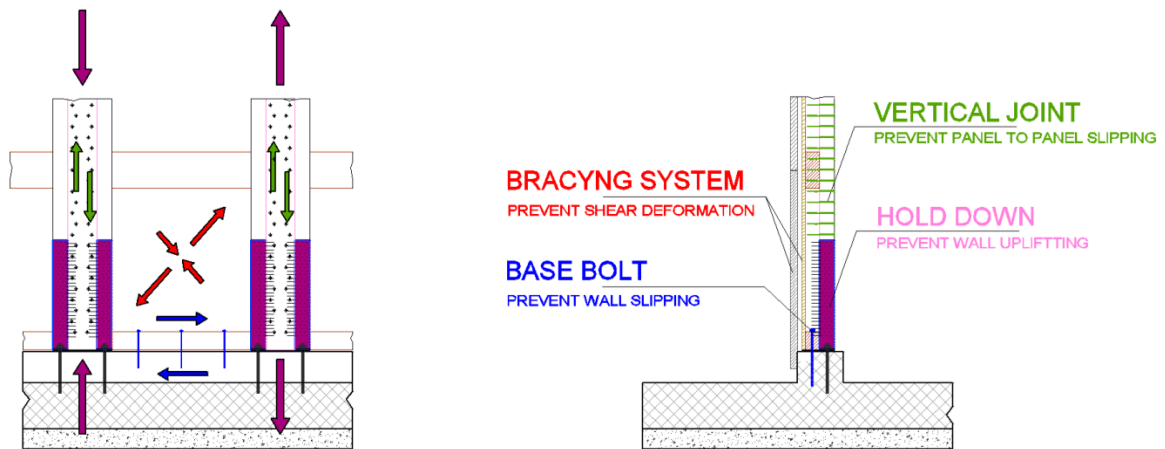


Fig. 7.10 – Connection systems used in the developed mixed wood-concrete shearwalls.

Regarding to hysteretic behaviour, these connection systems shows a “pinched” load displacement response and exhibits degradation under cyclic loading. In order to faithfully reproduce the actual hysteretic behaviour of these connectors the research-oriented numerical code “Open System for Earthquake Engineering Simulation” [7.17] was used. The hysteresis model developed by K. Elwood [7.18] was used to reproduce the ‘pinched’ load-deformation response and degradation under cyclic loading. Its skeleton curve is completely defined by 11 parameters identified in the following Fig. 7.11 and which values assigned for the performed analyses are reported in Fig. 7.12.

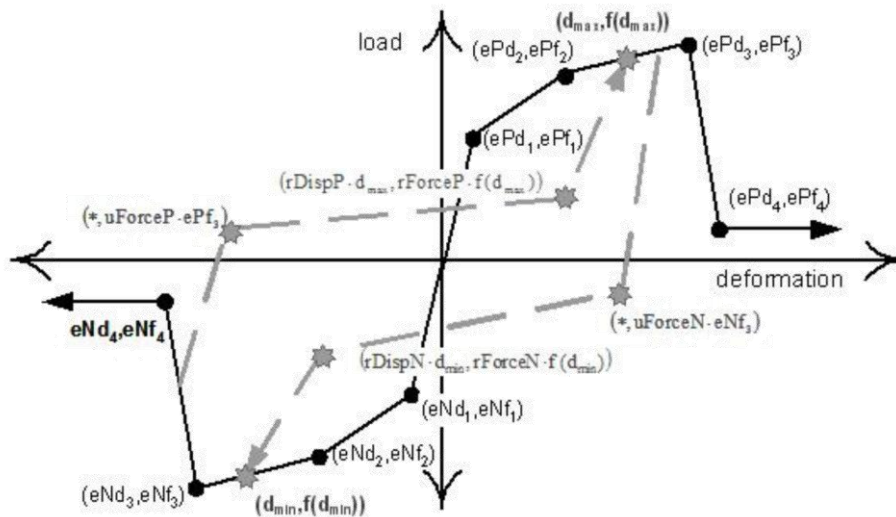


Fig. 7.11 – Elwood hysteretic model and characteristic parameters [7.17]

A comprehensive description of the analytical formulation and of the damage models of the adopted nonlinear element is reported in the previous paragraph 1.2.2.7 and in [7.17].

7.5.1 Modeling of the single fasteners

The calibration of the nonlinear element able to reproduce the connections behaviour has been made with reference to the load-displacement curves of single connectors obtained from the experimental tests. Fig. 7.12 shows as example, the comparison between experimental cyclic tests on base bolts, holdowns, bracing systems and vertical panel to panel connection elements related to “Wall B” and the respective numerical simulations. The model parameters are also reported for each nonlinear spring.

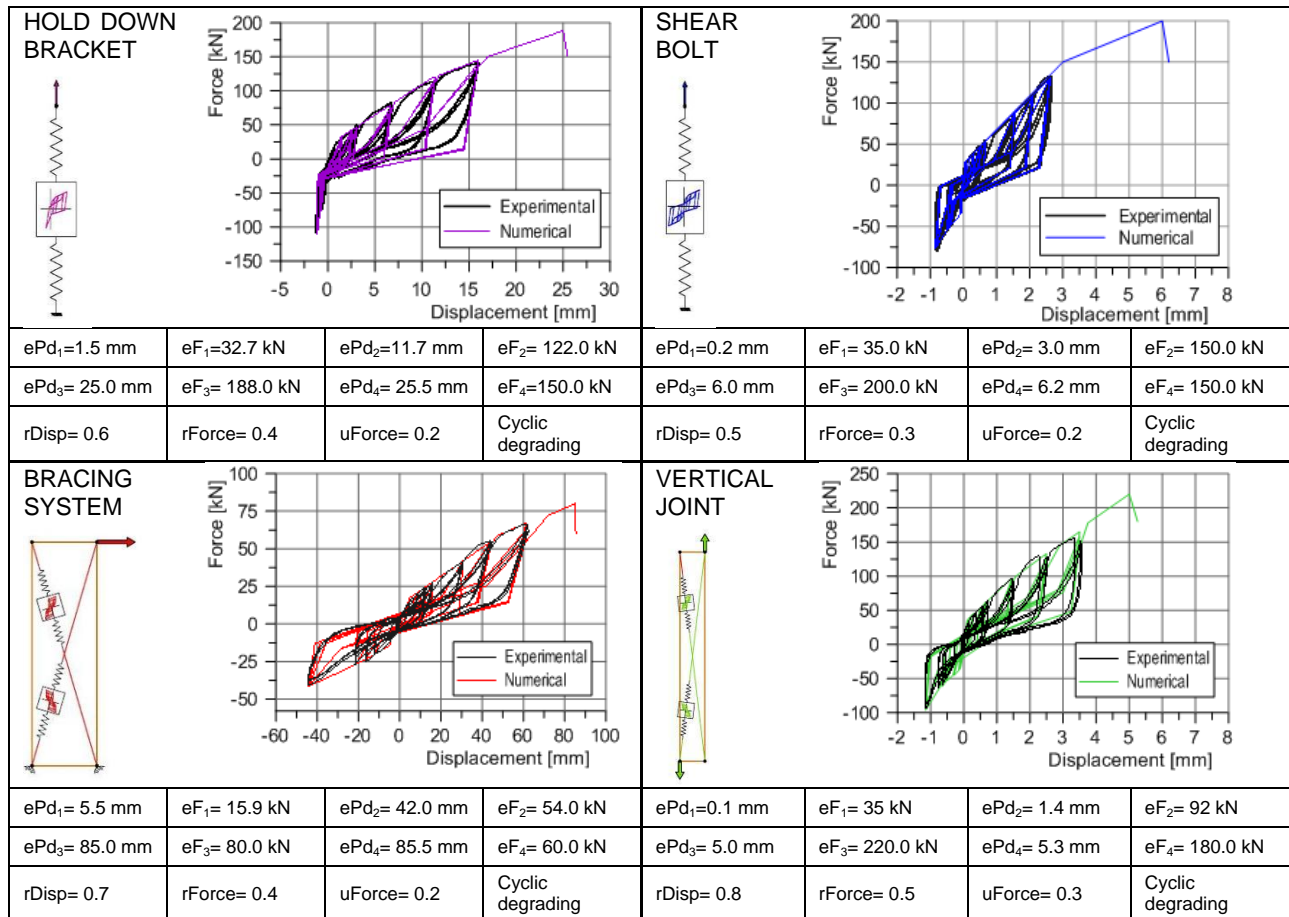


Fig. 7.12 - Comparison between experimental results and numerical load-displacement curve. The parameters of the numerical models are listed on the bottom of the plots and they are relative to the tensile branch of the cyclic curve.

The proposed nonlinear numerical model shows the typical pinched behaviour in the load-displacement curves, the reduction in stiffness for the reloading cycles and the strength degradation phenomena as stated in the initial hypotheses. The numerical results fit well the experimental ones also in terms of energy dissipation, with maximum differences of 12% for holddown, 8% for base bolt, 7% for bracing system and 6% for panel to panel joint (values refer to the maximum amplitude cycle reached on the tensile branch).

7.5.2 Numerical model of whole shearwalls

In order to assess the wall panel-basic joints interaction and the effect of the vertical load, the complete cyclic tests on “Wall B” and “Wall C” have been simulated. The numerical model is based

on the hypothesis that the nonlinear behaviour of the wall is concentrated in the connectors, whereas the wood frame remains in its elastic field. The used Finite Element models consist of a perimeter frame made by stiff elastic truss element braced and connected to the base by the nonlinear springs defined above. The cyclic test has been simulated by imposing an horizontal displacement to the node located on the upper part of the wall. The vertical load was reproduced applying a nodal force on the top of the wall. A sketch of the numerical model used in the analysis is reported in the following Fig. 7.13.

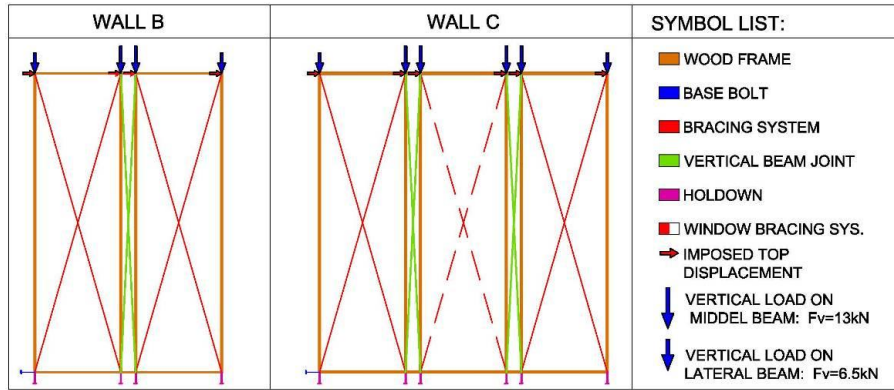


Fig. 7.13 - FEM model “Wall B” (left) and “Wall C” (right)

The load-displacement curve, reported in Fig. 7.14 shows the good correspondence between the results of the experimental test and the numerical simulation at each cycle.

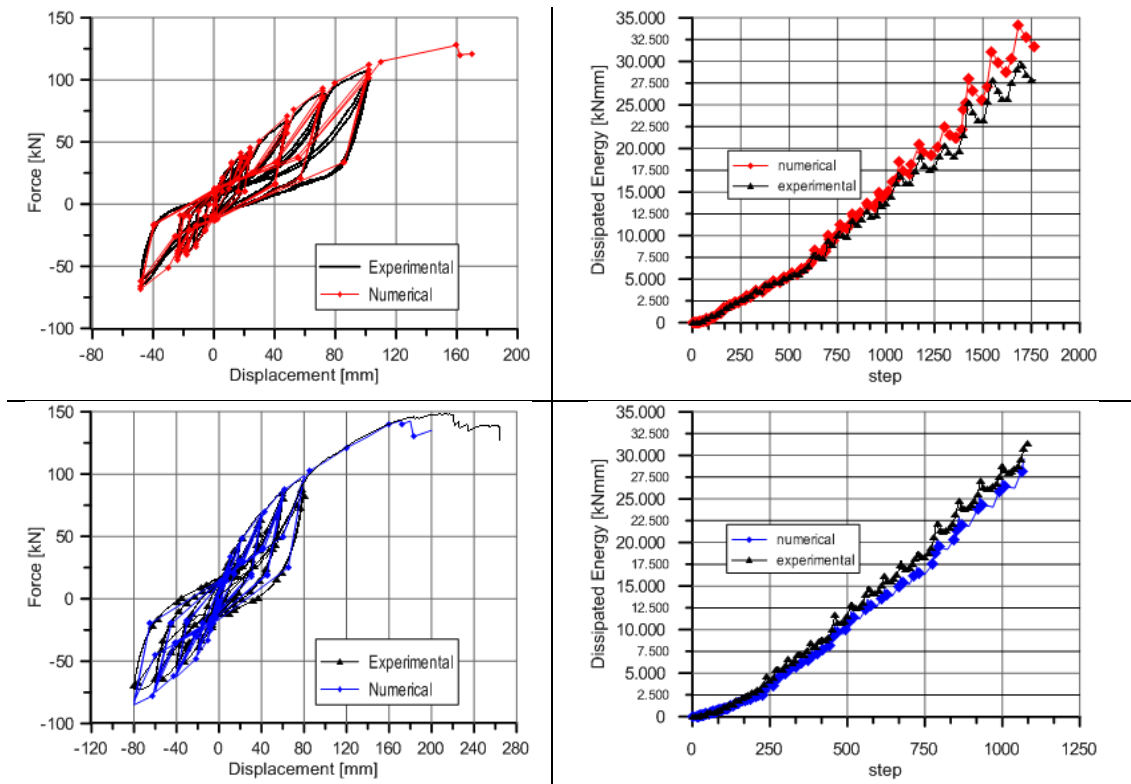


Fig. 7.14 - Comparison between the experimental results and the FEM simulation in terms of load slip curve and dissipated energy “Wall B” (top) and “Wall C” (bottom)

The good quality of the model is further confirmed by the assessment of the dissipated energy: Fig. 7.14 shows the difference in terms of dissipated energy per cycle between the experimental test

and the numerical simulation. The correspondence is very good at every cycle, the maximum difference is 11.5% for “Wall B” and 8.5% for “Wall C” (values refer to the maximum amplitude cycle reached on the tensile branch).

7.6 Assessment of the q-ductility factor

FMD method [7.19] is a really engineering approach for the seismic design of building because it refers to the inertial forces induced in the structures by earthquake. The application of these methods requires the evaluation of the most suitable q-factor which resumes the post-elastic behaviour and the ductility of the building. The definition of this q-factor is not immediate for wooden structure because it depends strongly on the criteria used to identify the yielding condition. A detailed treatment about this issue is reported in the previous Chapter 3. This condition gives the inelastic seismic design load and, according to the code provisions, EC8 [7.5], it can be obtained with a properly linearization of the building response, represented through its pushover curve.

As explain in the previous paragraph 7.4.1, the yielding limit is not univocally defined especially for an entire building. Due to this drawback and according to [7.20] and [7.21], in this work it was considered appropriate using the PGA-based approach. This method disregards the actual yielding limit of the structures defining the q-factor as the ratio between the acceleration that leads the structure to the “near collapse condition” (i.e. PGA_{u_eff}) and that used for the elastic design of the building (i.e. PGA_{u_code}). As reported in [7.16] the PGA-based method consists of the following steps:

- I. Choice of a case study building and design according to the relevant static [7.4] and seismic code [7.5] assuming $q=1$ so as to elastically resist to PGA_{u_code} value.
- II. Modeling of the test buildings using the proposed Finite Element models capable of reproducing the hysteretic behaviour of the connection elements and calibrated on the basis of experimental tests;
- III. Definition of an ultimate or near-collapse condition of the building, which coincides with the ultimate displacement of fastening elements.
- IV. Assessment of the seismic intensity (PGA_{u_eff}) that leads to the ultimate condition through a series of nonlinear analyses in the time domain with gradual increasing of the PGA intensity;
- V. Determination of the most suitable q behaviour factor according to the PGA-based approach.

As reported in the previous Chapter 3 such definition of the q-factor takes into account for the overstrength effect Ω_d [7.23]. The following paragraph describes the steps of the PGA-based approach pointing out the basic hypothesis and the encountered limitations.

7.6.1 Case study building

In order to define the actual seismic performance of the plated shearwall system and to make a direct comparison with crosslam one, the same three storeys CLT building tested on shaking table during SOFIE project was considered [7.22]. The B configuration with symmetric opening at the ground floor was investigated. The geometrical layout of this three storey building was compatible with the precast modular wood concrete panel dimension as depicted in Fig. 7.15.

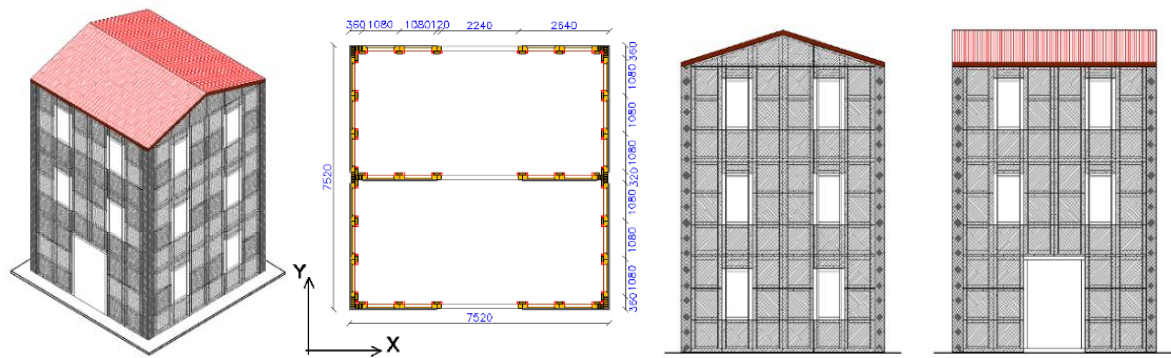


Fig. 7.15 - Case study: modular wall panel arrangement

Thanks to the in plant symmetrical distribution of the shearwalls it was possible to study the investigated building with two decoupled 2D plane model for x and y direction. In this work the analyses focus on the walls placed along the X direction which present two metre large opening at the ground floor. Fig. 7.16 reports the studied walls geometry, fasteners and bracing system arrangement.

Two different mass configurations were investigated in order to verify the influence of the principal period of vibration on the seismic response of the building. The difference between the two case studies in terms of total mass is about 25%. Table 7.5 reports the storey mass distribution and principal elastic period T_1 of each studied building.

Table 7.5 - Different mass distribution considered

Building	1 st storey	2 nd storey	3 rd storey	Total	T_1
N.1	16.5 t	16.5 t	12.7 t	45.7 t	0.48 sec
N.2	10.7 t	10.7 t	8.4 t	29.8 t	0.32 sec

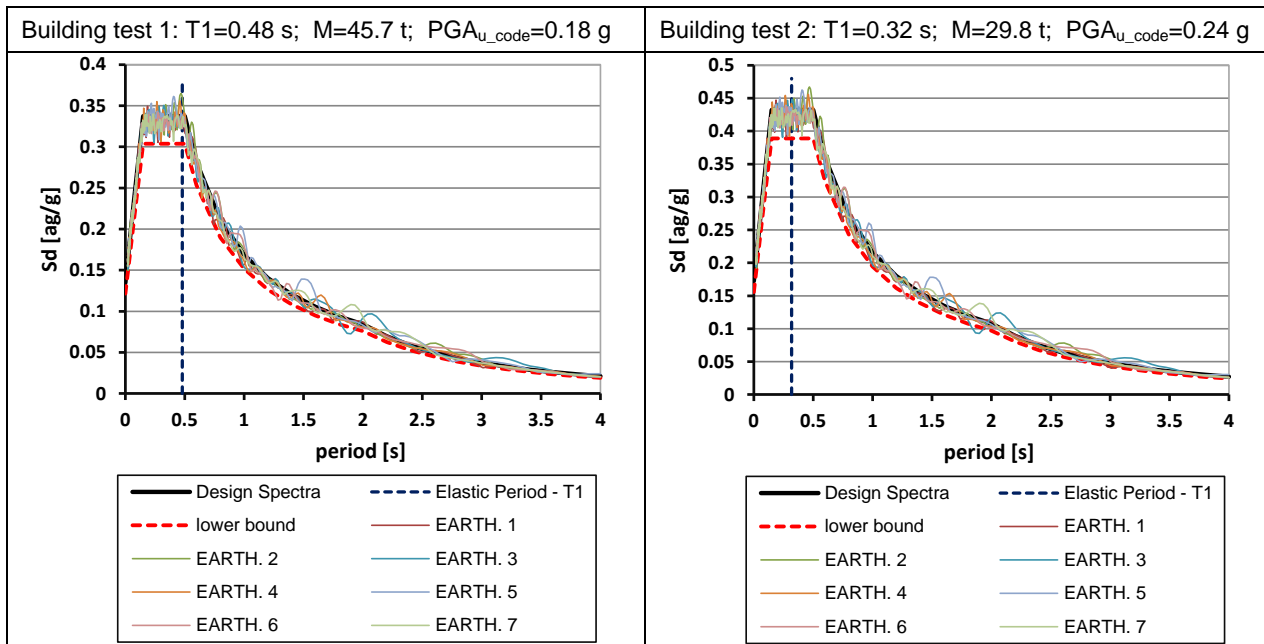
7.6.2 Seismic design of the case study building

It was assumed that the case study building was made by assembling the same modular wall panels subjected to the cyclic tests described in the previous paragraphs. The seismic design of the case studied building is based on the lateral shear resistance of the single precast modular panel and consists of the following two steps [7.16]:

- evaluation of the base shear resistance F_h according to the analytical evaluation based on the code provisions [7.4] (see Appendix A)
- evaluation of the maximum PGA_{u_code} compatible with the base shear resistance adopting a Linear Static Analysis performed considering the following data [7.5]:
 - type 1 elastic response spectra
 - rock foundation (type A soil according to EN 1998-1 [7.5], corresponding to $S=1.0$, $T_B=0.15$ sec, $T_C=0.4$ sec, $T_D=2.0$ sec),
 - behaviour factor $q=1$,
 - lowest bound factor for the design spectrum $\beta=0.20$
 - building importance factor $\gamma_I=1$.

Table 7.6 summarizes the outcomes of seismic design in terms of maximum PGA_{u_code} values compatible with the base shear resistance of the modular precast panels.

Table 7.6 - Seismic design parameters and response spectrum for both the examined buildings. The spectra compatibility requirement of the 7 artificially generated earthquakes is also reported.



As reported in Table 7.6 the lower value of PGA_{u_code} corresponds to the heavier configuration.

7.6.3 Numerical model of the case study building

The wall placed along the X direction with two meters large opening at the ground floor (see Fig. 7.15) was modelled based on the assumption that the nonlinear behaviour of the wall is concentrated in the connectors whereas the wood frame remains in its elastic field. The calibration of the numerical model was made referring to the outcomes from experimental tests described above. Fig. 7.16 reports a sketch of the numerical model used for analysis with the indication of type and position of nonlinear springs and of storey masses.

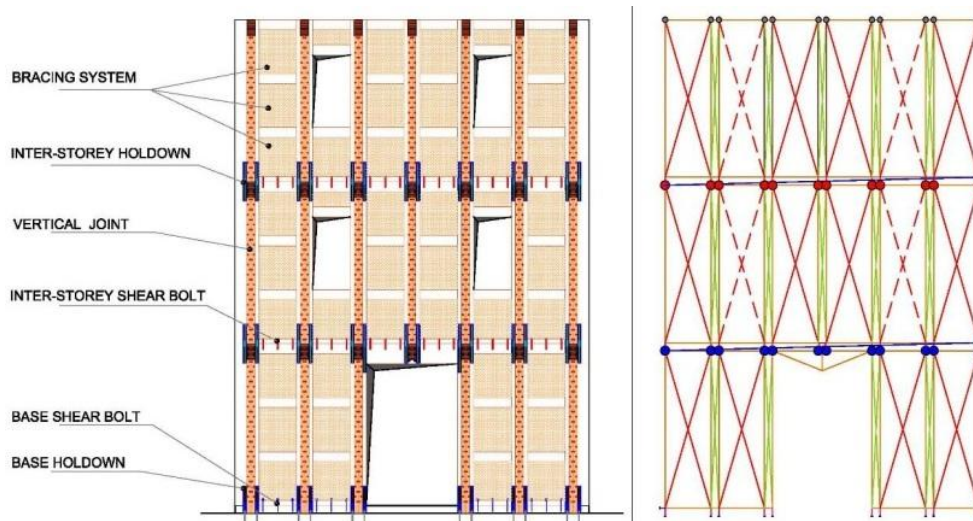


Fig. 7.16 - Investigated wall panels: fasteners and bracing system arrangement (left) and FEM model, type and position of the nonlinear elements (right)

7.6.4 Evaluation of the q-factor

Using the numerical model described above several nonlinear dynamic analyses were performed in order to evaluate the most suitable q-ductility factor for the plated shearwall system. With the aim to define the influence of the frequency content of the earthquakes on the building response the nonlinear dynamic analysis was performed considering 7 different artificially generated seismic shakes, as to meet the spectrum compatibility requirement. The spectra compatibility requirement of the seven considered earthquakes is summarized in Table 7.6.

The dynamic equilibrium equations have been integrated with a time step of 0.001 sec, by adopting an equivalent viscous damping of 2%, according to the Rayleigh model. The choice of such damping coefficient was made according to [7.16]. Both test buildings have been subjected to a growing level of seismic intensity, from the peak acceleration value equal to PGA_{u_code} to the collapse condition (PGA_{u_eff}) which was stated as the first achievement of the ultimate displacement of the bracing system or of base connectors.

The near collapse condition of the building was defined with the same criteria reported in [7.21]. In detail the effective failure condition of the connection elements were used as reference: for the holdown such condition corresponds to an uplift of 25 mm while for the shear connections (i.e. base bolt, vertical pane to panel joint and bracing system) the failure condition corresponds to an inter-storey drift equal to 3%. Table 7.7 reports the PGA_{u_eff} that leads the buildings to the near collapse condition and the related q factor values.

Table 7.7 - PGA_{u_eff} values and q-factor for the considered earthquakes and for both the examined buildings

	Building test 1		Building test 2	
	PGA_{u_eff}	q	PGA_{u_eff}	q
EARTH. 1	0.82	4.6	1.05	4.4
EARTH. 2	0.77	4.3	0.91	3.8
EARTH. 3	0.72	4.0	0.97	4.0
EARTH. 4	0.78	4.3	1.02	4.3
EARTH. 5	0.70	3.9	1.07	4.5
EARTH. 6	0.75	4.2	0.96	4.0
EARTH. 7	0.73	4.1	0.99	4.1
AVERAGE	0.75	4.2	1.00	4.1
MIN	0.70	3.9	0.91	3.8
MAX	0.82	4.6	1.07	4.5

Despite the usage of a procedure that fixes a priori the yielding limit of the structure, the obtained q values show a moderate variability as reported in Table 7.7. The q-factor spans between 3.9 and 4.6. It means that the effect of the frequency content of the shakes on the building dynamic response is not so relevant for the definition of the failure condition.

Based on the performed analyses, the q-ductility factors settle on a value up to 4 confirming the good dissipative capability of this construction system. Furthermore such q-factor estimation confirms the high dissipative capacity of this new developed plated shearwall system and results strictly in line with the previously obtained q-factor evaluation. In fact such q-factor estimation is comprised in the range defined by the Ductility Class criteria [7.5].

In detail the average value obtained using the numerical method is closely similar to that defined by the new developed expeditious procedure (see paragraph 4.5.3) which provides a lower bound

of the q-value range equal to 4.2. Such circumstance represents an additional validation of the new developed procedure for the q-factor estimation. Furthermore the obtained results highlight that the Elastic perfect Plastic by-linearization criteria provide the most reliable approximation of the capacity curve.

However the obtained results cannot be used to derive general conclusions about the correct q-factor to be used in the design of the investigated plated shearwall system since they are based on the analysis of a unique and specific three storeys case study building. In order to obtain a more accurate and reliable evaluation on the variability of the q-factor value with the building characteristics (i.e. number of storeys, arrangement of the resistant plated shearwall...) more case studies have to be numerically investigated. Furthermore three dimensional numerical models should be used to account for the effects of plan irregularities and that of the T or angle intersections between the shearwalls.

7.7 Conclusions

The new developed wood-concrete system presented in this section appears to be a viable alternative to the more traditional and common timber building system such as the conventional Platform frame system but also as the massive CLT one.

The major innovation is represented by the outer RC skin that has a dual function: it improves the thermal and acoustic performance of the system and gives strength and ductility against horizontal loads (e. g. earthquake). Furthermore the prefabrication with the consequently study of all the typological details and the structure modularization makes this innovative building system economical and profitable for the site management.

The experimental tests carried out for the characterization of the mechanical performances of this new developed building system have confirmed the reliability of the results obtained by applying the analytical formulations given by the available regulations on wood structures (i.e. Eurocode 5 [7.4]). Furthermore the performed experimental cyclic tests have highlighted that this new developed system is characterized by limited strength and stiffness degradation phenomena, good dissipative capacity and high ductility. Such properties make this new building system suitable for the use in seismic zone.

The seismic design of this high ductility wood-concrete system can be performed using the well-known FMD method [7.19] adopting a q-factor up to 4 as demonstrate by the performed analytical and numerical analyses.

Finally it is possible to affirm that thanks to its optimal robustness, massiveness, insulation properties and high seismic performance this new developed building system represents an effective alternative also to the more common CLT system especially in hot climate zone such as the Mediterranean area.

References - Chapter 7

- [7.1] Vahik E., 2006. *TF2000 Timber-frame building was tested at BRE Cardington. Barrier to the enhanced use of wood in construction. Time for Timber in Europe Conference. Gdansk, Poland, 24-25 May 2006*
- [7.2] Karacabeyli E., Ceccotti A. 1997. *Seismic force modification Factor for design of multy storey wood-frame platform construction. Meeting 30 of the Working Commission W18-Timber Structures, CIB. Vancouver, Canada, 1997, paper CIB-W18/30-15-3.*
- [7.3] Amadio C., Gatetsco N., Urban F. 2007. *Experimental study of timber shear walls made with OSB or wood fiber-reinforced gypsum panels. Proceeding of ANIDS 2007, Pisa Italy, 2007, CD.*
- [7.4] European Committee for Standardization (CEN). 2004. "Design of timber structures - Part 1-1 General: Common rules for buildings", Eurocode 5, Standard EN 1995-1-1, Brussels, Belgium.
- [7.5] European Committee for Standardization (CEN), 2004. "Design of structures for earthquake resistance - Part 1 General rules seismic actions and rules for buildings", Eurocode 8, Standard EN 1998-1, Brussels, Belgium.
- [7.6] Piron H.G.L., Lam F. 2003. *Shear walls and diaphragms, timber Engineering, by Thelandersson S., Larsen H.J., pp. 383-408*
- [7.7] Folz, B., Filiatrault, A. 2004. *Seismic analysis of wood frame structures. I: model formulation. Journal of Structural engineering, ASCE, Vol 130 pp 1353-1360*
- [7.8] Folz, B., Filiatrault, A. 2004. *Seismic analysis of wood frame structures. II: model implementation and verification. Journal of Structural engineering, ASCE, Vol 130 pp 1361-1370*
- [7.9] European Committee for Standardization (CEN). *EN 12512 – Timber structures – Test methods – Cyclic testing of joints made with mechanical fasteners. Brussels, Belgium, 2001.*
- [7.10] European Committee for Standardization (CEN). *EN 594, 1996. Timber Structures – Test methods – Racking strength and stiffness of timber frame wall panels.*
- [7.11] Munoz W., Mohammad M., Slaenikovich A., Quenville P. 2008. *Need for a harmonized approach for calculations of ductility of timber assemblies. Meeting 41 of the Working Commission W18-Timber Structures, CIB. St. Andrews, Canada, 2008, paper CIB-W18/41-15-1.*
- [7.12] Stehn L., Björnfort A. 2002. *Comparison of different ductility measurements for a nailed steel-to-timber connection. Proceeding of the 7th World Conference on Timber Engineering WCTE 2002. Shah Alam, Selangor Darul Ehsan, Malaysia, 12th-15th August 2002.*
- [7.13] Foschi RO., Bonac t. 1977. *Load slip characteristic for connections with common nails. WOOD SCI Technol 1977;9(3):118-23*
- [7.14] *EN 14358, 2007. Timber structures – Calculation of characteristic 5-percentile values and acceptance criteria for a sample. CEN, Brussels, Belgium.*
- [7.15] *Italian Ministry for the Infrastructures. New technical regulation for construction. Decree of the Ministry for the Infrastructures, Ministry of Interior, and Department of the Civil Defence. 2008.*
- [7.16] Ceccotti A., Sandhaas C. *A proposal for a standard procedure to establish the seismic behaviour factor q of timber buildings. Proceeding of the 11th World Conference on Timber Engineering WCTE 2010. Riva del Garda, Italy, June 20–24, 2010, CD.*

- [7.17] Fenves G.L., 2005, *Annual Workshop on Open System for Earthquake Engineering Simulation*, Pacific Earthquake Engineering Research Center, UC Berkeley, <http://opensees.berkeley.edu/>.
- [7.18] Elwood, K.J., and Moehle, J.P., (2006) "Idealized backbone model for existing reinforced concrete columns and comparisons with FEMA 356 criteria", *The Structural Design of Tall and Special Buildings*, vol. 15, no. 5, pp. 553-569.
- [7.19] Chopra AK. *Dynamics of structures—theory and applications to earthquake engineering*. Upper Saddle River: NJ: Prentice Hall; 1995.
- [7.20] Pozza, L., Scotta, R., Vitaliani, R. 2009. A non linear numerical model for the assessment of the seismic behaviour and ductility factor of X-lam timber structures. *Proceeding of international Symposium on Timber Structures, Istanbul, Turkey, 25-27 June 2009*, 151-162.
- [7.21] Pozza L., Scotta R., Polastri A, Ceccotti A. 2012. Seismic behaviour of wood concrete frame shear-wall system and comparison with code provisions. *Meeting 45 of the Working Commission W18-Timber Structures, CIB. Växjö, Sveden, 2012*, paper CIB-W18/45-15-2.
- [7.22] Ceccotti A. New technologies for construction of medium-rise buildings in seismic regions: the XLAM case. *IABSE Struct Eng Internat* 2008;18:156–65. *Tall Timber Buildings (special ed.)*.
- [7.23] Elnashai, S. and Mwafy, A. M., (2002), 'Overstrength and force reduction factors of multi-storey reinforced-concrete buildings' *Struct. Design Tall Build.* 11, 329–351 (2002) DOI:10.1002/tal.204

Appendix A - Geometrical and resistant characteristics of the newly developed wood-concrete building system.

A.1 Introduction

This appendix reports a comprehensive and detailed description of the geometrical properties and of the constructive details that characterize this new developed wood-concrete building system. The structural layout and the constructive concept are described both with regard to the single precast modular panel and to the entire building.

Once described the constructive technique this appendix reports the analytical evaluation of the lateral load bearing capacity and stiffness carried out referring to the available code provisions and the calculation criteria given by the science of the construction.

A.2 Geometrical characteristics and structural details

The new developed wood concrete building system combines a typical platform frame building system with an external thin reinforced concrete slab acting as a diaphragm against the horizontal forces and having also thermal and acoustic functions.

Manufacturing limitations combined with common inter storey height imposed a maximum dimension of the concrete slab side equal to 1080 mm. Hence the wood frame differs from the standard platform frame building: the spacing of the vertical stud doesn't depend on the size of the OSB sheets but on that of the external square precast concrete slabs. These dimensional limitations have inspired the development of a prefabricated modular system for buildings where the mixed wood-reinforced concrete shearwalls are made by connecting single modulus preassembled in the factory. On site the single precast modular panels are then assembled:

- connecting the adjacent panels by means of wood joints and screws;
- fixing the single panels at the inter-storey and at the foundation with mechanical connectors (mainly nailed holdowns and bolts).

The following Fig. A.1 reports a sample home built using this new modular constructive system.



Fig. A.1 Sample of a residential building made with this constructive system – Mestre (VE).

The structural layout is similar to wood frame constructive system but the walls are made of modular precast panel with aspect ratio of 3:1 (3.24m high and 1.08m long). A sketch of the typical modular panel is reported in Fig. A.2.

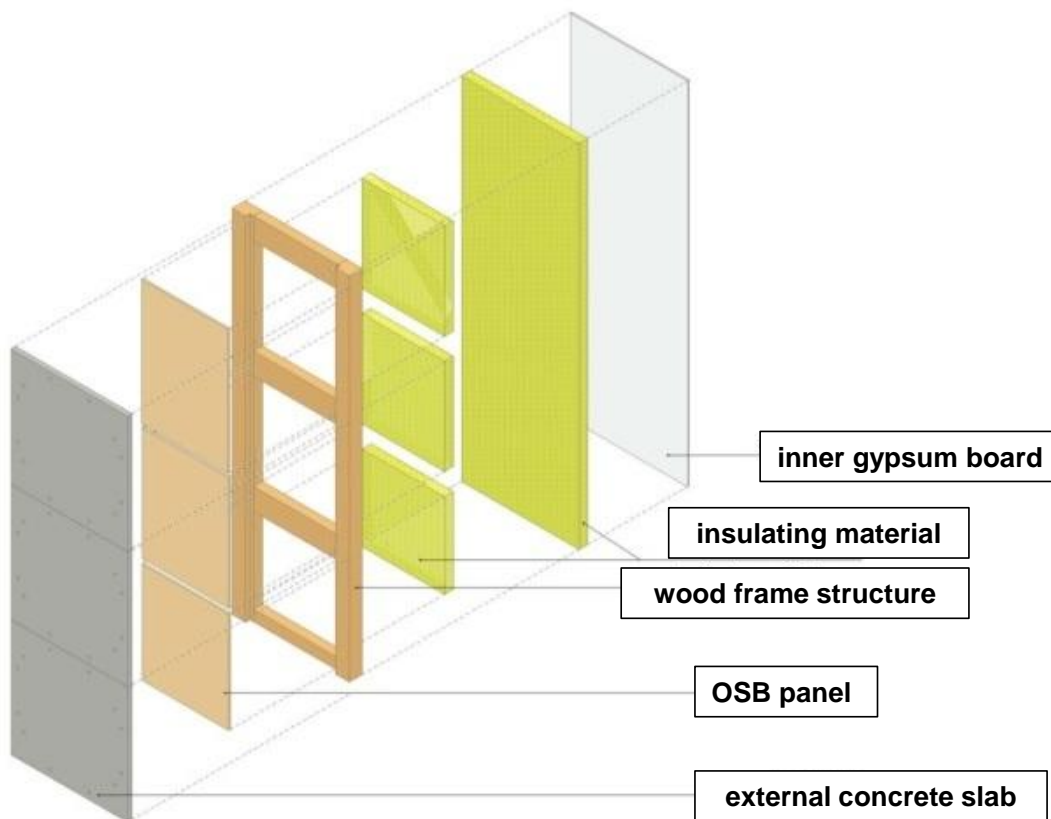


Fig. A.2 Exploded view of the modular wall panel.

The following Fig. A.3 reports the geometrical characteristics of the single precast modular panel.

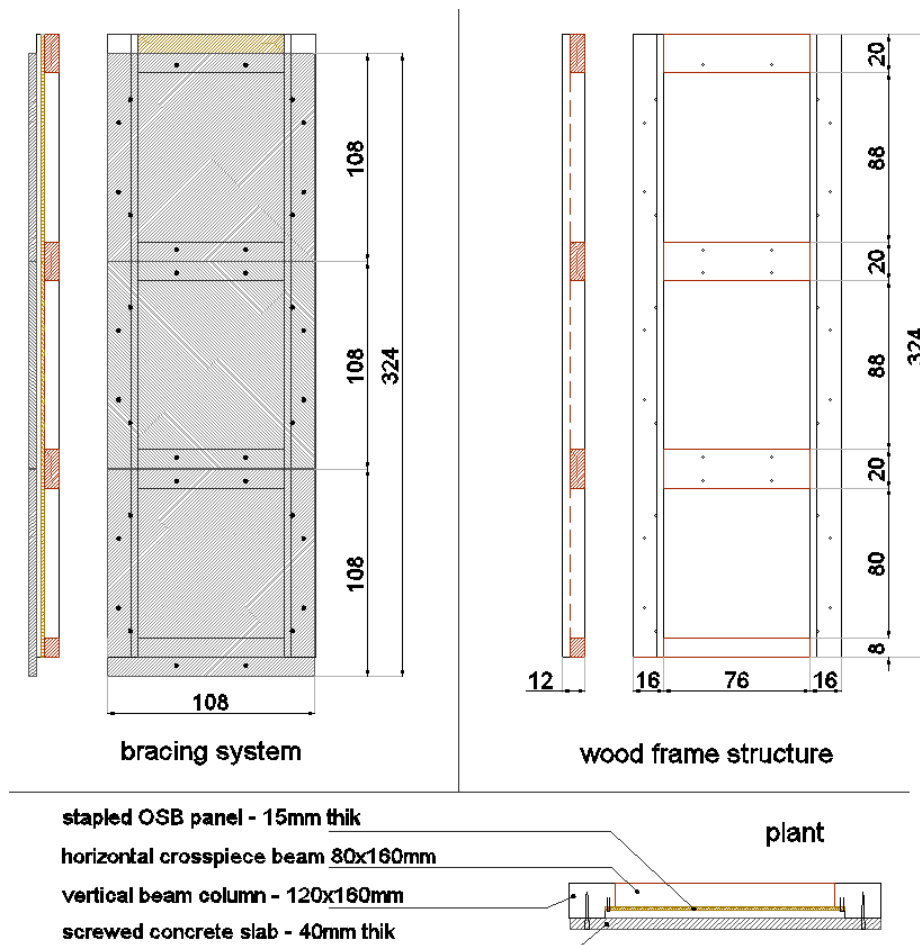


Fig. A.3 Geometrical characteristics of the precast modular panel

The particular arrangement of the OSB panel and concrete slab provides a continuous ventilation cavity from foundation to the roof. The presence of this continuous air layer between the two diaphragms, guarantees an optimal thermo-hygrometric performance and keeps dry the wood-concrete interface avoiding the wood deterioration.

A.2.1. Structural layout

The structural layout of each wood-concrete modular wall panel consists of two resistant systems with different structural functions: (1) elements engaged for vertical actions and (2) elements which react to the horizontal actions (wind and earthquake).

System used to resist vertical loads: consists of wood frame structures made of two vertical beam columns (rectangular section 160 mm x 120 mm) and four horizontal crosspiece beam (rectangular section 80 mm x 160 mm) screwed to the vertical columns. The beam columns transfer to the foundation the vertical load due to structural weight and the assembly with the horizontal beams realized the frame where the bracing system is fixed. Such assembly is made by means of screws. The adjacent modular wall panels are jointed together using a vertical joint cover beam (rectangular section 160 mm x 80 mm) screwed to the vertical beam column. This joint cover beam realized the vertical support for the floor and roof beams (place at interval of 1080 mm) and

transfers their structural weight and the dead and live loads to the foundation. More details on the wood frame structures are reported in Fig. A.3.

Bracing system reacting to horizontal actions: consists of two different types of rigid diaphragms connected to wood frame. The first bracing system is made by three square OSB panels of side 1080 mm and 15 mm thick connected with staples to the wood frame. The second bracing system consists of three square reinforced concrete slabs of side 1080 mm and 40 mm thick connected to the wood frame with screws. The reinforcement of the slabs is made of wire mesh knitted of side 60 mm. The diameter of the reinforcement is 4 mm. The characteristics of the RC slab are reported in the following Fig. A.4.

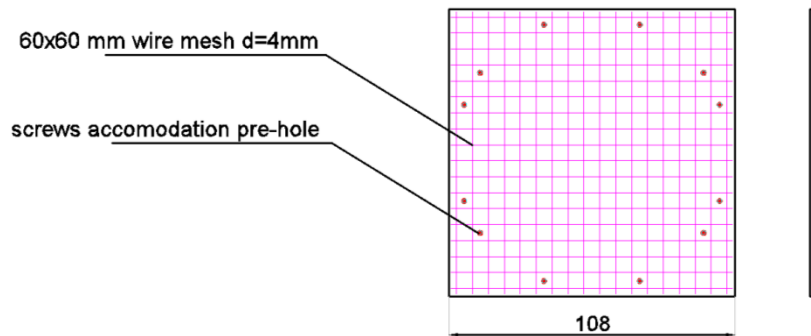


Fig. A.4 Geometrical characteristics of the RC slab

Hereafter is described the specifically developed connection system used to fix such RC slab to the wood frame.

A.2.2. Connection system between RC slab and wood frame

The concrete slab is fixed to the wood frame using large diameter screws coupled with plastic bushes. Such plastic bush follows the shape of the screw and serves these important functions:

- Reduces the clearance between the concrete slab and the screw without using sealant products. At the end of the screwing the screws contrast on the bush which tanks to its conical shape and to the presence of the notches goes in in perfect contact with the lateral surface of the hole. The clearance is reduced to the minimum as well as the initial slip of the connection.
- Acts as spacer between the horizontal cross beam of the wood frame and the concrete slab ensuring the ventilation cavity and avoiding the concrete slab deflection due to the tightening of the screw.
- Increases bearing resistance of the screws arranged along the vertical beam column where the concrete slab is adjacent to the wood frame without any space. By means of pre-holes the bushing is driven into the wood thereby increasing the surface of bearing failure of the screw. The holes arranged along the vertical beam columns for the housing of the bush also serve as template for the correct positioning of the concrete slab.

The conical shape of the screw also provides:

- A greater area of steel in the critical interface section between concrete slab and wood frame where it could form the plastic hinge of the screw.
- A natural expulsion of the water that enters between the bush and the concrete slab.

The specific characteristic of this new developed plastic bush are reported in the following Fig. A.5.

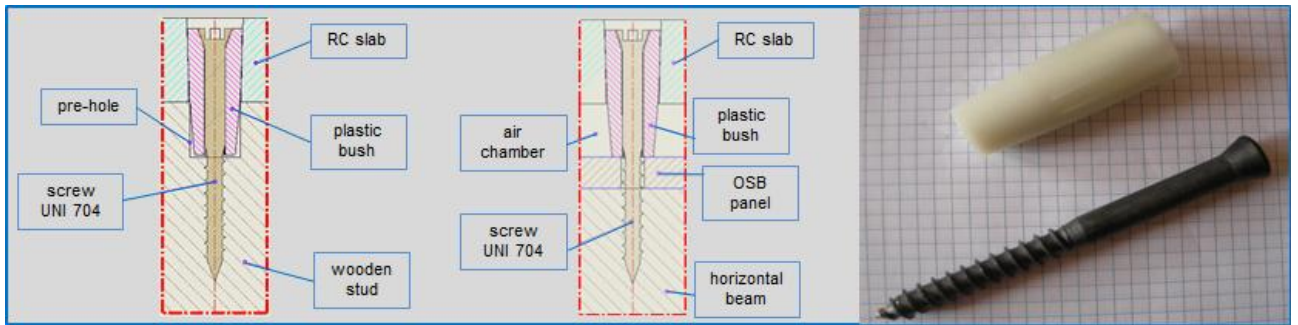


Fig. A.5 Characteristic of the plastic bush along the vertical beam column (left) and along the horizontal crossbeam (center) of the wood frame. Detail of plastic bush and screws (right).

The bracing system described above against the shear deformation of the wall panel while rigid motions, due to the rocking and the slip of the entire wall panel, are prevented by specific holdown and mechanical connectors.

A.2.3. Mechanical connections at the foundation

The modular wall panel is anchored to foundation using special home-made holdown and standard bolt which avoid respectively the rocking and the slip effects. The holdown is made by press-bent L-profile 3 mm thick nailed at the corner formed by the vertical beam columns and the joint cover beam. This holdown is connected to the concrete foundation with bolts as the standards holdown. The wall panel slip is prevented fixing the bottom horizontal crosspiece beam and the bottom concrete slab to the foundation by bolts. The shear action of OSB bracing is transferred to the foundation anchoring the bottom horizontal beam. The foundation anchor system is shown in Fig. A.6.

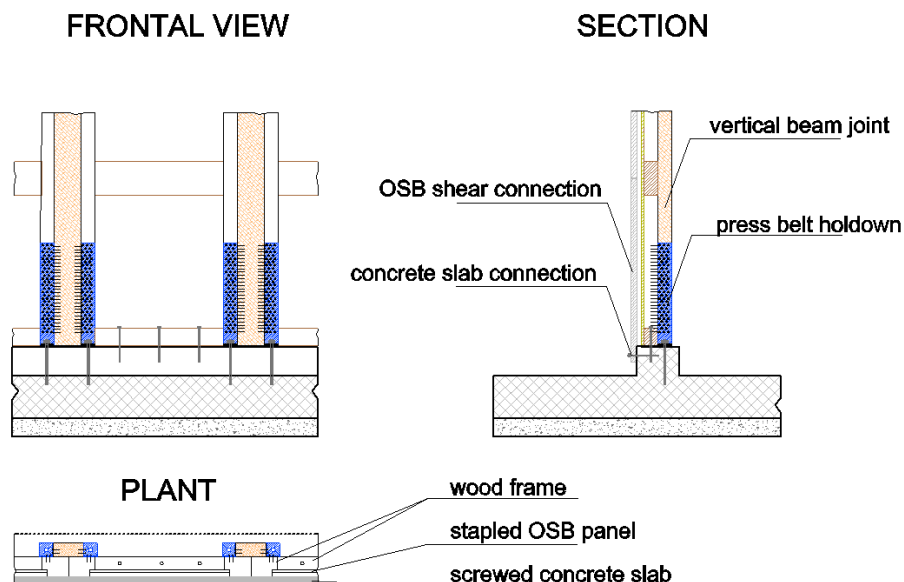


Fig. A.6 Foundation anchor system

Such foundation anchor system provides a direct and efficient transfer of the horizontal action to the foundation and divides the resistant mechanisms that counteract the rocking and the shear effects.

A.2.4. Mechanical connections at the inter-storey

At the inter-storey the wall panels are connected together by screws and mechanical connectors. The vertical beam column of upper modular panel are anchored to the bottom one using special holdown made by press-bent L-profile 3 mm thick nailed to the wood elements. These connections transfer the tensile actions, due to the rocking deformation, from the upper modular panel to the bottom one.

The OSB shear action is transferred from the upper modular panel to the bottom one by screwing the adjacent horizontal crosspiece beam. Otherwise the concrete slab of the upper modular panel is screwed to the horizontal crosspiece beam of the bottom one providing an efficient and direct transfer of the shear actions. The inter-storey connection systems are represented in Fig. A.7.

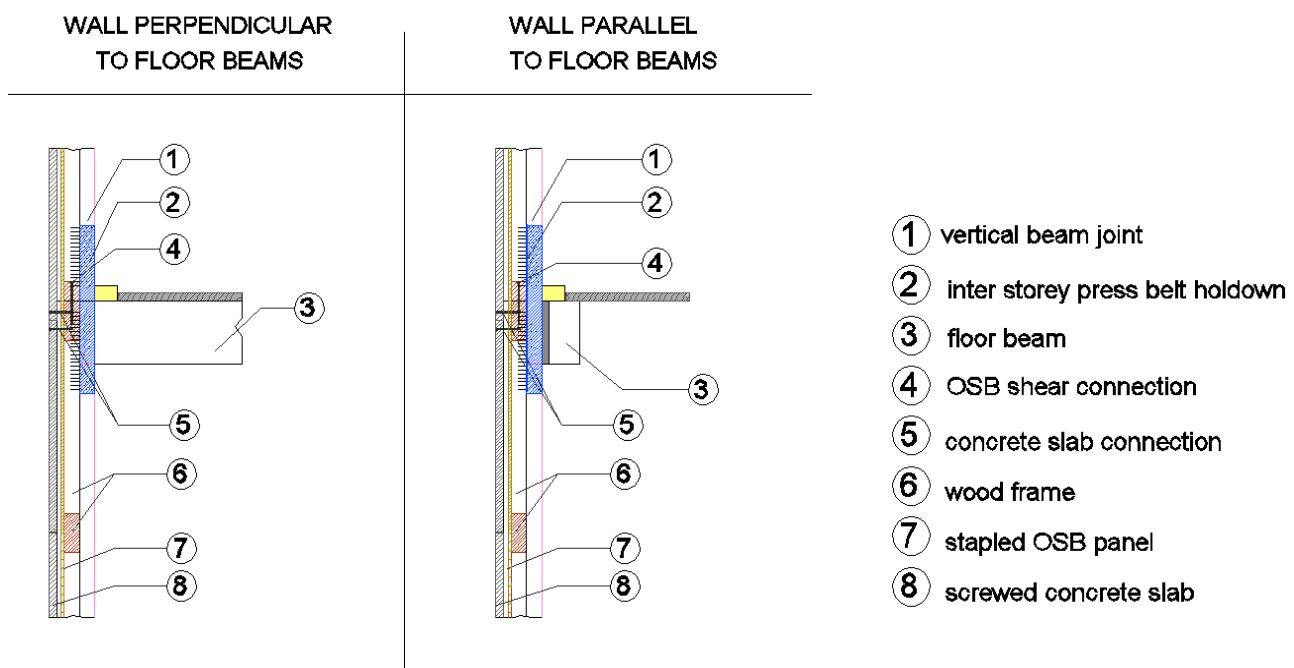


Fig. A.7 Inter-storey connection element

Such specifically developed inter-storey connection elements ensure a quick, easy and safe assembling because:

- the inter storey holdown are preventively nailed to the lower module;
- the concrete slab and the pre-assembled holdown represent a template for an accurate placement of the upper precast module;
- the installation work is carried from the inner side once the lower floor is positioned and fixed.

These specific features represent an important advantageous for the site management.

A.2.5. Joint system between adjacent modular panels

The adjacent modular wall panels are jointed together using a vertical joint cover beam fixed to the vertical beam column by means of self-drilling 8 x 140 mm screws. Such screws are 150 mm spaced. This joint cover beam is made by glued timber with a rectangular section of 160 mm x 80 mm and realized also the vertical support for the floor and roof beams. In Fig. A.8 a global view of

a composed wall is reported, where the vertical wood joints are used both as connection element and vertical column.

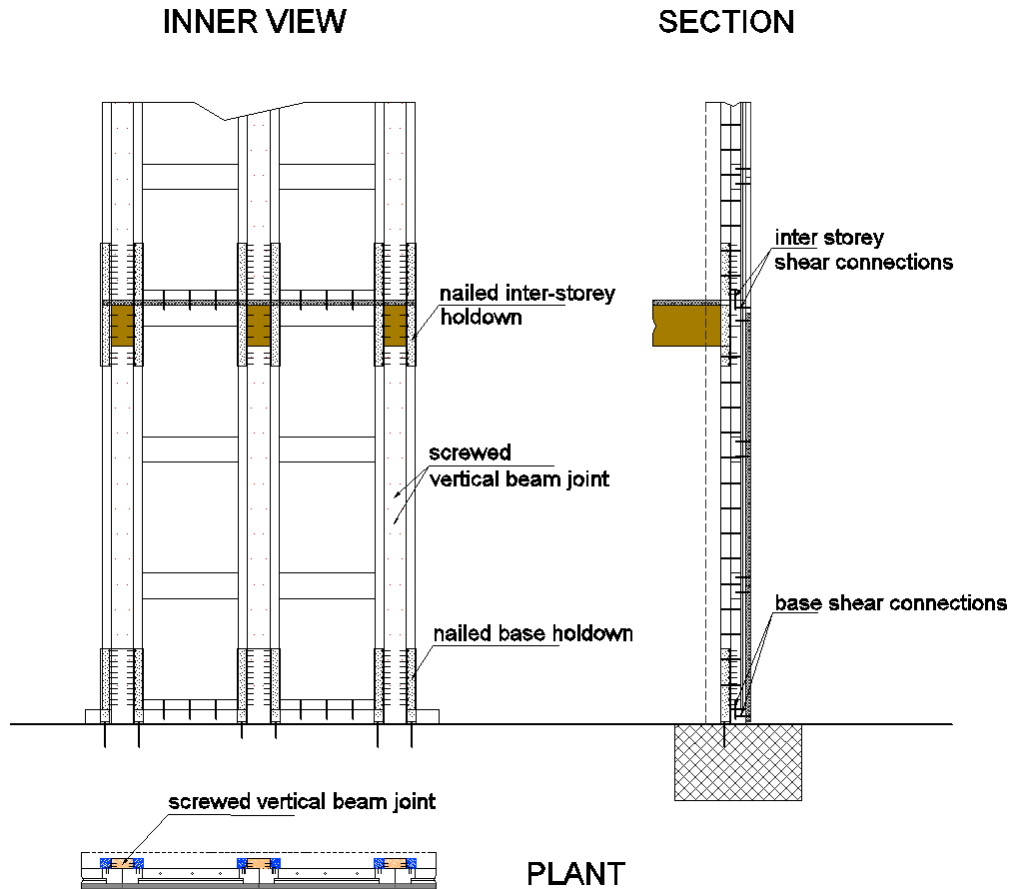


Fig. A.8 View of a two storeys composite wall with indication of the connection elements

Finally this innovative modular construction system is completely defined by a series of typological node at 90° angle and at T intersection of the wall as depicted in the following Fig. A.9.

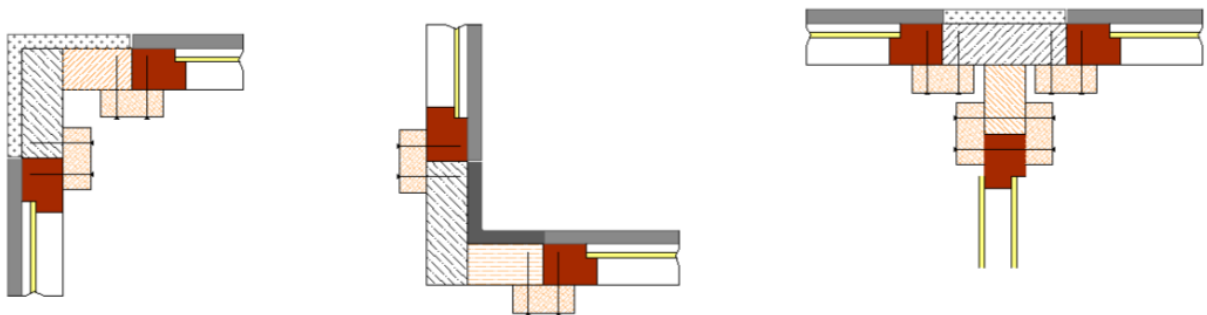


Fig. A.9 Typological node of the wood concrete building system – external angle (left), falling angle (center) and T intersection (right).

All typological constructive details and connection elements of this new developed building technology are specifically studied and optimized in order to obtain high modularization of the systems so as to simplify the design and the installation.

A.3 Lateral load bearing capacity and stiffness

The lateral load strength and stiffness of each single modular wall panel is given by three different contributions: bracing system (nailed OSB + screwed concrete slab), holdown bracket, and base shear bolt. In this section the strength and stiffness of these three contributions are defined referring to the analytical equations reported into EN 1995:2009 1-1 - Eurocode 5 [A.1]. The calculations mainly focus on the shear resistance of bracing system which is the innovative aspect of the new developed wood-concrete building system.

A.3.1 Analytical evaluation of wall panel lateral shear resistance

The lateral shear resistance of the modular wall panel is given by two different contributions. The first one consists of the OSB panel nailed to the wood frame with staples while the second one of the concrete slab screwed to the wood frame using large diameter screws. According to Eurocode 5 [A.1] it is not possible to sum up resistance contributions of different connection system without taking into account the effective stiffness and load displacement behaviour.

In this innovative building typologies the traditional bracing system made by stapled OSB panels reacts in parallel with the innovative one made by screwed concrete slabs. The two bracing system behave differently under horizontal loads but if they achieved the maximum force with the same value of displacement it is possible to sum up their resistance without committing relevant approximations. Such circumstance was verified by means of preliminary experimental tests conducted on single modular wall panels braced by single stapled OSB panel and single screwed concrete slabs. The obtained load slip curves are reported in the following Fig. A.10.

Modular panel braced by screwed RC slabs



Modular panel braced by stapled OSB panel

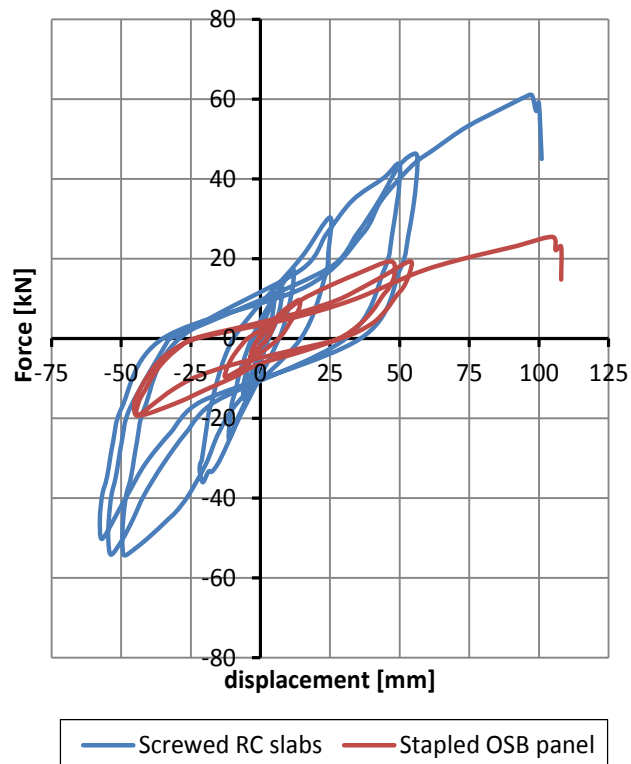


Fig. A.10 Load-slip curves of modular panel braced by stapled OSB panels or screwed concrete slabs

As reported in Fig. A.10 the load displacement curves of the two connection systems show different load carrying capacity but the peak values are achieved at the same displacement level. Due to this particular behavior of the two fasteners, in this work the lateral resistance of the bracing system will be defined summing up the peak resistance of the two connection typologies.

A.3.1.1. Stapled OSB panel shear resistance

The evaluation of the stapled OSB panel shear resistance is based on the provisions for stapled connections give in section 8.4 of EN 1995:2009 1-1 [A.1]. The main parameters used for the strength calculation are summarized in Table. A.1.

Table. A.1 Mechanical and geometrical properties of staples, wood frame and OSB panels

STAPLES PROPERTIES			
b_1	1.35	mm	1 st width of the rectangular cross-section
b_2	1.59	mm	2 st width of the rectangular cross-section
d_{eq}	1.46	mm	Equivalent diameter
b	12	mm	Width of the staple crown
L	60	mm	Length of the staple
θ	min 30°		Angle between the crown and grain direction
α	0	°	Angle between the grain and the force direction
f_u	800	MPa	Tensile strength of the wire
M_k	886.8	Nmm	Yielding moment per leg
$F_{ax,Rk}$	95.1	N	Characteristic load-carrying capacity for axial load
WOOD AND OSB PANEL PROPERTIES			
ρ_k	350	Kg/m ³	Characteristic timber density
t_{OSB}	15	mm	OSB panel thickness
$f_{h,1,k}$	59.94	MPa	OSB panel characteristic embedment strength
$f_{h,2,k}$	24.68	MPa	Timber Frame characteristic embedment strength
β	0.41	-	Member embedment strength ratio

Once defined the wood and staples properties, the characteristic load-carrying capacity of the connection could be evaluated referring to the Johansen + rope effect equations given in section 8.2.2 “Timber to Timber and Panel to Timber connections” of EN 1995 1-1:2009 [A.1]. Table. A.2 reports the strength calculation for staples in single shear.

Table. A.2 5% characteristic strength for staples in single shear according to Johansen equations

Load carrying capacity of the single staple			
$R_{k,III}$	368.2	N	Min. load carrying capacity per shear plane per single leg – failure mode f
ΔR_k	23.8	N	Additional contribution due to the rope effect per shear plane per single leg
R_k	0.78	kN	Load carrying capacity per single shear plane per staple

The characteristic shear resistance of the OSB bracing system is defined considering the characteristic load-carrying capacity of the connection elements and their spacing along the boundary of the wall panel. Table. A.3 explains such calculation.

Table. A.3 5% characteristic lateral shear resistance of OSB stapled panel bracing system

WALL PANEL SHEAR RESISTANCE – OSB CONTRIBUTION			
i	40	mm	Spacing of the staples along the edge
n	25	-	Number of staples per side
n _{eff}	1	-	Effective number of staples
R _{k,OSB}	19.5	kN	Characteristic wall panel lateral resistance – OSB contribution

A.3.1.2. Screwed concrete slab shear resistance

The concrete slab is fixed to wood frame using large diameter screws arranged along the boundary non-uniformly on all 4 sides. On the horizontal sides there are two screws, on the vertical ones four. Due to this asymmetry in the arrangement of the screws a plausible resistant mechanism for the screwed concrete bracing system was define as shown in Fig. A.11.

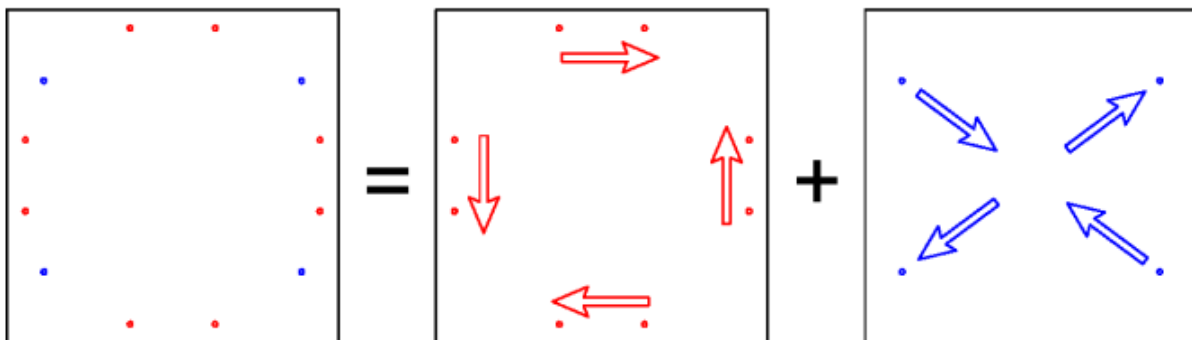


Fig. A.11 Resistant mechanism of screwed concrete bracing system

This resistant mechanism provides two different contributions of the concrete bracing system: the first one involves two screws for each side and presents a shear like behavior while the second one involves the two additional screws on the vertical sides and presents a strut and tie like behavior.

Referring to the resistant mechanisms define above the lateral resistance of the screwed concrete bracing system was calculated according to the Johansen + rope effect equations given in section 8.2.3 “Steel to Timber connections” of EN 1995 1-1:2009 [A.1] for the single screw. This calculation is summarized in Table. A.4 where the concrete slab was treated as a thick steel plate.

Table. A.4 5% characteristic lateral shear resistance of screwed concrete bracing system

SCREWS PROPERTIES			
d	8	mm	Screw diameter
L	120	mm	Screw length
f _u	800	MPa	Tensile strength of the screw

Appendix A

WOOD FRAME AND CONCRETE SLAB PROPERTIES			
ρ_k	350	Kg/m ³	Characteristic timber density
t_{slab}	40	mm	Concrete slab thickness.
$f_{h,k}$	25.83	MPa	Timber frame characteristic embedment strength
SHEAR LIKE MECHANISM CHARACTERISTIC LATERAL RESISTANCE			
α	0	°	Angle between the grain and the force direction
$R_{k_III d}$	9.08	kN	Minimum load carrying capacity per shear plane per single screw – failure mode e
ΔR_k	1.36	kN	Additional contribution due to the rope effect per shear plane per single screw
n_{ef}	2	-	Effective number of screw
n	2	-	Number of screws per side
$R_{k,slab_shear}$ like contrib.	20.88	kN	5% characteristic wall panel lateral resistance – concrete slab shear like mechanism contribution
STRUT AND TIE LIKE MECHANISM CHARACTERISTIC LATERAL RESISTANCE			
α	52	°	Angle between the grain and the force direction
$R_{k_III d}$	7.7	kN	Minimum load carrying capacity per shear plane per single screw – failure mode e
ΔR_k	1.36	kN	Additional contribution due to the rope effect per shear plane per single screw
n_{ef}	1	-	Effective number of screw
n	2	-	Number of strut and tie mechanism
$R_{k,slab_strut}$ and tie contr.	11.15	kN	5% characteristic wall panel lateral resistance – concrete slab shear like mechanism contribution
WALL PANEL SHEAR RESISTANCE – CONCRETE SLAB CONTRIBUTION			
$R_{k,slab.}$	32.3	kN	5% characteristic wall panel lateral resistance – concrete slab contribution

A.3.1.3. Single modular wall panel lateral resistance

In this section the lateral resistance of the modular wall panel is obtained summing up the peak resistance values define above as states in the following Equation A.1. Such calculation is in line with the initial hypothesis about achieving the peak resistance of the bracing system fasteners with the same displacement level.

$$R_{k_tot} = R_{OSB\ panel} + R_{concrete\ slab} = 51.8\ kN \quad (A.1)$$

To switch from the characteristic values to design one the partial safety coefficient γ_M prescript for the connection and the coefficient for the duration of the load K_{mod} , must be applied as shown in Equation A.2. According to EN 1995 – 1-1: 2009 for the connections the partial safety coefficient γ_M is equal to 1.3 and for instantaneous action (e.g. earthquakes and wind) K_{mod} is equal to 1.1.

$$R_{d_tot} = \frac{K_{mod}}{\gamma_m} (R_{OSB\ panel} + R_{concrete\ slab}) = \frac{1.1}{1.3} (R_{OSB\ panel} + R_{concrete\ slab}) = 43.8\ kN \quad (A.2)$$

The design of the modular wall panel is completed calculating the strength of holddown and base shear bolt.

The base and inter-storey connectors ensure a specific capacity design: the bracing system is the weakest structural element while holddown and base bolt are overstrength according to the criteria proposed by Fragiaco et al.[A.2]. In this work an overstrength factor equal to $\gamma_{overstrength} = 1.1$ was assumed for the design of the base fasteners in order to induce the shear deformation and the consequently energy dissipation of the bracing system.

To evaluate the force induced by the bracing system into base connection it was assumed that the holddown bracket avoids only the rocking effect of the wall while the base shear bolt avoids only the slip effect as shown in Fig. A.12. In this approach it was considered that each modular panel works alone for horizontal loads without any contribution from the adjacent panels.

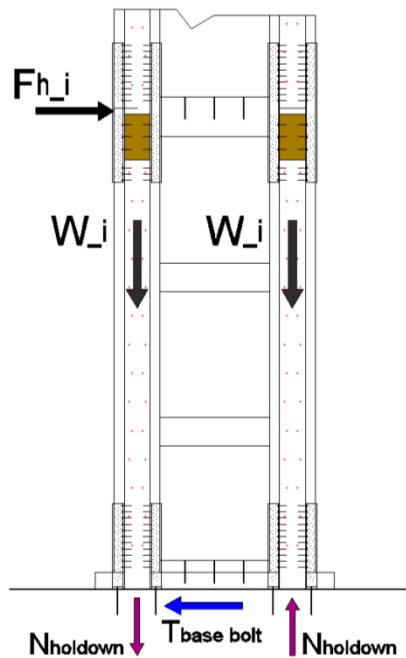


Fig. A.12 Force induced into base fasteners by bracing system

According to this simplified approach the forces acting into the holddown and in the base shear bolts are provided by the following Equation A.3 and A.4 which involve the overstrength factor $\gamma_{overstrength}$.

$$N_{holddown} = (R_k \cdot \frac{h}{b} - W \cdot \frac{b}{2}) \cdot \gamma_{overstrnght} \quad (A.3)$$

$$T_{base\ bolt} = (R_k - W \cdot f) \cdot \gamma_{overstrnght} \quad (A.4)$$

Where:

- ***h*** is the height of the wall
- ***b*** is the base of the wall
- ***f*** is the wood-concrete friction coefficient
- ***W*** is the sum of the weight of the wall panel and of the applied vertical load

The vertical dead and live loads act only on the walls perpendicular to the beams of the floor. In order to obtain the heaviest condition for the holdown, the stabilizing contribution of the vertical load was not considered.

The tensile strength used to verify the nailing and the steel blade of the holdown was obtained from the following relation A.5:

$$N_{\text{holdown}} = R_k \cdot \frac{h}{b} \cdot \gamma_{\text{overstrnght}} = 51.8 \cdot 3 \cdot 1.10 = 170.9 \text{ kN} \quad (\text{A.5})$$

The rocking effect is avoided by two press belt L holdown nailed to the wood frame with 24 4 x 60 mm anker nails per side. The fixing results very strong because in total it is made by 96 nails.

The load bearing capacity of each nail was calculate according to the Johansen + rope effect equations given in section 8.2.3 “Steel to Timber connections” of EN 1995 1-1:2009 [A.1] for the single nail in single shear as reported in the following Table. A.5:

Table. A.5 5% characteristic load bearing capacity of the holdown nailing

NAILS PROPERTIES			
d	4	mm	Nail diameter
L	60	mm	Nail length
f _u	600	MPa	Tensile strength of the nail
WOOD FRAME AND STEEL PLATE PROPERTIES			
ρ _k	350	Kg/m ³	Characteristic timber density
t _{steel}	3	mm	Steel plate thickness
f _{h,k}	27.55	MPa	Timber frame characteristic embedment strength
HOLDOWN RESISTANCE			
α	0	°	Angle between the grain and the force direction
R _k	1.53	kN	Minimum load carrying capacity per shear plane per single nail – failure mode e
ΔR _k	0.31	kN	Additional contribution due to the rope effect per shear plane per single nail
n _{ef}	1	-	Effective number of screw
n	48	-	Number of nails per holdown
N	2	-	Number of holdown per column
R _{k,tot_holdown.}	176.6	kN	5% characteristic holdown resistance-nails failure

As shown in Table. A.5 the load bearing capacity of the holdown nailing is greater than the force induce by the rocking effect amplified through the overstrength factor. The steel blade of the holdown must be overstrength respect to the nailing in order to ensure a ductile failure in the connection.

The following Table. A.6 reports the verification of the steel blade according to the ENV 1993-1-1 Eurocode 3 [A.3].

Table. A.6 5% characteristic tensile strength of holdown steel blade

STEEL PLATE PROPERTIES			
B	80	mm	Steel blade base
t	3	mm	Steel blade thickness
d	5	mm	Hole diameter
n	2	-	Number of aligned hole per blade
A _{eff}	245	mm ²	Effective area of the steel blade
MATERIAL PROPERTIES – STEEL S275-JR			
f _{y,k}	275	MPa	Characteristic yielding stress
n	2	-	Number of blade per holdown
N	2	-	Number of holdown per column
N _{Rk}	207.9	kN	Characteristic holdown resistance-steel blade failure

The overstrength factor of the steel blade results equal to 1.14 if compared to the nailing tensile strength and to 1.33 if compared to the load lateral resistance of the bracing system.

The base shear acting into the bolt connection is given by the following relation A.6 where the friction between the base wood beam and the concrete foundation has been neglected.

$$T_{\text{base bolt}} = R_k \cdot \gamma_{\text{overstrnght}} = 51.8 \cdot 1.1 = 57.0 \text{ kN} \quad (\text{A.6})$$

The base connection was made of 3 bolts with a diameter equal to 12 mm. Their resistance was evaluated according to the Johansen + rope effect equations given in section 8.2.3 “Steel to Timber connections” of EN 1995 1-1:2009 [A.1] for the single bolt in single shear as reported in Table. A.7.

Table. A.7 5% characteristic load bearing capacity of the base bolt

NAILS PROPERTIES			
d	12	mm	Bolt diameter
L	80	mm	bolt length
f _u	800	MPa	Tensile strength of the nail
WOOD FRAME AND CONCRETE FOUNDATION PROPERTIES			
ρ _k	350	Kg/m ³	Characteristic timber density
t _{concrete}	>80	mm	Concrete slab thickness
f _{h,k}	27.42	MPa	Timber frame characteristic embedment strength
BASE BOLT RESISTANCE			
α	0	°	Angle between the grain and the force direction
R _k	19.19	kN	Min. load carrying capacity per shear plane per single bolt – failure mode d
ΔR _k	3.44	kN	Additional contribution due to the rope effect per shear plane per single bolt
n	3	-	Number of bolt
n _{ef}	1	-	Effective number of bolt
R _{k,tot_base bolt}	67.9	kN	5% characteristic base bolt resistance – wood failure

The proposed design of the base connection ensures a ductile failure of the modular panel: the weakest structural element is the bracing system. The same design criteria and procedure are used to design the inter-storey tensile and shear connection systems.

A.3.2 Analytical evaluation of wall panel lateral shear stiffness

The top displacement of the single modular panel is composed from three different contributions according to the following Equations A.7.

$$\delta_{tot} = \delta_{shear} + \delta_{slip} + \delta_{rocking} \quad (A.7)$$

Where:

- δ_{tot} = total top displacement;
- δ_{shear} = top displacement due to the shear deformation of the bracing system;
- δ_{slip} = top displacement due to the base slip of the base bolt connections;
- $\delta_{rocking}$ = top displacement due to the rocking effect.

The subdivision of the total top displacement in these three contributions is depicted in the following Fig. A.13:

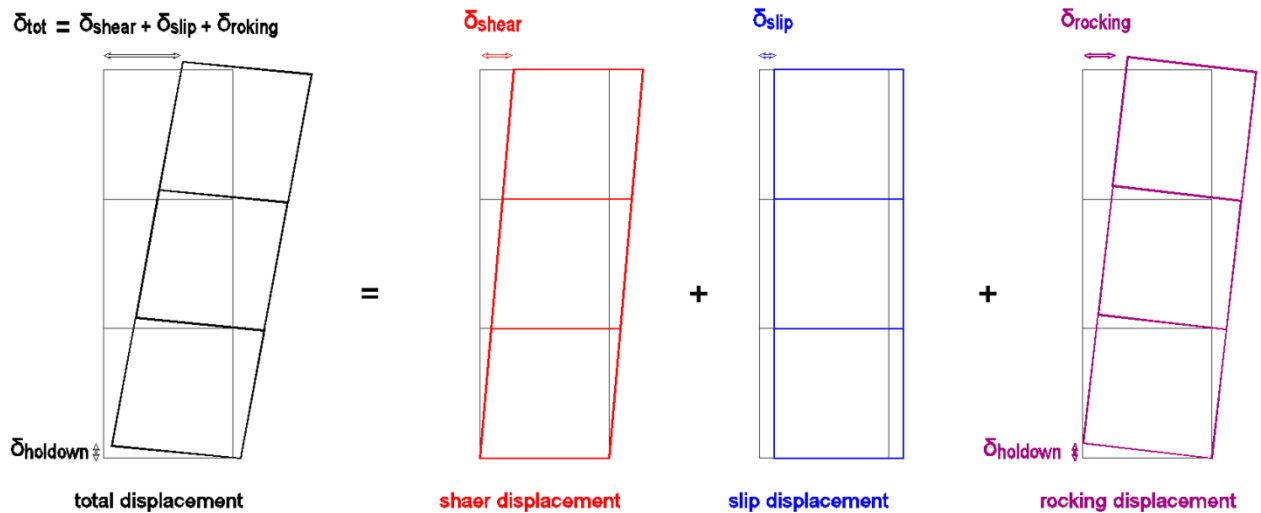


Fig. A.13 Decomposition of the top displacement in the shear, slip and rocking contributions

The value of each just defined top displacement depends on:

- the stiffness of each fasteners used in the modular panel;
- the force applied on the top of the wall;
- the vertical load acting on the wall.

Below the analytical evaluation of the stiffness of each connection element used to assemble the modular panel: bracing system, hold down and base bolt is reported. This analytical evaluation is based on the calculation of the stiffness of each connector (i.e. K_{ser}) according to Eurocode 5 [A.1] provisions.

A.3.2.1. Bracing system stiffness

Two different elements give the stiffness of the bracing system: the stapled OSB panel and the screwed concrete slab. The top shear force can be subdivided into two parts according to the following Equation A.8:

$$F_h = F_{h_OSB} + F_{h_concrete\ slab} \quad (A.8)$$

The bracing system of the modular panel is made of three square elements therefore the total shear displacement is equal to the sum of the deformation of each square bracing element.

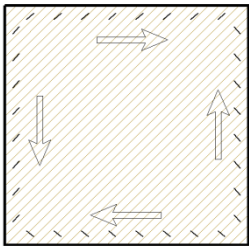
Stapled OSB panel

According to the Eurocode 5 § 7.1 “Joint slip” [A.1] the medium slip modulus per shear plane per staples is given by the following Equation A.9:

$$K_{ser_staples} = \rho_m^{1.5} d^{0.8} / 80 \quad (A.9)$$

Where ρ_m is the medium density of the connected wood elements and d the diameter of the connector. The following Table. A.8 summarizes the calculation of the stapled OSB panel stiffness.

Table. A.8 Stapled OSB panel stiffness calculation

	$d = 1.46 \text{ mm}$	staples diameter (according to EN 1995-1 §8.4-(2) [A.1])
	$\rho_m = 380 \text{ kg/m}^3$	medium density of the wood
	$K_{ser} = 125 \text{ N/mm}$	slip modulus per shear plane per staples
	$i_{staples} = 40 \text{ mm}$	Spacing of staples along the side
	$L = 1000 \text{ mm}$	length of side OSB panel
	$N_{staples} = 25$	number of staples along each side
$F_{h_OSB} = \frac{\delta_{top}}{3} \times (N_{staples} \times K_{ser_staples}) = \delta_{top} \times 1042$		Relation between the stiffness of each staples and the top force due to the OSB bracing shear resistance

Screwed concrete slab stiffness

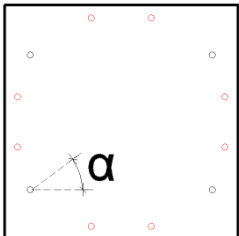
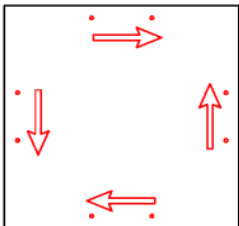
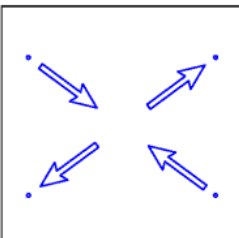
As states for the strength evaluation, the screws used to fix the concrete slab to the wood frame are arranged along the boundary non-uniformly on all 4 sides. On the horizontal sides there are two screws, on the vertical ones four. Due to this asymmetry two different contributions of the concrete bracing system were defined: the first one involves two screws for each side and presents a shear like behavior while the second one involves the two additional screws on the vertical sides and presents a strut and tie like behavior.

The stiffness of both these resistant mechanisms was evaluated referring to the Eurocode 5 § 7.1 “Joint slip” [A.1] and based on the medium slip modulus per shear plane per screws defined by the following Equation A.10:

$$K_{ser_screws} = \rho_m^{1.5} d / 23 \quad (A.10)$$

Where ρ_m is the medium density of the connected wood elements and d the diameter of the connector. Table. A.9 summarizes the calculation of the screwed concrete slab stiffness.

Table. A.9 Screwed concrete slab stiffness calculation

	$d = 8 \text{ mm}$	screws diameter
	$\rho_m = 380 \text{ kg/m}^3$	medium density of the wood
	$K_{ser} = 2577 \text{ N/mm}$	slip modulus per shear plane per screw
	$\alpha = 52^\circ$	angle of strut and tie mechanism
	$F_{h_shear \text{ concrete slab}} = \frac{\delta_{top}}{3} \cdot (N_{screws} \cdot K_{ser_screws}) = \delta_{top} \cdot 1727$	
<p>Relation between the stiffness of each screws and the top horizontal force due to the shear like behaviour of the concrete bracing system</p>		
	$F_{h_strut \& tie \text{ concrete slab}} = \frac{\delta_{top}}{3} \cdot (2 \cdot \cos \alpha \cdot K_{ser_screws}) = \delta_{top} \cdot 1057$	
<p>Relation between the stiffness of each screws and the top horizontal force due to the strut and tie like behaviour of the concrete bracing system</p>		
$F_{h_concrete \text{ slab}} = F_{h_shear \text{ concrete slab}} + F_{h_strut \& tie \text{ concrete slab}} = \delta \cdot 2784$		
<p>Relation between the stiffness of each screws and the top horizontal force due to the concrete slab bracing system</p>		

Total bracing system stiffness

As states for the lateral resistance of the modular panel it is possible to obtain the total wall stiffness summing up the stiffness contribution of the two bracing system. In fact they work in parallel in the elastic field and to obtain the total top shear force the two just defined contributions must be summed up according the following Equation A.11:

$$F_h = F_{h_OSB} + F_{h_concrete \text{ slab}} = \delta_{shear} \cdot (1042 + 2784) = \delta_{shear} \cdot 3826 \quad (A.11)$$

Once defined the relation between the top horizontal force and the top displacement, the elastic shear stiffness of the bracing system is obtained from the following Equation A.12:

$$F_h = K_{shear} \delta_{shear} \Rightarrow K_{shear} = \frac{F_h}{\delta_{shear}} = 3826 \text{ N/mm} \quad (A.12)$$

It should be noted that the obtained value of the bracing system stiffness is strictly in line with the typical stiffness value of shearwall braced using double OSB layer (see as way as example the experimental results summarize in [A.6]).

A.3.2.2. Base bolt stiffness

The slipping of the modular panel depends on the stiffness of the base bolt and on the entity of the friction between the concrete foundation and the base wood beam according the following Equation A.13:

$$\delta_{sl} = \frac{F_h - Wf}{K_{sl}} \quad (A.13)$$

Where:

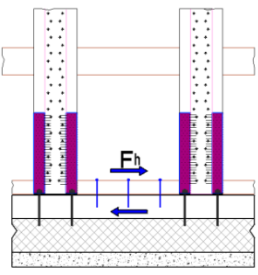
- F_h is the horizontal shear force
- W is the global load acting on the modular panel
- f is the wood-concrete friction coefficient
- K_{sl} is the base bolt stiffness

The dead and live vertical loads of the floors and roof are transferred to the foundation through specific vertical beam columns. The friction force is very small and caused only by the wall self-weight therefore it is reasonable to neglect its contribution. The slip stiffness k_{sl} corresponds to the stiffness of the base bolt and is evaluated according to the Eurocode 5 § 7.1 “Joint slip” [A.1]. The medium slip modulus per shear plane per bolts is given by the following Equation A.14:

$$K_{ser_bolts} = \rho_m^{1.5} d / 23 \quad (A.14)$$

Where ρ_m is the medium density of the connected wood elements and d the diameter of the connector. Table. A.10 summarizes the calculation of the base bolts stiffness.

Table. A.10 Base bolt stiffness calculation

	$d = 10 \text{ mm}$	bolts diameter
	$\rho_m = 380 \text{ kg/m}^3$	medium density of the wood
	$K_{ser} = 6442 \text{ N/mm}$	slip modulus per shear plane per staples
	$N_{bolts} = 3$	number of base bolts
$\delta_{bolts} = \frac{F_h}{N_{bolts} \cdot K_{ser_bolts}} = \frac{F_h}{19325}$		Relation between the stiffness of each staples and the top displacement due to the OSB bracing shear deformation

Once defined the top displacement due to the wall slipping the elastic shear stiffness of the base slip is obtained from the following Equation A.15:

$$F_h = K_{slip} \delta_{slip} \Rightarrow K_{slip} = \frac{F_h}{\delta_{slip}} = \frac{F_h}{F_h / 19325} = 19325 \text{ N/mm} \quad (A.15)$$

The use of large diameter bolts gives a high stiffness to the base connection consequently the base displacements are very small if compared to the bracing system ones.

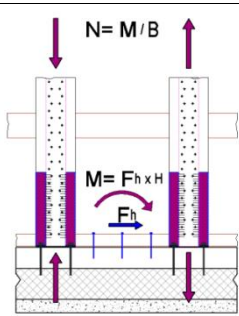
A.3.2.3. Holddown stiffness

The holddown prevents the wall uplifting and the consequent top displacement due to the rocking effect. The base uplift depends on the axial force induced in the vertical beam column by the top shear force. This axial force is reduced by the vertical load acting in the wall panel according the scheme reported in Fig. A.12 and the Equation A.3. The vertical dead and live loads act only on the walls perpendicular to the beams of the floor. In order to get the minimum values of the holddown stiffness the stabilizing contribution of the vertical load was not considered. The holddown stiffness is defined starting from the slip modulus of the nails according to the Eurocode 5 § 7.1 “Joint slip” [A.1]. The slip modulus per shear plane per nail is given by the following Equation A.16:

$$K_{ser_nails} = \rho_m^{1.5} d^{0.8} / 30 \tag{A.16}$$

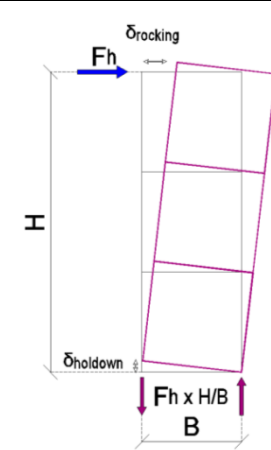
Where ρ_m is the medium density of the connected wood elements and d the diameter of the connector. Such Equation A.16 gives the medium slip modulus for a wood-wood connection but the holddown is a wood-steel connection for which the k_{ser} modulus is twice the wood-wood connection. Table. A.11 summarizes the calculation of the holddown stiffness.

Table. A.11 Holddown stiffness calculation

	$d = 4\text{mm}$	nails diameter
	$\rho_m = 380 \text{ kg/mm}^3$	medium density of the wood
	$K_{ser_nails} = 1497.0 \text{ N/mm}$	slip modulus per shear plane per nails
	$N_{nails} = 48$	number of nails on the base holddown
$\delta_{holddowns} = \frac{F_h \cdot H/B}{N_{nails} \cdot K_{ser_nails}} = \frac{F_h}{23952}$		Relation between the stiffness of each staples and the top displacement due to the OSB bracing shear deformation

Once defined the base uplift of the wall the top displacement can be obtained with simple relations of similarity of triangles as reports in the following Table. A.12.

Table. A.12 Relation between the base uplift and the top rocking displacement

	$\frac{\delta_{holddowns}}{B} = \frac{\delta_{rocking}}{H}$ $\frac{H}{B} = \text{aspect ratio} = 3$ $\delta_{rocking} = \frac{H}{B} \delta_{holddowns} = 3 \delta_{holddowns} = \frac{F_h}{7984}$
	Relation between the base uplift and the top horizontal displacement due to the specific aspect ratio of the modular wall panel

Once defined the top displacement due to the rocking effect it is possible to define the correspondent elastic stiffness using the following Equation A.17:

$$F_h = K_{\text{rocking}} \delta_{\text{rocking}} \Rightarrow K_{\text{rocking}} = \frac{F_h}{\delta_{\text{rocking}}} = \frac{F_h}{F_h/7984} = 7984 \text{ N/mm} \quad (\text{A.17})$$

The rocking stiffness due to the holdown base connection is greater than twice the bracing system one. This confirms that the deformability of the wall is mainly due to the bracing system.

A.3.2.4. Single modular wall panel lateral stiffness

In the previous section the stiffness of each fastener used to assemble the structural elements of the wall panel was defined. The top total displacement δ_{tot} and the top horizontal force F_h are linked using the following Equation A.18:

$$F_h = K_{\text{wall}} \cdot \delta_{\text{tot}} = K_{\text{wall}} \cdot (\delta_{\text{shear}} + \delta_{\text{slip}} + \delta_{\text{rocking}}) \quad (\text{A.18})$$

By expressing the displacements as a function of applied force F_h and relative stiffness the Equation A.18 becomes:

$$F_h = K_{\text{wall}} \cdot \delta_{\text{tot}} = K_{\text{wall}} \cdot \left(\frac{F_h}{k_{\text{shear}}} + \frac{F_h}{k_{\text{slip}}} + \frac{F_h}{k_{\text{rocking}}} \right) \Rightarrow \frac{1}{K_{\text{wall}}} = \left(\frac{1}{k_{\text{shear}}} + \frac{1}{k_{\text{slip}}} + \frac{1}{k_{\text{rocking}}} \right) \quad (\text{A.19})$$

Such formulation coincides with that proposed by Gavric et al.[A.4] and gives values of the wall stiffness defined by the following Equation A.20.

$$\frac{1}{K_{\text{wall}}} = \left(\frac{1}{k_{\text{shear}}} + \frac{1}{k_{\text{slip}}} + \frac{1}{k_{\text{rocking}}} \right) = \left(\frac{1}{3826} + \frac{1}{19325} + \frac{1}{7984} \right) = \frac{1}{2281} \Rightarrow K_{\text{wall}} = 2281 \text{ N/mm} \quad (\text{A.20})$$

Such stiffness value if referred to the wall length, results closely similar to that of the CLT wall. For a direct comparison see the stiffness values obtained from the experimental tests on massive CLT walls reported in [A.6].

A.3.3 Strength and stiffness of composed and windowed walls

The strength and stiffness evaluations reported in previous paragraphs are specific for a single modular wall panel without openings. This section gives the basic criteria for the estimation of the strength and stiffness of composed walls that can also include windows.

A.3.2.4. Composed wall lateral shear and stiffness

In the previous section it was investigate the global strength and stiffness of the single modular panel. When these single modular panels are assembled together to form an entire wall the global stiffness of this composite wall is affected by the interaction between the vertical joints used to connect the adjacent modular panel and the base holdowns. In order to understand the effects of vertical joints deformation two different limit conditions should be analysed. The first condition is characterized by strengthless vertical joint while the second one by very strong and stiff vertical

joints so as to consider the wall as a rigid element. The deformed shapes related to these two configurations are reported in the following Fig. A.14 where base holdowns constraints are not considered.

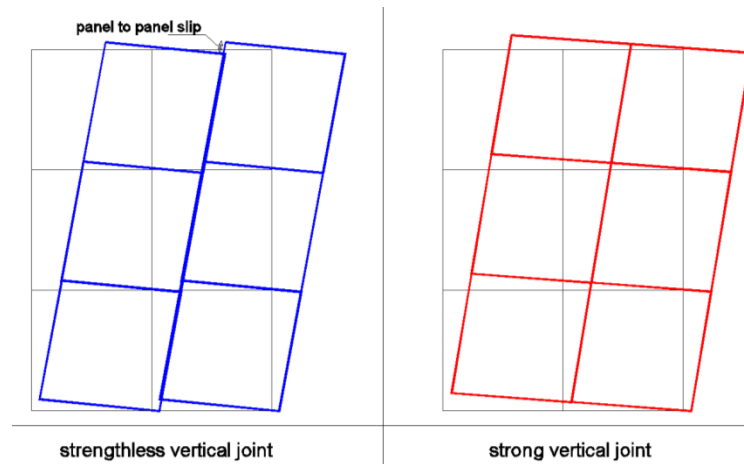


Fig. A.14 Deformed shape of assembled wall with different stiffness of vertical joint –base holdowns constraints are not considered

As shown in Fig. A.14 with a very stiff vertical joints the entire wall behaves as a rigid body without any slipping between the adjacent modular panels. Otherwise with strengthless vertical joint the single modular panel reacts independently from the adjacent one.

It should be noted that the constrictions given by the base holddown placed on the sides of each modular panel and nailed to the vertical wood joint (see Fig. A.8) avoid the uplift of the middle studs. Consequently the actual behaviour of the composite wall is intermediate respect to the two limit conditions described above.

The analytical evaluation of the effective behaviour results difficult because it depends also from the constraints degree given by upper perimetral floor beams. Such effect can be evaluated referring to full scale experimental tests performed on composite wall specimens. As reported in the paragraph 7.3.4 the relative displacement between adjacent modular panel results about equal to the holddown uplift as also confirmed by the deformed shape at the end of the tests. It means that each modular panel used to former a composed wall reacts independently from the adjacent one. Such condition confirms that the strength and stiffness characteristic of a composed wall could be defined by summing the contribution given by each modular panels.

A.3.2.5. Windowed wall lateral shear and stiffness

In this new developed building system windows and doors can be realized into two different manners depending upon the opening width. The 1st methodology concerns opening larger than the single modular panel. In this case an upper beam is required to former the opening. Otherwise the 2nd methodology concerns opening large as the interspace between the vertical studs of the modular panel. In this last case the opening is directly incorporate in the modular panel.

Such different methodologies for the realization of the opening are depicted in the following Fig. A.15.

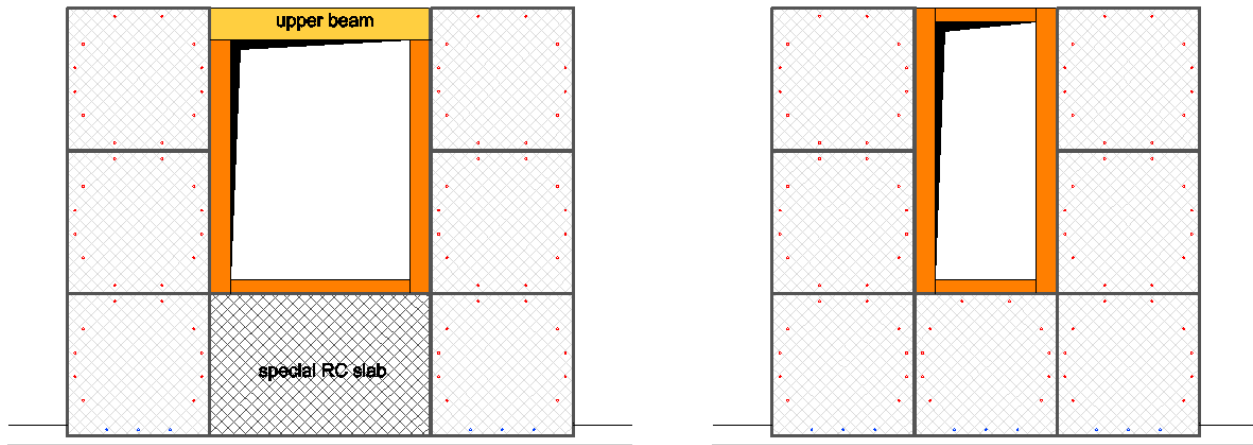


Fig. A.15 Construction methodology for wide (left) and small (right) opening.

The evaluation of the effects of the opening in the global response of the wall is a crucial issue for the shearwall systems. An extensive treatment about this aspect is reported in karacabeyli et al. [A.7]. In such study a number of wall specimens with different opening levels were tested in order to define the influence of doors and windows on the strength and the stiffness of the entire shearwall. The experimental tests show that the resistance and stiffness contribution given by the portion of the wall with opening is negligible. Such results provide the basis for the so called “method A” specifically implemented into the paragraph 9.2.4 of the Eurocode 5 [A.1] for the design of the shearwall.

According to these studies and code provisions the resistant contribution given by the portion of wall with incorporated openings should not be considered. This specific design criterion is also confirmed by the results from the experimental tests as reported in the paragraph 7.3.4 where walls composed by the same number of whole modular panels but with different openings are characterized by the same initial stiffness. Finally it should be noted that despite the strength and stiffness of the portions of wall with opening are negligible, a significant contribution in the energy dissipative capacity is provided by such openings.

References - Appendix A

- [A.1] *European Committee for Standardization (CEN). 2004. "Design of timber structures - Part 1-1 General: Common rules for buildings", Eurocode 5, Standard EN 1995-1-1, Brussels, Belgium.*
- [A.2] *Fragiacomo M, Dujic B, Sustersic I. Elastic and ductile design of multy-storey crosslam wooden buildings under seismic actions. Engineering Structures 33, 2011, 3043-3053.*
- [A.3] *European committee for standardization (CEN). ENV 1993-1-1 Eurocode 3 – Design of steel structures Part 1-1: General rules and rules for building. 2005*
- [A.4] *Ni, C., Popovski, M., Karacabeyli, E., Varoglu, E., Stierner, Midply wood shear wall system: Concept, performance and code implementation (2007) Proceedings Of Meeting 40 Of CIB-W18 paper 40-15-3, Bled, Slovenia*
- [A.5] *Gavric I, Ceccotti A, Fragiaco M. Experimental tests on cross-laminated panels and typical connections. Proceeding of ANIDS 2011, Bari Italy, 2011, CD.*
- [A.6] *Ceccotti A, Lauriola M.P, Pinna M, Sandhaas C. SOFIE Project – Cyclic Tests on Cross-Laminated Wooden Panels. World Conference on Timber Engineering WCTE 2006. Portland, USA, August 6-10, 2006, CD.*
- [A.7] *Karacabeyli E., Ceccotti A., (1998), "Nailed wood-frame shear walls for seismic loads: Test results and design considerations", in Proceedings "Structural Engineering World Congress", Structural Engineering World Wide, (San Francisco, USA, July 18-23, 1998), edited by Srivastava N.K., London, England, Elsevier Science Ltd, paper T207-T206*

List of Figures

Fig. I.1 - Destruction of a residential house after Northridge earthquake 1994 [I.5] (left) and Kobe earthquake 1995 [I.6] (right).....	2
Fig. I.2 – typical fastener used in mechanical joints [I.7].....	3
Fig. I.3 – Typical woodwork joints [I.7].....	4
Fig. I.4 – Detail of the woodwork joints of a Japanese pagoda [I.8].....	4
Fig. I.5 – Schematic diagram of the path of lateral forces in a simple building [I.9].....	5
Fig. I.6 – The two anchoring cases: sliding caused by base shear and uplift caused by overturning [I.10].....	5
Fig. I.7 – Typical anchorage system of Platform Frame building (left) [I.11] and CLT building (right) [I.9].....	6
Fig. I.8 – S. Francisco soft-storey building damage – Loma Prieta earthquake 1989 [I.12].....	6
Fig. I.9 – View of the seismic-resistant building of Lefkas Island – Greek (left). Resistant mechanisms under earthquake (right). In static condition masonry bear vertical load (A) but in case of partial collapse of the wall under earthquake the gravity load are bore by the wooden pillars (B) [I.1].....	7
Fig. I.10 – Lisbon area rebuild with “Pompalino” system after 1755 (left) and typical “gaiola” wall [I.2].....	8
Fig. I.11 – Example of a “Colombage” building in France [I.15] (left) and of a “Fackwerk” building in Germany (right) [I.16].....	8
Fig. I.12 – Example of sun-Dried Brick infill himis structure [I.14].....	9
Fig. I.13 – Example of stone infill himis structure [I.14].....	9
Fig. I.14 – Example of Brick infill himis structure [I.14].....	10
Fig. I.15 – Example of the section and picture of Daigo-ij Pagoda [I.13].....	10
Fig. I.16 – Simple wood-block system [I.14].....	11
Fig. I.17 – Glulam arch roof for Stockholm central railway station - 1925. [I.19].....	12
Fig. I.18 – 8-storey brick-and-beam office buildings built in Vancouver in 1905 (left) and in Toronto in 1920 (right) [I.20].....	13
Fig. I.19 – Novello factory – Varese Italy [I.21].....	14
Fig. I.20 – S. Francesco Church – Imola, Italy (top left), Carrefour Shopping Center – Milan, Italy (top right) and Palasport – Livorno, Italy (bottom) [I.21].....	14
Fig. I.21 – Typical beam-column intersections [I.7].....	15
Fig. I.22 – Basic concept of hybrid jointed for heavy frame systems [I.22].....	15
Fig. I.23 – Structural scheme of platform frame system [I.23].....	16
Fig. I.24 – Medium rise Platform Frame building in Växjö - Sweden [I.25].....	17
Fig. I.25 – CLT panel configuration [I.20] (left) and typical connection assemblies (right) [I.23].....	18
Fig. I.26 – Murray Grove 9-storey CLT Building, London [I.20].....	18
Fig. I.27 – Multi-family buildings in Austria [I.20].....	19
Fig. I.28 – 8-storey CLT buildings Melbourne – Australia [I.26].....	19
Fig. I.29 – Social houses. 9-storey CLT buildings in Italy [I.27].....	19
Fig. I.30 – Structural concept of the 6-storey hybrid wood-concrete building [I.20].....	20
Fig. I.31 – Heavy frame timber structure with steel bracing [I.29].....	21

Fig. I.32 – Hybrid CLT-concrete system [I.20].....	21
Fig. I.33 – Table 8.1 of Eurocode 8 [I.31].....	23
Fig. 1.1 - Failure modes for steel-timber (left) and timber –timber (right) connections according to EC5 [1.3].	33
Fig. 1.2 - Example of nailed wood- panel connection [1.4].....	33
Fig. 1.3 -Typical hysteretic behaviour of a ductile timber connection, suitable for energetic dissipation [1.4].	34
Fig. 1.4 – Illustration of hysteresis models for various structures from Loh et al.[1.11]	36
Fig. 1.5 – Typical pushover (left) and hysteresis (right) curve defined by Foschi model [1.23]	38
Fig. 1.6 – Pushover curve defined by Dolan model [1.24].....	39
Fig. 1.7 – Hysteresis loop defined by the Dolan model [1.24]	39
Fig. 1.8 – Richard & Yasumura model [1.15].....	41
Fig. 1.9 – Monotonic curve (left) and hysteretic loop (right) of CUREE model [1.18].....	42
Fig. 1.10 – Slope parameters for the Ceccotti & Vignoli model [1.27].....	43
Fig. 1.11 - Piecewise linear law of screws and angle bracket springs [1.16]	45
Fig. 1.12 - Definition of Elwood K. hysteresis model [1.30]	46
Fig. 2.1 - Connection macro-element.	53
Fig. 2.2 – Sensitivity of different hysteresis model to reproduce the behaviour of wood joints [2.3].....	54
Fig. 2.3 - Characteristic parameters of the connection hysteretic cycle for typical symmetrical connectors ..	56
Fig. 2.4 - Skeleton curve of wood (left) and of steel (right) springs for symmetrical hysteretic cycle.....	56
Fig. 2.5 – Comparison between experimental and numerical load-displacement curve of angle bracket, hold-down and panel to panel connection. Parameters of numerical models are listed on the side of plots. For holddown parameters are relative to the tensile branch of the cyclic curve.....	57
Fig. 2.6 – Numerical model of tested CrossLam wall with indication of connectors, horizontal imposed displacement (left) and applied vertical load (right).	58
Fig. 2.7 - Comparison between the results of the complete experimental cyclic test and the numerical simulation.....	59
Fig. 2.8- Comparison between accumulation of dissipated energy per cycle between experimental cyclic test and the numerical simulation.	59
Fig. 2.9 - Views of the model of the entire building with indications of the connections, storey masses and displacement measurement points.	60
Fig. 2.10 - Test results versus model prediction at point 3NE under Nocera Umbra earthquake scaled up to 1.2g.....	61
Fig. 3.1 – Relationships between the force reduction factor, R , structural overstrength, Ω , and the ductility reduction factor, R_{μ} [3.10].....	68
Fig. 3.2 – Q-factor values for each ductility class and for each building typology according to EC8 [3.1].....	70
Fig. 3.3 - Scheme of the actual method for the building system q-factor evaluation.....	71
Fig. 3.4 – Shearwall load-slip curve and correspondent ductility levels - EN_a (b) stands for EN12512 a (b) approach while E.A. stands for Equivalent Energy Strain Approach [3.26]	73
Fig. 3.5 – Q-factor definition according to the pushover procedure [3.30].	77
Fig. 4.1 - Main steps of the new developed procedure.....	86
Fig. 4.2 – Bi-linearization criteria proposed by NTC 2008 [4.12].....	88
Fig. 4.3 - Identification of yielding and failure limit according to the proposed energetic approach.	89
Fig. 4.4 – Bi-linearization criteria.	90
Fig. 4.5 – Yielding limit and ductility given by each considered bi-linearization criteria.	91
Fig. 4.6 – Reference CLT building tested on shaking table (left) and 3D numerical model (right) [4.17].....	92
Fig. 4.7 – q-factor estimation for the tested three storeys CLT building [4.17].....	92
Fig. 4.8 – Choice of the wall elements representative of the investigated building system [4.17].	93
Fig. 4.9 – Influence of the bi-linearization criteria over the q-factor value.	103
Fig. 5.1 – Main experimental tests on CLT specimen carried out during SOFIE project.	110
Fig. 5.2 – DRAIN 3D numerical model used to investigate the CLT building seismic response during SOFIE project (left) and “Ceccotti Vignoli” hysteretic model for connectors (right) [5.10].....	111
Fig. 5.3 – Main experimental tests conducted at the University of Ljubljana, Slovenia.....	111
Fig. 5.4 – Main experimental tests carried out in FPInnovations laboratory – Canada [5.14].....	112
Fig. 5.5 - Fasteners configuration and load slip curve of the tested walls.....	113

Fig. 5.6 - Parameters with influence over the q-factor.	114
Fig. 5.7 – Views of the considered three storeys building.	116
Fig. 5.8 – Plant view of the considered three storeys building.	116
Fig. 5.9 - Seismic resistant walls distribution with evidenced the walls analyzed with a 2D plane model.	117
Fig. 5.10 – Perspective view of the examined façade A (left) and B (right).	117
Fig. 5.11 – Case study configurations.	118
Fig. 5.12 - Fasteners arrangement for each junction levels and reference facades - the three storeys case study was taken as reference.	119
Fig. 5.13 – Detail of LVL panel to panel joints and relative holdown arrangement on the wall - the three storeys case study was taken as reference.	119
Fig. 5.14 – Total of case study configuration and indication of the respectively slenderness, storeys mass and principal elastic period.	120
Fig. 5.15 – Force distribution on base angular bracket and holdown under earthquake.	121
Fig. 5.16 – Force distribution on the vertical panel to panel joints (a) and middle holdown (b) under earthquake.	121
Fig. 5.17 - Pushover curve for three different wall configuration of the three storeys building.	123
Fig. 5.18 – Scheme of the three storeys building numerical model.	124
Fig. 5.19 – Example of main fasteners used in CLT building.	124
Fig. 5.20 – Example of calibration of the numerical model on the experimental test.	125
Fig. 5.21 – Example of force distribution used in the NLSAs.	126
Fig. 5.22 - Seismic signals used in NLDA (left) and demonstrating of the fulfillment of spectrum-compatibility requirement (right).	127
Fig. 5.23 – Pushover curve and near collapse condition load-displacement values for building configuration with reference to façade A (left) and B (right).	130
Fig. 5.24 – Summary pushover curve and near collapse condition load-displacement values for building configuration with reference to façade A (top) and B (bottom).	131
Fig. 5.25 – Modification of the behaviour factor q with the overstrength levels for each examined configurations.	135
Fig. 6.1 - Definition of the reference (left) and actual (right) junction indexes.	142
Fig. 6.2 – Histograms and correspondent normal distributions for the two slenderness levels considered.	143
Fig. 6.3 – Histograms and correspondent normal distributions for the three junction levels considered.	144
Fig. 6.4 – 5% - 95% characteristic q-factor ranges versus junction levels β for each examined slenderness λ	145
Fig. 6.5 – Comparison between the 5% percentile numerical and analytical q-factors, separately for each analyzed slenderness.	147
Fig. 6.6 – linear (top) and power (bottom) abacus for the q-factor estimation.	148
Fig. 6.7 – Deformed numerical models and connectors distribution for configurations “A” (left) and “B” (right).	150
Fig. 6.8 - Relationship between the $PGA_{near\ collapse}$ values and principal Eigen frequency of the building.	152
Fig. 6.9 - Time history of base shear for the earthquake N. 7 amplified to near collapse condition for elastic and inelastic connections behaviour.	153
Fig. 6.10 - q-factors for configuration “A” buildings calculated with the PGA-based approach (left) and the base shear based approach (right).	153
Fig. 6.11 - q-factors for configuration “B” buildings calculated with the PGA-based approach (left) and the base shear based approach (right).	154
Fig. 6.12 - Relationship between the q-values and principal elastic period of the studied building.	155
Fig. 6.13 - Building plan (left) and view of the shaken table test (right) [6.6].	157
Fig. 6.14 - Building plan (left) and axonometric view of the shaken table test (right) [6.3].	159
Fig. 6.15 - Sketch of the building model used for the numerical simulation (left) and view of the shaken table test (right) [6.3].	159
Fig. 6.16 - Time trend of the various energy contributions for the case study building for the seismic signal scaled up to near collapse condition.	162

Fig. 6.17 - Examples of hysteretic load displacement curve of angle bracket (left) and hold down (right) from nonlinear dynamic analysis.....	163
Fig. 6.18 - Time trend of energy dissipated for each specific connection element.	163
Fig. 6.19 - Shear-drift curves for each level of the case study building in the analyses with the seismic signal scaled up to near collapse condition.....	164
Fig. 6.20 - Energetic response for each level of the case study building –analyses with seismic signal scaled up to near collapse condition.....	164
Fig. 6.21 - Absolute (right) and relative (left) values of viscous and hysteretic dissipated energy contributions for each connection type (in this figure: H stands for hold-down, A for angles and P for panel-to-panel joints).	165
Fig. 6.22 - Relative values of viscous and hysteretic energy dissipation by each connection type at each level (left) and relative values of total dissipated energy contributions at each level. (right).....	166
Fig. 7.1 – Crown House, Manchester Five Storey Brick Clad Timber Frame [7.1].....	171
Fig. 7.2 – Brick Clad Timber Frame at BRE Cardington (left) and Typical Movement Joint (right) [7.1].....	172
Fig. 7.3 – View of the precast modular panel.....	174
Fig. 7.4 – View of the foundation anchor system.....	174
Fig. 7.5 - Sketch of the setup, “Wall B” and “Wall C”.....	176
Fig. 7.6 - Load displacement curve, cyclic test for “Wall B” (left) and “Wall C” (right).....	176
Fig. 7.7 - Wall configuration at the end of the cyclic test - “Wall B” (left) and “Wall C” (right).....	177
Fig. 7.8 - “Wall C”- configuration at the end of the monotonic ramp test and failure details.	177
Fig. 7.9 - Dissipated and potential energy used to define the equivalent viscous damping [7.9].....	180
Fig. 7.10 – Connection systems used in the developed mixed wood-concrete shearwalls.	183
Fig. 7.11 – Elwood hysteretic model and characteristic parameters [7.17].....	183
Fig. 7.12 - Comparison between experimental results and numerical load-displacement curve. The parameters of the numerical models are listed on the bottom of the plots and they are relative to the tensile branch of the cyclic curve.	184
Fig. 7.13 - FEM model “Wall B” (left) and “Wall C” (right).....	185
Fig. 7.14 - Comparison between the experimental results and the FEM simulation in terms of load slip curve and dissipated energy “Wall B” (top) and “Wall C” (bottom).....	185
Fig. 7.15 - Case study: modular wall panel arrangement.....	187
Fig. 7.16 - Investigated wall panels: fasteners and bracing system arrangement (left) and FEM model, type and position of the nonlinear elements (right).....	188
Fig. A.1 – Sample of a residential building made with this constructive system – Mestre (VE).....	194
Fig. A.2 – Exploded view of the modular wall panel.....	194
Fig. A.3 – Geometrical characteristic of the precast modular panel.....	195
Fig. A.4 – Geometrical characteristic of the RC slab.....	196
Fig. A.5 – Characteristic of the plastic blush along the vertical beam column (left) and along the horizontal crossbeam (center) of the wood frame. Detail of plastic blush and screws (right).....	197
Fig. A.6 – Foundation anchor system.....	197
Fig. A.7 – Inter-storey connection element.....	198
Fig. A.1 – View of a two storey composite wall with indication of the connection elements.....	199
Fig. A.8 – Typological node of the wood concrete building system – external angle (left), falling angle (center) and T intersection (right).....	199
Fig. A.9 – Load-slip curve of modular panel braced by stapled OSB panel or screwed concrete slabs.....	200
Fig. A.10 – Resistant mechanism of screwed concrete bracing system.....	202
Fig. A.11 – Force induced into base fasteners by bracing system.....	204
Fig. A.12 – Decomposition of the top displacement in the shear, slip and rocking contribution.....	207
Fig. A.13 – Deformed shape of assembled wall with different stiffness of vertical joint – the base holdowns constraints are not considered.....	213
Fig. A.14 – Construction methodology for wide (left) and small (right) opening.....	214

List of Tables

Table 2.1 - Mechanical characteristics of the CrossLam panel.....	58
Table 2.2 – Comparison between test and model results	61
Table 4.1 – Geometrical characteristic of the case study wall specimens.....	94
Table 4.2 – Hysteresis loop and correspondent bilinear approximation of the case study wall specimens. ...	97
Table 4.3 – q-factor definition for each case studies and bi-linearization criteria	100
Table 5.1 – Fasteners failure limit according to experimental tests [5.6].....	122
Table 5.2 - PGA_{max} and $PGA_{near\ collapse}$ for each investigated case study building.....	128
Table 5.3 – Q-factor estimation for all the investigated building configuration.....	132
Table 5.4 – q-factors values for the additional case study configurations designed for various fasteners overstrengthening levels.....	134
Table 6.1 – Values of the coefficient β , q-factor range and slenderness for each of the examined facades.	142
Table 6.2 – q-factor range for each slenderness and junction level	145
Table 6.3 - Storey masses and principal vibration period for each of the investigate buildings. In bold is evidenced the configuration tested on shaking table test with the SOFIE Project [6.3].....	151
Table 6.4 - PGA values for the near collapse condition registered in the analysis; letter A near to acceleration value corresponds to failure of the angular brackets while the letter H corresponds to failure of holdowns.	152
Table 6.5 – Statistical analysis of the obtained q-factor values	154
Table 6.6 - Comparison between analytical and numerical q-factor values.....	154
Table 6.7 - Geometrical characteristic of the case study N.1 – NEES Wood building.....	158
Table 6.8 - q-factor analytical evaluation of the case study N.1 - NEESWood building.....	158
Table 6.9 - Geometrical characteristic of the case study N.2 - SOFIE building	160
Table 6.10 - Q-factor analytical evaluation of the case study N.2 - SOFIE building.	160
Table 7.1 - Test results and interpretation according to the energetic and EN 12512 [7.9] approaches.....	179
Table 7.2 - Equivalent viscous damping values obtained from the cyclic test	180
Table 7.3 - Strength degradations at each cycle amplitude	181
Table 7.4 - Comparison between the experimental results and the code provisions.....	181
Table 7.5 - Different mass distribution considered.....	187
Table 7.6 - Seismic design parameters and response spectrum for both the examined buildings. The spectra compatibility requirement of the 7 artificially generated earthquakes is also reported.	188
Table 7.7 - $PGA_{u_{eff}}$ values and q-factor for the considered earthquakes and for both the examined buildings	189
Table A.1 - Mechanical and geometrical properties of staples, wood frame and OSB panels.....	201
Table A.2 - 5% characteristic strength for staples in single shear according to Johansen equations.....	201
Table A.3 - 5% characteristic lateral shear resistance of OSB stapled panel bracing system.....	202
Table A.4 - 5% characteristic lateral shear resistance of screwed concrete bracing system.....	202
Table A.5 - 5% characteristic load bearing capacity of the holdown nailing.....	205
Table A.6 - 5% characteristic tensile strength of holdown steel blade.....	206

Table A.7 - Stapled OSB panel stiffness calculation.....	208
Table A.8 - Screwed concrete slab stiffness calculation.....	209
Table A.9 - Base bolt stiffness calculation.....	210
Table A.10 - Holdown stiffness calculation.....	211
Table A.11 - Relation between the base uplift and the top rocking displacement.....	211